

Summer 2017

# Electrogenerated Chemiluminescent Studies of 9,10-Diphenylanthracene, Rubrene, Tris(2,2'- Bipyridine)Ruthenium(II) Species, and Their Derivatives For Sensitive Detection of Biomolecules

Pradip Bastola  
*University of Southern Mississippi*

Follow this and additional works at: <https://aquila.usm.edu/dissertations>

 Part of the [Analytical Chemistry Commons](#)

---

## Recommended Citation

Bastola, Pradip, "Electrogenerated Chemiluminescent Studies of 9,10-Diphenylanthracene, Rubrene, Tris(2,2'-Bipyridine)Ruthenium(II) Species, and Their Derivatives For Sensitive Detection of Biomolecules" (2017). *Dissertations*. 1429.

<https://aquila.usm.edu/dissertations/1429>

This Dissertation is brought to you for free and open access by The Aquila Digital Community. It has been accepted for inclusion in Dissertations by an authorized administrator of The Aquila Digital Community. For more information, please contact [aquilastaff@usm.edu](mailto:aquilastaff@usm.edu).

ELECTROGENERATED CHEMILUMINESCENT STUDIES OF 9,10-  
DIPHENYLANTHRACENE, RUBRENE, TRIS(2,2'-BIPYRIDINE)  
RUTHENIUM(II) SPECIES, AND THEIR DERIVATIVES FOR  
SENSITIVE DETECTION OF BIOMOLECULES

by

Pradip Bastola

A Dissertation  
Submitted to the Graduate School,  
the College of Science and Technology,  
and the Department of Chemistry and Biochemistry  
at The University of Southern Mississippi  
in Partial Fulfillment of the Requirements  
for the Degree of Doctor of Philosophy

August 2017

ELECTROGENERATED CHEMILUMINESCENT STUDIES OF 9,10-  
DIPHENYLANTHRACENE, RUBRENE, TRIS(2,2'-BIPYRIDINE)  
RUTHENIUM(II) SPECIES, AND THEIR DERIVATIVES FOR  
SENSITIVE DETECTION OF BIOMOLECULES

by Pradip Bastola

August 2017

Approved by:

---

Dr. Wujian Miao, Committee Chair  
Associate Professor, Chemistry and Biochemistry

---

Dr. J. Paige Buchanan, Committee Member  
Research Physical Scientist, US Army Corps of Engineers

---

Dr. Song Guo, Committee Member  
Assistant Professor, Chemistry and Biochemistry

---

Dr. Douglas S. Masterson, Committee Member  
Associate Professor, Chemistry and Biochemistry

---

Dr. Karl J. Wallace, Committee Member  
Associate Professor, Chemistry and Biochemistry

---

Dr. Sabine Heinhorst, Chair  
Professor, Chemistry and Biochemistry

---

Dr. Karen S. Coats  
Dean of the Graduate School

COPYRIGHT BY

Pradip Bastola

2017

*Published by the Graduate School*



THE UNIVERSITY OF  
**SOUTHERN**  
**MISSISSIPPI**®

## ABSTRACT

# ELECTROGENERATED CHEMILUMINESCENT STUDIES OF 9,10-DIPHENYLANTHRACENE, RUBRENE, TRIS(2,2'-BIPYRIDINE) RUTHENIUM(II) SPECIES, AND THEIR DERIVATIVES FOR SENSITIVE DETECTION OF BIOMOLECULES

by Pradip Bastola

August 2017

This dissertation explored and investigated the coreactant electrogenerated chemiluminescent (ECL) properties of unmixed and mixed systems of highly efficient ECL emitters, such as 9,10-diphenylanthracene (DPA), rubrene (RUB), and tris(2,2'-bipyridine)ruthenium(II) [ $\text{Ru}(\text{bpy})_3^{2+}$ ] species as well as their water-soluble derivatives, which can serve as ECL labels for sensitive bioanalysis of single or multiple analytes. The screening of most favorable common ECL coreactants, their concentration effects along with the effect of working electrode materials on ECL behavior, and energy transfer related interactions between ECL emitters were systematically investigated. In addition, a strategy for improvement of ECL signals with the use of nitrate salt as an ECL enhancing agent was employed. A highly sensitive and selective immunosensor for the detection of viruses (zika virus or ZIKV and dengue virus or DENV4) has been developed.

A well-adaptable spectral ECL instrument that can be used for undergraduate analytical chemistry or instrumental analysis laboratories was first constructed. ECL

coreactant screening studies concluded that benzoyl peroxide (BPO) was the most suitable coreactant using Pt working electrode.

Water soluble analogues of DPA and RUB, i.e., DPAS and SRUB, were synthesized and characterized by electrochemical and ECL studies. ECL signals were enhanced by more than 10 times when a nitrate salt was added to anodic ECL systems. A nitrate radical was seen using electron paramagnetic resonance (EPR) spectroscopy, which supported the proposed ECL enhancement mechanism was obtained.

Efforts were made on looking for direct evidence of ECL coreactant intermediates using EPR spectroscopy. Benzyloxy free radical ( $C_6H_5CO_2^{\bullet}$  or  $BPO^{\bullet}$ ) and sulfate anion radical ( $SO_4^{\bullet-}$ ) were detected using solid or solution-phase coreactant with or without a spin trapping agent 5,5-dimethyl-1-pyrroline-*N*-oxide (DMPO) under UV irradiation or through chemical reduction reactions.

Finally, zika virus (ZIKV) is a globally emerging mosquito-transmitted flavivirus that can cause severe fetal abnormalities. Any serotype of dengue virus (DENV1-4) shows flu like illness. As such, a highly sensitive and specific ECL based immunoassay was developed for detection of ZIKV and DENV-4 in human biological fluids with an impressive detection limit of 1 PFU of ZIKV in 100  $\mu$ L of saline, human plasma, or human urine.

## ACKNOWLEDGMENTS

I would like to pay my due gratitude and sincere appreciation to my mentor, advisor, my role model and my “guru”, Wujian Miao, PhD, for guiding, encouraging and directing me for my Ph.D. degree. I am so blessed and fortunate to work with my advisor, Dr. Miao who has not only guided me in the contents of science but also taught me different practical lessons of my life. I would also like to thank my doctoral research committee members, Dr. J. Paige Buchanan, Dr. Song Guo, Dr. Douglas S. Masterson and Dr. Karl J. Wallace for their constant support and feedbacks on my research projects. I would also like to say “Thank you” to my lab mates Dr. Yiliyasi Wusimanjiang, Tamanna F. Shanta and Arun S. Sridhar for their all-time support. I am very thankful to Dr. Fengwei Bai, Department of Biology, University of Southern Mississippi for his collaborative support on virus projects. I am also thankful to Dhiraj Acharya, Linda Le Gates, Amber Paul for their contributions on my research accomplishments. I would also like to admire Prof. Michael S. Diamond, Washington University in St. Louis, MO for providing reagents and antibodies for zika virus detection. I would like to acknowledge all Miao group members, past and present. I am equally thankful to all faculty, graduate and undergraduate and staff members from the Chemistry and Biochemistry Department, University of Southern Mississippi, Hattiesburg Campus. I would like to pay due regards to Professor Dr. Sabine Heinhorst, head of department for continuous support. I am indebted to acknowledge NSF career award (CHE-0955878) for funding my research. I am very thankful to Ms. Tina Masterson for teaching me how to teach undergraduate lab courses professionally. I express my thanks to Dr. Casey Simons for helping with EPR spectroscopy. I would like to acknowledge MS-INBRE facility for microscopy works and

Jessica Douglas for helping with TEM imaging. I would also like to thank Mrs. Pratikshya Adhikari for helping me with confocal imaging imaging and Mr. Krishna Sapkota for helping me with NMR and ESI-MS experiments.

Thank you so much my mother, Ishwari Devi Bastola, my father, Sitaram Bastola, for being amazing parents for not only giving me birth but also showing how beautiful this world is. I am very blessed to have my wife, Tulasha, son Prashal, and daughter Pransi for supporting my every endeavor towards my accomplishments.

Many thanks to my family members for supporting and encouraging me towards my research accomplishments.

## DEDICATION

This dissertation is dedicated to those six hundred million innocent children living on this planet who are deprived of good food, better health, and quality education. Approximately 3.1 million children die each year from hunger or hunger-related causes. Nearly 17,000 children die each day mostly from preventable health issues such as malaria, diarrhea and pneumonia. About 22,000 children die each day due to conditions of poverty. Every day, mother Earth loses nearly 1,000 innocent children due to preventable water and sanitation-related diseases.

## TABLE OF CONTENTS

ABSTRACT .....	ii
ACKNOWLEDGMENTS .....	iv
DEDICATION .....	vi
LIST OF TABLES .....	xiii
LIST OF ILLUSTRATIONS .....	xiv
LIST OF SCHEMES.....	xix
LIST OF ABBREVIATIONS.....	xx
CHAPTER I - INTRODUCTION AND BACKGROUND .....	1
1.1 Electroanalytical Techniques .....	1
1.1.1 Cyclic voltammetry.....	2
1.1.2 Differential pulse voltammetry .....	4
1.2 Electrogenenerated Chemiluminescence .....	5
1.2.1 Ion annihilation ECL.....	6
1.2.2 Coreactant ECL.....	9
1.3 Unique Features of ECL <sup>69,71</sup> .....	13
1.4 Implications of ECL.....	14
1.5 Selected Examples of Application of ECL for Detection of Analytes .....	16
1.5.1 Analyte binding methods used in ECL based detection .....	16
1.5.2 Sensitive detection of specific ion .....	18

1.5.3 “High amplification” strategy of ECL detection .....	19
1.5.4 Lab on a chip and paper based ECL .....	22
1.6 Ultraviolet-Visible Spectroscopy .....	23
1.6.1 Application of UV-Vis in ECL .....	24
1.7 Fluorescence Spectroscopy .....	24
1.7.1 Application of fluorescence in ECL .....	25
1.8 Electron Paramagnetic Resonance (EPR) Spectroscopy .....	26
1.8.1 Application of EPR in ECL .....	28
1.9 Scope of This Dissertation .....	28
CHAPTER II - COREACTANT ECL STUDIES OF UNMIXED AND MIXED SYSTEMS OF 9,10-DIPHENYLANTHRACENE, RUBRENE, AND TRIS(2,2'- BIPYRIDINE)RUTHENIUM(II) IN ACETONITRILE .....	30
2.1 Introduction.....	30
2.2 Experimental Section .....	32
2.2.1 Chemicals.....	32
2.2.2 Spectral ECL Instrument Setup .....	32
2.2.3 Electrochemical and ECL measurements .....	33
2.3 Results and Discussion .....	34
2.3.1 Selection of ECL emitters and their CV studies .....	34
2.3.2 Selection of ECL coreactants and working electrodes .....	39

2.3.3 Validation of the spectral ECL instrument .....	47
2.3.4 Study of unmixed systems of ECL emitters .....	50
2.3.5 Study of binary mixed systems of ECL emitters .....	52
2.3.6 Study of ternary mixed systems of ECL emitters .....	62
2.4 Hazards .....	67
2.5 Conclusion .....	67
CHAPTER III - SYNTHESIS, ELECTROCHEMISTRY AND ECL STUDIES OF WATER SOLUBLE ANALOGUES OF 9,10-DIPHENYLANTHRACENE AND RUBRENE WITH NITRATE AS ECL ENHANCING AGENT .....	69
3.1 Introduction.....	69
3.2 Experimental Section .....	70
3.2.1 Chemicals.....	70
3.2.2 Apparatus and methods.....	70
3.3 Synthesis .....	74
3.3.1 Synthesis of water soluble analogue of DPA — Sodium-9,10- diphenylanthracene sulfonate (SDPAS) .....	74
3.3.2 Synthesis of water soluble sulfonated rubrene (SRUB) .....	76
3.4 Results and Discussion .....	77
3.4.1 Structural characterization and elucidation.....	77
3.4.2 Electrochemistry of DPAS and SRUB .....	83

3.4.3 Effect of ECL coreactant and electrode material on ECL production .....	87
3.4.4 ECL enhancement with nitrate ions .....	96
3.4.5 Direct EPR Evidence of Nitrate Free Radical (NO <sub>3</sub> <sup>•</sup> ).....	106
3.4.6 ECL Studies of Mixed Systems of DPAS, SRUB, and Ru(bpy) <sub>3</sub> <sup>2+</sup> .....	110
3.5 Conclusion .....	114
 CHAPTER IV – DIRECT ELECTRON PARAMAGNETIC RESONANCE EVIDENCE OF CATHODIC ECL COREACTANT INTERMEDIATES OF BENZOYL PEROXIDE AND AMMONIUM PERSULFATE .....	
	116
4.1 Introduction.....	116
4.2 Experimental Section .....	119
4.2.1 Chemicals and materials .....	119
4.2.2 EPR parameters and acquisition .....	120
4.2.3 Spin labels (traps) .....	121
4.3 Results and Disussion .....	122
4.3.1 Measurement of EPR spectra of benzoyloxy free radical (BPO <sup>•</sup> or PhCO <sub>2</sub> <sup>•</sup> )	122
4.3.2 Measurement of EPR spectra of sulfate anion radical (SO <sub>4</sub> <sup>•-</sup> ) .....	125
4.4 Conclusion .....	127
 CHAPTER V – ULTRASENSITIVE ELECTROGENERATED CHEMILUMINESCENCE BASED IMMUNOASSAYS FOR THE DETECTION OF ZIKA AND DENGUE VIRUSES .....	
	129

5.1 Introduction.....	129
5.2 Experimental.....	132
5.2.1 Chemicals and reagents.....	132
5.2.2 Preparation and titration of virus stocks .....	132
5.2.3 ECL label loading and avidin conjugation of PSBs.....	133
5.2.4 Attachment of biotinylated antibodies to the surface of ECL-label loaded PSBs and MBs.....	133
5.2.5 ECL and electrochemical measurements .....	134
5.2.6 Confocal Microscopy.....	135
5.2.7 Transmission Electron Microscopy .....	135
5.2.8 Real time-quantitative PCR (RT-qPCR).....	135
5.2.9 Western blotting.....	136
5.3 Results.....	136
5.3.1 Assay design, ECL-label loading and antibody conjugation of polystyrene and magnetic beads.....	136
5.3.2 Anti-ZIKV-PSB capture of ZIKV .....	138
5.3.3 Anti-ZIKV-PSB specifically detects ZIKV in a highly sensitive manner .....	141
5.3.4 ECL-based immunoassay can detect ZIKV in human biological fluids.....	146
5.3.5 ECL Detection of DENV4.....	150
5.4 Discussion.....	154

5.5 Conclusion .....	156
CHAPTER VI – CONCLUDING REMARKS .....	157
REFERENCES.....	160

## LIST OF TABLES

Table 2.1 Redox potential, ECL efficiency, and ECL emission values of DPA, RUB, and Ru(bpy) <sub>3</sub> <sup>2+</sup> species. ....	36
--	----

## LIST OF ILLUSTRATIONS

Figure 1.1 Cyclic voltammogram (CV) of $K_3Fe(CN)_6$ .....	3
Figure 1.2 Potential-excitation signals and voltammogram for DPV (from ref. <sup>68</sup> ). .....	5
Figure 1.3 Molecular structures of some common ECL emitters.....	6
Figure 1.4 Molecular structures of some common ECL coreactants.....	10
Figure 1.5 Examples of solid-phase ECL assay formats (from ref. <sup>72</sup> ). .....	18
Figure 1.6 Working principle of the $Hg^{2+}$ -ECL detection (from ref. <sup>199</sup> ). .....	19
Figure 1.7 Schematic diagram of (a) DNA hybridization, and (b) sandwich type ECL immunoassay (from ref. <sup>72</sup> ). .....	21
Figure 1.8 Fabrication and operation of a paper-based microfluidic ECL sensor. (from ref. <sup>203</sup> ). .....	23
Figure 1.9 Schematic of FRET process (from ref. <sup>176</sup> ). .....	26
Figure 1.10 Energy diagram showing splitting of the energy levels is directly proportional to the strength of magnetic field. ....	27
Figure 2.1 Schematic diagram of spectral ECL instrument setup. ....	33
Figure 2.2 Molecular structures of ECL emitters under study (a) DPA, (b) RUB, and (c) $Ru(bpy)_3^{2+}$ . .....	35
Figure 2.3 CVs of individual ECL emitters. ....	39
Figure 2.4 Molecular structures of ECL coreactants under study (a) TPrA, (b) DBAE, and (c) BPO. ....	40
Figure 2.5 CVs of individual ECL coreactants. ....	41
Figure 2.6 CVs of 10.0 mM BPO at different electrodes. ....	42
Figure 2.7 ECL spectra obtained from a mixture of DPA, RUB, and $Ru(bpy)_3^{2+}$ . .....	44

Figure 2.8 Effect of electrode material on ECL intensity. ....	47
Figure 2.9 ECL responses of various coreactant ECL systems measured with a PMT based ECL instrument. ....	49
Figure 2.10 ECL spectra of (A) DPA, (B) RUB, and (C) Ru(bpy) <sub>3</sub> <sup>2+</sup> at various concentrations using BPO as coreactant. (D) Relationship between the emitter concentration and ECL peak intensity. ....	52
Figure 2.11 ECL spectra of the (DPA-RUB)/BPO system with a constant concentration of RUB mixed with various concentrations of DPA. ....	54
Figure 2.12 Fluorescence spectra of DPA and absorption spectrum of RUB. ....	55
Figure 2.13 ECL spectra of the (DPA-Ru(bpy) <sub>3</sub> <sup>2+</sup> )/BPO system with a constant concentration of (A) DPA and (B) Ru(bpy) <sub>3</sub> <sup>2+</sup> mixed with various concentrations of (A) Ru(bpy) <sub>3</sub> <sup>2+</sup> and (B) DPA. ....	57
Figure 2.14 Fluorescence spectra of DPA and absorption spectra of Ru(bpy) <sub>3</sub> <sup>2+</sup> . ....	58
Figure 2.15 Fluorescence spectra of DPA with the addition of various amounts of Ru(bpy) <sub>3</sub> <sup>2+</sup> . ....	59
Figure 2.16 ECL spectra of the (RUB-Ru(bpy) <sub>3</sub> <sup>2+</sup> )/BPO system with a constant concentration of (A) Ru(bpy) <sub>3</sub> <sup>2+</sup> and (B) RUB mixed with various concentrations of (A) RUB and (B) Ru(bpy) <sub>3</sub> <sup>2+</sup> . ....	62
Figure 2.17 Deconvolution of ECL spectra obtained from a mixture of DPA, RUB, and Ru(bpy) <sub>3</sub> <sup>2+</sup> . ....	63
Figure 2.18 ECL spectra of the (DPA-RUB- Ru(bpy) <sub>3</sub> <sup>2+</sup> )/BPO system with the concentration change of (A) DPA, (B) RUB, and (C) Ru(bpy) <sub>3</sub> <sup>2+</sup> while two other ECL emitter concentrations remained unchanged. ....	66

Figure 3.1 Homemade ECL instrument setup.....	71
Figure 3.2 Liquid nitrogen cooled CCD camera-based ECL spectral instrument setup...	72
Figure 3.3 FTIR spectra of (A) DPA and DPAS, and (B) RUB and SRUB.....	79
Figure 3.4 ESI-MS data of DPAS.....	80
Figure 3.5 <sup>1</sup> H-NMR spectroscopy data of (A) DPA, and (B) DPAS, (C) RUB, and (D) SRUB.....	83
Figure 3.6 (A) CVs, and (B) DPVs of DPAS in aqueous media. ....	85
Figure 3.7 (A) CVs, and (B) DPVs of SRUB in aqueous media. ....	87
Figure 3.8 Effect of electrode material on the ECL intensity of (A) DPAS/DBAE and (B) DPAS/TPrA system. ....	89
Figure 3.9 Effect of electrode material on the ECL intensity of (A) SRUB-DBAE and (B) SRUB-TPrA system.....	90
Figure 3.10 ECL-CV profiles of the DPAS-DBAE system.....	93
Figure 3.11 Effect of coreactant concentration and electrode material on ECL intensity.	96
Figure 3.12 Effect of nitrate ions on ECL from (A) DPAS/DBAE, and (B) SRUB/DBAE. ....	99
Figure 3.13 CVs of (a) NaNO <sub>3</sub> , (b) DBAE-NaNO <sub>3</sub> , and (c) DBAE.....	100
Figure 3.14 Effect of [NaNO <sub>3</sub> ] on the ECL enhancement of (a) SRUB/DBAE and (b) DPAS/DBAE system. ....	102
Figure 3.15 Demonstration of ECL enhancement by NaNO <sub>3</sub> using the mixed (DPAS-Ru(bpy) <sub>3</sub> <sup>2+</sup> )/DBAE system.....	103
Figure 3.16 Effect of different nitrate salts on the ECL enhancement of the Ru(bpy) <sub>3</sub> <sup>2+</sup> /DBAE system. ....	104

Figure 3.17 Experimental and simulated EPR spectra for nitrate mixed with DMPO in water under UV irradiation. ....	109
Figure 3.18 ECL spectra of (A) (DPAS-SRUB) /DBAE-NaNO <sub>3</sub> and (B) (DPAS-Ru(bpy) <sub>3</sub> <sup>2+</sup> )/DBAE-NaNO <sub>3</sub> .....	112
Figure 3.19 ECL spectra (DPAS-SRUB-Ru(bpy) <sub>3</sub> <sup>2+</sup> )-NaNO <sub>3</sub> /DBAE with the concentration change of (A) Ru(bpy) <sub>3</sub> <sup>2+</sup> and (B) SRUB. ....	114
Figure 4.1 Block diagram of EPR instrumentation.....	120
Figure 4.2 Chemical structures of common nitroxide spin labels (traps). ....	121
Figure 4.3 EPR spectra of DMPO/ <sup>•</sup> OOC <sub>6</sub> H <sub>5</sub> adduct. ....	123
Figure 4.4 EPR spectra obtained from (A) solid BPO without DMPO under UV irradiation, and (B) solid BPO mixed with a drop of 200 mM DMPO solution under UV irradiation.....	125
Figure 4.5 EPR spectra of (A) solid persulfate with DMPO under UV irradiation, and (B) persulfate in water with hydrazine and DMPO without UV irradiation. ....	127
Figure 5.1 Assay design and preparation of immuno-conjugated and ECL-loaded beads. ....	138
Figure 5.2 Immuno-conjugated and ECL label loaded polystyrene beads capture ZIKV. ....	140
Figure 5.3 TEM images during detection of ZIKV. ....	141
Figure 5.4 Anti-ZIKV-PSB specifically detects ZIKV in a highly sensitive manner. ...	146
Figure 5.5 ECL-based immunoassay detects ZIKV in human biofluids. ....	150
Figure 5.6 (A) PSB(RUB)-anti-4G2 conjugates, (B) PSB(RUB)<DENV4>MB final aggregates and (C) Free (unbound) PSB(RUB) from the supernatant. ....	152

Figure 5.7 ECL-responses from PSB-DENV4-MB aggregates obtained from samples containing different concentrations of DENV4 viruses..... 154

## LIST OF SCHEMES

Scheme 1.1 Schematic diagram showing general principles of ion annihilation ECL process. <sup>73</sup> .....	7
Scheme 1.2 Coreactant mechanisms route in typical ECL processes. (from ref. <sup>71,83</sup> ).....	12
Scheme 2.1 ECL mechanism with BPO as cathodic ECL coreactant. ....	46
Scheme 3.1 Synthesis of SDPAS using the sulfonation of DPA.....	75
Scheme 3.2 Synthesis of SRUB using the sulfonation of RUB.....	77
Scheme 3.3 ECL mechanism with DBAE as an anodic ECL coreactant. ....	91
Scheme 3.4 Proposed ECL mechanism of the R/DBAE-NO <sub>3</sub> <sup>-</sup> system using DBAE as an anodic ECL coreactant and NO <sub>3</sub> <sup>-</sup> as an ECL enhancing agent. ....	106
Scheme 3.5 Formation of DMPO/NO <sub>3</sub> <sup>•</sup> and DMPO/OH <sup>•</sup> adducts. ....	107
Scheme 4.1 A general ECL mechanism of an anodic ECL system with R served as an ECL emitter and C as a coreactant.....	116
Scheme 4.2 A general ECL mechanism of a cathodic ECL system with R served as an ECL emitter and C as a coreactant.....	117
Scheme 4.3 Formation of benzoyloxy radical (BPO <sup>•</sup> ) by chemically reducing BPO with hydrazine, followed by spin trapping with DMPO.....	122

## LIST OF ABBREVIATIONS

<i>CL</i>	chemiluminescence
<i>ECL</i>	electrogenerated chemiluminescence or electrochemiluminescence
<i>UV-Vis</i>	ultraviolet-visible
<i>FL</i>	fluorescence
<i>CV</i>	cyclic voltammetry
<i>DPV</i>	differential pulse voltammetry
<i>PMT</i>	photomultiplier tube
<i>CCD</i>	charged coupled device
<i>EPR</i>	electron paramagnetic resonance
<i>SECM</i>	scanning electrochemical microscopy
<i>TEM</i>	tunneling electron microscopy
<i>PAH</i>	polycyclic aromatic hydrocarbon
<i>DPA</i>	9,10-diphenylanthracene
<i>RUB</i>	rubrene
<i>Ru(bpy)<sub>3</sub><sup>2+</sup></i>	tris(2,2'-bipyridine)ruthenium(II)
<i>BPO</i>	benzoyl peroxide
<i>TPrA</i>	tri- <i>n</i> -propylamine
<i>DBAE</i>	2-(dibutylamino)ethanol
<i>MeCN</i>	acetonitrile
<i>GCE/GC</i>	glassy carbon electrode
<i>DPAS</i>	9,10-diphenylanthracene sulfonate
<i>SRUB</i>	sulfonated rubrene

<i>PB</i>	sodium phosphate buffer
<i>PBS</i>	phosphate buffer saline
<i>mAb</i>	monoclonal antibody
<i>ZIKV</i>	zika virus
<i>DENV</i>	dengue virus
<i>WNV</i>	west nile virus
<i>CKV</i>	chikungunya virus
<i>PSB</i>	polystyrene bead
<i>MB</i>	magnetic bead
<i>DMPO</i>	5,5-dimethyl-1-pyrroline- <i>N</i> -oxide

## CHAPTER I - INTRODUCTION AND BACKGROUND

The essence of this dissertation is to study the electrochemical and electrogenerated chemiluminescent (ECL) properties of ECL emitters, namely 9,10-diphenylanthracene (DPA), rubrene (RUB), and tris(2,2'-bipyridine)ruthenium(II) complex ( $\text{Ru}(\text{bpy})_3^{2+}$ ) for their potential applications towards detection and quantification of biomolecules, such as antigens, viruses, and proteins. Their analysis could be realized by designing highly efficient ECL based biosensors involving the combination of the most favorable ECL emitters and coreactants. This chapter briefly reviews various electroanalytical techniques, ECL and its bio-detection, and spectroscopic methods associated with ECL studies.

### 1.1 Electroanalytical Techniques

Electroanalytical techniques are the analytical techniques that study to infer crucial information, such as concentration and chemical reactivity of the analyte of interest by measuring electrical responses in the form of e.g., current, charge, oxidation states, or potential. In other words, these techniques deal with the interaction of electricity and analyte (usually a chemical species) resulting in chemical change and production of electrical energy by chemical change. The most common process of carrying out electrochemical analysis is in an electrochemical cell containing electrodes.<sup>1-3</sup> Depending upon which aspects of the cell are controlled, electroanalytical techniques are classified as: (a) potentiometry (potential difference is measured in the absence of current flow), (b) coulometry (current is measured over time), and (c) voltammetry (current is measured with varying potential).

A wide range of studies employing electroanalytical techniques can be found in the literature (e.g., scifinder scholar). Recently electroanalytical techniques have been deployed for analyzing polyphenols in red wine,<sup>4</sup> determination of anti HIV drugs,<sup>5</sup> identifying lead white pigment,<sup>6</sup> analyzing food samples,<sup>7-14</sup> pharmaceutical drug analysis,<sup>15-29</sup> probing neurochemical mechanisms and brain chemistry,<sup>30-40</sup> understanding of temperature effects on metal chemodynamics,<sup>41</sup> environmental monitoring,<sup>42-45</sup> and analyzing carcinogenic polycyclic aromatic hydrocarbons (PAHs).<sup>46</sup>

### 1.1.1 Cyclic voltammetry

Cyclic voltammetry (CV) is a versatile electroanalytical and potentiodynamic technique, which has been widely used in the understanding of organometallic,<sup>47-50</sup> organic,<sup>51-55</sup> and polymer chemistry.<sup>56-58</sup> CV is a simple and widely employed technique to obtain qualitative as well as quantitative information of the redox process under study.<sup>59,60</sup> For ferricyanide/ferrocyanide  $[\text{Fe}^{\text{III}}(\text{CN})_6^{3-}]/\text{Fe}^{\text{II}}(\text{CN})_6^{4-}$  system to demonstrate how this technique can be applied to fundamentally understand the redox process of this couple. The one electron redox process for ferricyanide/ferrocyanide can be written as:



Nernst equation for Equation 1.1 can be expressed as:

$$E = E_{\text{Fe}(\text{CN})_6^{3-}/\text{Fe}(\text{CN})_6^{4-}}^0 + 0.059 \log \frac{[\text{Fe}^{\text{III}}(\text{CN})_6^{3-}]}{[\text{Fe}^{\text{II}}(\text{CN})_6^{4-}]} \quad (\text{at } 298 \text{ K}) \quad (1.2)$$

where  $E$  and  $E^0$  are the measured and formal potentials, respectively. Figure 1.1 shows a cyclic voltammogram of  $\text{K}_3\text{Fe}(\text{CN})_6$  solution. The formal potential can be calculated as:

$$E^{0'} = \frac{E_{pa} + E_{pc}}{2} \quad (1.3)$$

where  $E_{pa}$  and  $E_{pc}$  are the anodic and cathodic peak potential, respectively. The separation of peak potential of a reversible redox process:

$$\Delta E_p = E_{pa} - E_{pc} = \frac{0.057}{n} \quad (\text{at } 298 \text{ K}) \quad (1.4)$$

where  $n$  is the number of electron transfer involved in the redox process. For the process shown in Equation (1.1)  $n = 1$ , thus  $\Delta E_p = 57 \text{ mV}$  is the expected value.

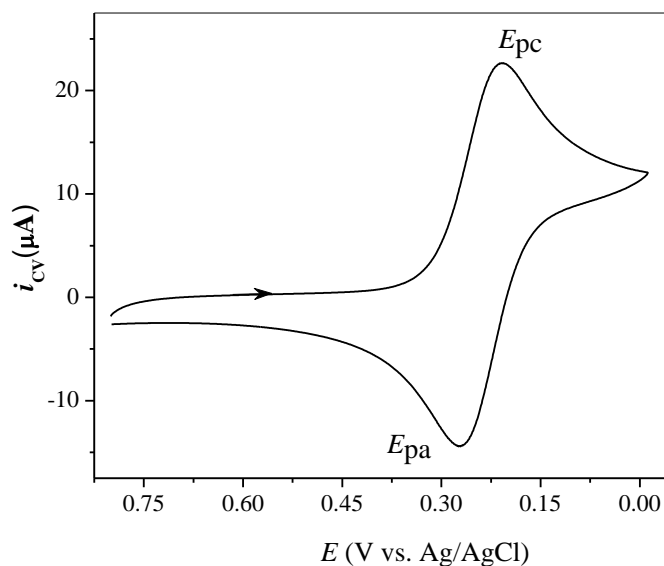


Figure 1.1 Cyclic voltammogram (CV) of  $\text{K}_3\text{Fe}(\text{CN})_6$ .

Note: Cyclic voltammogram was obtained from 6.0 mM  $\text{K}_3\text{Fe}(\text{CN})_6$  and 1.0 M  $\text{KNO}_3$  at a 3.0 mm-diameter glassy carbon working electrode at a scan rate of 100 mV/s.

For a reversible system, the peak current on the forward scan ( $i_p$ ) is given by the Randles-Sevcik equation:<sup>2,61</sup>

$$i_p = (2.69 \times 10^5) n^{3/2} A D^{1/2} C \nu^{1/2} \quad (1.5)$$

where  $n$  is the number of electrons transfer involved,  $A$  is the surface area of electrode ( $\text{cm}^2$ ),  $D$  is the coefficient of diffusion ( $\text{cm}^2/\text{s}$ ),  $C$  is the concentration of the electroactive species ( $\text{mol}/\text{cm}^3$ ), and  $\nu$  is the scan rate ( $\text{V}/\text{s}$ ). Therefore, the magnitude of peak current is proportional to the concentration of analyte and the square root of scan rate.

CV is often used to check the stability of reaction products, the presence of intermediates in redox reactions, electron transfer kinetics,<sup>62</sup> and the reversibility of a reaction.<sup>63</sup> CV is used to determine the electron stoichiometry of a system,<sup>64,65</sup> the diffusion coefficient of an analyte and the formal reduction potential. Because the concentration is proportional to current in a reversible nernstian system, concentration of an unknown analyte can be determined by generating a calibration curve of current vs. concentration.<sup>66,67</sup>

### **1.1.2 Differential pulse voltammetry**

Differential pulse voltammetry (DPV) is often the electrochemical technique of choice when the sensitivity of CV is not enough. In other words, if the redox peaks in CV are not obvious, one normally considers DPV technique to speculate where the electroactive species is oxidized or reduced. DPV is none other than the first order differentiation or derivative of linear sweep voltammetry or staircase voltammetry where a series of regular voltage pulses applied in a potential linear sweep or stairsteps fashion. Like all potentiometric methods, the current is measured immediately before each potential change. A differential pulse voltammogram is a plot of current change of each

cycle of pulse vs. potential. During a potential step, the faradaic current decay is much slower than the charging current decay. Thus, all pulsed techniques could provide much sensitive and low detection limit results for quantifying an electroactive species as compared with linear scan or cyclic voltammetry. Figure 1.2 shows a typical potential waveform of DPV and its voltammogram, where  $\tau$  is the time of each pulse cycle,  $t_p$  is the pulse time,  $\Delta E_p$  is the pulse potential, and  $\Delta E_s$  is the change in potential per cycle.

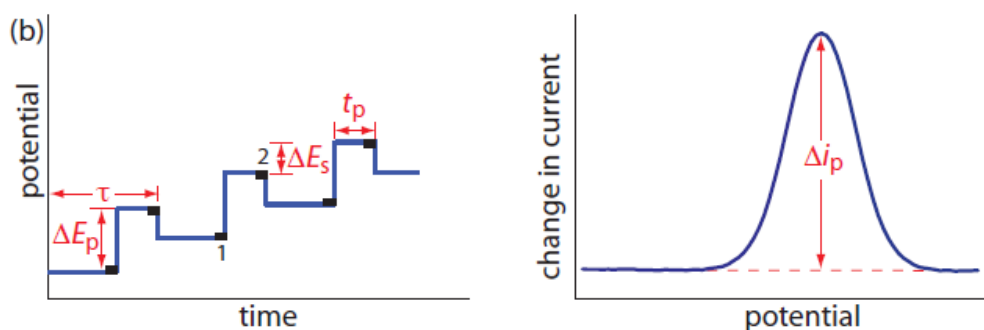


Figure 1.2 Potential-excitation signals and voltammogram for DPV (from ref.<sup>68</sup>).

Note: The current is sampled at the time intervals shown by the black rectangles.  $\Delta i$ , the current changed is measured by current at point subtracted from the current at point 2.

## 1.2 Electrogenerated Chemiluminescence

Electrogenerated chemiluminescence (ECL) is a light emission process as a consequence of electrochemical reaction and is generally potential (voltage) controlled. The wavelength of the emitted light corresponds to the energy gap between the excited and ground states of the emitter (luminophore). ECL emitters can be organic, such as dipyrrometheneboron difluoride (BODIPY) as shown in Figure 1.3 (a), inorganic metal complexes, such as tris(2,2'-bipyridine)osmium(II) [ $\text{Os}(\text{bpy})_3^{2+}$ ] as shown in Figure 1.3

(b), and semiconductor nanoparticles (quantum dots), such as CdSe/ZnS quantum dots as shown in Figure 1.3 (c). ECL has been classified into two main categories, namely ion annihilation ECL and coreactant ECL.

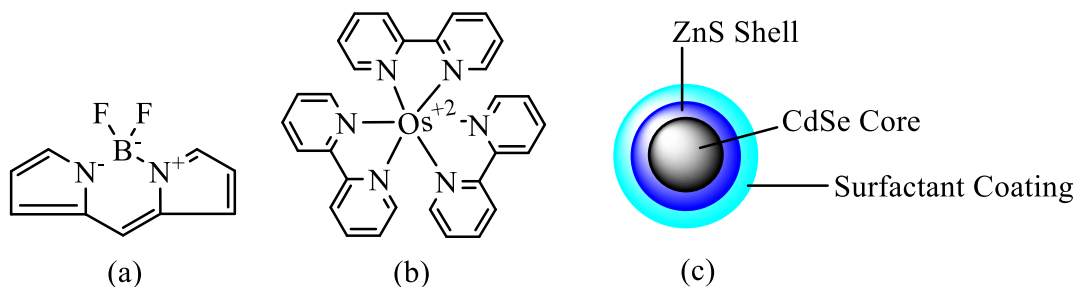


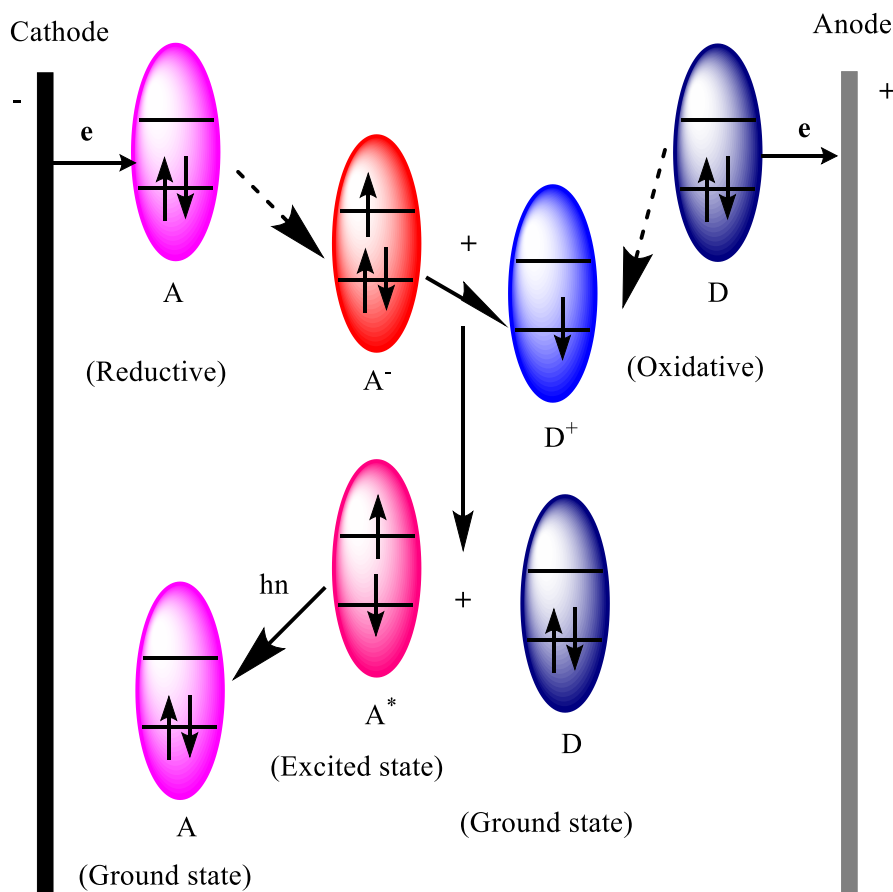
Figure 1.3 Molecular structures of some common ECL emitters

Note: Molecular structures of (a) BODIPY, (b)  $\text{Os}(\text{bpy})_3^{2+}$ , and (c) cartoon representation of CdSe (ZnS shell) quantum dot.

### 1.2.1 Ion annihilation ECL

ECL has been investigated since 1960s as a method of producing light at an electrode,<sup>69</sup> and has been widely used in analyte binding studies.<sup>70-72</sup> A typical ECL process is illustrated in Scheme 1.1, where species A accepts an electron at the cathode to form a reductive species  $\text{A}^-$ , while species D loses an electron at the anode to form an oxidative species  $\text{D}^+$ . When both  $\text{A}^-$  and  $\text{D}^+$  species diffuse from the electrode and meet, a highly energetic electron transfer process from  $\text{A}^-$  to  $\text{D}^+$  occurs, resulting in the formation of the excited state  $\text{A}^*$  that emits light (i.e., ECL emission). The emitted light intensity is generally proportional to the ECL emitter's concentration initially present in the solution, and the emission wavelength reflects the identity of the emitter. Based on the above two characteristic properties of an ECL system, qualitative and quantitative analysis of a target analyte associated with an ECL label can be realized. Because both radical anion

and cation are produced electrochemically before their annihilation to form ECL, this type of ECL is called ion annihilation ECL. Note that the chemical species used in ion annihilation ECL can be the same, for example,  $A = D = R$  (i.e.,  $R = 9,10$ -diphenylanthracene (DPA), rubrene (RUB), or tris(2,2'-bipyridine)ruthenium(II) ( $\text{Ru}(\text{bpy})_3^{2+}$ )). After one cycle ion annihilation process, the ECL emitter is regenerated resulting in high sensitivity of the technique.



Scheme 1.1 Schematic diagram showing general principles of ion annihilation ECL process.<sup>73</sup>

Equations (1.6-1.9) list each step of a typical type of ion annihilation ECL.



Depending on the energy available in an ion annihilation, Equation 1.8, the produced  $R^*$  could be either the singlet state species ( $^1R^*$ ) or the triplet state species ( $^3R^*$ ).

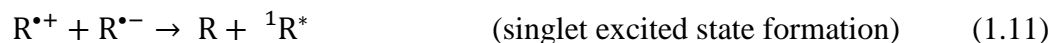
Instead of two working electrodes, in which one is applied with a positive potential and the other with a negative potential, ion annihilation ECL can also be obtained from an electrochemical system with only one working electrode. In this case, however, the working electrode must be scanned or pulsed between a positive and a negative potential alternatively. When  $R^{\bullet+}$  or  $R^{\bullet-}$  species is not stable enough for ECL reaction, or when the ECL solvent has a narrow potential window (e.g., in aqueous solution) so that  $R^{\bullet+}$  or  $R^{\bullet-}$  cannot be formed, no or weak ECL emission can be produced via the ion annihilation pathway.

The energy available or enthalpy for ion annihilation in Equation 1.8 can be estimated using modification of the standard Gibbs-Helmholtz equation,  $\Delta G = \Delta H - T\Delta S$  from the redox potential for oxidation and reduction processes in Equations 1.6 and 1.7 using

$$-\Delta H_{\text{ann}} = E_p \left( \frac{R}{R^{\bullet+}} \right) - E_p \left( \frac{R}{R^{\bullet-}} \right) - 0.16 \quad (1.10)$$

where  $-\Delta H_{\text{ann}}$  is measured in eV.  $E_p$  is the peak potential (in volts) for electrochemical redox process. The numerical value of 0.16 in Equation 1.10 is the entropy approximation term ( $T\Delta S$ ). If the energy ( $-\Delta H_{\text{ann}}$ ) is larger than the energy required for the formation of lowest excited singlet state and is said to follow “energy sufficient” or S-route, otherwise it is called “energy deficient system” and follow T-route. If neither route persists, a third route called ST route arises.

The ion annihilation for S route is summarized as:



In contrast, the ion-ion annihilation for T route is summarized as:



9,10-diphenylanthracene (DPA) system, more specifically,  $DPA^{\bullet+}/DPA^{\bullet-}$  system displays the typical S route system,<sup>74,75</sup> whereas N,N,N',N'-tetramethyl-p-phenylenediamine/9,10-diphenylanthracene, i.e.  $TMPD^{\bullet+}/DPA^{\bullet-}$  generates the excited state utilizing the T-route.<sup>75,76</sup> ST route is usually adopted by  $RUB^{\bullet+}/RUB^{\bullet-}$  system.<sup>77-80</sup>

### 1.2.2 Coreactant ECL

To overcome the aforementioned problems, coreactant ECL strategies can be used,<sup>72,81,82</sup> in which ECL is generated from a system containing an ECL emitter (e.g.,  $Ru(bpy)_3^{2+}$ ) and a deliberately added substance called coreactant (e.g., tri-*n*-propylamine

(TPrA), or benzoyl peroxide (BPO)) upon anodic or cathodic potential scanning or pulsing. Chemically, a coreactant is a species that, upon electrochemical oxidation or reduction, immediately undergoes chemical decomposition to form a strongly reducing or oxidizing intermediate that can react with an oxidized or reduced ECL emitter to generate excited states. Use of coreactant ECL allows many ECL related studies to be able to conduct in aqueous media. Depending on the electrode potential scanning direction, coreactant ECL can be classified as either anodic coreactant ECL or cathodic coreactant ECL.<sup>81</sup> In fact, coreactants are the intermediate species when electrochemically oxidize or reduce yield high redox power radical species for further chemical reactions in ECL processes. This ECL route has been used to enhance ECL greatly even for strong ECL emitters such as  $\text{Ru}(\text{bpy})_3^{2+}$ . Figure 1.4 shows three commonly used ECL coreactants.

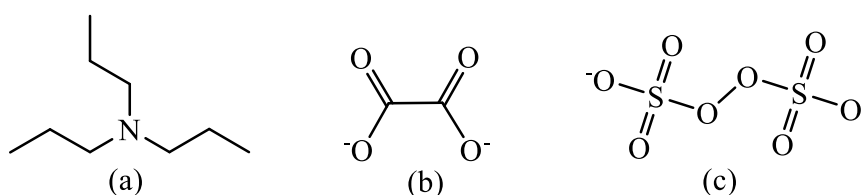
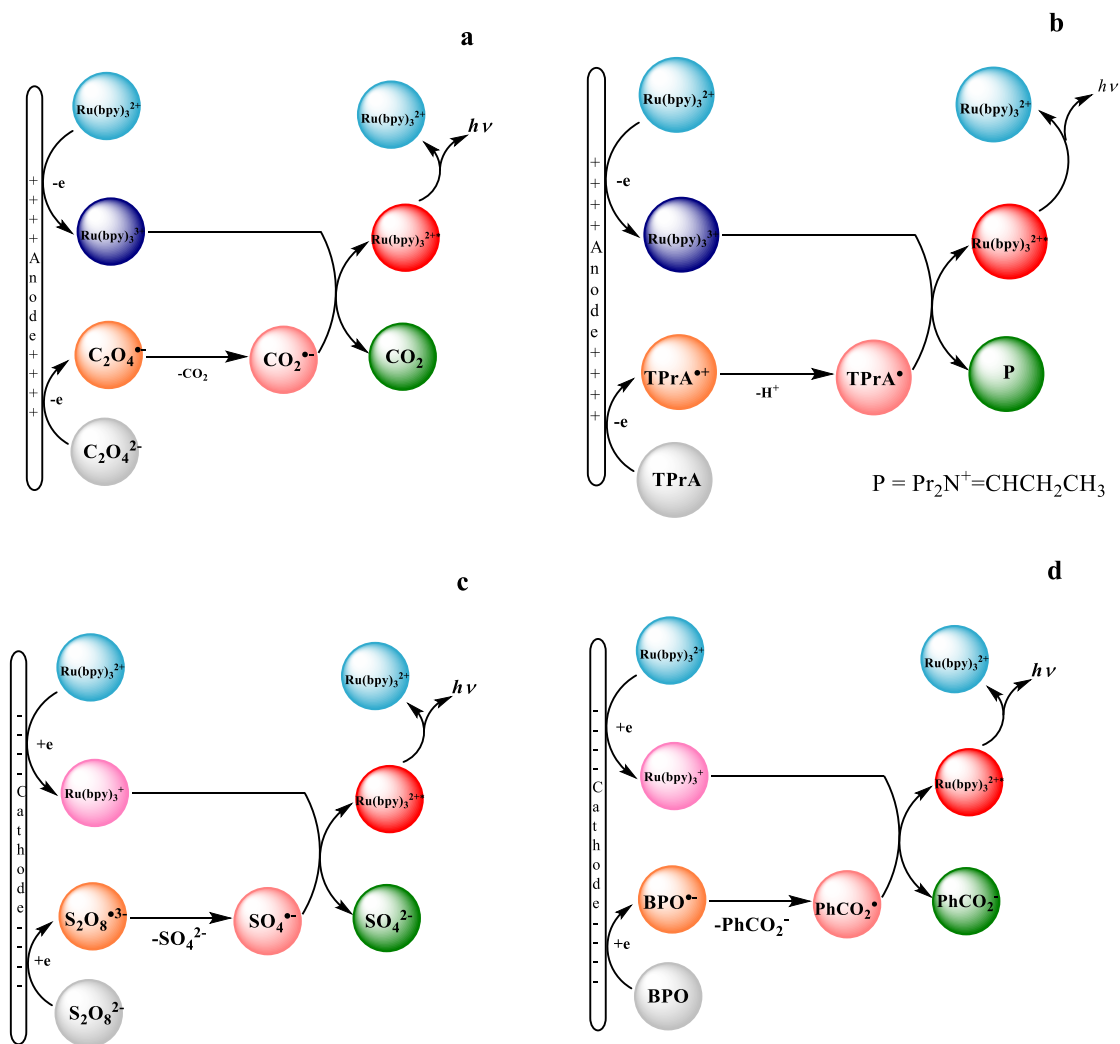


Figure 1.4 Molecular structures of some common ECL coreactants.

Note: (a) Tri-*n*-propylamine (TPrA), (b) oxalate, and (c) persulphate salt.

The used coreactant should not itself generate any ECL, otherwise there would be an interference with the analyte in solution. Additionally, the oxidation and reduction of the coreactant and analyte should be simultaneous after which there occurs chemical reaction followed by the electrochemical redox reaction at the surface of the electrode. As demonstrated in Scheme 1.2, the coreactant approach was first introduced by Bard et al., where ECL was studied in acetonitrile in the absence and presence of several

luminophores such as rubrene, DPA,  $\text{Ru}(\text{bpy})_3^{2+}$ , and  $\text{Os}(\text{bpy})_3^{2+}$ . TPrA and oxalate belong to the class of anodic ECL coreactants, whereas BPO and persulfate belong to the class of cathodic ECL coreactants. As shown in Scheme 1.2a., electrochemical oxidation of oxalate and  $\text{Ru}(\text{bpy})_3^{2+}$  occurs simultaneously in the anodic region (upon application of positive potential), a strong reducing agent,  $\text{CO}_2^{\cdot-}$  with a high reduction power is then produced after oxidized. Thus, in situ formed radical anion undergoes e.g., chemical reaction with the oxidized cation  $\text{Ru}(\text{bpy})_3^{3+}$  to yield the excited state of  $\text{Ru}(\text{bpy})_3^{2+}$  (i.e.,  $\text{Ru}(\text{bpy})_3^{2+*}$ ) generating ECL.



Scheme 1.2 Coreactant mechanisms route in typical ECL processes. (from ref.<sup>71,83</sup>).

Note: ECL mechanistic pathways for  $\text{Ru}(\text{bpy})_3^{2+}$  with both reductive ((a) Oxalate, (b) TPrA) and oxidative ((c) persulfate, (d) BPO) coreactants.

Similarly, the oxidation of TPrA and  $\text{Ru}(\text{bpy})_3^{2+}$  occurs simultaneously in the anodic region, a strong reducing agent  $\text{TPrA}^\bullet$  with a high reduction power is produced after oxidized. This  $\text{TPrA}^\bullet$  free radical produced chemically after deprotonation

encounters the oxidized cation  $\text{Ru}(\text{bpy})_3^{3+}$  to yield the excited state  $\text{Ru}(\text{bpy})_3^{2+}$  (i.e.,  $\text{Ru}(\text{bpy})_3^{2+*}$ ) producing ECL as illustrated in Scheme 1.2b.

The ECL mechanism with cathodic coreactants, such as BPO and persulfate, is completely reverse to that of ECL mechanism of anodic coreactants described previously. With cathodic coreactant, such as persulfate ( $\text{S}_2\text{O}_8^{2-}$ ), the reduction of persulfate and  $\text{Ru}(\text{bpy})_3^{2+}$  occurs simultaneously at the cathode, a strong oxidant,  $\text{SO}_4^{\cdot-}$  with a high oxidizing power, is then produced after reduction. Thus,  $\text{SO}_4^{\cdot-}$  anion free radical produced encounters reduced cation  $\text{Ru}(\text{bpy})_3^+$  to form the excited state of  $\text{Ru}(\text{bpy})_3^{2+}$  (i.e.,  $\text{Ru}(\text{bpy})_3^{2+*}$ ) producing ECL as seen in Scheme 1.2c. Similarly, when BPO is used as cathodic ECL coreactant, the reduction of BPO and  $\text{Ru}(\text{bpy})_3^{2+}$  occurs simultaneously at the cathode, a strong oxidant,  $\text{BPO}^{\cdot-}$  with a high oxidizing power is then produced after reduction of BPO.  $\text{BPO}^{\cdot-}$  quickly undergoes chemical decomposition to yield  $\text{BPO}^{\cdot}$  free radical that chemically reacts with the reduced cation  $\text{Ru}(\text{bpy})_3^+$  to yield the excited state of  $\text{Ru}(\text{bpy})_3^{2+}$  (i.e.,  $\text{Ru}(\text{bpy})_3^{2+*}$ ) generating ECL as illustrated in Scheme 1.2d.

### **1.3 Unique Features of ECL<sup>69,71</sup>**

ECL bridges the traditional fields of analytical electrochemistry with luminescence spectroscopy, and offers several distinct advantages over other spectroscopic-based detection system.

(1) Compared with fluorescence (FL) methods, ECL does not need a light source, which effectively frees the ECL from scattered-light and luminescent impurity interferences.

(2) Although ECL is a form of chemiluminescence (CL), in which both ECL and CL involve the light production by species that can undergo highly energetic electron transfer reactions. CL is initiated by the mixing of needed reagents with carefully controlling of their fluid flows. In contrast, ECL starts with electrochemical reactions by controlling electrode potential, scan rate, and position.

(3) ECL can be more selective than CL because the type of excited states may be controlled by varying the electrode potential.

(4) ECL generally is a nondestructive technique, in which the ECL emitter can be re-generated after the ECL emission, thereby providing high sensitivity.

The above statements are supported by several recent studies,<sup>84-86</sup> where different immunoassays based on enzyme-linked immunosorbent assay (ELISA), chemiluminescence (CL), ECL, and FL were compared, and ECL-based immunoassays were found to have excellent reproducibility and sensitivity over other assays. Therefore, ECL-based sensing systems will offer several unique features, which include high sensitivity, good selectivity, low background, integrated versatility, excellent reproducibility, and fast sample analysis.

#### **1.4 Implications of ECL**

Sensitivity and selectivity are desirable attributes of any ECL based detection system for detecting specific molecules of interest with many components. Sensitivity, in DNA hybridization and other bioassays for the detection of biomolecules of interest, is important in clinical diagnostics,<sup>87-90</sup> forensic chemistry,<sup>90,91</sup> environmental investigations,<sup>92,93</sup> pharmaceutical studies,<sup>94,95</sup> and biological warfare agent detection.<sup>96-103</sup> Thus, ECL provides sensitive and selective detection of molecules of interest should have broad applicability in all of these fields. A number of ECL reviews<sup>83,104-115</sup> have been available as ECL has been aggressively employed in clinical diagnostics because of the sensitivity, selectivity, and stability of ECL based biosensors.

Since ECL itself is not the stand alone technique, ECL needs to be coupled with various separation techniques, specifically liquid chromatographic techniques (high performance liquid chromatography or HPLC<sup>116-123</sup>, flow injection,<sup>124-129</sup> capillary electrophoresis or CE<sup>130-135</sup>) for determination and analysis of analytes in matrix. Biological threat agents have been detected with ECL and fluorogenic-chemiluminescence (FCL) based assays. ECL detection was found to be more sensitive for the detection of bacteria, viruses, and toxins whereas FCL has been considered as more versatile for effective sample clean-up and high throughput screening of complex samples.

Magnetic beads based ECL assays have been used with conjecture with a technology called systematic evolution of ligands by exponential enrichment (SELEX).<sup>136</sup> Instead of using protein-based antibodies in most common immunoassay formats, highly specific receptors formed from oligonucleotides called aptamers have been utilized.

Numerous label free aptamer based ECL detection has been investigated.<sup>137-154</sup> Amplification of binding receptors can be procured via PCR (polymerase chain reaction). Various immobilization ECL formats (immunoassays as well as DNA hybridization) can be found in ECL literature utilizing classical ECL luminophores,<sup>155-161</sup> semiconductor nanoparticles or quantum dots (QDs),<sup>162-165</sup> metal nanoparticles (NPs),<sup>105,166-171</sup> carbon nanotubes (CNTs)<sup>172-177</sup> and graphene,<sup>139,178-186</sup> for improving performance of developed ECL biosensors. Very sensitive and precise DNA assays labeled with Ru(bpy)<sub>3</sub><sup>2+</sup> derivatives have been presented.<sup>187</sup> Recent reports on DNA assays witnessed the limit of detection (LOD) as 20 DNA copies per mL in plasma or serum and 80 copies per mL in whole blood of varicella-zoster virus.<sup>188</sup> On a separate paper, a threshold of 10 DNA copies of Epstein–Barr virus has been mentioned.<sup>189</sup> Quantification of DNA or messenger RNA by reverse transcription PCR based on Ru(bpy)<sub>3</sub><sup>2+</sup>-ECL has been performed using commercial QPCR System 5000<sup>®</sup> from Perkin–Elmer<sup>190</sup> and the Origen<sup>®</sup> Analyser from Igen<sup>191</sup> down to attomolar level immobilized on a solid support (magnetic beads) using biotin-streptavidin chemistry. Latest ECL applications include lab-on-a-chip approaches paper based ECL.<sup>192-195</sup>

## **1.5 Selected Examples of Application of ECL for Detection of Analytes**

### **1.5.1 Analyte binding methods used in ECL based detection**

There is an increasing need for rapid, highly specific methods of detecting and quantifying small quantities of analytes such as chemical, biochemical, and biological substances. The presence of these materials can often be determined by binding methods that exploit the high degree of specificity which characterizes many biological systems.

Known methods that rely on binding to detect a molecule of interest in a sample include nucleic acid hybridization techniques and protein-ligand interactions such as antibody-antigen binding (Figure 1.5).<sup>72</sup> In these methods, a positive value is typically indicated either by the presence or the absence of an observable label (e.g., an ECL label) that has been attached to one or more of the materials comprising a diagnostic complex. For example, in the first case of DNA detection (Figure 1.5a), a target single-stranded DNA (ssDNA) with an ECL label attached hybridizes with a ssDNA probe that immobilized on a solid substrate.<sup>196,197</sup> Under the same experimental conditions, ECL produced from the complementary ssDNA hybridization will be higher than that obtained from non-complementary one. The sandwich type format shown in Figure 1.5d<sup>196,198</sup> is the most commonly used means of ECL detection of an antigen (or a biomarker). Also, direct interaction between the capture antibody and corresponding labeled antigen is possible (Figure 1.5e), although in this case the pretreatment of the antigen (analyte) with the ECL label, and subsequent separation of the free ECL labels from the antigen-ECL label conjugates would be required, which could dramatically slow down the entire detection progress as compared with the sandwich type assays, where both surface-confined and ECL labeled antibodies can be pre-prepared. In a competition assay format (Figure 1.5f), the unlabeled antigen blocks the ability of the labeled antigen to bind. As a result, less label measured in the assay means more of the unlabeled (test sample) antigen is present. In other words, the amount of antigen in the test sample is inversely related to the amount of label measured in the competitive format.

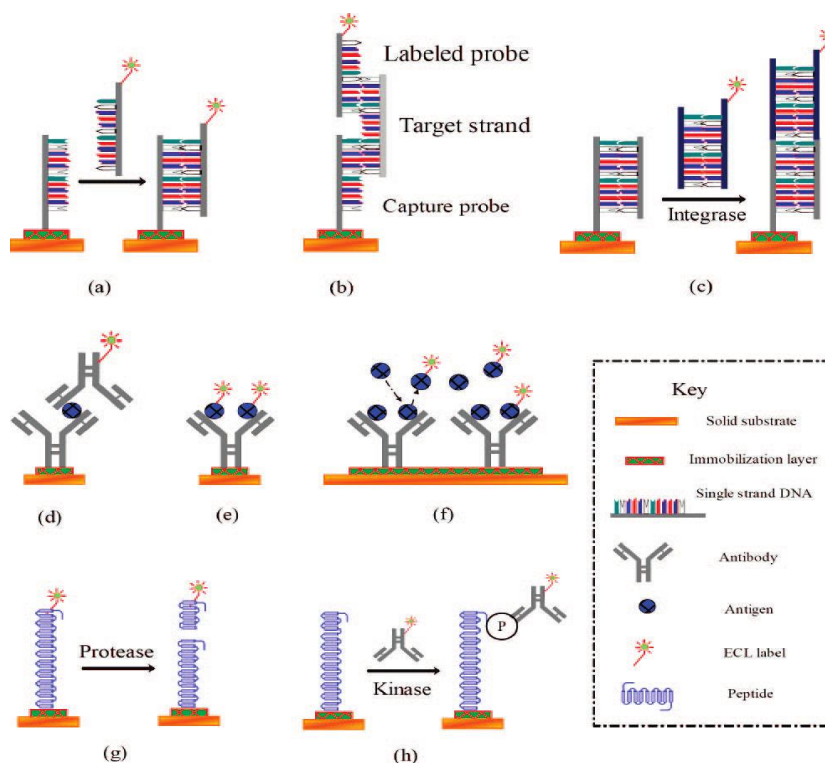


Figure 1.5 Examples of solid-phase ECL assay formats (from ref.<sup>72</sup>).

Note: (a) DNA hybridization assay based on an immobilized ssDNA hybridizes with a labeled target ssDNA., (b) sandwich type DNA biosensor, (c) an assay used for integrase activity test with immobilized and free labeled dsDNA, (d) sandwich type immunoassay, (e) direct immunoassay, (f) competitive assay in which analyte competes with labeled analyte for antibody binding sites on immobilized antibody, (g) protease activity assay where cleavage of the immobilized peptide results in the decrease in ECL emission due to the removal of the ECL label, (h) kinase activity assay using a labeled antibody to recognize the phosphorylated product.

### 1.5.2 Sensitive detection of specific ion

A new type of  $\text{Hg}^{2+}$  selective ECL biosensor with an extremely low detection limit of 2.4 pM and high stability has been recently reported on the basis of mercury-specific oligonucleotide (MSO). MSO served as a molecular recognition element and a  $\text{Ru}(\text{bpy})_3^{2+}$  derivative as an ECL emitting species. As shown in Figure 1.6, the MSO is covalently attached to the surface of carboxylated single-wall carbon nanotubes (SWNTs) on a glassy carbon electrode via an appropriate length of spacer. G4 PAMAM dendrimer

with heavily loaded  $\text{Ru}(\text{bpy})_3^{2+}$  derivatives are tethered to the other end of the MSO. In the presence of  $\text{Hg}^{2+}$  ions, the initial linear MSO bends to form a “hairpin” type structure after the complexation reaction between  $\text{Hg}^{2+}$  ions and thymine bases, which leads to the ECL labels become closer to the electrode surface. Thus, a significant increase in ECL intensity was observed with the  $\text{Hg}^{2+}$  bound ECL biosensor upon the anodic potential scanning or pulsing in the presence of TPrA coreactant.



Figure 1.6 Working principle of the  $\text{Hg}^{2+}$ -ECL detection (from ref.<sup>199</sup>).

### 1.5.3 “High amplification” strategy of ECL detection

In ECL analysis, ECL active labels that are attached to the target biomolecule produce a measurable signal. The intensity of the measured signal is generally proportional to the amount of the target species bound on the electrode. Traditionally, only one or few labels can be attached directly to one target biomolecule, so that nonspecific adsorption can be avoided and the bioactivity of the target biomolecule remains. By utilizing polystyrene microspheres/beads (PSB) as the carrier of a large

number of hydrophobic ECL labels (i.e.,  $\text{Ru}(\text{bpy})_3^{2+}$ ) an ultrasensitive methodology for DNA hybridization detection,<sup>156</sup> sandwich-type immunoassay of C-reactive protein (CRP),<sup>155</sup> and the detection of high explosive 2,4,6-trinitrotoluene (TNT)-contaminated soil and creek water samples<sup>161</sup> has been demonstrated.

The principle of this type of strategy is shown in Figure 1.7. For DNA detection (Figure 1.7a), a known sequence ssDNA (probe ssDNA) is first immobilized on the surface of a magnetic bead (MB). The complementary ssDNA (target ssDNA)-coated PSB bead that contains a large number of ECL labels (e.g., water insoluble  $\text{Ru}(\text{bpy})_3^{2+}$ ,  $\sim 10^9$  molecules/bead) hybridizes with the probe ssDNA to form a [(probe ssDNA-MB)/(target ssDNA-PSB)] aggregate. Finally, this aggregate is magnetically separated from the reaction mixture and transferred into an acetonitrile (MeCN) solution, in which the PSBs dissolve and the ECL label is released. Light emission from the released ECL labels is subsequently measured in MeCN in the presence of a coreactant, such as TPrA, at a Pt electrode. A similar approach based on a sandwich-type of immunoassay can be used for the detection of an antigen (e.g., CRP and TNT), as displayed in Figure 1.7b. Clearly, there is no need for direct attachment of the ECL labels to ssDNA or antibodies in the present technique, therefore a high loading capacity of the ECL labels per PSB, hence a very large amplification factor of the ECL label molecules for each molecule of analyte can be achieved, given that a limited number of capture ssDNA or antibody species are attached to one PSB via the immobilization layer (of avidin).

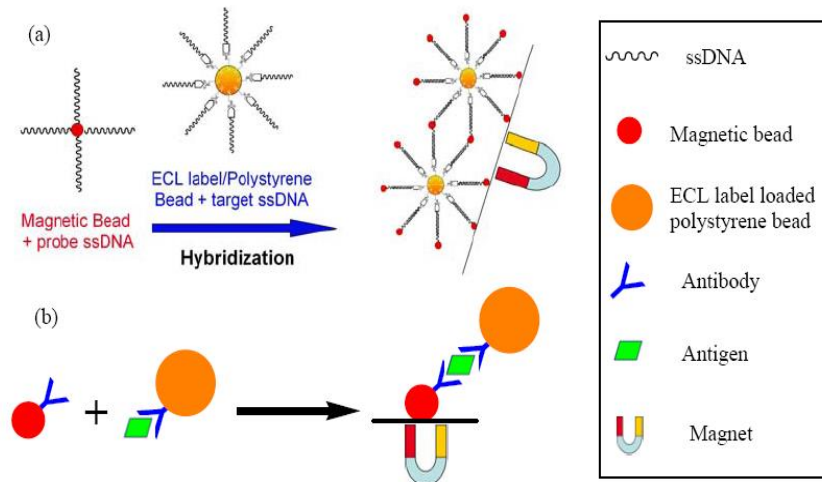


Figure 1.7 Schematic diagram of (a) DNA hybridization, and (b) sandwich type ECL immunoassay (from ref.<sup>72</sup>).

Note: Polystyrene beads were used as the ECL label carrier and magnetic beads were used for the separation of analyte-containing ECL label/polystyrene beads.

With the above PSB-based “high amplification” technique, a detection limit of 1.0 fM ( $1.0 \times 10^{-15}$  M) for a t-ssDNA was achieved,<sup>197</sup> along with a 100-fold improvement in the sensitivity in the CRP determination<sup>198</sup> compared to a previously reported surface immobilized ECL method.<sup>196</sup> Likewise, a limit of detection of 0.10 ppt TNT was obtained,<sup>200</sup> which is about 600 times lower than recently reported data using “a novel surface plasmon resonance immunosensor.”<sup>201</sup>

Similar idea has been extended to ECL detection in aqueous media. Instead of 10  $\mu$ m in diameter PSBs, ~100 nm in diameter sized liposomes as the ECL label carrier were used in CRP detection.<sup>202</sup> The release of the ECL label from liposomes was realized by using 0.1 M TPrA and 0.1 M phosphate buffer (pH 7.6) containing 0.1 M NaCl and 1% (v/v) Triton X-100.

#### **1.5.4 Lab on a chip and paper based ECL**

Recent advancement in the field of ECL has made possible an exciting invention of a kind of paper substrate micro-fluidic chip of bipolar electrode ECL and application in imaging and sensing. This can be realized in practice by utilizing carbon paste as bipolar electrode on paper for development of ECL chip for imaging, sensing, and detection of TPrA. This invention exploits the proof of concept of paper substrate micro-fluidics.

Another recent report<sup>203</sup> described the development of an ECL sensor fabricated utilizing paper microfluidics with and without the use of conventional photodetectors. Paper based microfluidic sensor was designed with inkjet printing were combined with screen-printed electrodes (SPEs) to create simple, cheap, disposable using conventional as well as mobile phone camera. Using conventional photodetector, a LOD of 2-(dibutylamino)ethanol (DBAE) and nicotinamide adenine dinucleotide (NADH) was 0.9  $\mu\text{M}$  and 72  $\mu\text{M}$ , respectively, whereas 250  $\mu\text{M}$  DBAE was detected using the phone.

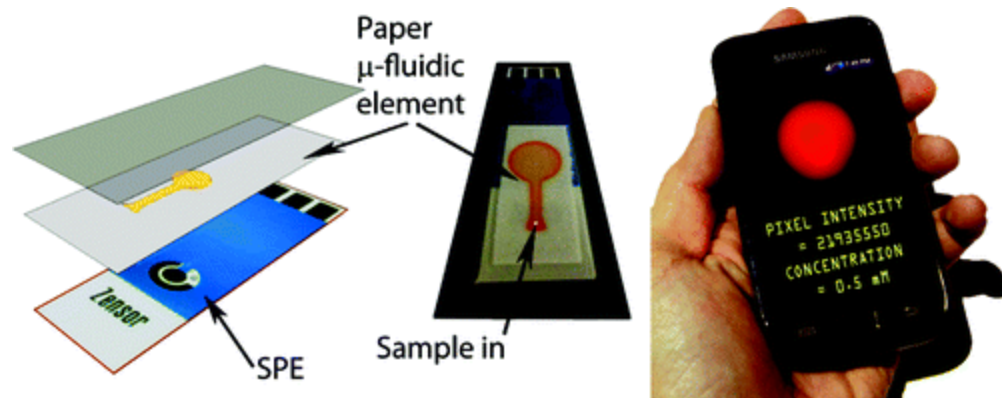


Figure 1.8 Fabrication and operation of a paper-based microfluidic ECL sensor. (from ref.<sup>203</sup>).

Note: The individual paper fluidic elements were cut to size and the hydrophilic portion filled with a 10 mM Ru(bpy)<sub>3</sub><sup>2+</sup> solution before drying. The paper substrate was then aligned and fixed onto the face of the SPE by laminating with transparent plastic. Finally, a drop of sample is introduced through a small aperture in the plastic at the base of the channel, and when the detection zone was fully wetted, the sensor was placed close to the lens of the camera phone, a potential of 1.25 V was applied, and the resulting emission was captured and analyzed.

A wide range of ultrasensitive detection of analytes using ECL can be found in the literature.<sup>113,138,143,148,153,156,161,204-206</sup>

## 1.6 Ultraviolet-Visible Spectroscopy

Ultraviolet–visible spectroscopy (UV-Vis or UV/Vis) is an absorption spectroscopic technique in which absorption of light intensity by a molecule in a sample in UV-Vis region. UV-vis technique is based on Beer’s law, which can be expressed as shown below in Equation 1.14 as:

$$A = \epsilon \cdot b \cdot C \quad (1.14)$$

where  $A$  is the absorbance,  $\epsilon$ , the molar extinction coefficient (molar absorptivity) in the units of  $\text{L mol}^{-1}\text{cm}^{-1}$ ,  $b$ , the path length of the cuvette (cm), and  $C$  is the concentration in  $\text{mol L}^{-1}$ . During an absorption process, an electron from the ground energy state promotes to the higher energy level of excited state. Because we measure the absorbed light by the sample of interest, the detector is aligned along with the light source and sample holder.

### **1.6.1 Application of UV-Vis in ECL**

UV-Vis spectroscopy is employed to obtain an optimum fluorescence. For optimum fluorescence, one needs a right excitation wavelength that can be obtained by speculating at what absorption wavelength the molecule absorption is maximum in UV-Vis spectra. This wavelength is often the correct excitation wavelength in fluorescence. UV-Vis spectroscopy could help us to understand the energy or electron transfer mechanism and has found many applications in biomolecule detection.<sup>181,207-211</sup>

### **1.7 Fluorescence Spectroscopy**

Fluorescence spectroscopy is an emission spectroscopic technique utilized to record fluorescence or emissive light from a sample when UV or visible light is externally applied to excite the electrons in a molecule. The energy of light emitted is the energy level difference between the lower and upper energy levels before and after the promotion of electron(s) by irradiation of external light source. Absorption and emission are the complementary processes. Because, light source is applied externally to excite the electrons, the emissive light or fluorescence is measured by placing the detector 90 degrees against the light source-sample array to measure the emitted light.

### **1.7.1 Application of fluorescence in ECL**

Theoretically, ECL emission spectrum could overlap with the fluorescence emission spectrum from the same luminophore under study. However, this is not always the case. For example, in the case of quantum dot luminophores that are not properly capped, there could be some shift in the peak emission wavelengths. To verify whether the ECL has been generated from the same luminophore or luminophore with some redox impurities contaminated with, one can compare the ECL spectrum with the fluorescence spectrum using identical solvent system. Absorption and emission are the crucial steps to understand the energy transfer between acceptor and donor molecules in mixed ECL emitter systems. One example of such energy transfer is the fluorescence resonance energy transfer (FRET) between two luminophores that emit light at two different or close emission wavelengths (Figure 1.8). One way of investigating this type of energy or electron transfer between two luminophores is to see if there is any spectral overlap between the emission of donor luminophore and the absorption of acceptor luminophore.

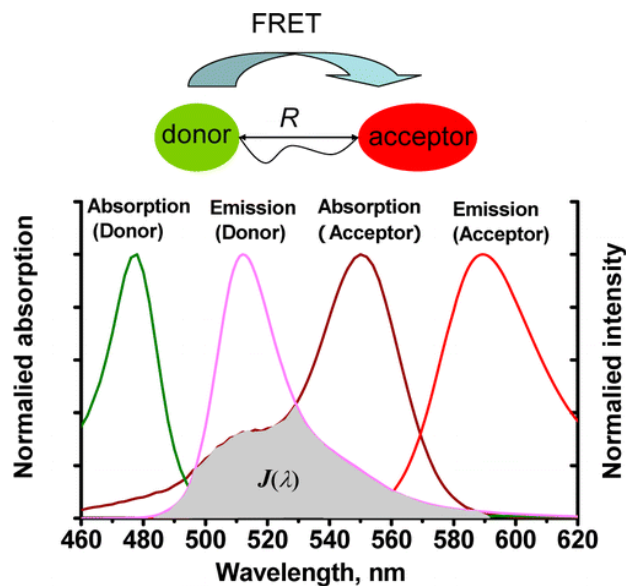


Figure 1.9 Schematic of FRET process (from ref.<sup>176</sup>).

### 1.8 Electron Paramagnetic Resonance (EPR) Spectroscopy

Electron paramagnetic resonance (EPR) or electron spin resonance (ESR) spectroscopy is a technique utilizing for studying materials with unpaired electrons. The fundamental principles behind EPR spectroscopy are analogous to that of nuclear magnetic resonance (NMR). EPR utilizes the excitement of electron spin whereas in NMR, the spins of atomic nuclei are excited. EPR offers great specificity because ordinary chemical solvents and matrices do not give rise to EPR spectra. For understanding origin of an EPR signal,<sup>212-215</sup> the electronic levels of an atom in a molecule should be considered. Each electron has a magnetic moment and spin quantum number,  $s = 1/2$ , with magnetic components  $m_s = +1/2$  and  $m_s = -1/2$ . In the presence of an external magnetic field with strength  $B_0$ , the electron's magnetic moment aligns itself either parallel ( $m_s = -1/2$ ) or antiparallel ( $m_s = +1/2$ ) to the magnetic field (Figure 1.10), each alignment having a specific energy due to the Zeeman effect. The separation

between the lower and the upper state for unpaired free electrons is accompanied by either absorbing or emitting a photon of energy ( $\Delta E$ ) equal to  $h\nu$  such that the resonance condition is obeyed as shown in Equation 1.15.

$$\Delta E = h\nu \quad (1.15)$$

where  $h$  is the Planck's constant ( $h = 6.626 \times 10^{-34} \text{ J}\cdot\text{s}$ ) and  $\nu$  is the frequency of the radiation. This leads to the fundamental equations of EPR spectroscopy:

$$h\nu = g_e \mu_B B_0 \quad (1.16)$$

where  $g_e$  equals to 2.0023 for the free electron and  $\mu_B$  is the Bohr magneton.

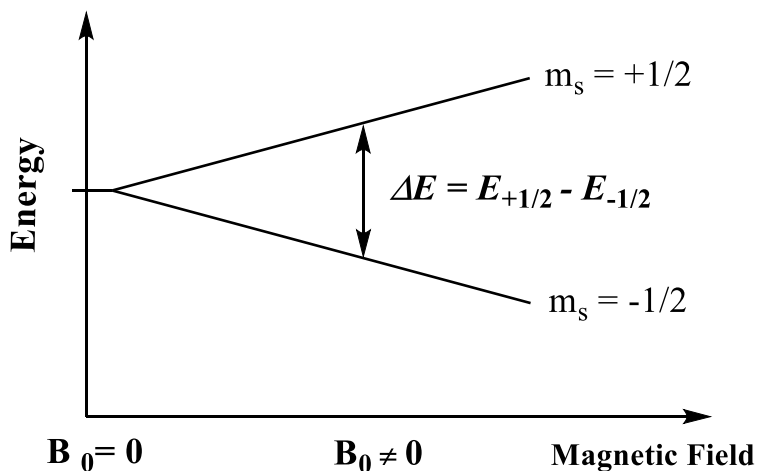


Figure 1.10 Energy diagram showing splitting of the energy levels is directly proportional to the strength of magnetic field.

### **1.8.1 Application of EPR in ECL**

ECL generation always involves anionic, cationic, and free radicals. As a result, EPR could play an important role in monitoring the reaction process and in providing critical information for proposing ECL mechanisms. Previously, EPR signals obtained from TPrA<sup>•+</sup> cation radical after its oxidation has been reported.<sup>216</sup> Very recently, hydroxyl radical OH<sup>•</sup>, which is an intermediate of cathodic ECL coreactant H<sub>2</sub>O<sub>2</sub> reduction, as well as its stability in H<sub>2</sub>O-CH<sub>3</sub>CN mixtures, has also been published.<sup>217</sup>

### **1.9 Scope of This Dissertation**

There has been ongoing rapid use of ECL in quantification and analysis of clinical, food, and environmental samples; however, there are very few studies found in the literature for ECL based multiplexed assays. Thus, there is a need for urgent and immediate measures to be taken to detect and quantify multiple analytes per assay with high throughput. One could save time, money, and effort by collecting multiple data at one time with the use of multiple emitters (labels). For this, it is important to study the systematic ECL titration behavior of mixed and unmixed systems of multiple efficient ECL emitters before their potential applications in multiplexing detection of biomolecules could be realized. This dissertation focuses on search for favorable ECL coreactants by screening various commonly used ECL coreactants that suit in both unmixed and mixed systems of emitter-coreactant combination. This dissertation also provides insights into optimizing experimental conditions, which include effects of electrode material, molecular oxygen (only applicable to cathodic coreactants), concentration of ECL emitter, coreactant, and solvent on ECL signal intensities. The

interaction studies of the multiple efficient ECL emitters with common favorable coreactant in their mixed systems are also the focused area of this dissertation. The synthesis of water soluble analogues of DPA and RUB, viz. 9,10-diphenylanthracene sulfonate (DPAS) and sulfonated rubrene (SRUB), electrochemical and ECL studies of the synthesized emitters, and methods to improve ECL signals of the emitters all comes under the scope of this dissertation. EPR studies of ECL coreactant intermediates of cathodic ECL coreactants, namely benzoyl peroxide and persulfate, that generate benzoyloxy free radical (BPO $\cdot$ ) and sulfate anion radical (SO $_4^{\cdot-}$ ) were conducted. Finally, sensitive and selective ECL detection of zika and dengue viruses is achieved with the use of effective and efficient emitter-coreactant combination.

CHAPTER II - COREACTANT ECL STUDIES OF UNMIXED AND MIXED SYSTEMS OF 9,10-DIPHENYLANTHRACENE, RUBRENE, AND TRIS(2,2'-BIPYRIDINE)RUTHENIUM(II) IN ACETONITRILE

## 2.1 Introduction

A biosensor is an analytical device for detection and quantification of biological species (e.g., bacteria, viruses, antigens, enzymes, nucleic acids) through a variety of transducers that convert chemical information (e.g., identity and concentration of analyte) into a measurable signal (e.g., current, voltage, mass change, and optical intensity). Electrogenerated chemiluminescence (ECL) based biosensors use the ECL emission to probe target biomolecules. The Ru(bpy)<sub>3</sub><sup>2+</sup>-TPrA system has been the most commonly used coreactant ECL system in the literature for determination of various analytes,<sup>1-20</sup> although the Ru(bpy)<sub>3</sub><sup>2+</sup>-DBAE (DBAE = 2-(dibutylamino)ethanol) system has recently shown some promising results.<sup>21-29</sup> To measure multiple analytes in a sample simultaneously, a multiplexing detection method must be developed. When ECL is used as a sensing element, multiple efficient ECL emitters present in the same sample matrix could be required. Spectroscopically, however, how these ECL emitters interact each other in the same solution under the ECL experimental conditions remains unclear.

ECL is a relatively new analytical technique, which has vast applications in the areas of e.g., (a) life sciences for the discovery of new drugs and important biological markers, (b) clinical utilities such as screening, monitoring, and diagnosing specific biomolecules associated with certain types of diseases, and (c) industrial management and bio-defense for monitoring and identification of bacteria, toxins, chemical warfare agents, explosives, and other pathogens in food and environmental samples.<sup>218</sup> It would

be beneficial to college students majoring in e.g., chemistry, biochemistry, forensic chemistry, and environmental sciences to be exposed to ECL technology. However, the current textbooks of analytical and instrumental analysis lack the relevant contents. In fact, ECL theory and ECL labs could fit perfectly with any modern analytical chemistry especially instrumental analysis textbooks. This is because, scientifically, ECL is a perfect connection among the three-traditional instrumental analysis course components — spectroscopy, electrochemistry, and separation methods. ECL is a process of light generation (spectroscopy) via redox reactions (electrochemistry), and has been used as a transducer (detector) in flow injection, liquid chromatography, and capillary electrophoresis (separation methods) and micro total analysis.

In this chapter, ECL behavior of unmixed and mixed systems of three efficient ECL emitters, namely 9,10-diphenylanthracene (DPA), rubrene (RUB), and  $\text{Ru}(\text{bpy})_3^{2+}$ , is studied with several common ECL coreactants, using an inexpensive homemade electrochemical-ECL-spectroscopic instrument. The data obtained will provide some fundamental information for future use in multiplexing ECL detection, and the constructed instrument can be used for college level ECL labs in instrumental analysis. Such electrochemistry-ECL-spectroscopy integrated labs will offer several advantages including (a) more efficient utilization of laboratory equipment, and (b) challenging students with critical thinking of different categories of instrumental techniques. Previously, there have been some efforts on constructing and conducting ECL labs for college students.<sup>219,220</sup> The instrumentation and experiments presented in this chapter, however, are new.

## 2.2 Experimental Section

### 2.2.1 Chemicals

Unless otherwise stated, all chemicals were of analytical grades and used as received. Tris(2,2'-bipyridyl)ruthenium perchlorate [Ru(bpy)<sub>3</sub>(ClO<sub>4</sub>)<sub>2</sub>], tri-*n*-propylamine (TPrA, 99+%), rubrene (RUB, 98%), hydrochloric acid (HCl, 37.5%), benzoyl peroxide (BPO, 97%), and 2-(dibutylamino)ethanol (DBAE, 99%) were purchased from Sigma Aldrich (St. Louis, MO). Methanol (spectroanalyzed grade), 9,10-diphenylanthracene (DPA, 98%), and tetra-*n*-butylammonium perchlorate (TBAP, 99+%, electrochemical grade) were obtained from Fluka (Milwaukee, WI). Acetonitrile (MeCN, 99.93+%, HPLC grade) was purchased from MP Biomedicals (Solon, OH).

### 2.2.2 Spectral ECL Instrument Setup

The schematic diagram of spectral ECL instrument setup is shown in Figure 2.1, where a portable “WaveNow” potentiostat (Pine Research Instrumentation) is coupled with a Hamamatsu TG-series mini-spectrometer (Hamamatsu Photonics Inc.).<sup>221</sup> A laptop computer installed with “AfterMath” software from Pine Instrumentation and “SpecEvaluation” software from Hamamatsu was used to control both the potentiostat and mini-spectrometer as well as to display both the electrochemical responses and ECL spectra. The connection between the computer and potentiostat or mini-spectrometer was done with a USB cable. ECL emissions generated at the working electrode were collected and sent to the mini-spectrometer via an optical fiber before displayed on the computer screen. Note that when electrochemical and ECL experiments were conducted, both

“AfterMath” and “SpecEvaluation” software must be open and run simultaneously. For the electrochemical cell system, either a screen-printed electrode (SPE, e.g., ceramic Au or Pt SPEs) or a traditional three-electrode system can be used.

The above constructed spectral ECL instrument is relatively inexpensive, easy to operate, very portable, and well adaptable to various levels of teaching and learning environments.

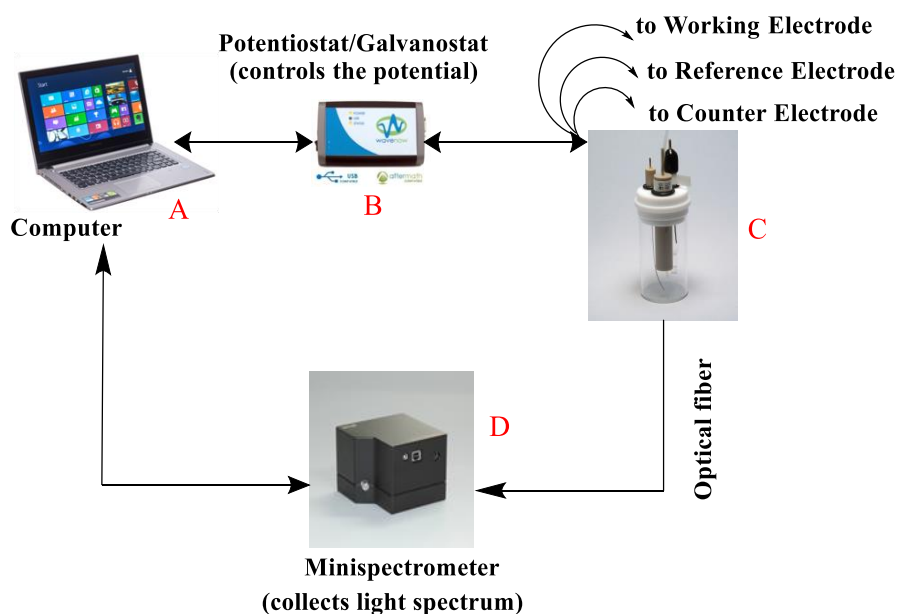


Figure 2.1 Schematic diagram of spectral ECL instrument setup.

Note: (A) computer, (B) potentiostat/galvanostat, (C) electrochemical cell with a three-electrode system, and (D) mini-spectrometer.

### 2.2.3 Electrochemical and ECL measurements

A traditional three-electrode electrochemical cell system was used, with either a Pt (2.0 mm), Au (2.0 mm), or glassy carbon electrode (GCE, 3.0 mm) as the working electrode, a Ag/Ag<sup>+</sup> (10 mM AgNO<sub>3</sub> in 0.10 M TBAP in MeCN) as the reference

electrode, and a Pt mesh as the counter electrode, respectively. All these electrodes were purchased from CH Instruments (Austin, TX). A disposable 5 mL glass vial was used as the cell. The working electrode was polished with 0.3  $\mu\text{m}$  alumina and washed with deionized (DI) water (Elix Advantage Water Purification System, EMD Millipore, Darmstadt, Germany), and sonicated in nitric acid and toluene, respectively. This was followed by rinsing the electrode with ethanol, DI water, and acetonitrile, respectively, and then drying with Kimwipes tissue. The vycor tip of the  $\text{Ag}/\text{Ag}^+$  reference electrode was replaced whenever needed to prevent from susceptible cross contamination. All solutions involving cathodic reduction reactions were pre-degassed with ultrapure nitrogen gas (Airgas, Hattiesburg, MS), and all experiments were conducted at room temperature  $20 \pm 1$   $^{\circ}\text{C}$ .

## **2.3 Results and Discussion**

### **2.3.1 Selection of ECL emitters and their CV studies**

There are a huge number of ECL emitters reported in the literature. For this study, however, 9,10-diphenylanthracene (DPA), rubrene (RUB), and  $\text{Ru}(\text{bpy})_3(\text{ClO}_4)_2$  (Figure 2.2) were chosen, because (a) they are readily available commercially, (b) they have shown well defined reversible redox behavior in acetonitrile (MeCN) that is the most commonly used organic solvent for electrochemical and ECL studies, (c) the ion annihilation ECL data indicated that their ECL efficiencies are among the highest in the ECL emitters ever studied, and (d) their ECL emission spectra are well separated from one to another, which is desirable for spectral separation based multiplexing ECL detection. Table 2.1 lists the redox potential, ECL efficiency, and ECL emission values of

DPA, RUB, and  $\text{Ru}(\text{bpy})_3^{2+}$  species. Note that 25% efficiency for DPA represents the theoretical maximum for ECL from DPA singlets.<sup>222</sup> Although the counter ion of  $\text{Ru}(\text{bpy})_3^{2+}$  will not affect the ECL behavior, to avoid possible influence of water,  $\text{Ru}(\text{bpy})_3(\text{ClO}_4)_2$  rather than hydrated  $\text{Ru}(\text{bpy})_3\text{Cl}_2 \cdot 6\text{H}_2\text{O}$  was used.

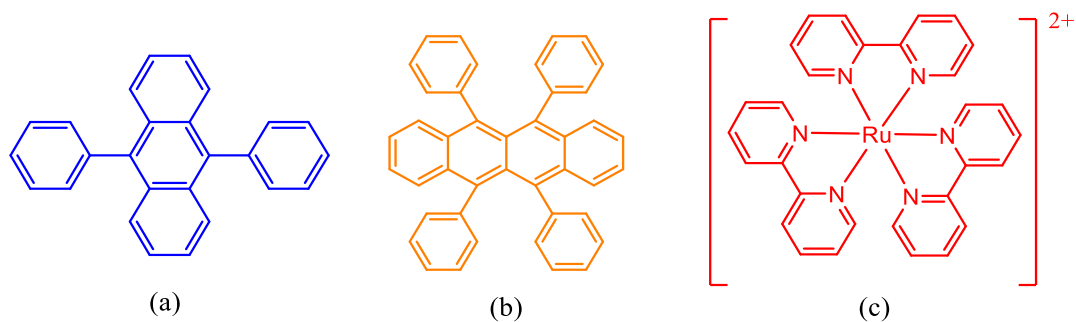


Figure 2.2 Molecular structures of ECL emitters under study (a) DPA, (b) RUB, and (c)  $\text{Ru}(\text{bpy})_3^{2+}$ .

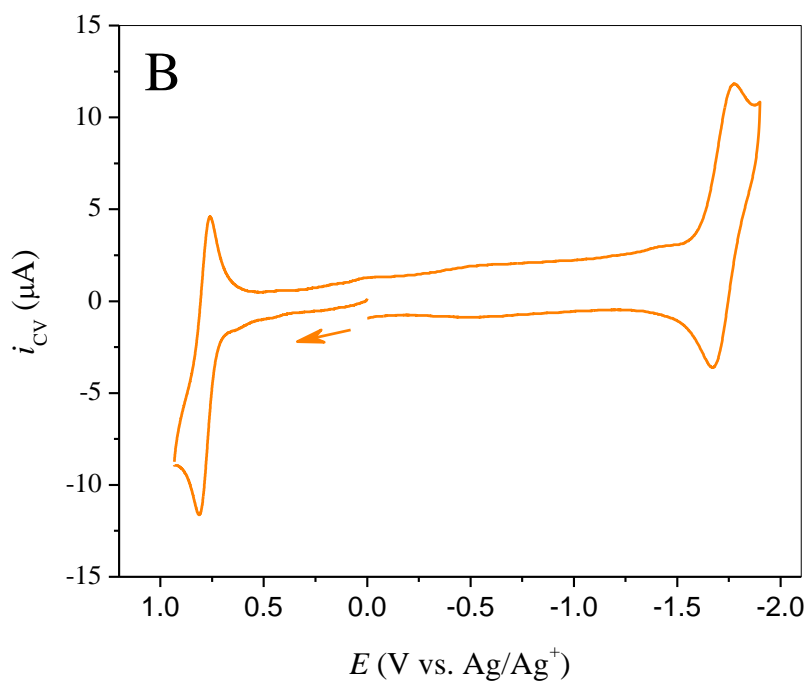
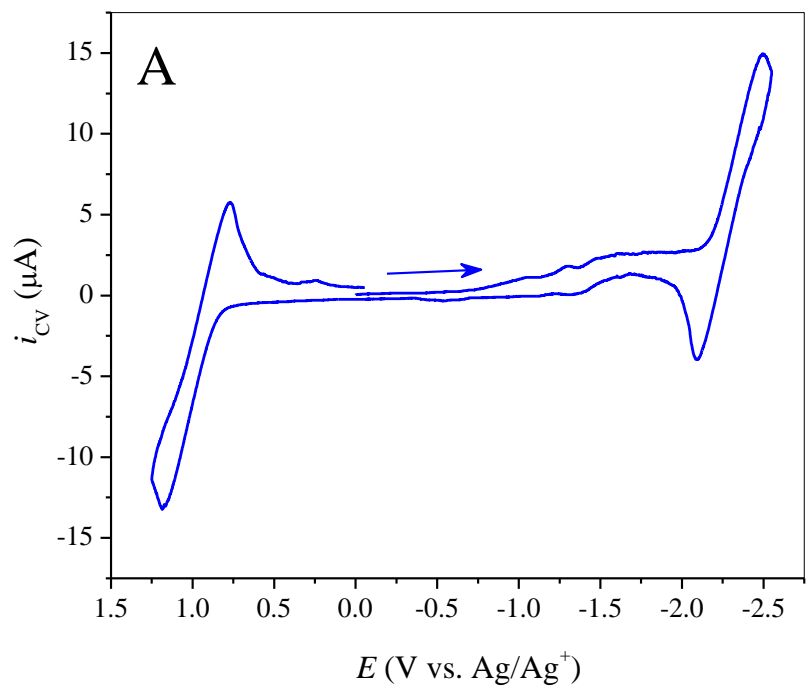
Table 2.1 Redox potential, ECL efficiency, and ECL emission values of DPA, RUB, and Ru(bpy)<sub>3</sub><sup>2+</sup> species.

ECL Labels	Redox Potential (V, vs SCE)				Media	Ion Annihilation ECL efficiency $\Phi_{\text{ECL}}$	ECL Emission ( $\lambda_{\text{max}}$ , nm)	
	$E_{1/2}(\text{ox})$		$E_{1/2}(\text{red})$				Ref. <sup>224</sup>	This work
	Ref. <sup>223</sup>	This work	Ref. <sup>223</sup>	This work				
DPA	+1.29	+1.03	-1.96	-2.24	MeCN	25% <sup>222</sup>	~420	~420
RUB	+0.82	+0.84	-1.56	-1.79	1:1 MeCN/PhH	25% <sup>225</sup>	~540	~545
Ru(bpy) <sub>3</sub> <sup>2+</sup>	+1.35	+1.05	-1.32	-1.63	MeCN	5% <sup>226</sup>	~620	~630

Figure 2.3 shows the cyclic voltammograms of DPA, RUB, and Ru(bpy)<sub>3</sub><sup>2+</sup>, respectively, in which a mixed solvent system of MeCN/PhH (1:1, v/v) is used for RUB study due to its poor solubility in pure MeCN solvent (< 100  $\mu\text{M}$ ). Although benzene and phenolic moieties help increase solubility of RUB but could quench ECL significantly.<sup>227-</sup>

<sup>229</sup> All three ECL emitters undergo reversible one-electron transfer oxidation and reduction reactions. It is believed that Ru(bpy)<sub>3</sub><sup>2+</sup> oxidation occurs at the metal center, i.e., [Ru<sup>II</sup>(bpy)<sub>3</sub><sup>2+</sup>]  $\rightarrow$  [Ru<sup>III</sup>(bpy)<sub>3</sub><sup>2+</sup>], whereas the reversible three one-electron transfer

processes are contributed to the reduction of the bpy ligand.<sup>230</sup> Table 2.1 lists the half-wave potential of the first oxidation and reduction process of the three emitters, where a potential value of 0.186 V vs standard hydrogen electrode (SHE) for Ag/Ag<sup>+</sup> (10 mM) in MeCN and 0.241 V vs SHE for saturated calomel reference electrode (SCE, Hg/Hg<sub>2</sub>Cl<sub>2</sub> (sat., KCl)) was used, respectively, for the conversion of the redox potential.<sup>2</sup> Close inspection of Table 2.1 reveals that the redox potential difference between the oxidation ( $E_{1/2}(\text{ox})$ ) and reduction ( $E_{1/2}(\text{red})$ ) is nearly identical when comparing the literature value with the one of this work for both DPA (3.25 vs 3.27 V) and Ru(bpy)<sub>3</sub><sup>2+</sup> (2.67 vs 2.68 V). This suggests that the difference in  $E_{1/2}$  value for the same redox process between the literature value and the present one is due to the use of two different reference electrodes. For RUB, however, a  $\Delta E_{1/2}$  value of 2.38 V and 2.63 V is obtained from the literature and present work, respectively. Considering the ECL emission of RUB at ~540 nm and Ru(bpy)<sub>3</sub><sup>2+</sup> emits at ~620 nm, one would expect a larger energy gap (or  $\Delta E_{1/2}$  value) between the excited and ground state for RUB as compared with that for Ru(bpy)<sub>3</sub><sup>2+</sup>. Thus, for RUB the  $E_{1/2}$  values obtained from the present work are more reasonable.



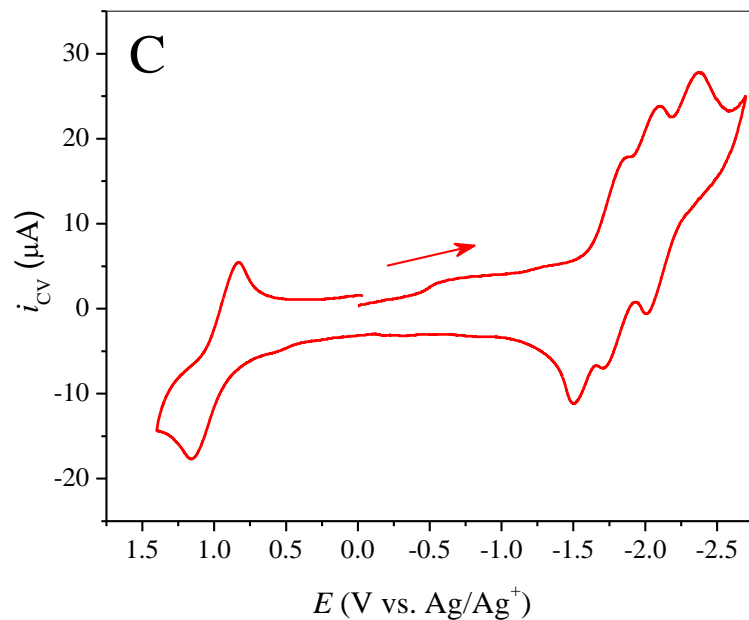


Figure 2.3 CVs of individual ECL emitters.

Note: CVs of (A) 1.0 mM DPA in 0.10 M TBAP in MeCN, (B) 1.0 mM RUB in MeCN/PhH (1:1, v/v), and (C) 1.0 mM Ru(bpy)<sub>3</sub>(ClO<sub>4</sub>)<sub>2</sub> at a 2-mm Pt electrode with a scan rate of 100 mV/s.

### 2.3.2 Selection of ECL coreactants and working electrodes

ECL coreactants are important species that are deliberately added into ECL emitter systems for obtaining efficient ECL emissions and ruling out the setbacks of working with solvents that cannot withstand a large potential window. They can also often overcome the problems associated with the instability of electrochemically generated emitter cations or anions or the ECL quenching by oxygen in the air.

Tri-*n*-propylamine (TPrA) and 2-(dibutylamino)ethanol (DBAE) are commonly used for anodic ECL, and benzoyl peroxide (BPO) and persulfate are for cathodic ECL. Figure 2.4 shows the molecular structures of TPrA, DBAE, and BPO. As persulfate salt,

such as ammonium persulfate or potassium persulfate is not soluble in acetonitrile, only the three coreactants shown in Figure 2.4 were used for further studies.

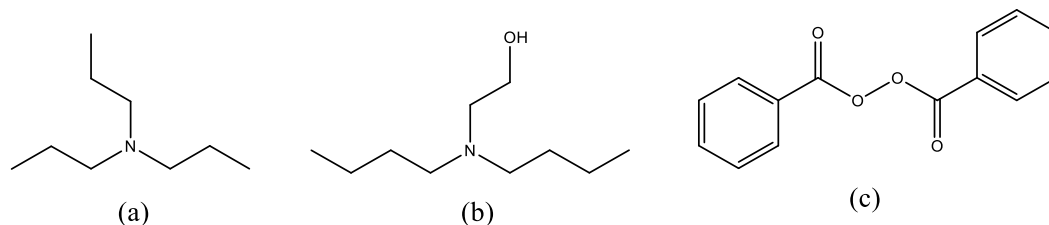


Figure 2.4 Molecular structures of ECL coreactants under study (a) TPrA, (b) DBAE, and (c) BPO.

The cyclic voltammograms of individual coreactants under study are shown in Figure 2.5. At a Pt electrode, TPrA oxidizes at an onset potential of 0.20 V  $\text{Ag}/\text{Ag}^+$  and a peak potential of 0.49 V vs  $\text{Ag}/\text{Ag}^+$  (Figure 2.5a). Similarly, an onset potential of 0.34 V vs  $\text{Ag}/\text{Ag}^+$  and a peak potential of 0.94 V vs  $\text{Ag}/\text{Ag}^+$  for DBAE oxidation are observed (Figure 2.5b). On the other hand, BPO reduction occurs at 0.50 V vs  $\text{Ag}/\text{Ag}^+$  with a peak reduction potential of -1.60 V vs  $\text{Ag}/\text{Ag}^+$  (Figure 2.5c). The irreversible CV behavior of all three coreactants is consistent with the fact that the newly generated chemical species at the electrode undergoes immediately a series of chemical reactions in the solution so that no electroactive species remain when the electrode potential is scanned on the reverse direction.<sup>112</sup>

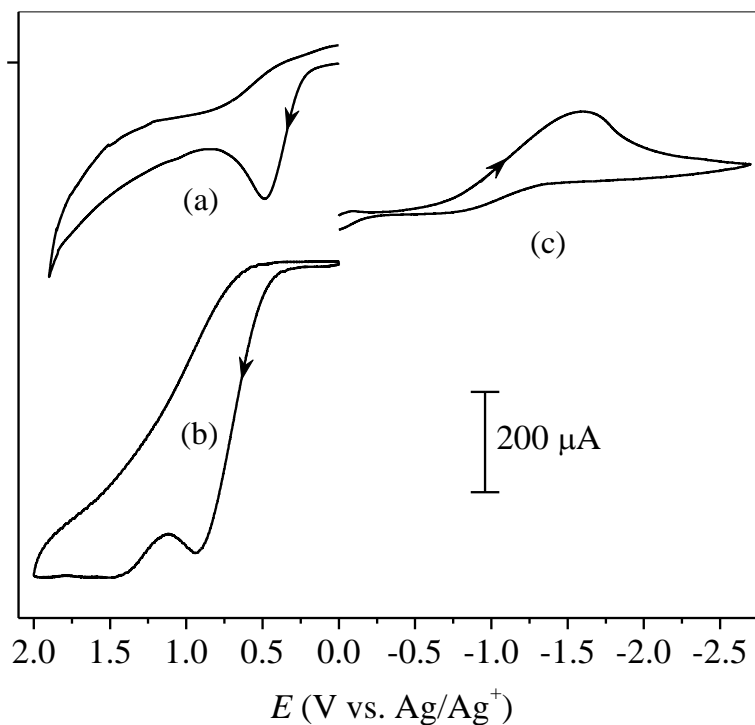


Figure 2.5 CVs of individual ECL coreactants.

Note: CVs of (a) 25.0 mM TPrA, (b) 25.0 mM DBAE, and (c) 10.0 mM BPO in MeCN containing 0.10 M TBAP at a 2-mm Pt electrode with a scan rate of 100 mV/s.

Electrode material can affect the redox behavior of coreactant, which is directly correlated to the ECL generation of a coreactant ECL system. Generally, the more coreactant reacts at the electrode, the more intermediates needed for ECL production are formed, thus the stronger the ECL intensity will be. Figure 2.6 shows the CVs of BPO at Pt, Au, and GCE. It is clear that in MeCN, Pt is the most favorable working electrode for BPO reduction, followed by Au electrode and then GCE. Previously, Pt has been shown to play a catalytic role towards many electrochemical processes.<sup>231-237</sup>

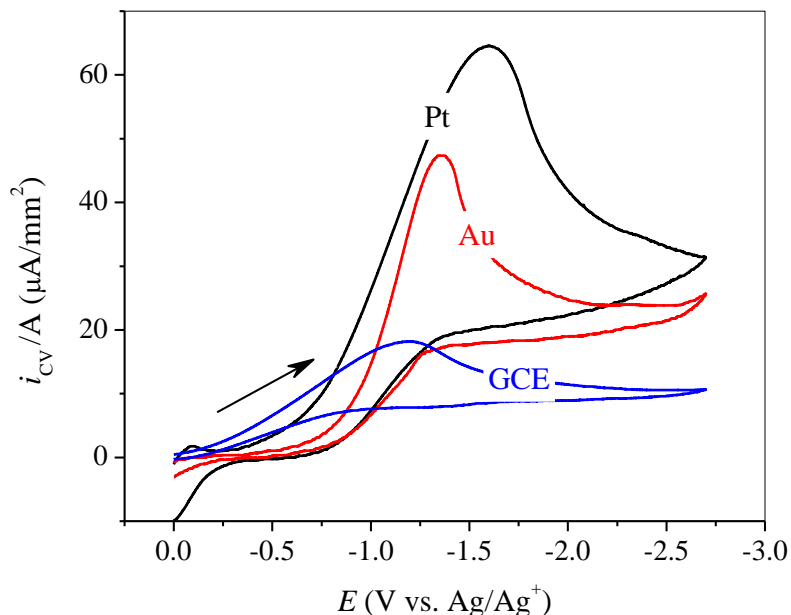


Figure 2.6 CVs of 10.0 mM BPO at different electrodes.

Note: All CVs were carried out in MeCN containing 10.0 mM BPO-0.10 M TBAP at a 2-mm Pt electrode with a scan rate of 100 mV/s. The solution was degassed for about 7 minutes with N<sub>2</sub>.

Initial ECL tests were conducted in a mixture solution of DPA, RUB, and Ru(bpy)<sub>3</sub><sup>2+</sup> using different ECL coreactants with linear sweep voltammetry. As shown in Figure 2.7, not detectable, weak, and strong ECL spectra are observed when ECL coreactant of TPrA (Figure 2.7a), DBAE (Figure 2.7b), and BPO (Figure 2.7c) are used, respectively. Clearly, neither TPrA nor DBAE is a suitable common coreactant for the mixture ECL system. This observation can be explained by the ECL mechanism.<sup>72</sup> To generate ECL from an ECL emitter DPA (or RUB), electrochemically oxidized DPA<sup>•+</sup> (or RUB<sup>•+</sup>) cation must annihilate with its DPA<sup>•-</sup> (or RUB<sup>•-</sup>) anion to form an excited state DPA\* (or RUB\*) that emits light. Because the redox potential of TPrA<sup>•</sup> free radical, i.e., -1.7 V vs SCE,<sup>223</sup> is less negative than that of -2.24 V for the DPA/DPA<sup>•-</sup> couple or -

1.79 V vs SCE for the RUB/RUB<sup>-</sup> couple (Table 2.1), no significant amount of DPA<sup>-</sup> (or RUB<sup>-</sup>) anion is expected to produce. As a result, no or very weak ECL can be generated. The redox potential of DBAE<sup>•</sup> free radical is not available in the literature; it is estimated to be around -2.2 V vs SCE, because weak ECL responses are seen in the ECL emission regions of the DPA/DBAE (~420 nm) and RUB/DBAE (~550 nm) systems (Figure 2.7b). Note that TPrA<sup>•</sup> and DBAE<sup>•</sup> free radicals are produced after the electrochemical oxidation of TPrA and DBAE and subsequent deprotonation reaction, respectively.<sup>72</sup> The above discussion, however, cannot be extended to the Ru(bpy)<sub>3</sub><sup>2+</sup> case, as this system follows different ECL mechanisms.<sup>72</sup>

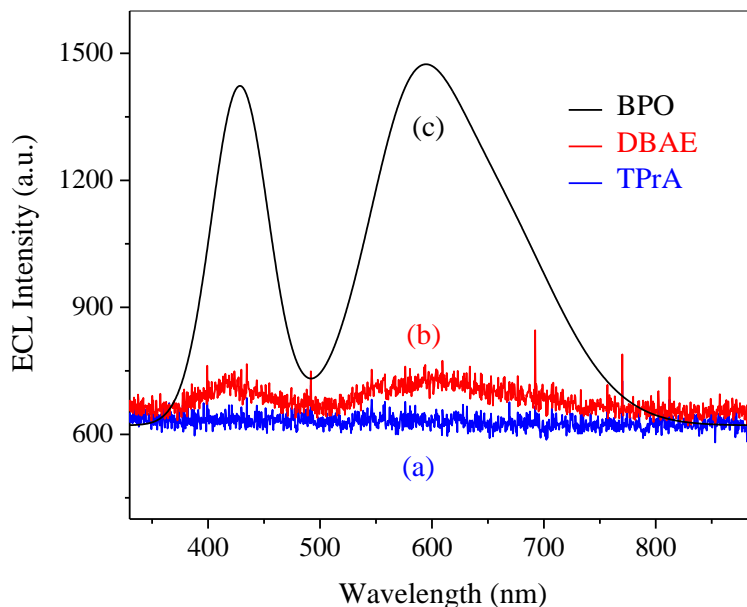
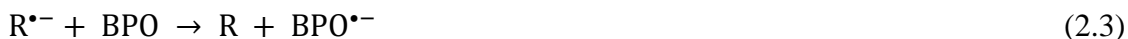


Figure 2.7 ECL spectra obtained from a mixture of DPA, RUB, and  $\text{Ru}(\text{bpy})_3^{2+}$ .

Note: ECL spectra were obtained from a mixture of DPA (250.0  $\mu\text{M}$ ), RUB (25.0  $\mu\text{M}$ ), and  $\text{Ru}(\text{bpy})_3^{2+}$  (25.0  $\mu\text{M}$ ) in MeCN containing 0.10 M TBAP with (a) 25.0 mM TPrA, (b) 25.0 mM DBAE, and (c) 10 mM BPO upon a linear potential sweep from 0 and 2.0 V for (a) and (b) or 0 and -3.0 V vs  $\text{Ag}/\text{Ag}^+$  for (c) at a 2-mm diameter Pt electrode at a scan rate of 100 mV/s. The solution was degassed for about 7 min with  $\text{N}_2$  before ECL spectra were recorded.

In contrast, when the cathodic ECL coreactant BPO is used, remarkably strong ECL emissions are observed for all the three ECL emitters (Figure 2.7c). Notably, emission spectra from RUB (~550 nm) and  $\text{Ru}(\text{bpy})_3^{2+}$  (~620 nm) are overlapped, which can be deconvoluted as will be demonstrated later. Scheme 2.1 summarizes the ECL mechanism of the R/BPO system (R = DPA, RUB, or  $\text{Ru}(\text{bpy})_3^{2+}$ ) involving both the energy-sufficient S-route and the energy-deficient T-route (Section 1.2.1 in Chapter I).<sup>72</sup> Briefly, upon the cathodic potential scanning, both BPO and ECL emitter R are electrochemically reduced to form  $\text{BPO}^{\cdot-}$  and  $\text{R}^{\cdot-}$  (Equations 2-1 and 2-2), and the former

further decomposes to produce a strong oxidizing intermediate, namely benzoate radical  $C_6H_5CO_2^\bullet$  (Equation 2.4), with a redox potential value of  $> +1.5$  V vs SCE.<sup>238</sup> This is followed by redox reactions between  $C_6H_5CO_2^\bullet$  and R (Equation 2.5) as well as  $R^{\bullet-}$  (Equation 2.6) to produce species (e.g.,  $R^{\bullet+}$ ,  $^1R^*$ , and  $^3R^*$ ) necessary for ECL generation.



(R = aromatic hydrocarbons such as DPA or RUB and  $Ru(bpy)_3^{2+}$ ).

Scheme 2.1 ECL mechanism with BPO as cathodic ECL coreactant.

Effect of electrode material on ECL production of the R/BPO system was examined with the spectral ECL instrument. As shown in Figure 2.8, under the same experimental conditions, among the three tested working electrodes (Pt, Au, and GCE), Pt electrode produces the strongest ECL spectra for all three ECL emitters (Figure 2.8a), whereas GCE only gives weak ECL responses (Figure 2.8c). The ECL intensity obtained from Pt, Au, and GCE has an approximate ratio of 2.8/1.8/1 for  $\text{Ru}(\text{bpy})_3^{2+}$ , 3.8/1.9/1 for RUB, and 3.7/2.2/1 for DPA, respectively. These findings are consistent with the CV data shown in Figure 2.6, suggesting that the electrochemical reduction of BPO is a determining step for the ECL generation of the R/BPO system. In addition, at Pt electrode, the  $\text{Ru}(\text{bpy})_3^{2+}$ /BPO system produces nearly the same intense ECL as the RUB/BPO system does, which is about 20% stronger than that from the DPA/BPO system (Figure 2.8a).

Based on the above discussion, it is concluded that the combination of BPO coreactant with Pt working electrode is the most favorable choice for ECL detection of a mixture of DPA, RUB, and  $\text{Ru}(\text{bpy})_3^{2+}$  emitters.

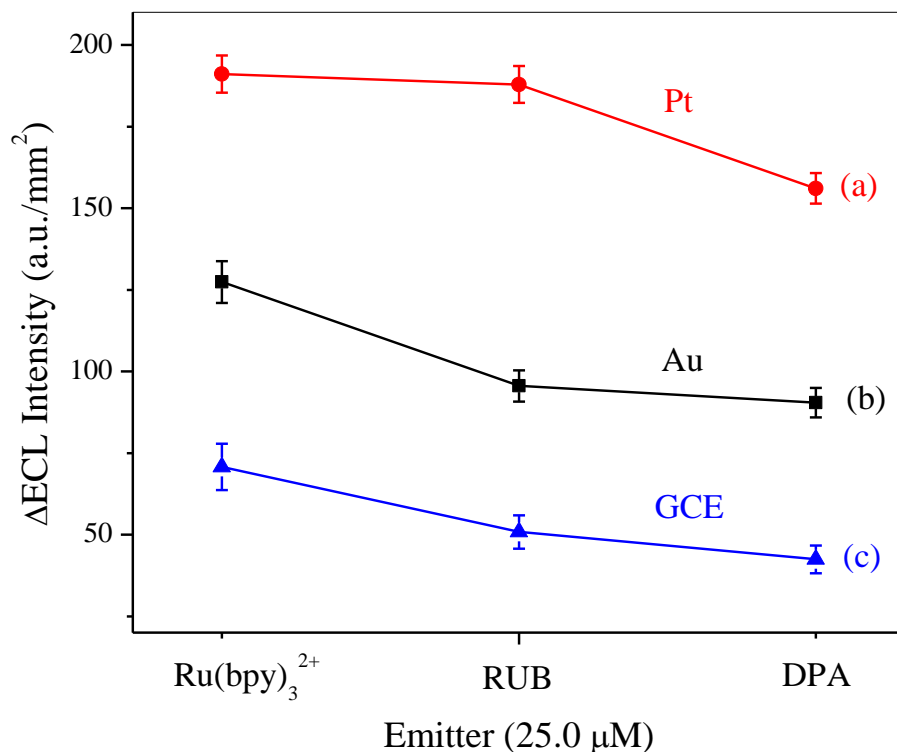


Figure 2.8 Effect of electrode material on ECL intensity.

Note: Plot of changes in ECL intensity per unit area vs a fixed concentration of ECL emitters (i.e., 25.0 μM) using 10.0 mM coreactant BPO (optimized concentration) in 0.10 M TBAP MeCN with a linear potential sweep from 0 to -3.0 V vs Ag/Ag<sup>+</sup> at a scan rate of 100 mV/s. Hamamatsu mini-spectrometer was used to collect ECL spectra.

### 2.3.3 Validation of the spectral ECL instrument

The performance of the newly constructed mini-spectrometer based spectral ECL instrument was compared and validated with a homemade ECL setup that used a photomultiplier tube (PMT) as a light detector.<sup>239</sup> Due to its extremely high sensitivity, the PMT based ECL instrument can detect ultra-low ECL emissions. Consequently, the ECL responses of all the three coreactants (i.e., TPrA, DBAE, and BPO) coupled with the

three ECL emitters (i.e., DPA, RUB, and  $\text{Ru}(\text{bpy})_3^{2+}$ ) were recorded. Figure 2.9 shows such results, where BPO yields the most efficient ECL intensities for all the three ECL emitters, with a slightly less ECL intensity over the entire coreactant concentration range from the DPA/BPO system as compared with the RUB/BPO or  $\text{Ru}(\text{bpy})_3^{2+}$ /BPO system. Also, maximum ECL intensities appear at 10.0 mM BPO, which likely is explained by the two opposing roles of BPO has during the ECL generation (Scheme 2.1). On the one hand, BPO is needed for the production of  $\text{BPO}^{\bullet-}$ ,  $\text{C}_6\text{H}_5\text{CO}_2^{\bullet}$ ,  $\text{R}^{\bullet+}$ ,  $^1\text{R}^*$ , and  $^3\text{R}^*$ , which is favorable to ECL generation. On the other hand, however, BPO can react with the electrogenerated  $\text{R}^{\bullet-}$  (Equation 2.3), which reduces the chance of the ion annihilation reaction of  $\text{R}^{\bullet+} + \text{R}^{\bullet-} \rightarrow \text{R}^*$  (Equation 2.11) and diminishes ECL generation. Significantly weak ECL responses are seen from the systems using TPrA or DBAE as an ECL coreactant, especially when DPA or RUB is used as an ECL emitter. As discussed earlier, the insufficient reducing capacity of TPrA $^{\bullet}$  and DBAE $^{\bullet}$  free radicals towards chemical reductions of DPA and RUB is probably the cause of such weak ECL emissions.

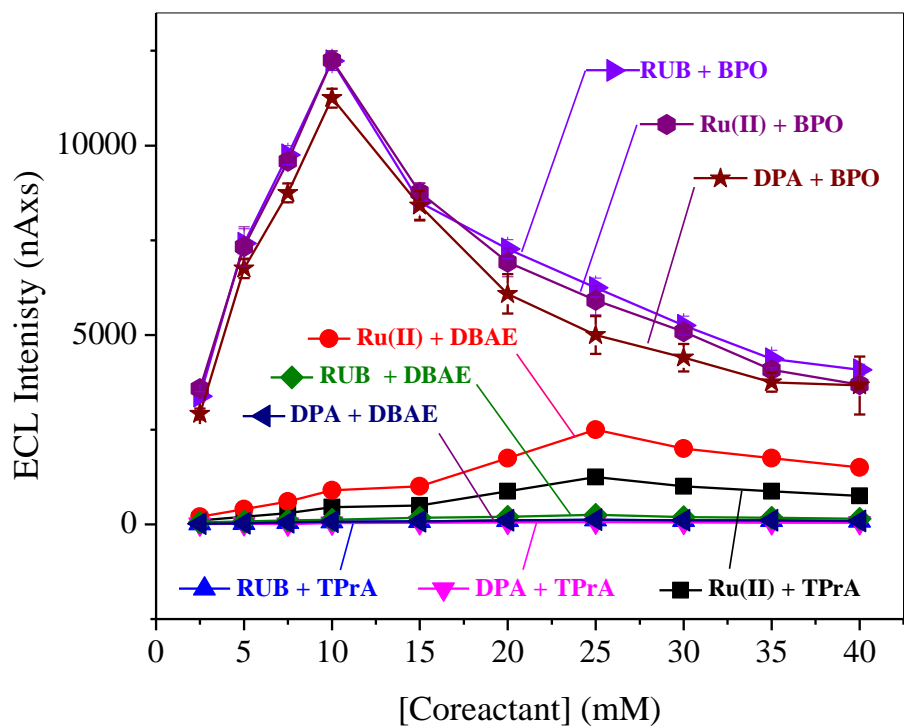


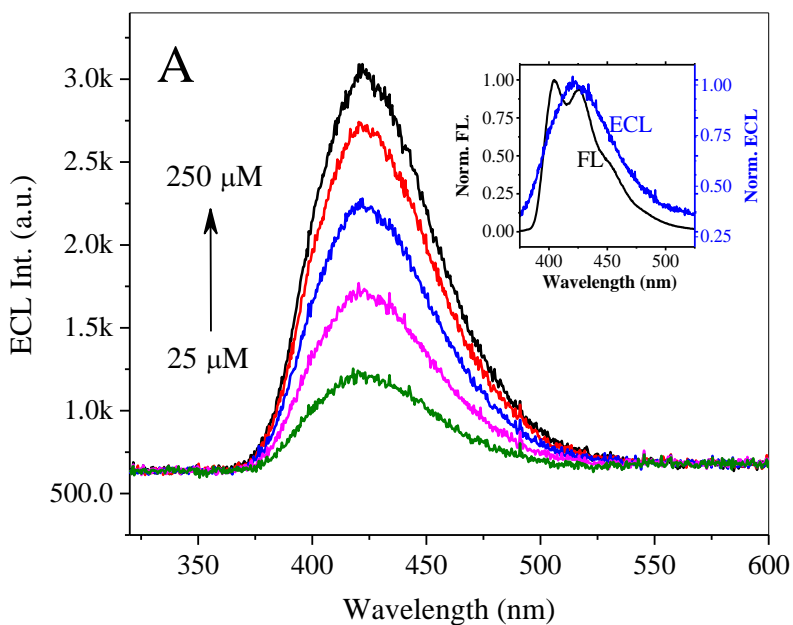
Figure 2.9 ECL responses of various coreactant ECL systems measured with a PMT based ECL instrument.

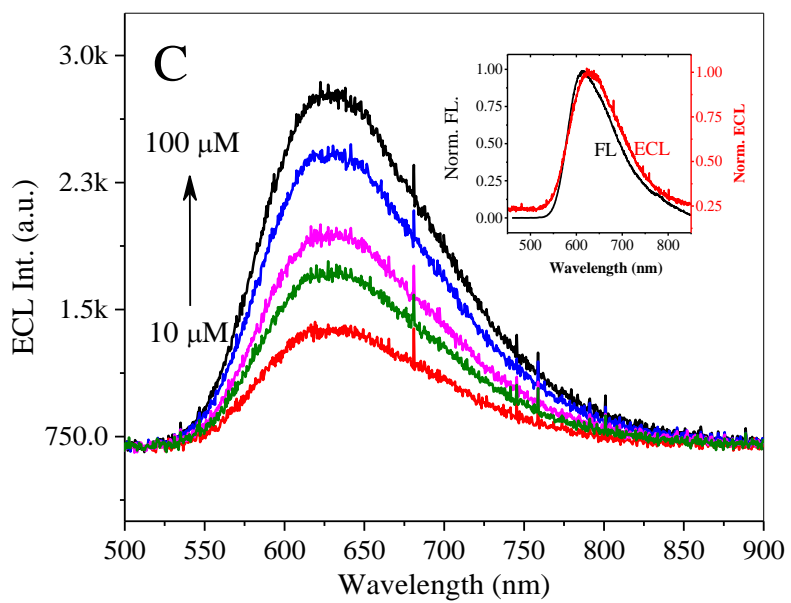
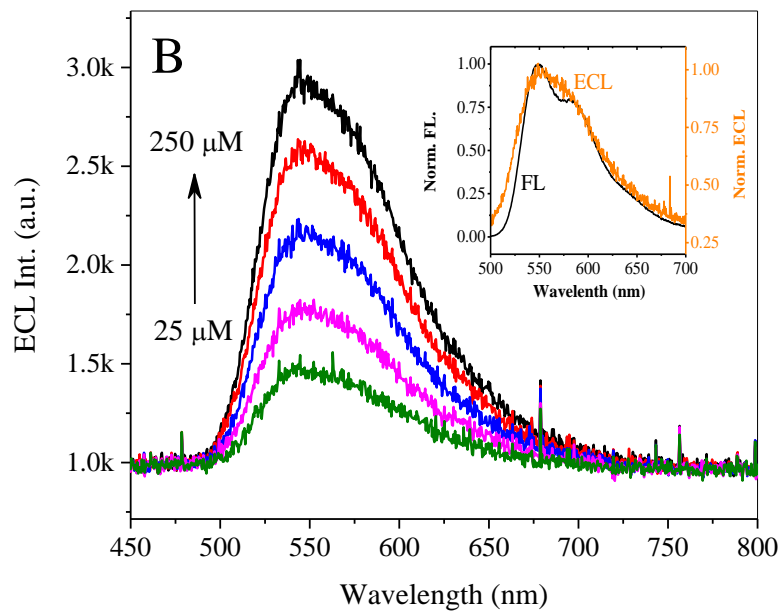
Note: Integrated ECL-intensities of three different ECL emitters (i.e., RUB,  $\text{Ru}(\text{bpy})_3^{2+}$ , and DPA,  $25.0 \mu\text{M}$  each) were plotted against various concentrations of three different co-reactants (i.e., BPO, DBAE, and TPrA). CV potential scanning between 0 and 2.0 V for TPrA and DBAE or 0 and -3.0 V vs  $\text{Ag}/\text{Ag}^+$  for BPO in 0.10 M TBAP MeCN at a 2-mm Pt electrode with a scan rate of 100 mV/s was used. The solution was degassed for about 7 min with  $\text{N}_2$  before ECL measurement was taken place.

It is evident that the data shown in Figure 2.9 are consistent with the data shown in Figures 2.7 and 2.8, verifying that the constructed mini-spectrometer based spectral ECL instrument performed well.

### 2.3.4 Study of unmixed systems of ECL emitters

Figure 2.10 shows the ECL spectra of individual ECL emitter DPA (Figure 2.10A), RUB (Figure 2.10B), and  $\text{Ru}(\text{bpy})_3^{2+}$  (Figure 2.10C) at various concentrations when 10.0 mM BPO is used as the cathodic ECL coreactant, with a maximum ECL emission at  $\sim 420$  nm,  $\sim 545$  nm, and 630 nm, respectively. These ECL peak values are in good agreement with those reported previously from ion annihilation reactions (Table 2.1) as well as with fluorescence spectra displayed as an inset of the respective ECL spectra (Figures 2.10A-C). An excellent linear relationship between the ECL emitter concentration and the ECL peak intensity is shown in Figure 2.10D. Such a calibration curve is useful for quantifying target analyte when the R/BPO system is used for ECL based single or multiplexed assays.





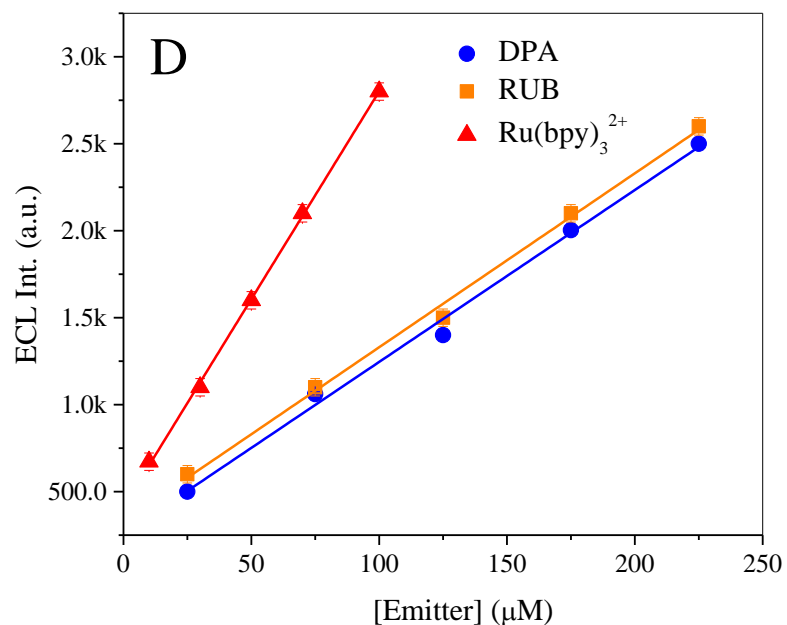


Figure 2.10 ECL spectra of (A) DPA, (B) RUB, and (C)  $\text{Ru}(\text{bpy})_3^{2+}$  at various concentrations using BPO as coreactant. (D) Relationship between the emitter concentration and ECL peak intensity.

Note: All ECL measurements were carried out with the spectral ECL instrument in 0.10 M TBAP MeCN solution containing 10.0 mM BPO and various concentrations of ECL emitter after degassed with  $\text{N}_2$  for 7 min at a 2-mm diameter Pt electrode over a linear potential sweep from 0 to -3.0 V vs  $\text{Ag}/\text{Ag}^+$  at 100 mV/s. Insets in (A)-(C) were comparisons between ECL and fluorescence spectra. For fluorescence experiments carried out with a PTI Qunata Master 40<sup>TM</sup> intensity based spectrofluorometer, 2.50  $\mu\text{M}$  of each ECL emitter in MeCN was used. The excitation wavelength for DPA, RUB, and  $\text{Ru}(\text{bpy})_3^{2+}$  was 370 nm, 490 nm, and 450 nm, respectively. These wavelengths were the maximum absorption peak wavelengths of the emitters measured with a Beckman Coulter DU 800 UV/Vis spectrophotometers.

### 2.3.5 Study of binary mixed systems of ECL emitters

Among DPA, RUB, and  $\text{Ru}(\text{bpy})_3^{2+}$  ECL emitters, three binary combinations of them, namely, DPA-RUB, DPA- $\text{Ru}(\text{bpy})_3^{2+}$ , and RUB-  $\text{Ru}(\text{bpy})_3^{2+}$ , were studied. Figure

2.11 shows the ECL spectra of the (DPA-RUB)/BPO system with a constant concentration of RUB (25.0  $\mu\text{M}$ ) mixed with different concentrations of DPA. With the increase of DPA concentration, ECL intensity at  $\sim 420$  nm for DPA emissions increases as expected. Meanwhile, the ECL intensity at  $\sim 540$  nm for RUB emissions also increases slightly. The inset in Figure 2.11 displays the linear responses of ECL intensities with the concentration of DPA. The increase in RUB ECL with the increase of [DPA] can be contributed to the energy transfer between  $\text{DPA}^*$  and RUB as  $\text{DPA}^* + \text{RUB} \rightarrow \text{RUB}^*$ . This explanation is supported by the fluorescence spectra of DPA and the absorption spectra of RUB (Figure 2.12), where partially overlap of the two spectra is evident.

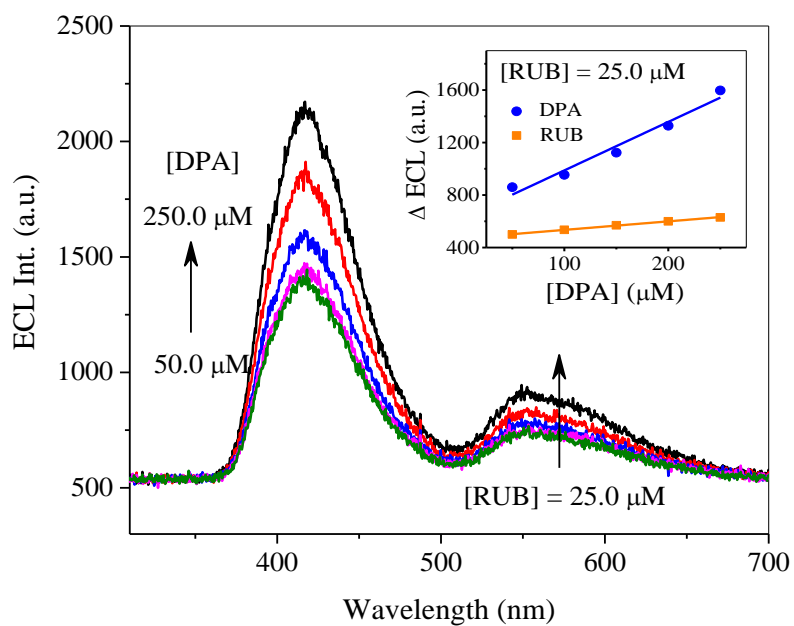


Figure 2.11 ECL spectra of the (DPA-RUB)/BPO system with a constant concentration of RUB mixed with various concentrations of DPA.

Note: [DPA] was increased from 50.0  $\mu\text{M}$  to 250  $\mu\text{M}$  while [RUB] at 25.0  $\mu\text{M}$  was held constant with 10.0 mM BPO as ECL coreactant. All ECL measurements were carried out using the spectral ECL instrument in MeCN solution containing 0.10 M TBAP supporting electrolyte after degassed with  $\text{N}_2$  for 7 min at a 2-mm diameter Pt electrode with a CV scan rate of 100 mV/s.

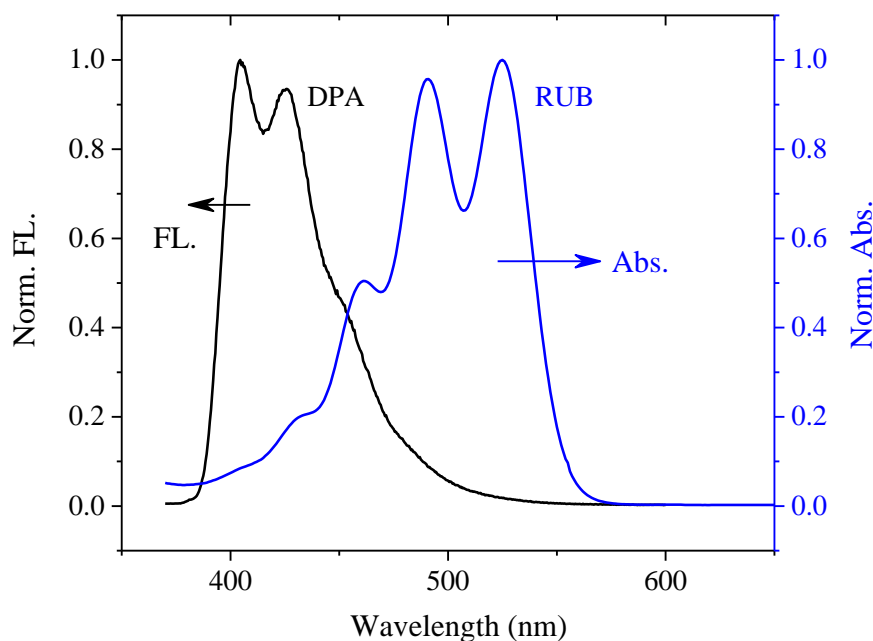
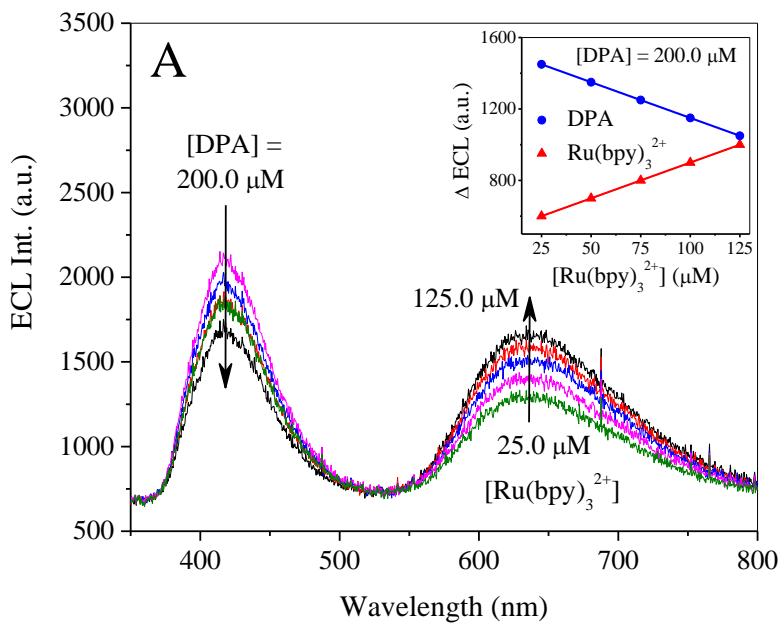


Figure 2.12 Fluorescence spectra of DPA and absorption spectrum of RUB.

Note: The experiments were carried out in MeCN. The slit width was 0.75 nm. The excitation wavelength for fluorescence experiment was 370 nm.

The ECL behavior of the (DPA-Ru(bpy)<sub>3</sub><sup>2+</sup>/BPO system is shown in Figure 2.13. Under a constant [DPA], the ECL intensity for Ru(bpy)<sub>3</sub><sup>2+</sup> emissions at ~630 nm increases with the increase of [Ru(bpy)<sub>3</sub><sup>2+</sup>], whereas the ECL signal for DPA emissions at ~420 nm decreases (Figure 2.13A). On the other hand, under a constant [Ru(bpy)<sub>3</sub><sup>2+</sup>], the ECL intensity of DPA as well as Ru(bpy)<sub>3</sub><sup>2+</sup> increases with the increase of [DPA] (Figure 2.13B), although in the latter case, the ECL intensity change is insignificant. These data can be explained with the energy transfer between DPA\* and Ru(bpy)<sub>3</sub><sup>2+</sup> through a reaction process of DPA\* + Ru(bpy)<sub>3</sub><sup>2+</sup> → Ru(bpy)<sub>3</sub><sup>2+\*</sup>, as illustrated by the partial overlapping of the fluorescence spectra of DPA and the absorption spectra of Ru(bpy)<sub>3</sub><sup>2+</sup>

(Figure 2.14). Fluorescence titration experiments of DPA with  $\text{Ru}(\text{bpy})_3^{2+}$  (Figure 2.15) further support the above explanation.



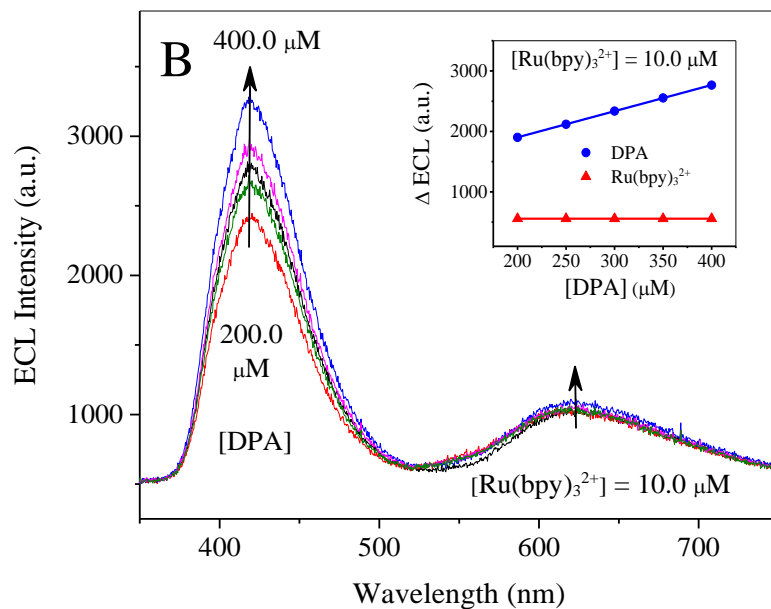


Figure 2.13 ECL spectra of the (DPA-Ru(bpy)<sub>3</sub><sup>2+</sup>)/BPO system with a constant concentration of (A) DPA and (B) Ru(bpy)<sub>3</sub><sup>2+</sup> mixed with various concentrations of (A) Ru(bpy)<sub>3</sub><sup>2+</sup> and (B) DPA.

Note: (A) [Ru(bpy)<sub>3</sub><sup>2+</sup>] was increased from 25.0 μM to 125.0 μM while [DPA] at 200.0 μM was held constant, and (B) [DPA] was increased from 200.0 μM to 400.0 μM while [Ru(bpy)<sub>3</sub><sup>2+</sup>] at 10.0 μM was held constant with 10.0 mM BPO as ECL coreactant. All ECL measurements were carried out using the spectral ECL instrument in MeCN solution containing 0.10 M TBAP supporting electrolyte after degassed with N<sub>2</sub> for 7 min at a 2-mm diameter Pt electrode with a CV scan rate of 100 mV/s.

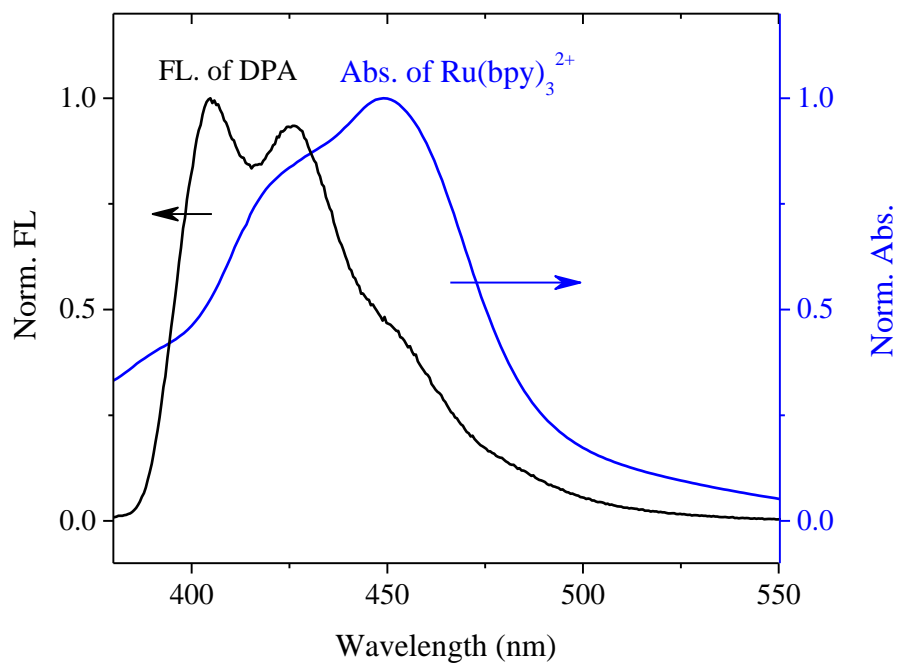


Figure 2.14 Fluorescence spectra of DPA and absorption spectra of Ru(bpy)<sub>3</sub><sup>2+</sup>.

Note: The experiments were carried out in MeCN. The excitation wavelength for DPA emission was 370 nm.

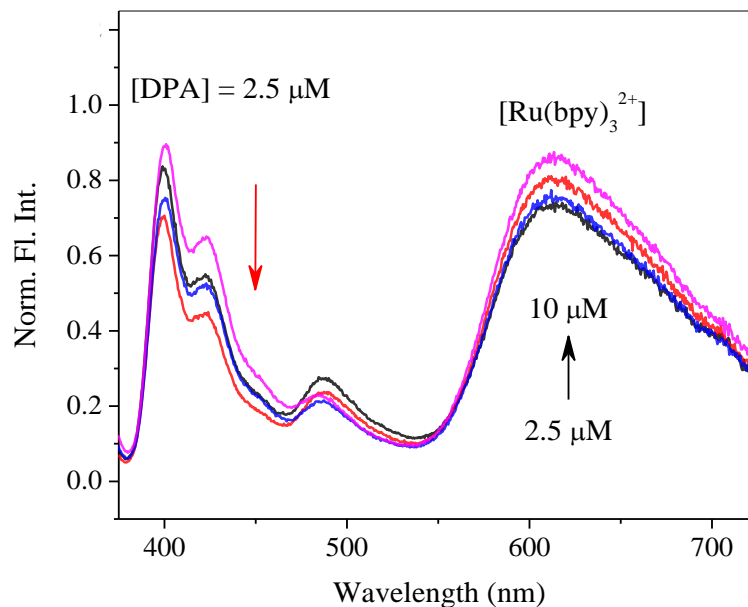
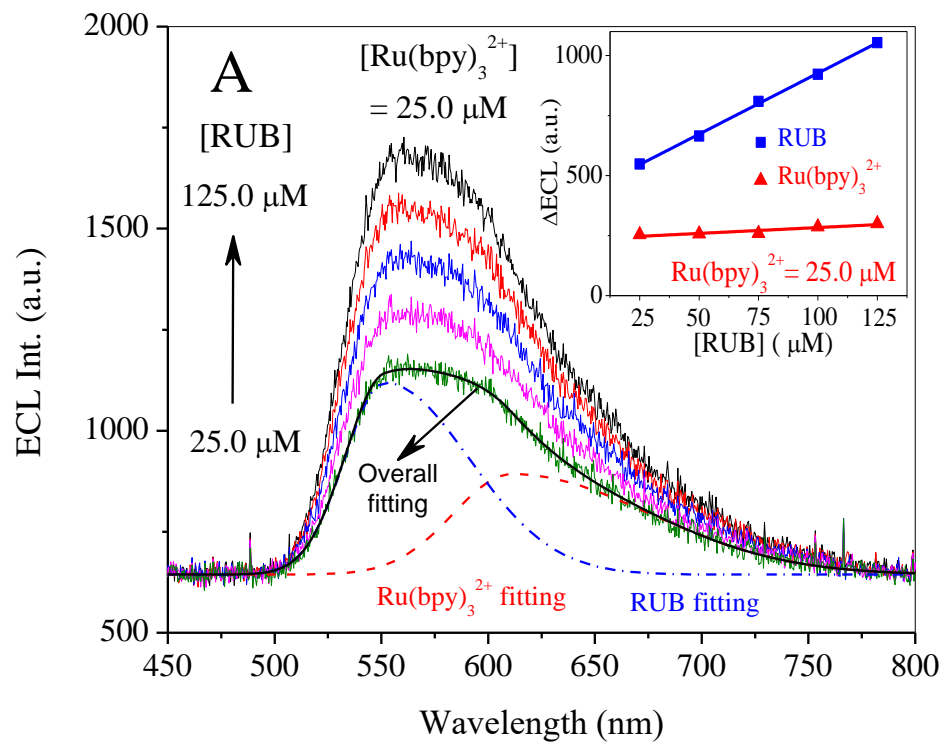


Figure 2.15 Fluorescence spectra of DPA with the addition of various amounts of  $\text{Ru}(\text{bpy})_3^{2+}$ .

Note:  $[\text{DPA}]$  was fixed at  $2.5 \mu\text{M}$  whereas  $[\text{Ru}(\text{bpy})_3^{2+}]$  was gradually allowed to increase from  $2.5 \mu\text{M}$  till  $20 \mu\text{M}$ . The fluorescence titration experiments were carried out in MeCN. The excitation wavelength was  $370 \text{ nm}$  and the slit width was  $0.75 \text{ nm}$ .

Finally, the ECL properties of the (RUB- $\text{Ru}(\text{bpy})_3^{2+}$ )/BPO system were investigated. Because the peak values of these two ECL emitters are relatively close ( $540$  vs  $630 \text{ nm}$ ) and their individual spectra are broad, experimentally obtained overall ECL spectra as shown in Figure 2.16 are significantly overlapped. To resolve the peak overlapping, “multiple peak fit” function within OriginLab software was used. Specifically, two “biguanssian” peak functions with one peak located at  $\sim 540 \text{ nm}$  for RUB and the other at  $\sim 630 \text{ nm}$  for  $\text{Ru}(\text{bpy})_3^{2+}$  were initialized. The calculated best overall fitting curve (solid line) was found to match well with the experimental data

(Figure 2.16), where individual ECL spectra for each emitter (dashed lines) were also displayed. As a result, the respective ECL intensity of RUB and  $\text{Ru}(\text{bpy})_3^{2+}$  in the binary system can be estimated. Note that such a spectral simulation or fitting is constrained by the known ECL emissions including  $\lambda_{\text{max}}$  values. Therefore, errors introduced by deconvolution of experimentally obtained spectra are small. Spectral fitting of severely overlapped peaks in high resolution X-ray photoelectron spectroscopy has been widely used for many years.<sup>240</sup> Figure 2.16A shows that the ECL intensity of RUB increases with the increase of its concentration and the ECL for  $\text{Ru}(\text{bpy})_3^{2+}$  remains unchanged when a constant  $[\text{Ru}(\text{bpy})_3^{2+}]$  is used. The opposite is also true. As shown in Figure 2.16B, when  $[\text{RUB}]$  remains constant, the ECL intensity of  $\text{Ru}(\text{bpy})_3^{2+}$  increases with the increase of  $[\text{Ru}(\text{bpy})_3^{2+}]$ , and the ECL of RUB is not influenced by the addition of RUB. These data suggest that, unlike in the cases involving DPA (Figures 2.11 and 12), no energy transfer between RUB and  $\text{Ru}(\text{bpy})_3^{2+}$  exists. This is not surprising because the energy difference between the two excited ECL emitters is rather close.



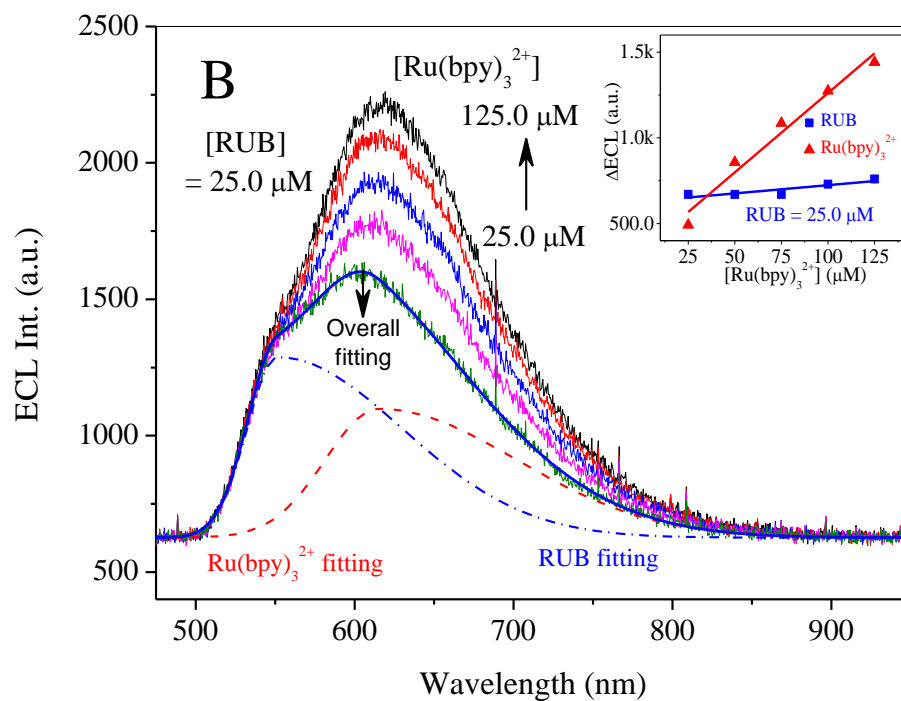


Figure 2.16 ECL spectra of the (RUB-Ru(bpy)<sub>3</sub><sup>2+</sup>)/BPO system with a constant concentration of (A) Ru(bpy)<sub>3</sub><sup>2+</sup> and (B) RUB mixed with various concentrations of (A) RUB and (B) Ru(bpy)<sub>3</sub><sup>2+</sup>.

Note: (A) [RUB] was increased from 25.0 μM to 125.0 μM while [Ru(bpy)<sub>3</sub><sup>2+</sup>] at 25.0 μM was held constant, and (B) [Ru(bpy)<sub>3</sub><sup>2+</sup>] was increased from 25.0 μM to 125.0 μM while [RUB] at 25.0 μM was held constant with 10.0 mM BPO as ECL coreactant. All ECL measurements were carried out using the spectral ECL instrument in MeCN solution containing 0.10 M TBAP supporting electrolyte after degassed with N<sub>2</sub> for 7 min at a 2-mm diameter Pt electrode with a CV scan rate of 100 mV/s.

### 2.3.6 Study of ternary mixed systems of ECL emitters

In this section, ECL behavior of ternary mixed systems of (DPA-RUB-Ru(bpy)<sub>3</sub><sup>2+</sup>/BPO is presented. Figure 2.17 shows a typical ECL spectra obtained from a mixture of DPA, RUB, and Ru(bpy)<sub>3</sub><sup>2+</sup> using BPO as the cathodic coreactant. The peak at

~420 nm for DPA emission is well separated from the overlapped broad peak at ~600 nm for emissions from RUB and Ru(bpy)<sub>3</sub><sup>2+</sup>. Using the same strategy for the deconvolution of mixed ECL spectra of RUB and Ru(bpy)<sub>3</sub><sup>2+</sup> (Figure 2.16 in Section 2.3.5), this ternary ECL spectra can be also well resolved with the “multiple peak fit” function in OriginLab as demonstrated in Figure 2.17. Consequently, ECL intensities of respective individual emitters can be estimated.

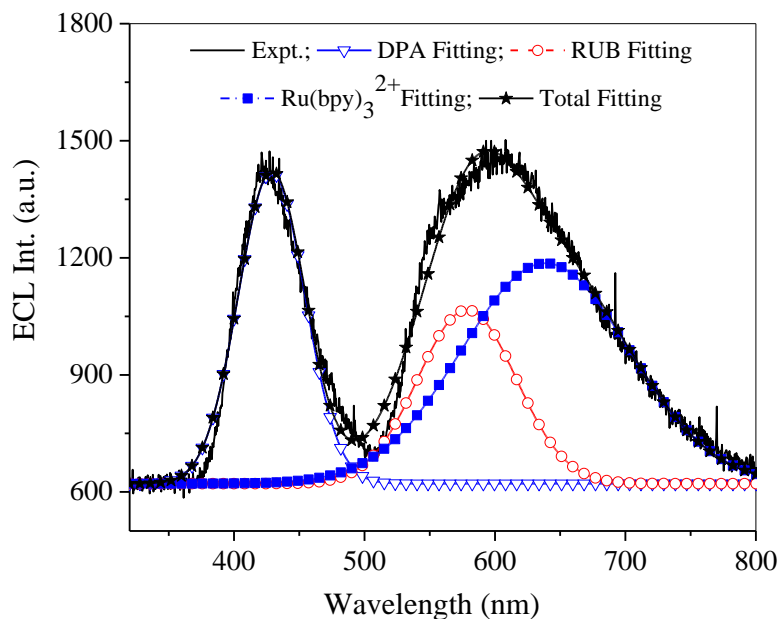
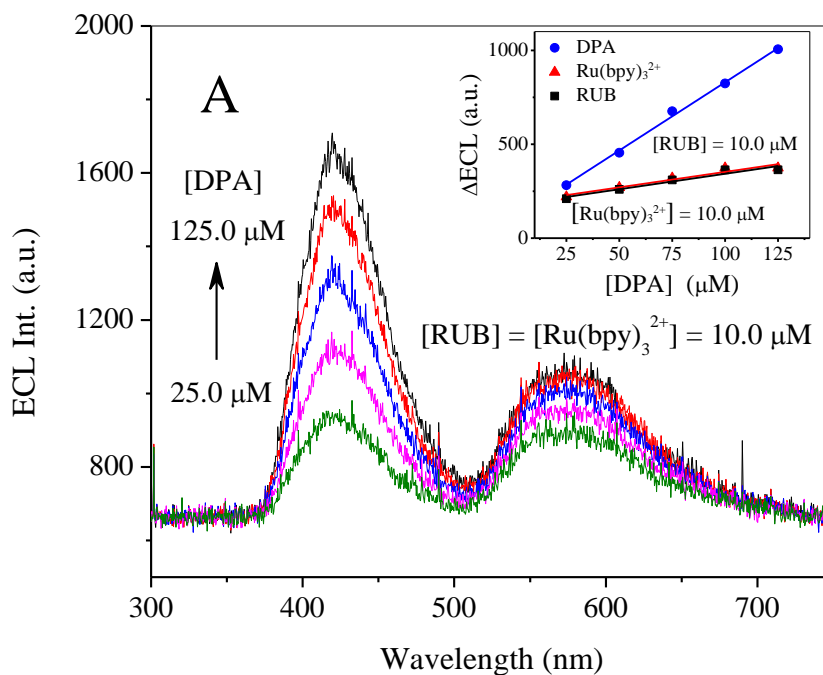
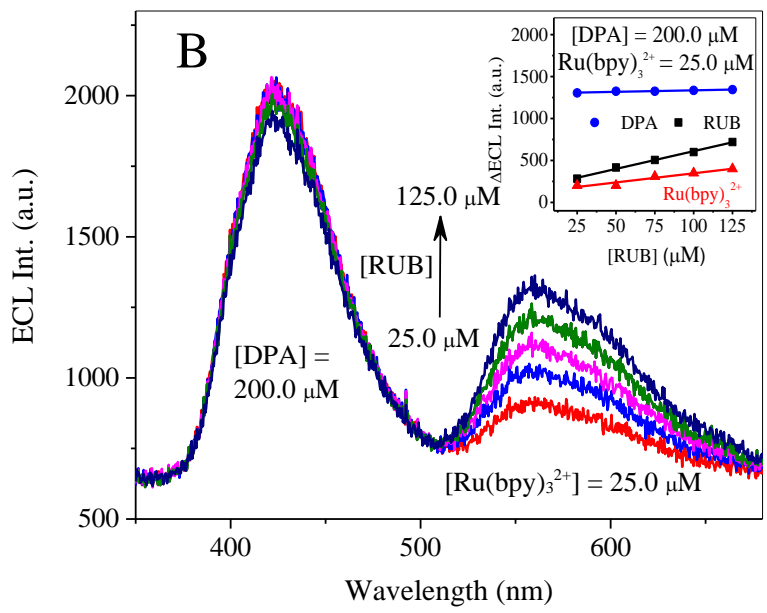


Figure 2.17 Deconvolution of ECL spectra obtained from a mixture of DPA, RUB, and Ru(bpy)<sub>3</sub><sup>2+</sup>.

Note: ECL spectra were obtained from a mixture of DPA (250.0 μM), RUB (25.0 μM), and Ru(bpy)<sub>3</sub><sup>2+</sup> (25.0 μM) in MeCN containing 10.0 mM BPO-0.10 M TBAP at a 2-mm diameter Pt electrode with a scan rate of 100 mV/s. The solution was degassed for ~7 minutes with pure nitrogen gas.

Figure 2.18 shows three examples of the ECL responses from ternary mixed systems of ECL emitters. In each case, concentrations of two of the three ECL emitters remain unchanged, and the ECL intensity of each emitter is examined along with the concentration change of the third emitter. Specifically, the effect of [DPA], [RUB], and [Ru(bpy)<sub>3</sub><sup>2+</sup>] on the overall ECL behavior is revealed in Figures 2.18A, B, and C, respectively. Detailed linear relationship between the individual ECL intensity and the third ECL emitter concentration is plotted and placed aside of the ECL spectra as an inset. These data can be explained using the energy transfer between the high energy excited DPA\* species and the ground state RUB or Ru(bpy)<sub>3</sub><sup>2+</sup> to form a relatively low energy excited state species of RUB\* or Ru(bpy)<sub>3</sub><sup>2+\*</sup>.





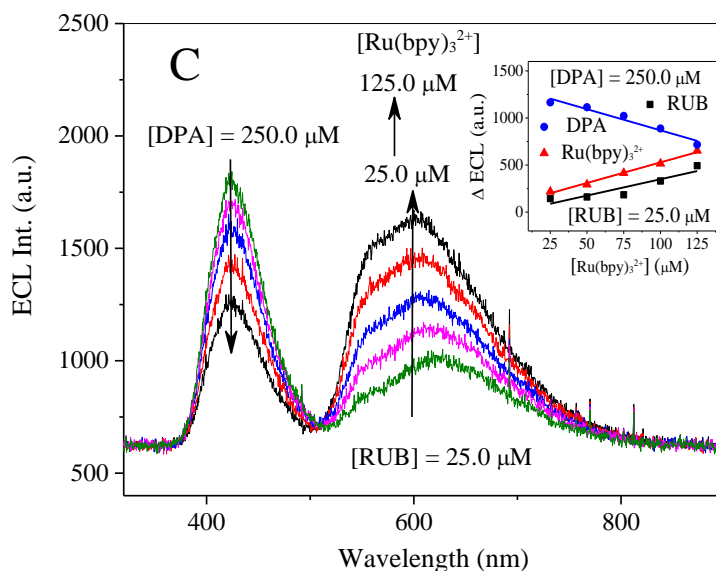


Figure 2.18 ECL spectra of the (DPA-RUB-  $\text{Ru}(\text{bpy})_3^{2+}$ )/BPO system with the concentration change of (A) DPA, (B) RUB, and (C)  $\text{Ru}(\text{bpy})_3^{2+}$  while two other ECL emitter concentrations remained unchanged.

Note: Experiments were carried out in MeCN solution containing 10.0 mM BPO-0.10 M TBAP after degassed with  $\text{N}_2$  for ~7 min at a 2-mm diameter Pt electrode with a CV scan rate of 100 mV/s.

Although energy transfer related interactions between ECL emitters were observed, which seems to make the proposed three ECL emitters a bit unfit for potential use in ECL based multiplexed assays, it is expected that this kind of interaction should become negligible at a lower concentration range (e.g., sub-micromolar or below) that is often the case in real sample analysis.

## 2.4 Hazards

Polycyclic aromatic hydrocarbons (PAHs) have carcinogenic effects. Acute (short-term) inhalation of acetonitrile exposure results in irritation of mucous membranes whereas its chronic (long-term) exposure results in central nervous system effects, such as headaches, numbness, and tremors. TPrA and DBAE are skin and eye irritants and the solutions of these must be prepared under hood. BPO can be explosive if exposed to heat, shock or friction.

## 2.5 Conclusion

An inexpensive and portable spectral ECL instrument was constructed. This setup consisted of a portable “WaveNow” potentiostat from Pine Research Instrumentation and a Hamamatsu mini-spectrometer, and was capable of conducting regular electrochemical experiments and measuring ECL spectra. The newly homemade instrument was used to study the cyclic voltammetry of individual ECL emitters (i.e., DPA, RUB, and Ru(bpy)<sub>3</sub><sup>2+</sup>) and coreactants (i.e., TPrA, DBAE, and BPO) as well as the ECL behavior of various combinations of ECL emitter-coreactant at different working electrodes (i.e., Pt, Au, and GCE). The results from ECL titration studies of unmixed and mixed systems of ECL emitters using the most efficient cathodic BPO coreactant at Pt electrode provided fundamental data for ECL spectral based multiplexing detection of analytes. Certain interactions between co-existing ECL emitters were explained with the energy transfer from a high energy excited state emitter to another relatively low energy ground state emitter, which was supported by the fluorescence and absorption spectroscopic data. Finally, the experimentally obtained overlapping ECL spectra were well resolved with

the “multiple peak fit” function of OriginLab program. Parts of the experiments reported in this chapter were carried out with the integrated homemade spectral ECL instrument can be well-adapted to various levels of analytical chemistry or instrumental analysis teaching laboratories.

CHAPTER III - SYNTHESIS, ELECTROCHEMISTRY AND ECL STUDIES OF  
WATER SOLUBLE ANALOGUES OF 9,10-DIPHENYLANTHRACENE AND  
RUBRENE WITH NITRATE AS ECL ENHANCING AGENT

### 3.1 Introduction

The sensitive ECL detection of biomolecules is highly desirable if the efficient ECL emitters are soluble in water so that ECL immunoassay can be performed in aqueous buffer media. This is because aqueous media generally is considered to be safer, greener, and more ecofriendly than organic solvents. Also, organic media are not compatible with commercial ECL instruments. Moreover, most in-vitro and in-vivo studies are performed in aqueous buffer conditions. Among the three studied ECL emitters in Chapter II, 9,10-diphenylanthracene (DPA) and rubrene (RUB) are water insoluble, whereas Ru(bpy)<sub>3</sub>Cl<sub>2</sub> is soluble in both aqueous and organic media. A wide range of publications on ECL detection in aqueous media utilize Ru(bpy)<sub>3</sub><sup>2+</sup> and its derivatives<sup>241-253</sup> as well as quantum dots (QDs)<sup>254-267</sup> as ECL labels. However, there has been no any report on usage of water soluble derivatives of efficient ECL emitters of DPA and RUB for ECL detection purposes in aqueous systems. Thus, it is important to synthesize their water-soluble derivatives so that all the three emitters could be used for spectral separation based multiplexing detection of analytes in aqueous media. Previously,<sup>268,269</sup> 9,10-diphenylanthracene-2-sulfonate has been shown to produce weak ECL with anodic coreactant tri-*n*-propylamine (TPrA) and cathodic coreactant persulfate in acetonitrile–water (1:1 v/v) mixture media.

This chapter presents the synthesis, electrochemistry and anodic coreactant (i.e., TPrA and 2-(dibutylamino)ethanol (DBAE)) ECL studies of water soluble sulfonated

9,10-diphenylanthracene (DPAS) and sulfonated rubrene (SRUB). ECL enhancement with nitrate was demonstrated. The direct electron paramagnetic resonance (EPR) spectroscopic evidence of nitrate radical was obtained, which further supported the proposed ECL enhancement mechanism.

## 3.2 Experimental Section

### 3.2.1 Chemicals

Rubrene (RUB,  $\geq 99\%$ ), tri-*n*-propylamine (TPrA, 99+%), 2-(dibutylamino)ethanol (DBAE, 99%), sodium phosphate monobasic monohydrate ( $\text{NaH}_2\text{PO}_4 \cdot \text{H}_2\text{O}$ , 99%), nitrobenzene, potassium nitrate ( $\text{KNO}_3$ , 98%), lithium nitrate ( $\text{KNO}_3$ , 98%),  $\text{CDCl}_3$  (chloroform-d, 99.6% atoms D and 0.3% v/v TMS) and hydrochloric acid (HCl, 37.5%) were obtained from Sigma-Aldrich. Fuming sulfuric acid was from Acros Organics. Dioxane, methylene dichloride, and ethylene dichloride were purchased from Thermo Fisher Scientific. Acetonitrile (MeCN, 99.93+%, HPLC grade) was from MP Biomedicals. Sodium nitrate ( $\text{NaNO}_3$ ) and ammonium nitrate ( $\text{NH}_4\text{NO}_3$ ) were purchased from Baker Chemical Co. Methanol (spectroanalyzed grade) and 9,10-diphenylanthracene (DPA, 98%) were obtained from Fluka. 2,2-diphenyl-1-picrylhydrazyl 5,5-dimethyl-1-pyrroline *N*-oxide (DMPO) was received from Cayman Chemical. All chemicals were used as received, unless otherwise stated.

### 3.2.2 Apparatus and methods

All electrochemical and ECL experiments were performed with a CHI 660A electrochemical workstation (CH Instruments, Austin, TX) coupled with a photomultiplier tube (PMT) (Hamamatsu R928, Japan) installed in a light tight black box

as shown in Figure 3.1. To prevent from external background light interferences, the electrochemical cell with testing solution was placed inside the light tight box that covered with a black blanket.<sup>113,270</sup> To supply a voltage of -700 V to the PMT, a model 472A Brandenburg PMT power supply (England) was used. A highly sensitive Keithley 6514 electrometer (Keithley, Cleveland, OH) was used to detect the photocurrent from the testing sample and converts to voltage ( $\pm 2.0$  V).

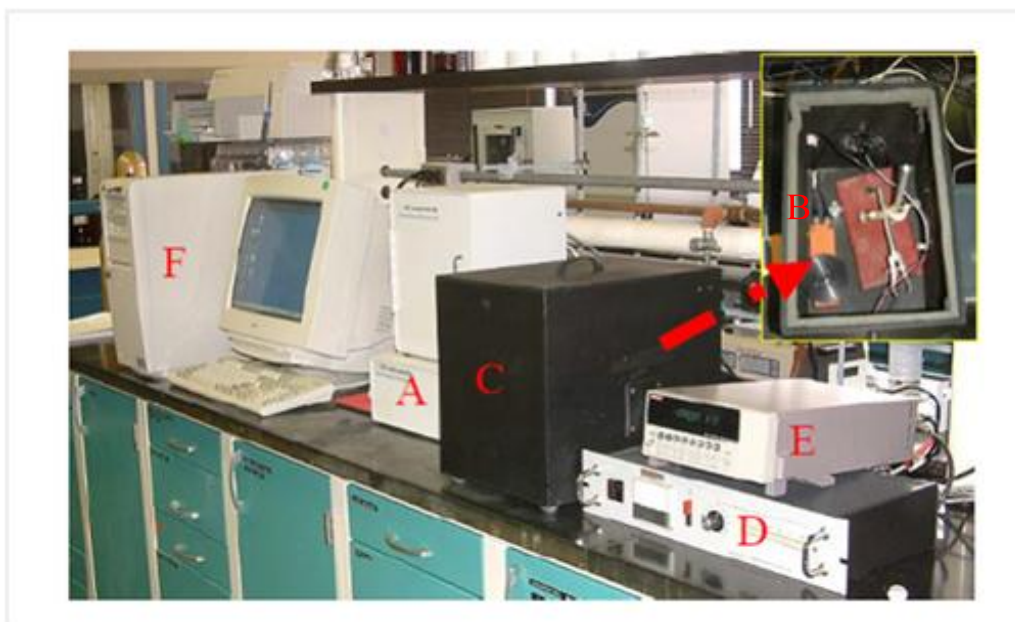


Figure 3.1 Homemade ECL instrument setup.

Note: The ECL setup consists of (A) potentiostat, (B) PMT, (C) light tight box with PMT installed, (D) PMT power supply, and (E) electrometer.

For recording ECL spectra, a workstation from Princeton Instrument (Acton, MA) comprising (A) a Spec-10:400B/LN-eXcelon digital charge coupled device (CCD) camera system cooled to  $-120$  °C with liquid nitrogen, (B) ST 133B controller, and (C) Acton SP-2156 imaging spectrograph was used. The system was controlled and data were

collected and displayed via “WinSpec/32” software. Electrochemical and ECL signals were generated with a model 173 potentiostat/galvanostat coupled with a model 175 universal programmer from Princeton Applied Research (Oak Ridge, TN). ECL emissions at the Pt working electrode were carried over by an optical fiber to the CCD detector through a 1.5 mm slit. Figure 3.2 shows a photograph of the above CCD based ECL spectral instrument.

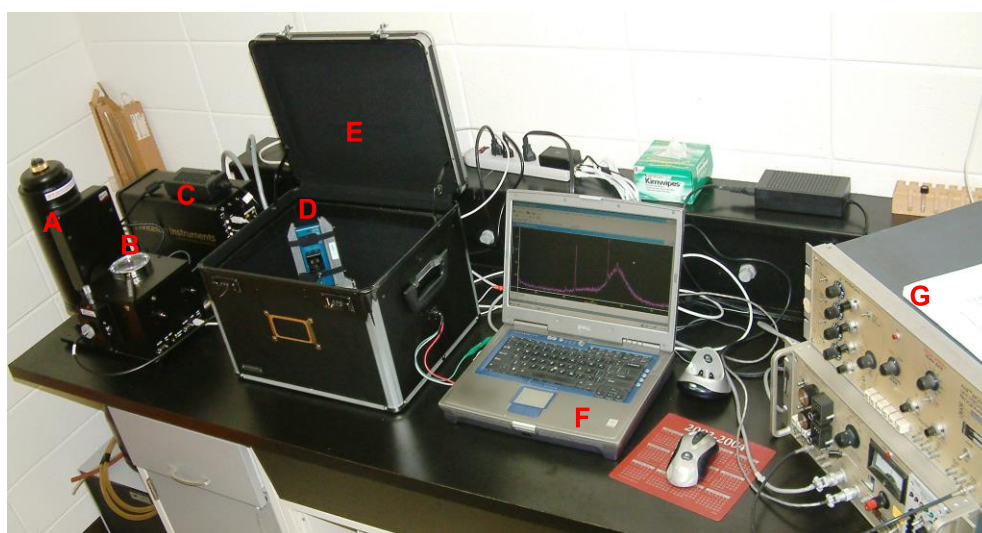


Figure 3.2 Liquid nitrogen cooled CCD camera-based ECL spectral instrument setup.

Note: The setup consists of (A) CCD Camera, (B) monochromator, (C) CCD camera controller, (D) three-electrode electrochemical cell, (E) light tight black box, (F) computer, and (G) potentiostat/galvanostat.

Diamond crystal attenuated total reflection Fourier transform infrared (ATR-FTIR) experiments were performed with a Nicolet Nexus 470 FTIR spectrometer (Thermo Electron Corp., Madison, WI). A pinch of crystalline precursors (RUB and DPA) and synthesized dried solid products (DPAS and SRUB) were used to collect FTIR spectra.

$^1\text{H}$  NMR spectroscopic experiments were performed using Bruker 400 MHz NMR spectrometer using a concentration of 5.0 mg/mL in  $\text{CDCl}_3$ .

Mass spectrometry experiments were performed on a Thermo-Finnigan LXQ electro-spray ionization (ESI)-ion trap mass spectrometer using negative ion mode with a concentration of 0.1 mg/mL and a flow rate of 100  $\mu\text{L}/\text{min}$  in MeCN/ $\text{H}_2\text{O}$  (50:50, v/v) mixed solvent systems.

Electron paramagnetic resonance (EPR) spectroscopy was performed with a Bruker EMX microX EPR spectrometer equipped with an ER 4119HS standard cylindrical resonator (Bruker BioSpin Corp.). A resonant frequency of 19.89 GHz, a modulation frequency of 100 kHz, and a microwave power of 20 mW were used. Pre-calibration of the EPR instrument was done using the manufacturer's 2,2-diphenyl-1-picrylhydrazyl (DPPH), 1, 3-bis diphenylene-2-phenyl allyl (BDPA), and weak pitch standard calibration samples. Nitrate radicals ( $\text{NO}_3^\cdot$ ) were produced in situ with UV irradiation from a Bruker illumination accessory using 0.10 M  $\text{KNO}_3$  in the presence of 0.20 M DMPO spin trap agent in aqueous media. Experimentally, the mixture solution was filled into a standard glass capillary (10 cm long, 2/1.2 OD/ID (mm), World Precision Instruments, Inc., Sarasota, FL) to a height of ~4 cm and sealed with "permanent avery glue stic" (Office Depot, Hattiesburg, MS) at the bottom to prevent any leakage of the sample. This capillary was then placed in a regular quartz EPR tube (Wilmad Lab Glass) for spectra acquisition. The experimentally obtained EPR spectra were simulated using PEST Winsim Software (National Institute of Environmental

Health Sciences, National Institute of Health, Research Triangle Park, NC) for calculating hyperfine coupling constants.

### 3.3 Synthesis

#### 3.3.1 Synthesis of water soluble analogue of DPA — Sodium-9,10-diphenylanthracene sulfonate (SDPAS)

DPAS was synthesized as reported in the literature<sup>269,271-273,274,275</sup> with some modifications. Briefly, 1.00 g (3.0 mmol) of 9,10-diphenylanthracene (DPA) was dissolved in 7.0 mL nitrobenzene to form a clear yellow solution, to which excess fuming sulfuric acid (500.0  $\mu$ L) was added slowly over a period of five minutes. The reaction was allowed to occur for 36 h under stirring before a volume of 200.0 mL water was added. The mixture was separated into two phases — the aqueous phase on the top and the organic phase on the bottom as nitrobenzene (specific density 1.20 g/mL) was heavier than water. The aqueous phase was separated from the organic phase with a separatory funnel, adjusted to pH 7.0 with 10.0 M NaOH, and heated to evaporate the solvent until ~10 mL. 300.0 mL of methanol was subsequently added to the above concentrated aqueous phase that immediately turned into white slurry (i.e., unreacted DPA). The filtered methanol solution was concentrated by distillation, yielding ~0.35 g (or ~0.85 g in the second batch of synthesis) of crude sulfonated DPA (e.g., SDPAS, light yellow solid).

The crude product was purified by ion-exchange column chromatography using Dowex 1 $\times$ 2-100 ion-exchange resin (50-100 dry mesh; 3 $\times$ 1 cm) and eluted with a gradient of 0 to 0.50 M HCl in methanol. Experimentally, the crude yellow product was

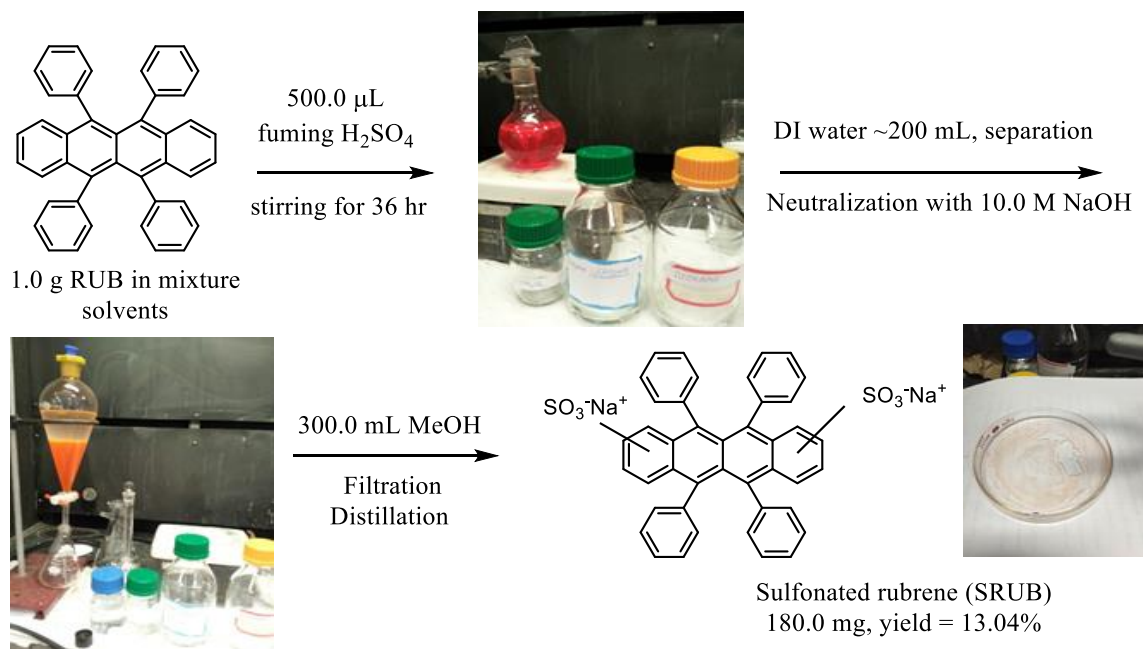
re-dissolved in 10.0 mL of methanol with stirring and sonication. The supernatant was applied to the ion-exchange column and eluted with (1) 5.0 mL methanol, (2) 5.0 mL of 0.25 M HCl in methanol, and (3) 5.0 mL of 0.50 M HCl in methanol. Fractions from the last two elution steps were collected and placed in a refrigerator overnight. The precipitates were transferred to a glass petri dish covered with a piece of filter paper and air-dried for several days under ambient conditions. Finally, ~45 mg (~3% yield) of light yellow-green DPAS was scraped from the petri dish with a razor blade. Theoretically, ~1.53 g of the final product should be obtained. The low yield in this synthesis could be due to (1) low efficiency of sulfonation reaction, and (2) the loss of the product during the ion-exchange purification process. In the latter case, it might be a good idea to collect all materials after vaporizing the fractions from the last two elution steps, because experimentally, no any precipitate was seen at 4 °C from the fraction of pure methanol elution (i.e., the first elution step), indicating that the later fractions should essentially contain pure products. Scheme 3.1 illustrates the synthesis of SDPAS.



Scheme 3.1 Synthesis of SDPAS using the sulfonation of DPA.

### 3.3.2 Synthesis of water soluble sulfonated rubrene (SRUB)

SRUB was synthesized as reported in the literature<sup>127,276</sup> with some modifications. Briefly, 1.00 g of rubrene (RUB, 1.8 mmol) was dissolved in a mixed solvent system consisting of 80.0 mL of 1,4-dioxane, 80.0 mL of ethylene dichloride, and 40.0 mL of methylene dichloride (2:2:1 in v/v) to form a clear red solution. Excess fuming sulfuric acid (500.0  $\mu$ L) was added to the above solution slowly over a period of five minutes. The reaction media was stirred for 36 h followed by adding 200.0 mL of water into the mixture, which produced two separate phases with aqueous phase containing the product on the top and the organic layer on the bottom due to density difference. The aqueous layer was then collected with a separatory funnel and neutralized with 10.0 M NaOH. Solution evaporation via heating was undertaken until ~10 mL of concentrated solution was obtained. Subsequently, 300.0 mL of methanol was added, turning the solution to be white slurry. The filtered methanol solution was finally concentrated by distillation, yielding 180.0 mg of SRUB product (light red crystalline, ~13.04% yield). The synthetic steps are outlined in Scheme 3.2.



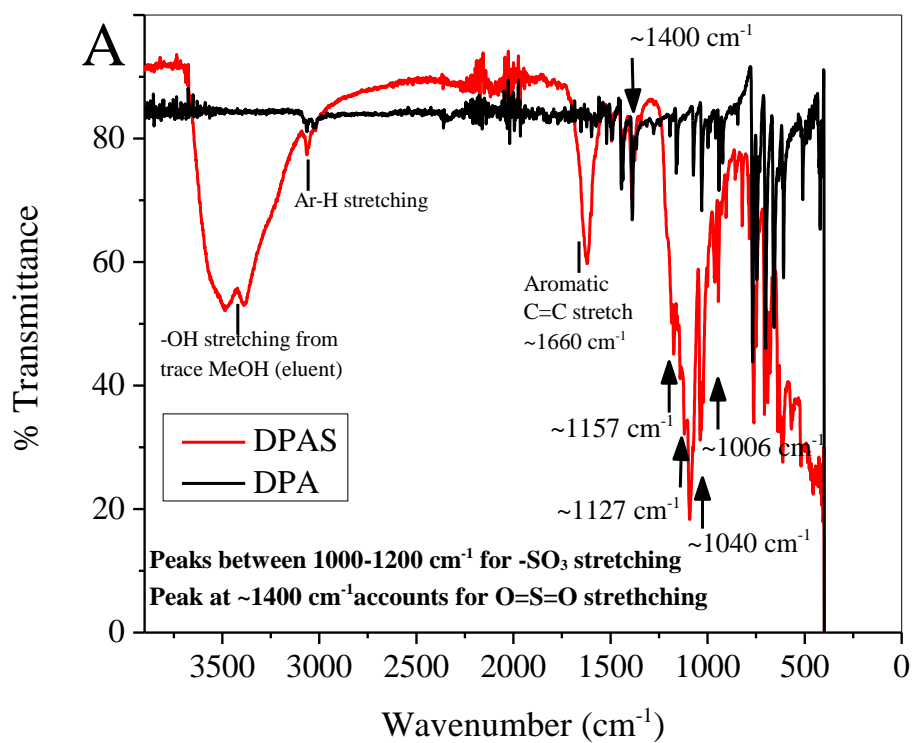
Scheme 3.2 Synthesis of SRUB using the sulfonation of RUB.

### 3.4 Results and Discussion

#### 3.4.1 Structural characterization and elucidation

Figure 3.3 shows the Fourier transform infrared (FTIR) spectra of pure precursors (DPA and RUB) along with their sulfonated products (DPAS and SRUB). The IR peaks between  $1000\text{-}1400\text{ cm}^{-1}$  correspond to sulfur-oxygen stretching vibrations. More specifically, the IR bands at positions  $\sim 1156\text{ cm}^{-1}$ ,  $\sim 1127\text{ cm}^{-1}$ ,  $\sim 1040\text{ cm}^{-1}$ , and  $\sim 1006\text{ cm}^{-1}$  all account for the  $-\text{SO}_3$  stretching vibrations of the sulfonate group<sup>277-280</sup> from the sulfonated products, providing solid proof of sulfonation during the synthesis of DPAS (Figure 3.3 A) and SRUB (Figure 3.3B). The band at  $\sim 1400\text{ cm}^{-1}$  is due to the symmetric and asymmetric stretching vibrations of  $\text{O}=\text{S}=\text{O}$  of the sulfonate group of the sulfonated products.<sup>280</sup> The broad peak between  $3000\text{-}3500\text{ cm}^{-1}$  in Figures 3.3A and B account for

the -OH stretching, possibly from a trace amount of water or MeOH used in the synthetic steps. The shoulder just above 3000  $\text{cm}^{-1}$  in both the Figures 3.3A and B was assigned for Ar-H stretching both the precursors and the sulfonated products containing benzene moieties (for instance DPA and DPAS contain 5 benzene rings while RUB and SRUB contains 8 benzene rings).



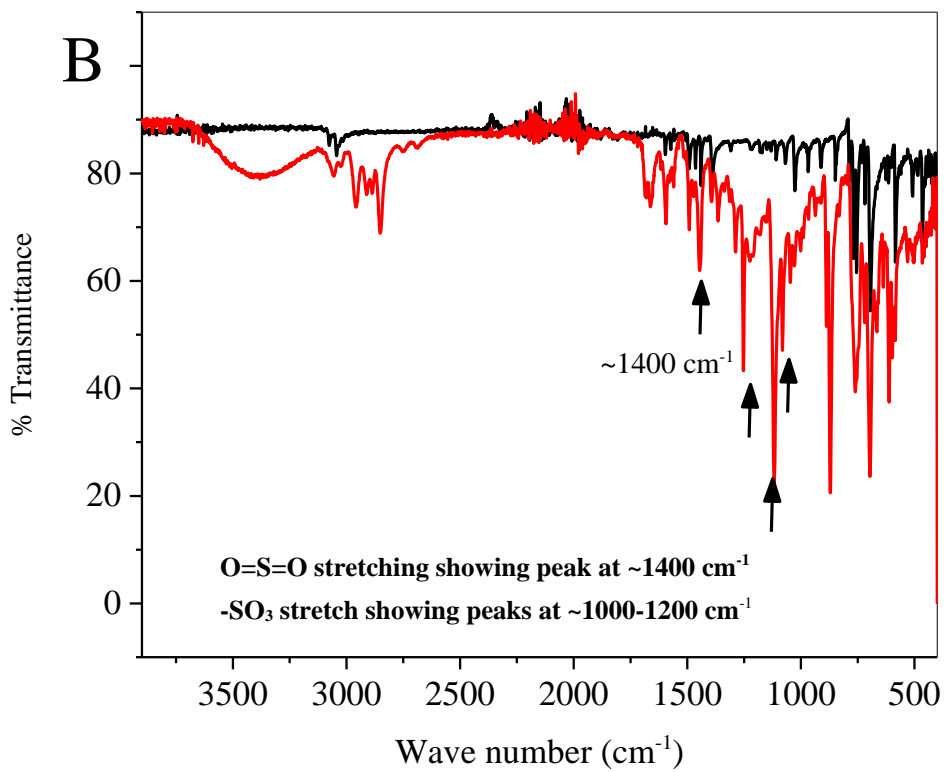


Figure 3.3 FTIR spectra of (A) DPA and DPAS, and (B) RUB and SRUB.

Note: The arrows marked are signature bands for  $\text{-SO}_2$  and  $\text{SO}_3$  stretching vibrations.

The evidence of successful sulfonation of DPA is also witnessed by electro-spray ionization mass spectrometry (ESI-MS) (Figure 3.4), where the  $m/z$  peak at 409 in negative mode scan corresponds to the molecular mass of DPAS having molecular mass of its precursor DPA plus one sulfonated group. Moreover, no ESI-MS peak for the precursor DPA (molecular weight = 330.45 g/mol) was seen, suggesting the high purity of the final DPAS product.

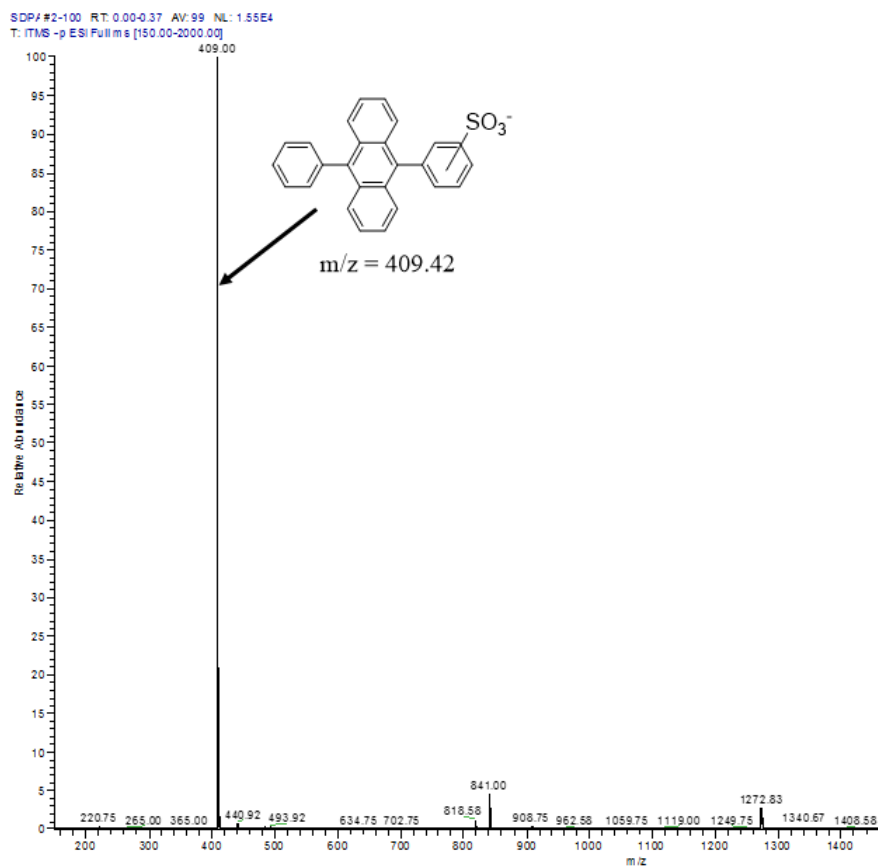
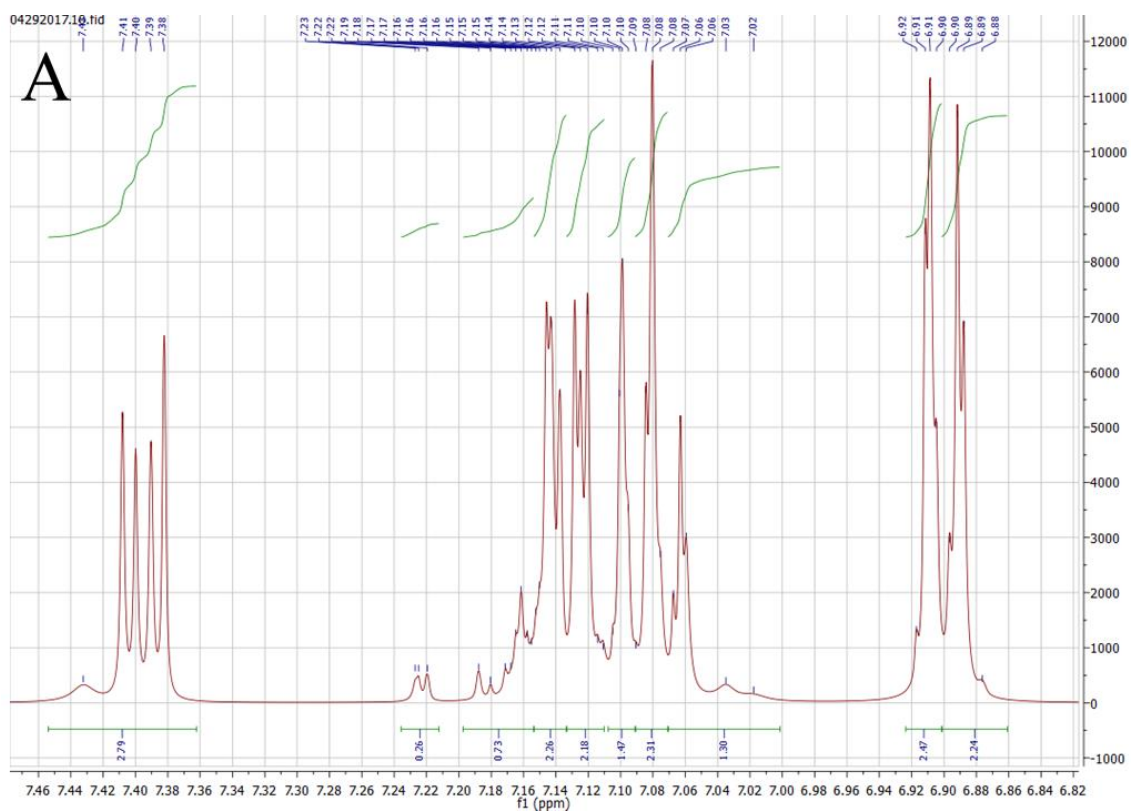


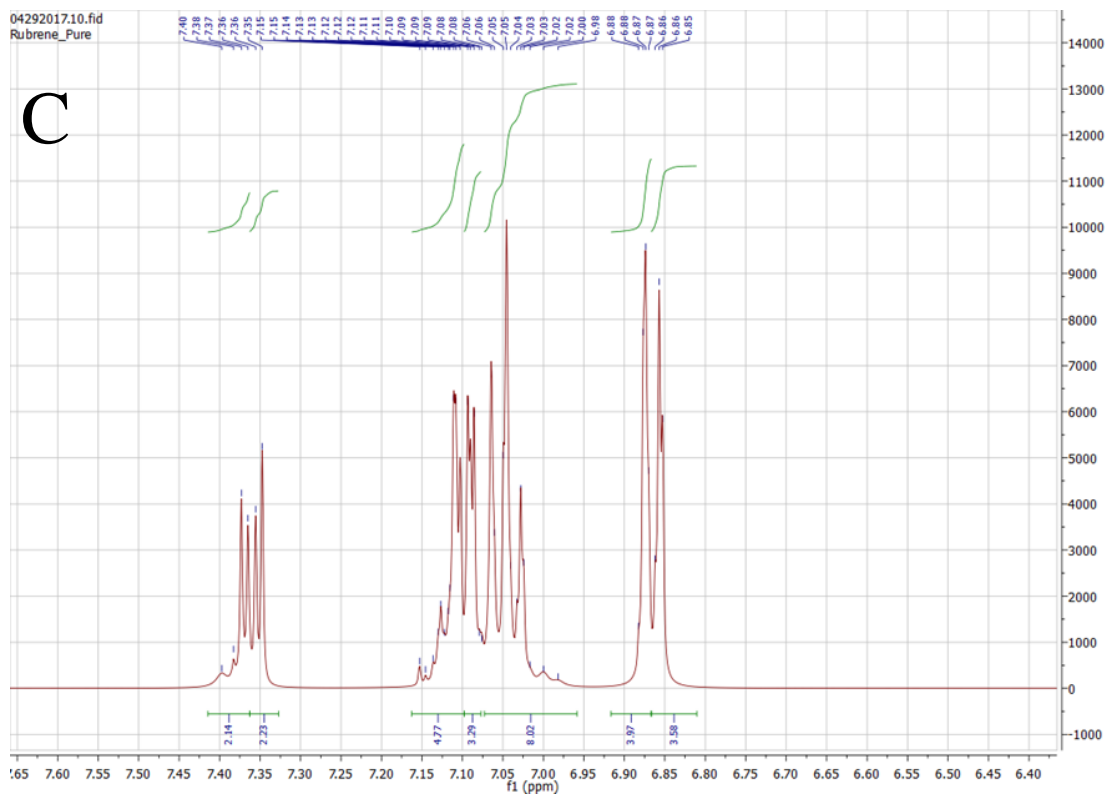
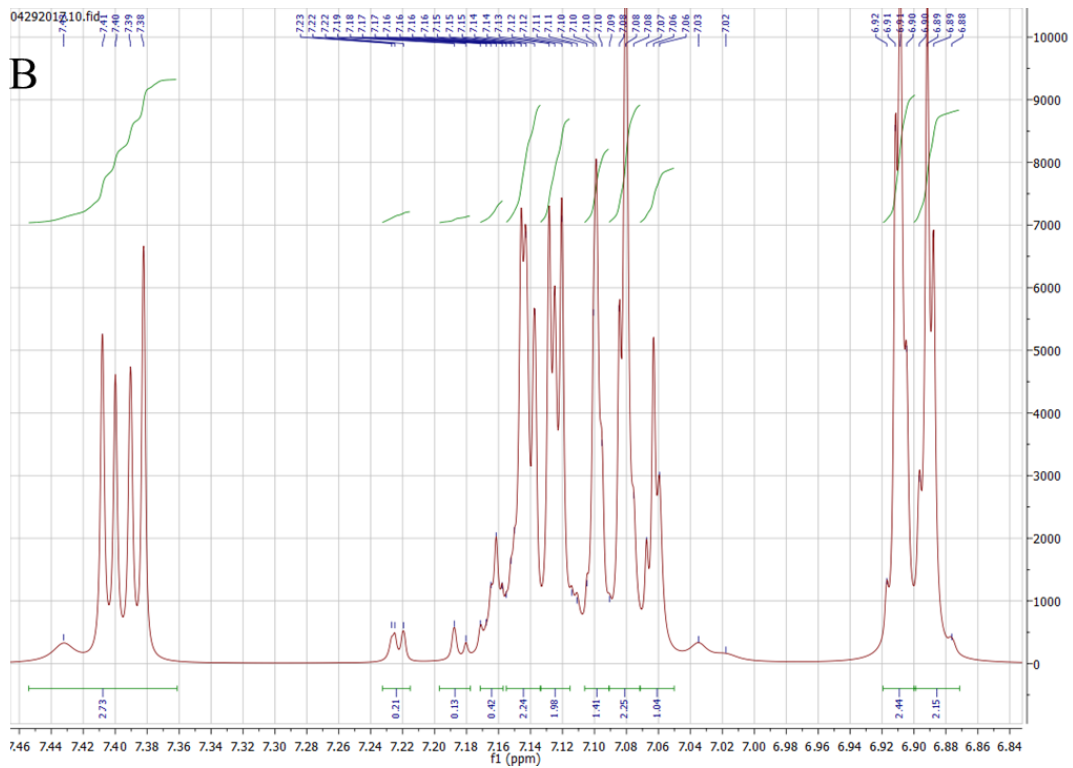
Figure 3.4 ESI-MS data of DPAS.

The ESI-MS data were obtained with 0.1 mg/mL DPAS in MeCN: H<sub>2</sub>O (50:50, v/v) at a flow rate of 100  $\mu$ L/min in negative mode scan.

Proton nuclear magnetic resonance (<sup>1</sup>H-NMR) spectroscopy data (Figure 3.5A) revealed a total of 18 protons upon integration when the precursor DPA was subjected to <sup>1</sup>H-NMR spectroscopy (molecular formula of DPA = C<sub>22</sub>H<sub>18</sub>). On the other hand, the integration of the <sup>1</sup>H-NMR of sulfonated DPAS data showed a total of 17 protons (Figure 3.5B), indicating that DPAS (molecular formula = C<sub>22</sub>H<sub>17</sub>SO<sub>3</sub>H) contains only one sulfonated group. This finding is consistent with the MS data described above. Similarly, the integration of all the NMR peaks from <sup>1</sup>H-NMR data of rubrene (RUB) (molecular

formula = C<sub>42</sub>H<sub>28</sub>) summed to a total of 28 protons (Figure 3.5C). On the other hand, the <sup>1</sup>H-NMR sulfonated rubrene (SRUB) data upon integration of all NMR peaks gave a total of 26 protons (Figure 3.5D), confirming that 2 protons were replaced by two sulfonated groups resulting in the synthesis of disubstituted sulfonated rubrene, i.e. the final product SRUB (molecular formula = C<sub>42</sub>H<sub>26</sub>S<sub>2</sub>O<sub>6</sub>H<sub>2</sub>).





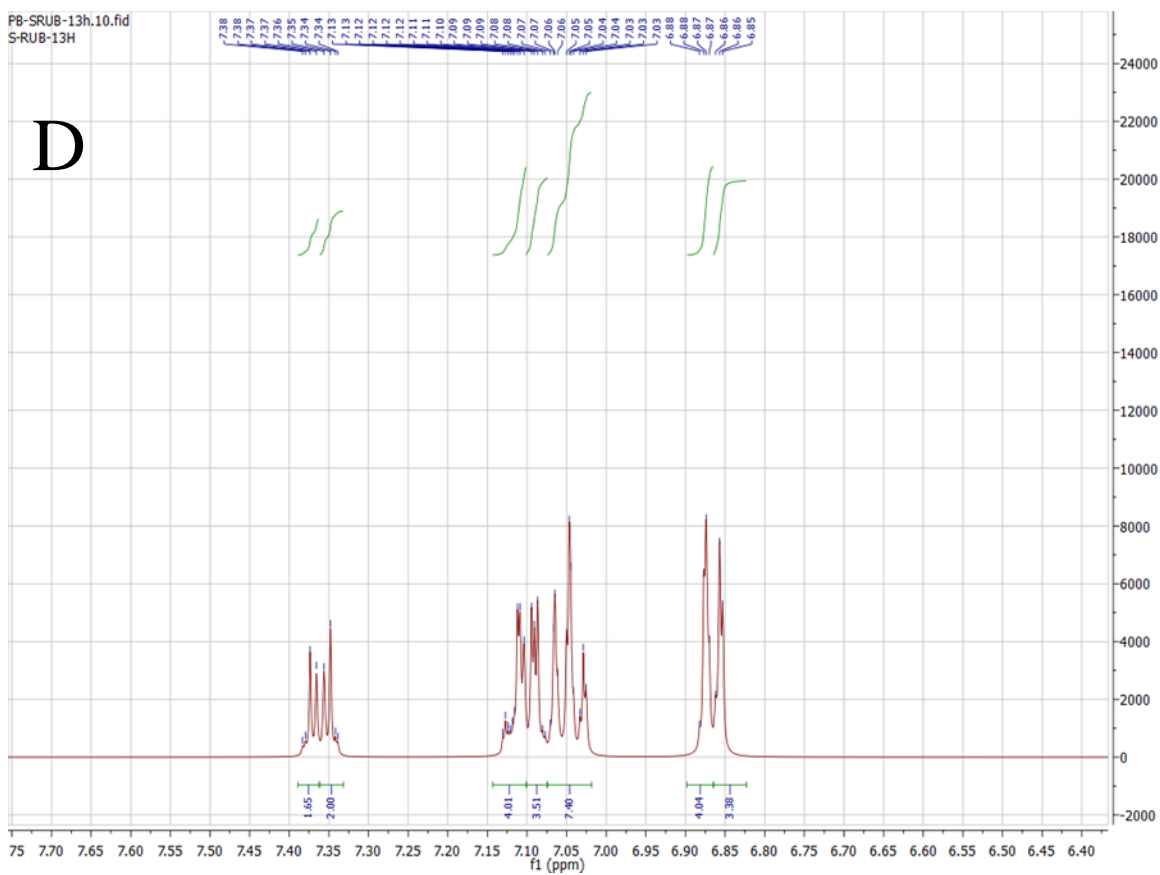


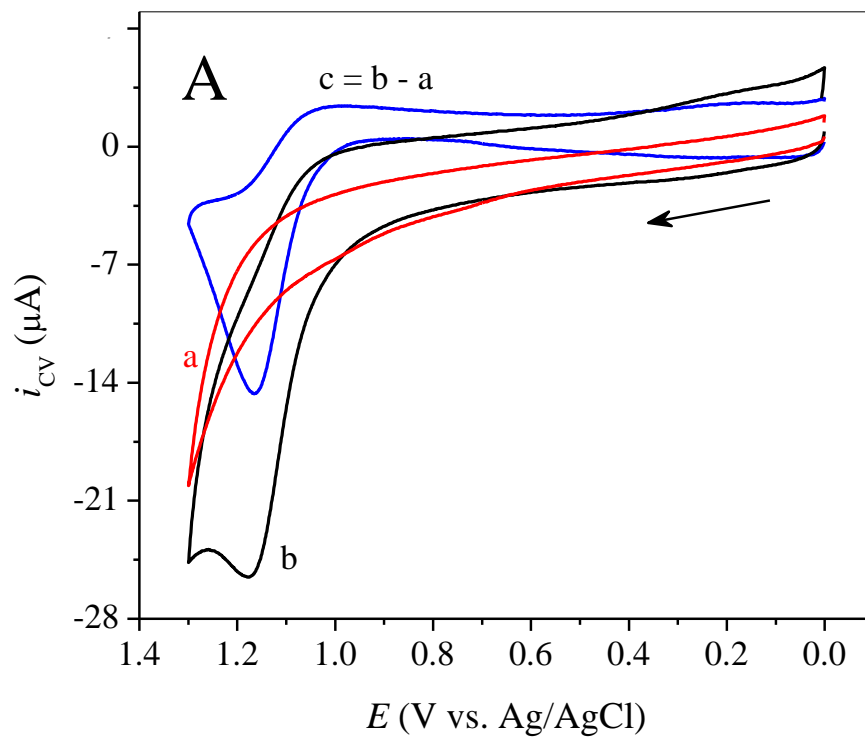
Figure 3.5  $^1\text{H-NMR}$  spectroscopy data of (A) DPA, and (B) DPAS, (C) RUB, and (D) SRUB.

Note:  $^1\text{H-NMR}$  spectroscopy experiments were performed with a concentration 5 mg/mL in  $\text{CDCl}_3$ .

### 3.4.2 Electrochemistry of DPAS and SRUB

The solubility of sulfonated DPA (DPAS) and sulfonated rubrene (SRUB) was very low ( $\sim 10 \mu\text{M}$ ) in sodium phosphate buffer (PBS, pH 7.5). To acquire good CV signals, DPAS and SRUB were dissolved in 95% PBS (pH 7.5)-5% MeCN (v/v) with an estimated concentration of  $50 \mu\text{M}$  (saturated). As shown in Figure 3.6A, DPAS irreversibly oxidizes at  $\sim 1.17 \text{ V}$  vs Ag/AgCl (3.0 M KCl) at a glassy carbon electrode (GCE), indicating that the DPAS radical cation is not sufficiently stable in the reaction

media within the time scale of the experiment. To better probe the electrochemical behavior of DPAS, differential pulse voltammetry (DPV) was applied, in which, DPAS oxidizes with a peak potential of 1.07 V vs Ag/AgCl (Figure 3.6B). The pre-wave appeared in DPV could result from the adsorption of DPAS on GCE.



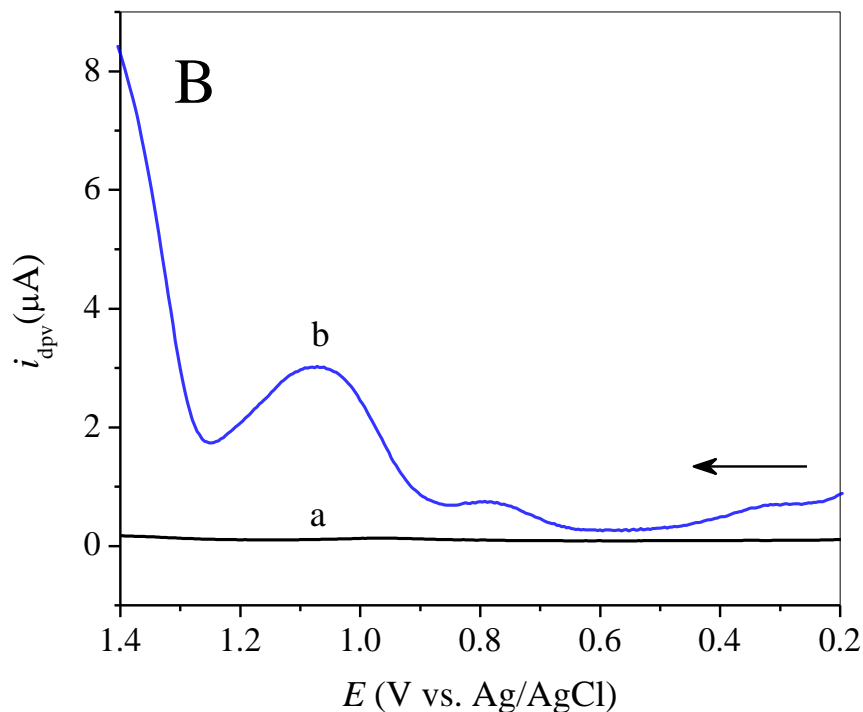
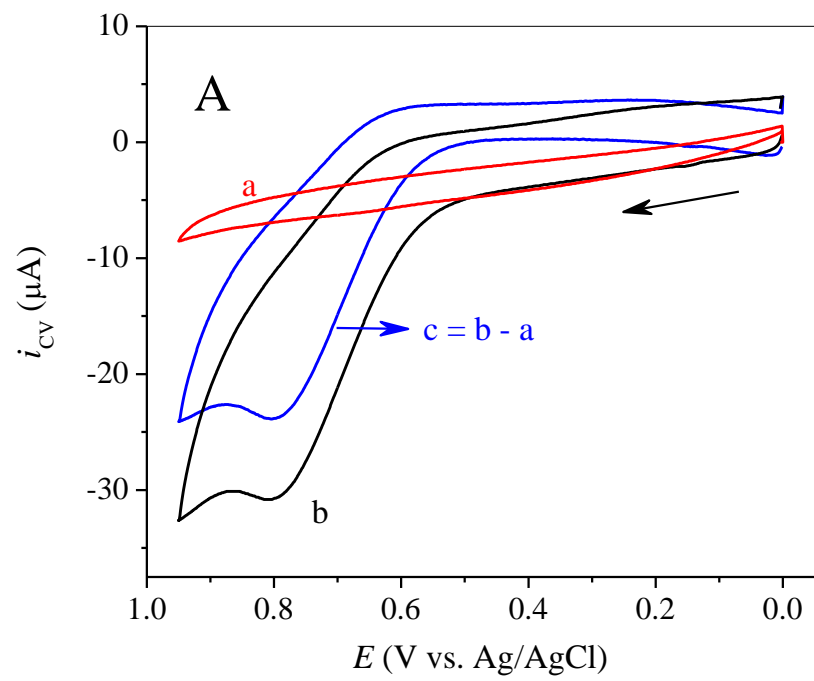


Figure 3.6 (A) CVs, and (B) DPVs of DPAS in aqueous media.

Note: In Figure 3.6A, (a) CV of the background (0.10 M PBS (pH 7.5 with 5% MeCN (v/v)), (b) CV of  $\sim 50 \mu\text{M}$  DPAS in 0.10 M PBS (pH 7.5) with 5% MeCN (v/v), and (c) CV after background subtraction. In Figure 3.6B, (a) background (0.10 M PBS (pH 7.5 with 5% MeCN (v/v)), (b) DPV of  $50 \mu\text{M}$  DPAS in 0.10 M PBS (pH 7.5) with 5% MeCN (v/v). Both CV and DPV experiments were performed using a 3-mm GCE. at (A) a scan rate of 100 mV/s and (B) pulse width = 0.2 s, sample width = 0.016 s, and pulse period = 0.5 s.

Similarly, the irreversible oxidation of SRUB occurs at  $\sim 0.80 \text{ V vs Ag/AgCl}$  on CV and  $\sim 0.86 \text{ V vs Ag/AgCl}$  on DPV as shown in Figure 3.7A and Figure 3.7B, respectively. The oxidation potentials for sulfonated DPA and RUB are close to their predecessors as discussed in Table 2.1 of Chapter II, although different solvents and electrodes were used.



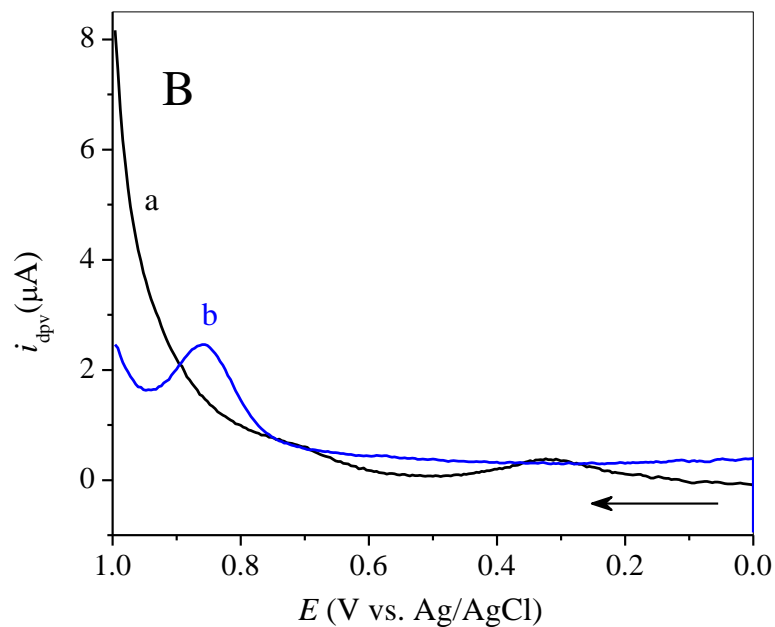


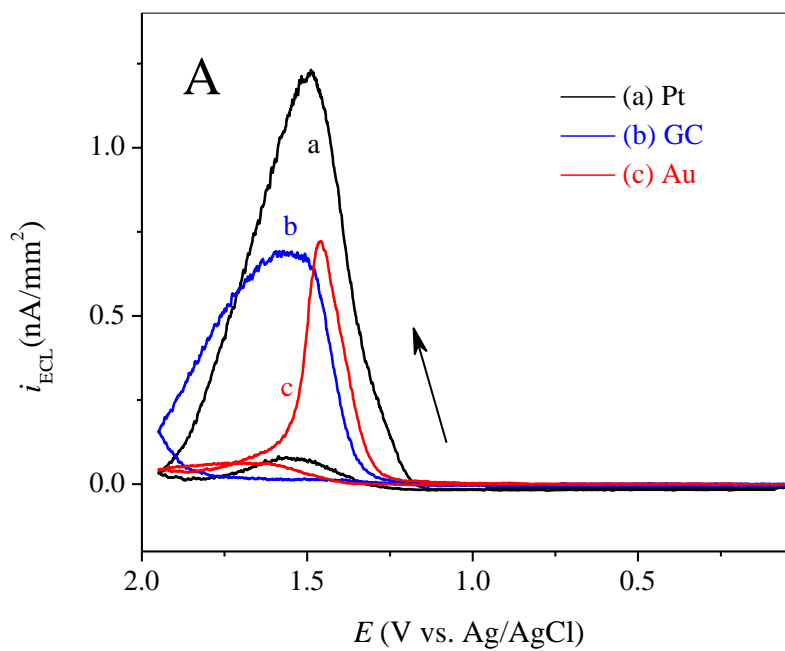
Figure 3.7 (A) CVs, and (B) DPVs of SRUB in aqueous media.

Note: In Figure 3.7A, (a) CV of the background (0.10 M PBS (pH 7.5 with 5% MeCN (v/v)), (b) CV of ~50  $\mu\text{M}$  SRUB in 0.10 M PBS (pH 7.5) with 5% MeCN (v/v), and (c) CV after background subtraction. In Figure 3.7B, (a) background (0.10 M PBS (pH 7.5 with 5% MeCN (v/v)), (b) DPV of 50  $\mu\text{M}$  SRUB in 0.10 M PBS (pH 7.5) with 5% MeCN (v/v). Both CV and DPV experiments were performed using a 3-mm GCE at (A) a scan rate of 100 mV/s and (B) pulse width = 0.2 s, sample width = 0.016 s, and pulse period = 0.5 s.

### 3.4.3 Effect of ECL coreactant and electrode material on ECL production

Various anodic and cathodic ECL coreactants were tested to find out the most suitable or favorable ECL coreactant for DAPS and SRUB. As only extremely weak ECL was observed from cathodic coreactant persulfate, the following discussion focuses on anodic ECL coreactants DBAE and TPrA. As shown in Figure 3.8, upon the anodic potential scanning, ECL is produced from the DPAS/DBAE system (Figure 3.8A) and the

DPAS/TPrA system (Figure 3.8B) at all three tested electrodes, namely, Pt, Au, and glassy carbon (GC) electrode.



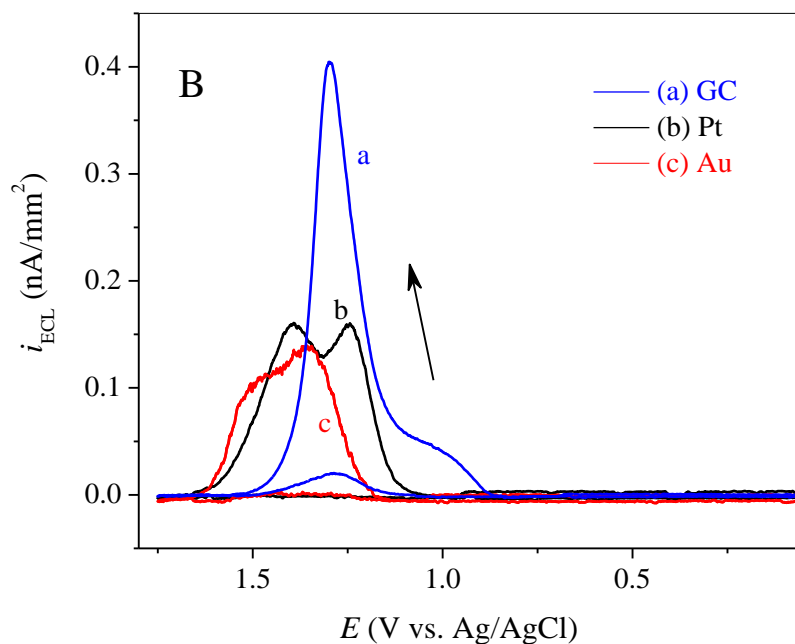


Figure 3.8 Effect of electrode material on the ECL intensity of (A) DPAS/DBAE and (B) DPAS/TPrA system.

Note: ECL was generated with DPAS using (A) 25 mM DBAE and (B) 25 mM TPrA. The concentration of DPAS was 7.5  $\mu$ M at different electrodes (indicted in the Figure) at a scan rate of 100 mV/s.

Similar behavior was observed for the SRUB/DBAE system (Figure 3.9A) and the SRUB/TPrA system (Figure 3.9B).

Several features are noticed: (1) ECL generated from DPAS occurs at a more positive potential than SRUB does, (2) for the same ECL emitter (DPAS or SRUB), much stronger ECL signals are produced when DBAE rather than TPrA is used as the coreactant, (3) relative weak ECL signals are produced from DPAS as compared with SRUB, and (4) electrode materials strongly affect the ECL behavior.

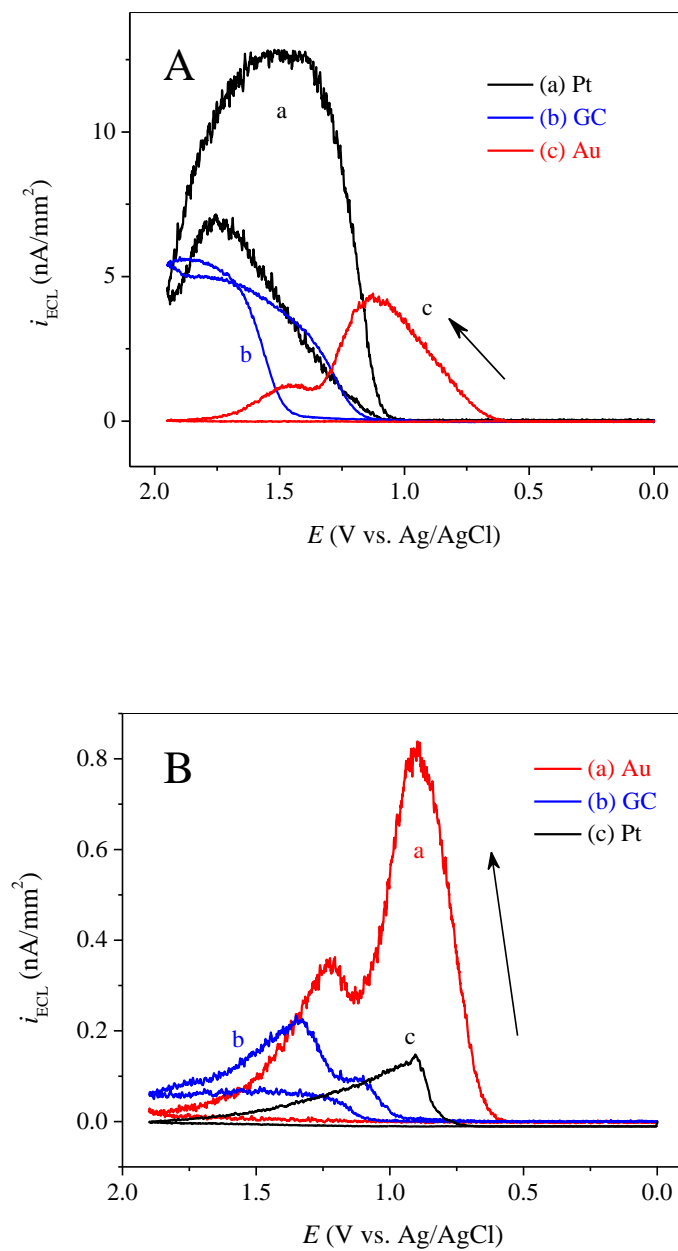
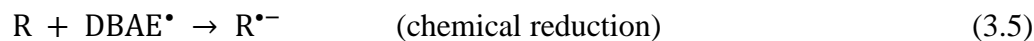
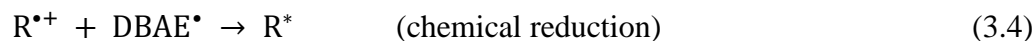


Figure 3.9 Effect of electrode material on the ECL intensity of (A) SRUB-DBAE and (B) SRUB-TPrA system.

Note: ECL was generated with SRUB using (A) 25 mM DBAE, and (B) 25 mM TPrA. The concentration of SRUB was 7.5  $\mu\text{M}$  at different electrodes (indicted in Figure) at a scan rate of 100 mV/s.

The striking features that summarize DPAS system are enlisted as: (1) ECL generated from DPAS occurs at a more positive potential than SRUB does, (2) for the same ECL emitter (DPAS or SRUB), much stronger ECL signals are produced when DBAE rather than TPrA is used as the coreactant, (3) relative weak ECL signals are produced from DPAS as compared with SRUB, and (4) electrode materials strongly affect the ECL behavior. These observations can be explained with the ECL mechanism shown in Scheme 3.3, where DBAE could be replaced with TPrA as both coreactants share the similar reaction pathways.<sup>30</sup>



(R = DPAS or SRUB, and DBAE = (CH<sub>3</sub>CH<sub>2</sub>CH<sub>2</sub>CH<sub>2</sub>)<sub>2</sub>NCH<sub>2</sub>CH<sub>2</sub>OH)

Scheme 3.3 ECL mechanism with DBAE as an anodic ECL coreactant.

To generate ECL, both coreactant and ECL emitter must be electrochemically oxidized (Equations 3.1-3.2). Because the oxidation of coreactant often occurs at a less positive potential region than that of ECL emitter, the onset potential of ECL generation is essentially determined by the oxidation potential of the emitter. As discussed earlier in Figures 3.6 and 3.7, DPAS oxidizes at  $\sim 1.1$  V vs Ag/AgCl but SRUB at  $\sim 0.8$  V vs Ag/AgCl, it is expected that the ECL system of DPAS appears at a more positive potential region. The ECL-CV profiles shown in Figure 3.10 further supports the above discussion. In this Figure 3.10, 25 mM of DBAE and  $7.5\mu\text{M}$  of DPAS are used, hence the CV responses should be predominated by the oxidation of DBAE. The ECL intensity is also directly proportional to the amount of the coreactant oxidized; the more coreactant oxidation is (Equation 3.1), the freer radicals of DBAE $\cdot$  (or TPrA $\cdot$ ) forms (Equation 3.3), the more excited state species  $\text{R}^*$  is produced (Equation 3.5), thus the stronger the ECL intensity (Equation 3.7). Electrochemical oxidation of DBAE has shown to be easier than that of TPrA (see Figure 2.5 in Chapter II for more details). As a result, the DBAE system gives stronger ECL signals than the TPrA system. To make Equation 3.5 occur, the reducing power of the free radical, i.e., the reduction potential of DBAE $\cdot$  (or TPrA $\cdot$ ), must be more negative than that of  $\text{R}^{\bullet-}$ . As shown in Table 2.1 of Chapter II, DPA has a much negative reduction potential ( $-2.24$  V vs SCE) than that of RUB ( $-1.79$  V vs SCE) in MeCN, it is likely that the reduction potential of DPAS in aqueous solution is much negative than that of SRUB. In other words, the chance of Equation 3.5 to occur is more likely for SRUB as compared with DPAS. Therefore, SRUB displays stronger ECL than DPAS does.

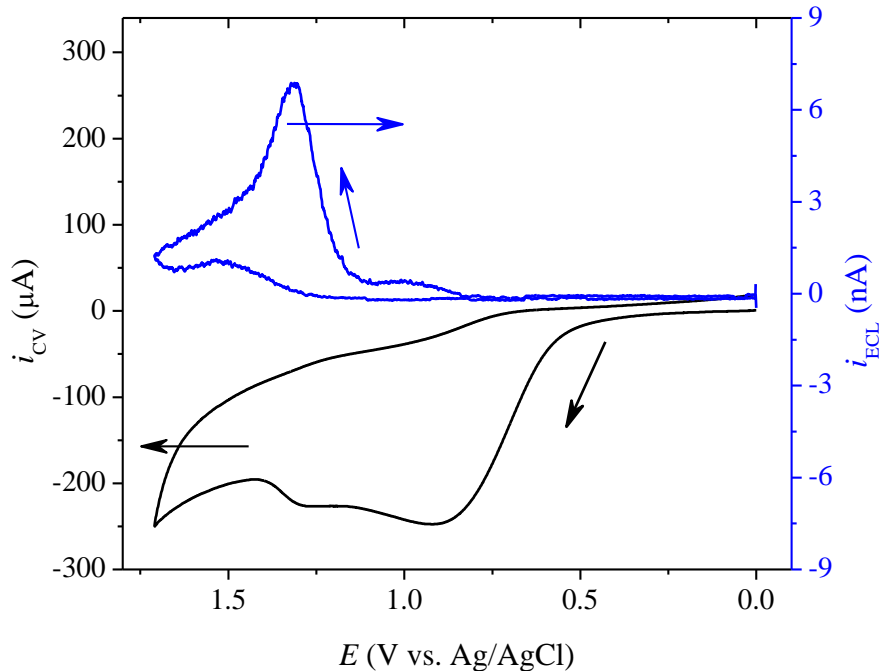
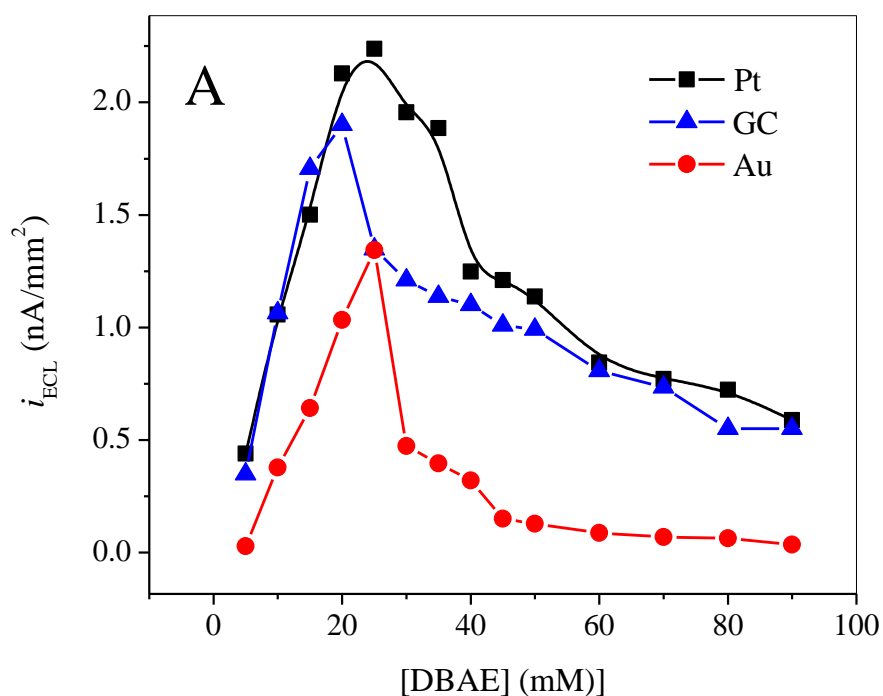


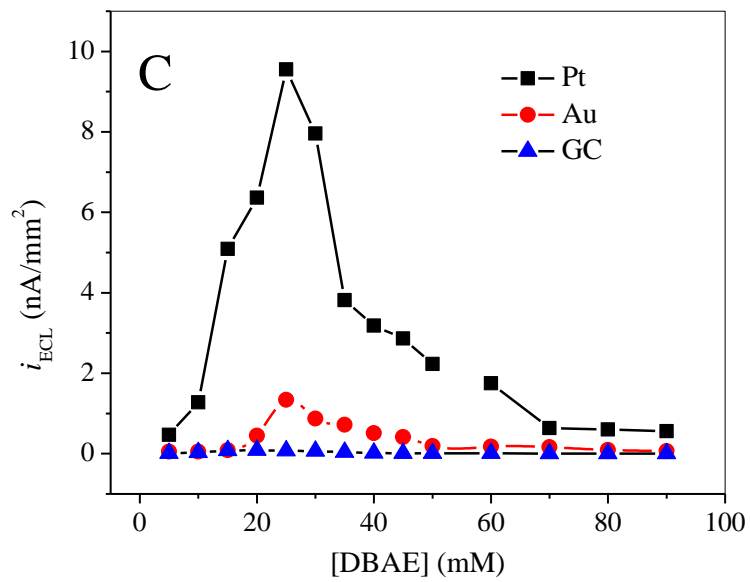
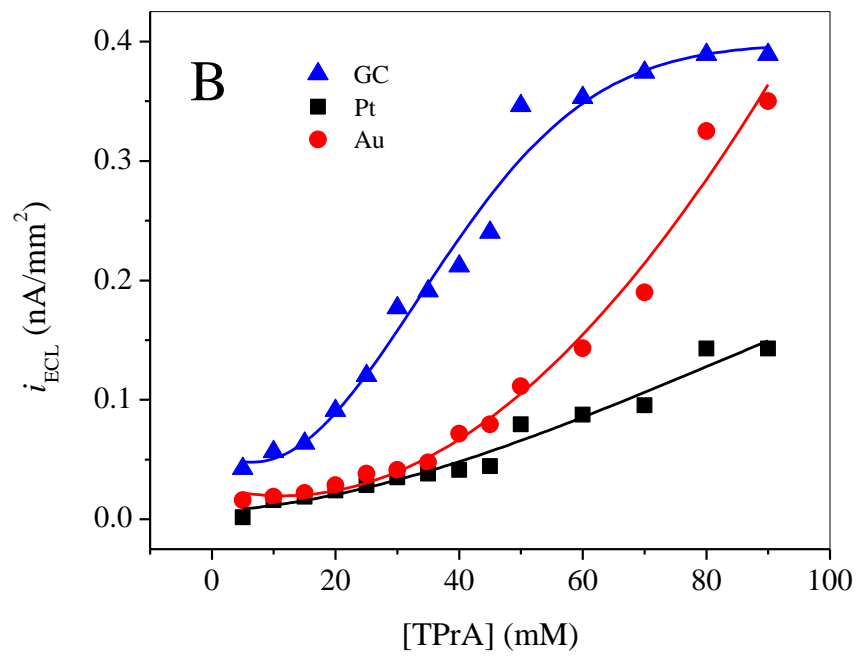
Figure 3.10 ECL-CV profiles of the DPAS-DBAE system.

Note: ECL-CV profiles were obtained with 7.5  $\mu\text{M}$  DPAS-25 mM DBAE at a 2-mm Pt electrode sweeping at 100 mV/s in 0.10 M PBS (pH 7.5).

Figures 3.11 shows the effect of coreactant concentration and electrode material on ECL intensity of the DPAS/DBAE system (Figures 3.11A and B) and the SRUB/TPrA system (Figure 3.11C and D). It is evident that for DBAE coreactant, the optimal concentration for both DPAS and SRUB ECL production is around 25 mM (Figures 3.11A and C). This could be because DBAE acts as both ECL coreactant and ECL quencher. For TPrA, however, the higher the concentration is, the higher the ECL signal is generated (Figures 3.11B and D). This is consistent with the fact that the higher the concentration of TPrA, the more TPrA<sup>+</sup> and TPrA<sup>•</sup> species can be produced, therefore the stronger the ECL (Scheme 3.3). As for the working electrode, Pt is clearly the most

favorable electrode for the DPAS/DBAE and SRUB/DBAE systems (Figures 3.11A and C), whereas mixed results are found when TPrA is used (Figures 3.11B and D). The combination of electrochemical oxidations of both ECL emitter and coreactant at a given electrode has probably played certain roles in determining the effect of the electrode material on ECL production.





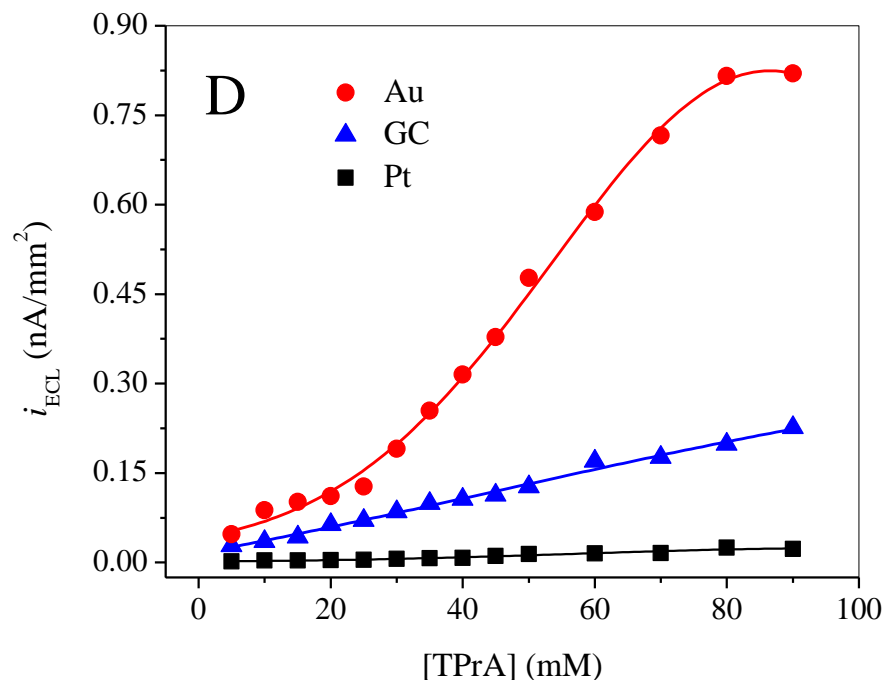


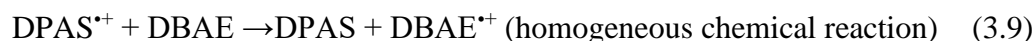
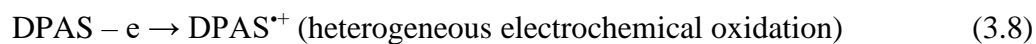
Figure 3.11 Effect of coreactant concentration and electrode material on ECL intensity.

Note: ECL measurements were conducted in 0.10 M PBS (pH 7.5) containing 7.5  $\mu$ M ECL emitter of (A) and (B) DPAS, or (C) and (D) SRUB using coreactant of (A) and (C) DBAE, or (C) and (D) TPrA with a scan rate of 100 mV/s. Each point in the figure was an average result of three replicated tests.

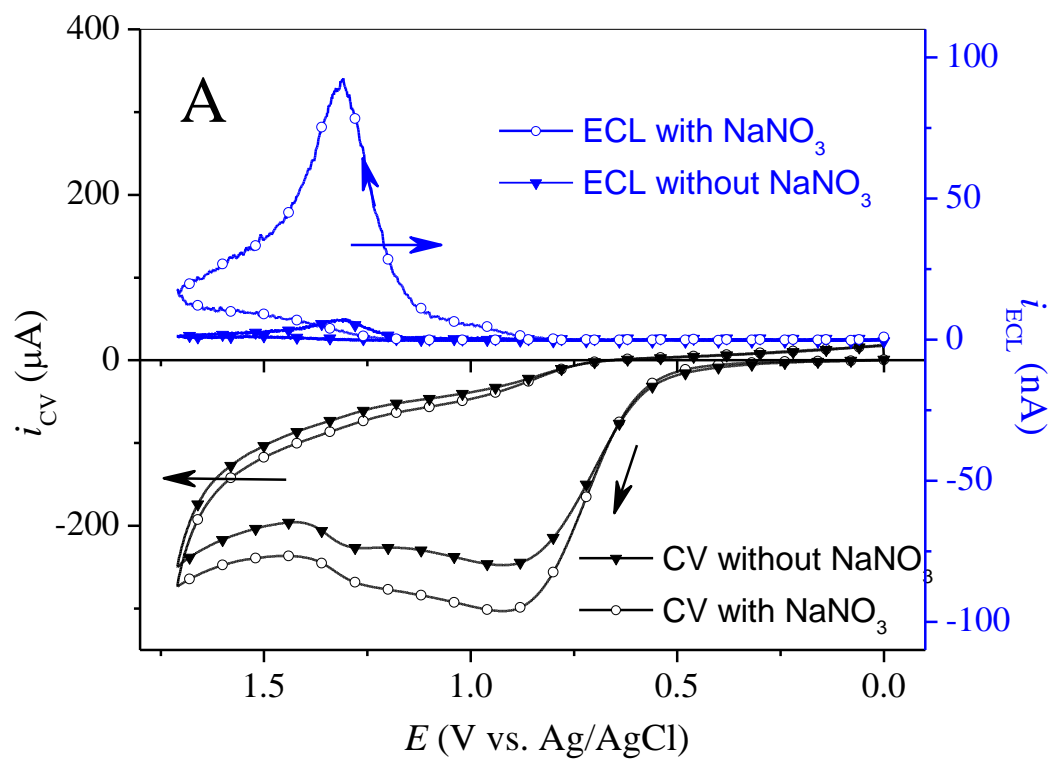
### 3.4.4 ECL enhancement with nitrate ions

The ECL signals generated from the water soluble DPAS/DBAE and SRUB/DBAE systems were relatively weak. Inspired by the study published previously from this research group,<sup>281</sup> where ECL determination of hexamethylene triperoxide diamine explosives was enhanced by silver nitrate in MeCN, we tested the effect of nitrate ions on the ECL production of the DPAS/DBAE and SRUB/DBAE systems. As shown in Figures 3.12, after addition of 10.0 mM NaNO<sub>3</sub> to the above two systems, the

ECL peak intensity is increased by a factor of 13 (Figure 3.12A) and 11 (Figure 3.12B), respectively. CV responses indicate that much higher oxidation currents on the forward scan are seen for the DPA/DBAE- $\text{NaNO}_3$  system as compared with the DPA/DBAE system alone (Figure 3.12A). On the other hand, however, only moderate increase in the forward oxidation currents is observed for the SRUB/DBAE- $\text{NaNO}_3$  system (Figure 3.12B). Moreover, CV responses are clearly shown to be affected by the ECL emitter present in the solution. This could be contributed partially to the electrocatalytic processes shown in Equations 3.8-3.9, where  $\text{DPAS}^{++}$  produced electrochemically at the electrode oxidizes DBAE chemically in the solution, resulting in regeneration of DPAS.



The above explanation is consistent with the oxidation peak potential of  $\sim 1.17$  V for DPAS (Figure 3.6A) and  $\sim 0.9$  V vs Ag/AgCl for DBAE, as well as with the small oxidation wave appeared at around 1.28 V vs Ag/AgCl on the forward scan of the CV in Figure 3.12A. Otherwise, the electrochemical oxidation of  $7.5 \mu\text{M}$  DPAS would not be seen in the presence of 25.0 mM DBAE. In the case of SRUB, the oxidation potential of  $\sim 0.86$  V vs Ag/AgCl (Figure 3.7A) for  $\text{SRUB}^{++}$  is not sufficiently positive enough to oxidize DBAE. The presence of SRUB seems also to inhibit the electro-oxidation of DBAE and nitrate ions, as in these cases, delayed and ill-defined oxidation processes are evident (Figure 3.12B) as compared with CVs in Figure 3.12A. Physical adsorption of SRUB on Pt could be responsible for this behavior.



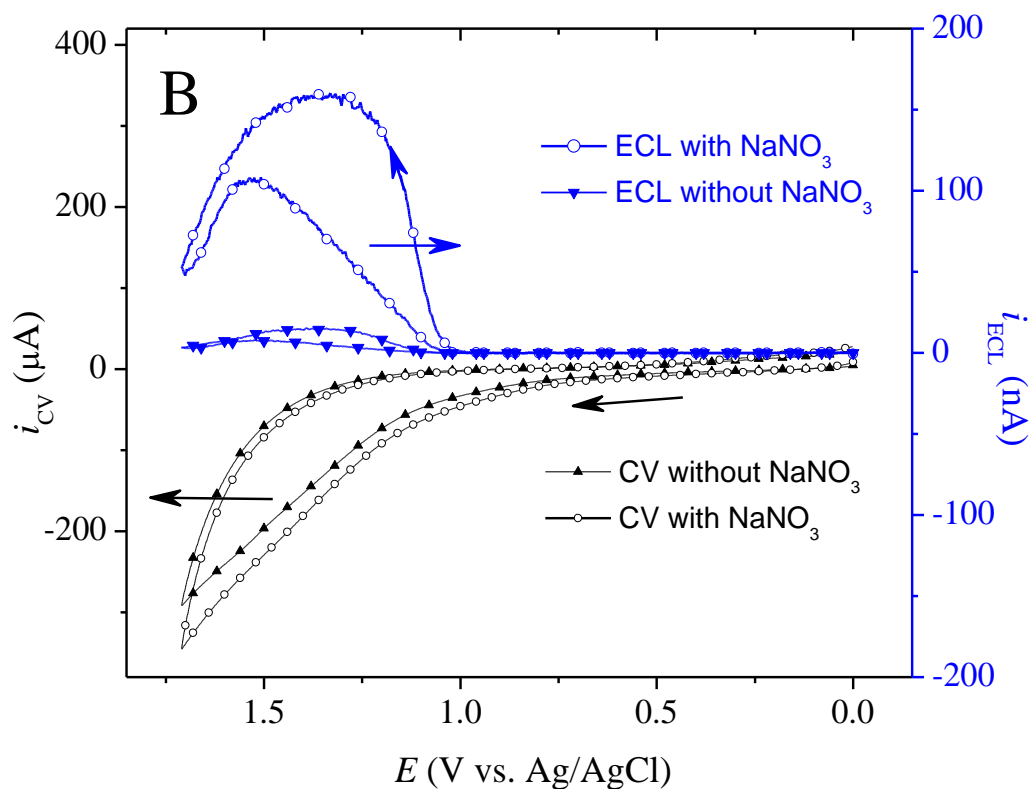


Figure 3.12 Effect of nitrate ions on ECL from (A) DPAS/DBAE, and (B) SRUB/DBAE.

Note: CV-ECL experiments were conducted in 0.10 M PBS (pH 7.5) containing (A) 7.5  $\mu\text{M}$  SRUB-25.0 mM DBAE and (B) 7.5  $\mu\text{M}$  DPAS-25.0 mM DBAE in the absence and presence of 10.0 mM  $\text{NaNO}_3$ . A 2-mm diameter Pt and a scan rate of 100 mV/s were used.

Close inspection of Figure 3.13 reveals that the enhanced ECL responses by nitrate ion have a less positive onset potential than that from a redox media without added  $\text{NaNO}_3$ . Besides, the enhancement starts at  $\sim 0.80$  V vs Ag/AgCl for the DPAS/DBAE- $\text{NaNO}_3$  system and  $\sim 1.00$  V vs Ag/AgCl for the SRUB/DBAE- $\text{NaNO}_3$  system. These two potential values are even less positive than the onset oxidation potential of  $\text{NaNO}_3$ , i.e.,  $\sim 1.05$  V vs Ag/AgCl (Figure 3.13a). As a result, the pre-enhancement of ECL is probably ascribed to the pre-oxidation of the ECL emitter and coreactant, which is facilitated by

the added  $\text{NaNO}_3$ . Previous studies using FTIR spectroscopy<sup>282</sup> and indirect radiotracer method<sup>283</sup> have confirmed the adsorption of  $\text{NO}_3^-$  ions on Pt and other metal surfaces. During anodic potential scanning, such adsorption could prevent the formation of platinum oxides (e.g., PtO and  $\text{PtO}_2$ ),<sup>284</sup> therefore promoting the oxidation of electroactive species. As shown in Figure 3.13b, the onset oxidation potential of DBAE is shifted from 1.10 V to 0.75 V vs Ag/AgCl after the addition of  $\text{NaNO}_3$ .

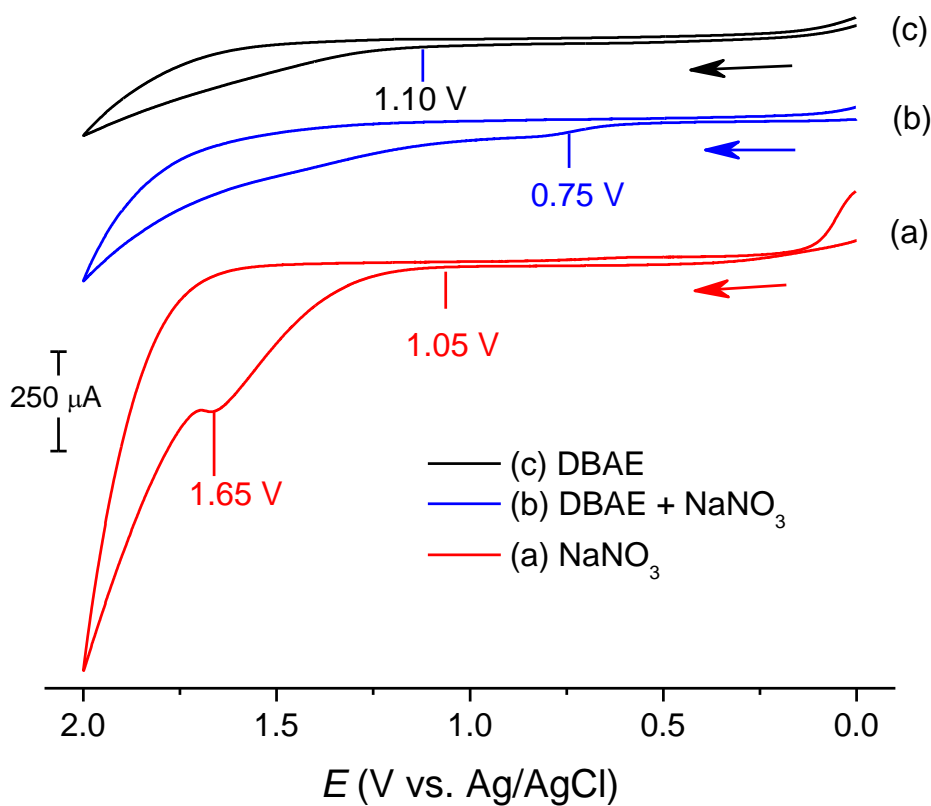


Figure 3.13 CVs of (a)  $\text{NaNO}_3$ , (b) DBAE- $\text{NaNO}_3$ , and (c) DBAE.

Note: (a) CV measurements were conducted in 0.10 M PBS (pH 7.5) containing (a) 10 mM  $\text{NaNO}_3$ , (b) 25.0 mM DBAE and 10.0 mM  $\text{NaNO}_3$ , and (c) 25.0 mM DBAE at a 2-mm diameter Pt electrode with a scan rate of 100 mV/s.

The electrochemical oxidation of  $\text{NaNO}_3$  starts at  $\sim 1.05$  V with an anodic peak potential of  $\sim 1.65$  V vs Ag/AgCl (Figure 3.13c), which matches the ECL generation window of the DPAS/DBAE as well as SRUB/DBAE system. As will be discussed in detail later, the ECL enhancement originates from the electrochemical oxidation of nitrate ions.

Figure 3.14 illustrates the effect of  $[\text{NaNO}_3]$  on the ECL enhancement. With the increase of  $[\text{NaNO}_3]$  from 0 to 8.0 mM, the ECL intensity for the DPAS/DBAE as well as the SRUB/DBAE system increases gradually. After  $[\text{NaNO}_3]$  reaches 9.0 mM, the enhancement levels off. Notice also that the effect of ECL enhancement by  $\text{NaNO}_3$  is more significant towards the SRUB/DBAE system than the DPAS/DBAE system.

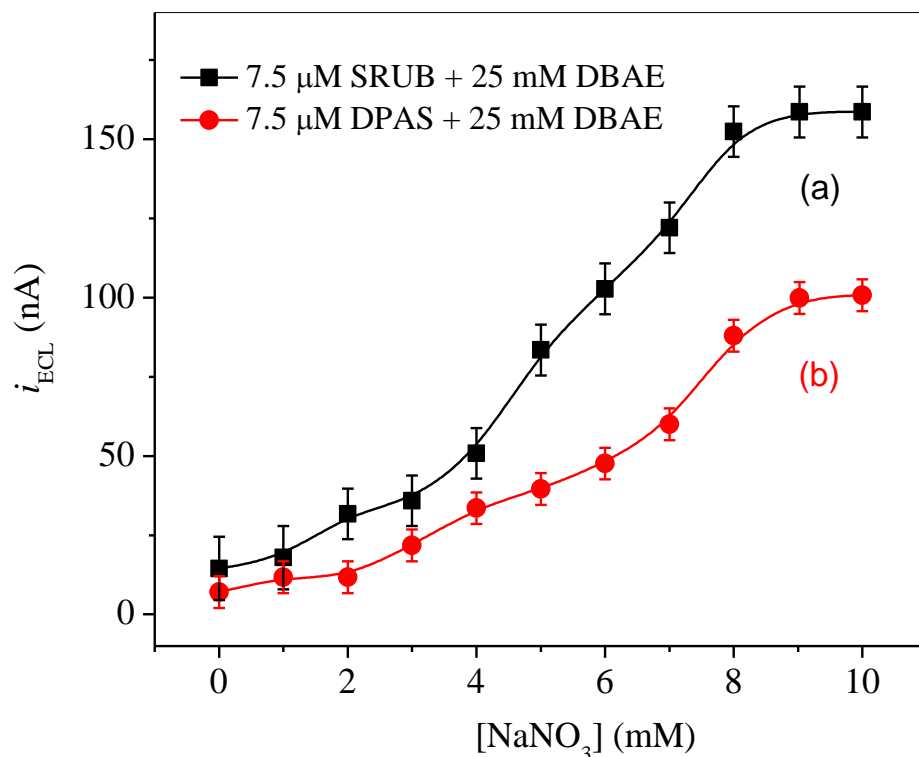


Figure 3.14 Effect of  $[\text{NaNO}_3]$  on the ECL enhancement of (a) SRUB/DBAE and (b) DPAS/DBAE system.

Note: ECL intensity at peak was used and other experimental conditions were the same as listed in Figure 3.9.

The above remarkable ECL enhancement by  $\text{NaNO}_3$  is further testified by the data shown in Figure 3.15, where ECL signals are acquired with the spectral ECL instrument reposted in Chapter II rather than a highly sensitive photodetector photomultiplier tube (PMT). With the addition of  $\text{NaNO}_3$  into the mixed (DPAS- $\text{Ru}(\text{bpy})_3^{2+}$ )/DBAE system, quantification of originally undetectable ECL signals is realized.

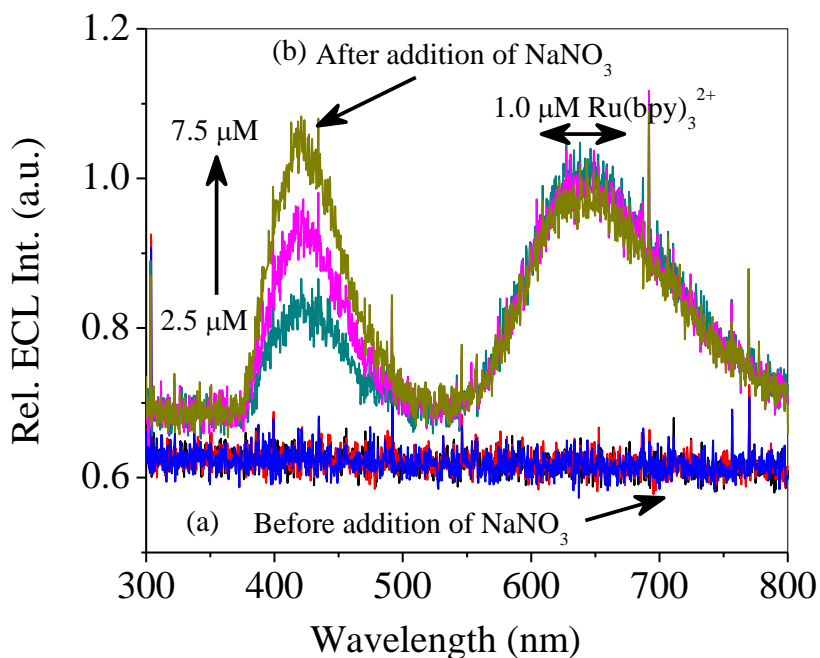


Figure 3.15 Demonstration of ECL enhancement by  $\text{NaNO}_3$  using the mixed (DPAS- $\text{Ru}(\text{bpy})_3^{2+}$ )/DBAE system.

Note: (a) ECL spectra of [DPAS] from 2.5 to 7.5  $\mu\text{M}$ , mixed with a constant  $[\text{Ru}(\text{bpy})_3^{2+}]$  of 1.0  $\mu\text{M}$ , and (b) ECL spectra obtained after addition of 10.0 mM  $\text{NaNO}_3$  to solutions described in (a). All data were collected from the homemade spectral ECL instrument with a linear sweep voltammetry from 0 to 2.0 V vs Ag/AgCl at 100 mV/s.

Previously,<sup>281</sup>  $\text{AgNO}_3$  was used as an ECL enhancing agent in MeCN, and both  $\text{Ag}^+$  and  $\text{NO}_3^-$  ions were found to be responsible for ECL enhancement. In the present study, however,  $\text{AgNO}_3$  cannot be used because  $\text{Ag}^+$  ion can react with phosphate buffer to form silver precipitates. To verify if the cations of nitrate salts would play any role during the process of ECL enhancement, nitrate salts with various cations M ( $\text{M} = \text{Li}^+$ ,  $\text{Na}^+$ ,  $\text{K}^+$ , and  $\text{NH}_4^+$ ) were added to a well-understood  $\text{Ru}(\text{bpy})_3^{2+}$ /DBAE system. The resultant ECL profiles are shown in Figure 3.16, suggesting that nitrate ion is solely

responsible for the ECL enhancement. Compared with data shown in Figure 3.12, ECL profiles of the  $\text{Ru}(\text{bpy})_3^{2+}/\text{DBAE-MNO}_3$  system are extended to a much broad potential range with a clear pre-enhancement feature. This broadening effect is consistent with the electrochemical oxidation behavior of  $\text{NaNO}_3$  (Figure 3.13a), and is probably an indication of  $\text{R}^{\bullet-}$  stability in the solution (see Scheme 3.4 for details). In other words, the anion radicals of the three tested ECL emitters follow a stability order of  $\text{Ru}(\text{bpy})_3^+ > \text{SRUB}^{\bullet-} > \text{DPAS}^{\bullet-}$ .

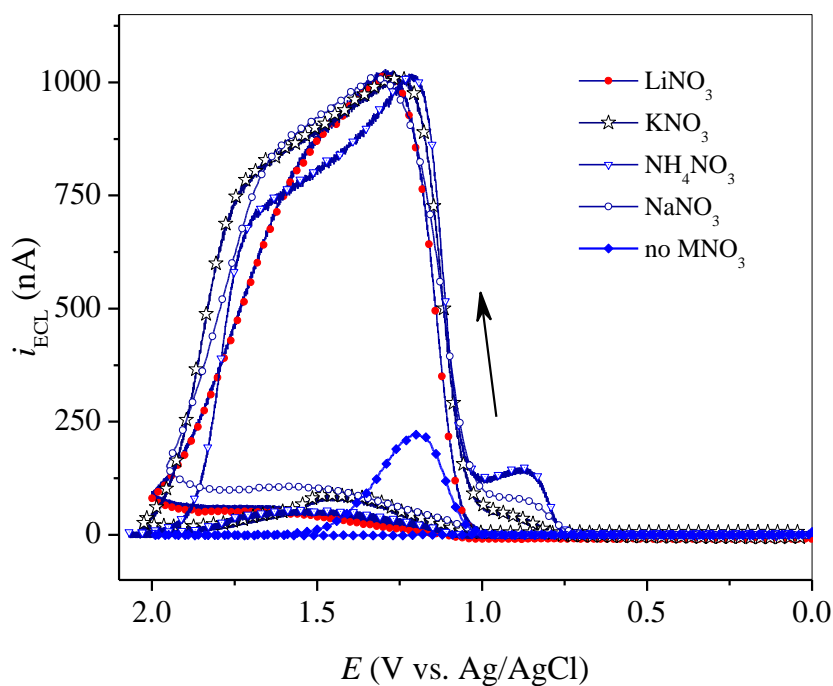
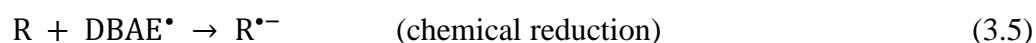


Figure 3.16 Effect of different nitrate salts on the ECL enhancement of the  $\text{Ru}(\text{bpy})_3^{2+}/\text{DBAE}$  system.

Note: ECL measurements were conducted in 0.10 M PBS buffer (pH 7.5) containing  $7.5 \mu\text{M}$   $\text{Ru}(\text{bpy})_3^{2+}$  and 25.0 mM DBAE in the absence and presence of 10.0 mM of  $\text{LiNO}_3$ ,  $\text{KNO}_3$ ,  $\text{NH}_4\text{NO}_3$ , and  $\text{NaNO}_3$  at a 2-mm diameter Pt electrode with a scan rate 100 mV/s.

On the basis of the data presented above and previous studies,<sup>281,285-287</sup> it is believed that the significant ECL enhancement of the R/DBAE system with nitrate ions is associate with the chemical oxidation reactions of nitrate free radical ( $\text{NO}_3^\bullet$ ) generated electrochemically (Equation 3.10) with the ECL emitter R (Equation 3.11), coreactant DBAE (Equation 3.12), and  $\text{R}^{\bullet-}$  (Equation 3.13), forming species that are crucial for ECL emissions. The  $\text{NO}_3^\bullet/\text{NO}_3^-$  couple has an estimated standard redox potential of  $\sim 1.80$  V vs Ag/AgCl,<sup>39</sup> which is consistent with the oxidation peak potential of 1.65 V vs Ag/AgCl for  $\text{NaNO}_3$  in aqueous media (Figure 3.13a) and that of  $\sim 1.63$ -1.9 V vs Ag/AgCl for  $\text{NO}_3^-$  in MeCN.<sup>285-287</sup> Scheme 3.4 is the proposed ECL mechanism of the R/DBAE- $\text{NO}_3^-$  system using DBAE as an anodic ECL coreactant and  $\text{NO}_3^-$  as an ECL enhancing agent, where Equations 3.10-3.13 are highlighted and contributed to the ECL enhancement.



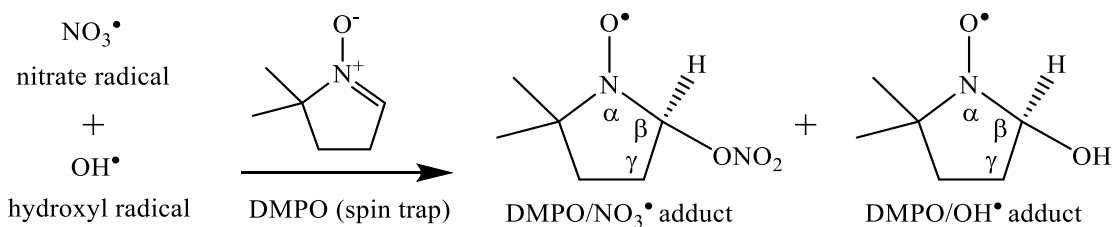


Scheme 3.4 Proposed ECL mechanism of the R/DBAE-NO<sub>3</sub><sup>-</sup> system using DBAE as an anodic ECL coreactant and NO<sub>3</sub><sup>-</sup> as an ECL enhancing agent.

### 3.4.5 Direct EPR Evidence of Nitrate Free Radical (NO<sub>3</sub><sup>•</sup>)

To verify if nitrate free radical exists in the chemical environment similar to the ECL media, EPR spectroscopy of potassium nitrate was performed in an aqueous solution. The use of a regular quartz EPR tube is not appropriate because the heating of the aqueous solution by microwave resulting in the tuning of the EPR instrument to be difficult. Consequently, a small glass capillary tube was used to hold the test solution. Although photolysis of nitrate can involve a series of complicated reactions,<sup>288-290</sup> both NO<sub>3</sub><sup>•</sup> and OH<sup>•</sup> free radicals are expected to form first before they are caught by spin trapping agent DMPO (Equations 3.14-18). The EPR signals are produced from the respective stable DMPO/radical adducts, whose chemical structures are shown in Scheme 3.5.





Scheme 3.5 Formation of  $\text{DMPO/NO}_3^\bullet$  and  $\text{DMPO/OH}^\bullet$  adducts.

Figure 3.17 shows the experimental and simulated EPR spectra of aqueous  $\text{KNO}_3$  mixed with DMPO under UV irradiation. The reason to choose  $\text{KNO}_3$  instead of  $\text{NaNO}_3$  was because  $\text{KNO}_3$  had higher purity than  $\text{NaNO}_3$ , thus potential impurity interfaces to EPR production were minimized. The experimentally obtained EPR spectra (Figure 3.17a) consist of peaks from two types of DMPO/radical adducts, where peaks labelled with “\*” are from  $\text{DMPO/OH}^\bullet$  radicals and ones with “&” labeling are from  $\text{DMPO/NO}_3^\bullet$  radicals. These assignments are supported by EPR simulations presented in Figures 3.17c and d, respectively, using Winsim software. Although  $\text{DMPO/OH}^\bullet$  EPR spectra have been widely reported,<sup>288,291-296</sup> no EPR spectra on  $\text{DMPO/NO}_3^\bullet$  radicals is found. For  $\text{DMPO/OH}^\bullet$  simulation, the hyperfine coupling of the unpaired electron with the  $\alpha$ -N nucleus and  $\beta$ -H nucleus was considered. The same coupling constants ( $a^{\text{N}} = 14.85$  G and  $a_{\beta}^{\text{H}} = 14.85$  G) taken from a previously published paper of this research group on hydroxyl radical EPR were used.<sup>281</sup> For  $\text{DMPO/NO}_3^\bullet$  simulation, in addition to the

coupling between the unpaired electron and the  $\alpha$ -N nucleus ( $a^N = 14.85$  G), contributions from the  $\beta$ -H with two possible conformation sites are included.<sup>293</sup> These two sites in chemical exchange should have close hyperfine coupling constants as found out during the optimization of simulation ( $a_{\beta}^{H1} = 13.85$  G and  $a_{\beta}^{H2} = 13.70$  G). The combination of the above two simulated EPR spectra is illustrated in Figure 3.17b, which matches well with the experimentally obtained one (Figure 3.17a).

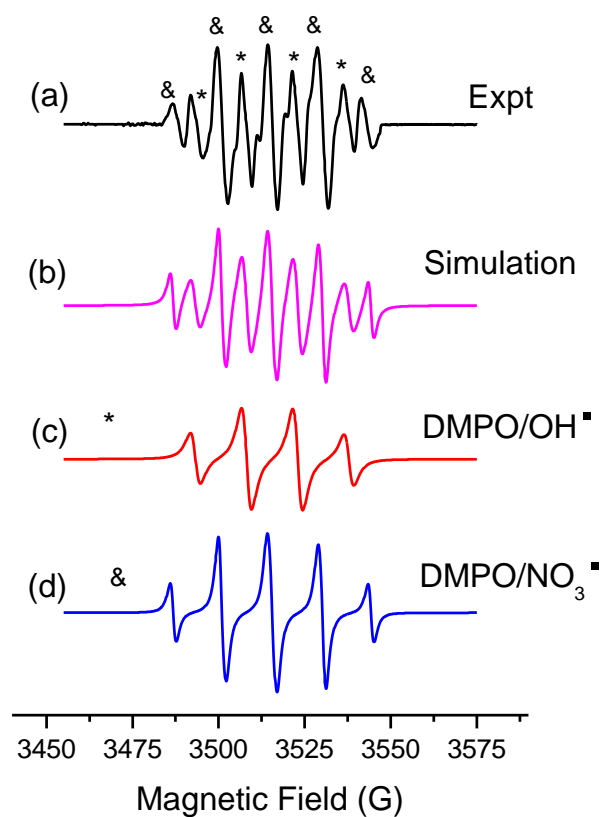


Figure 3.17 Experimental and simulated EPR spectra for nitrate mixed with DMPO in water under UV irradiation.

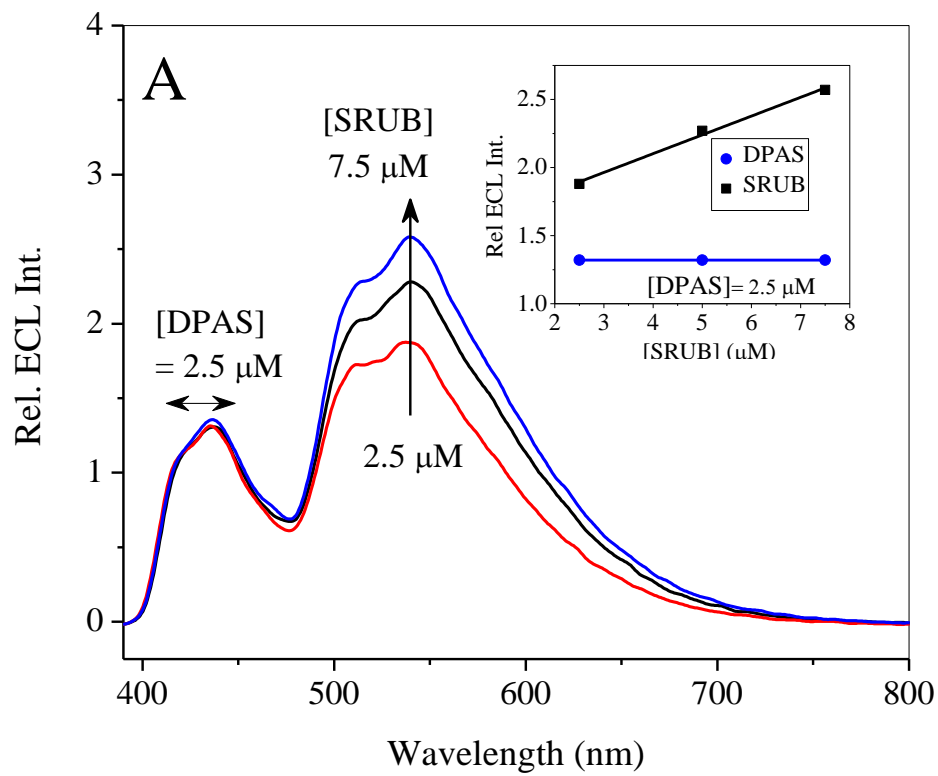
Note: EPR spectra were obtained from UV irradiation of 0.10 M  $\text{KNO}_3$  with 200 mM 5,5'-dimethyl pyrroline-*N*-oxide (DMPO as spin trap) in aqueous media, using a resonant frequency of 9.86 GHz, a modulation frequency of 100 kHz, a microwave power of 2.697 mW, and a time constant of 32 ms. The EPR spectra were the collection of 4 consecutive scans. (a) Experimental, (b) overall simulation, (c) simulation of  $\text{DMPO/OH}^\bullet$ , and (d) simulation of  $\text{DMPO/NO}_3^\bullet$ . The following hyperfine coupling constants were used: for (c)  $a^{\text{N}} = 14.85$  G and  $a_{\beta}^{\text{H}} = 14.85$  G, and for (d)  $a^{\text{N}} = 14.85$  G,  $a_{\beta}^{\text{H1}} = 13.85$  G, and  $a_{\beta}^{\text{H2}} = 13.70$  G.

EPR spectra from solid sodium nitrate irradiated with X or  $\gamma$  rays have been previously reported.<sup>297</sup>

### 3.4.6 ECL Studies of Mixed Systems of DPAS, SRUB, and Ru(bpy)<sub>3</sub><sup>2+</sup>

ECL titration study was first undertaken to examine possible interactions between DPAS and SRUB, whose ECL emissions are at ~ 420 nm and ~ 550 nm, respectively. Attempts to collect ECL spectra from the binary mixed system of DPAS-SRUB, where the concentration of SRUB was increased while keeping the concentration of DPAS constant, were unsuccessful, because concentrations of DPAS and SRUB larger cannot be larger than 10 μM in sodium phosphate buffer as mentioned in Chapter II. At such low concentrations, ECL spectra were too weak to be recorded. Upon addition of nitrate (10 mM optimal concentration) to the system, ECL spectra immediately became detectable. Figure 3.18A shows the ECL spectra of the (DPAS-SRUB)/DBAE-NO<sub>3</sub><sup>-</sup> system with a constant concentration of DPAS at 2.50 μM mixed with different concentrations of SRUB. With the increase of SRUB concentration, ECL intensity at ~550 nm for SRUB emissions increases as expected. Meanwhile, the ECL intensity at ~420 nm for DPAS remains essentially unchanged. The inset in Figure 3.18A displays the linear responses of ECL intensities with the increase in the concentration of SRUB. This finding suggests that the energy transfer interactions between the two emitters are insignificant at low concentrations, which is different from the cases in Chapter II when higher concentrations of emitters were used.

Figure 3.18B shows the ECL spectral data for the mixed (DPAS-Ru(bpy)<sub>3</sub><sup>2+</sup>)/DBAE-NaNO<sub>3</sub> system, where ECL emissions from DPAS and Ru(bpy)<sub>3</sub><sup>2+</sup> increase with the increase of Ru(bpy)<sub>3</sub><sup>2+</sup> concentration due to the energy transfer interactions as described in Chapter II.



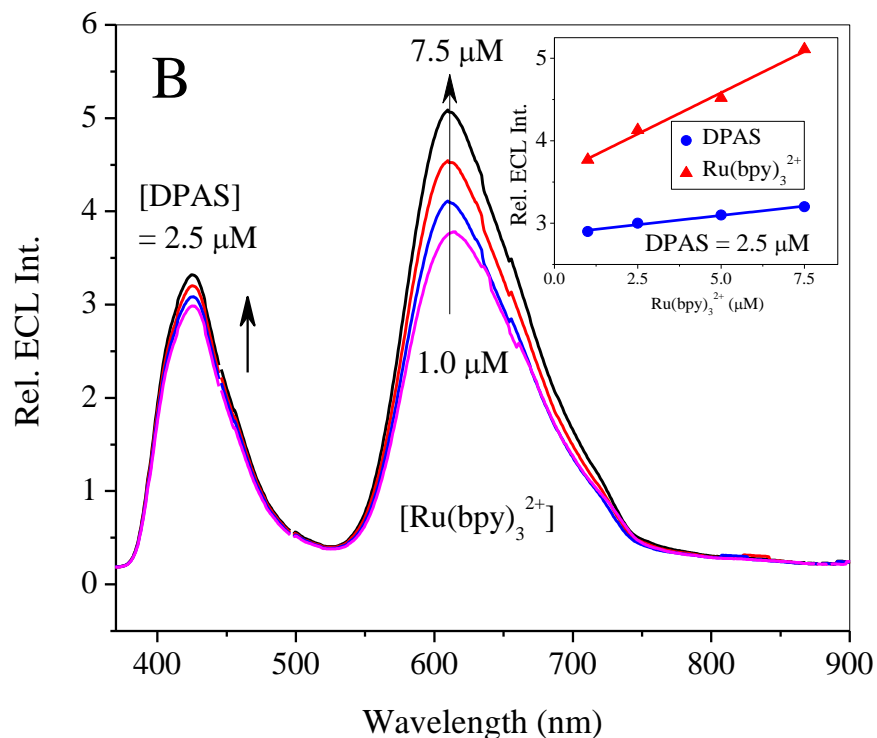
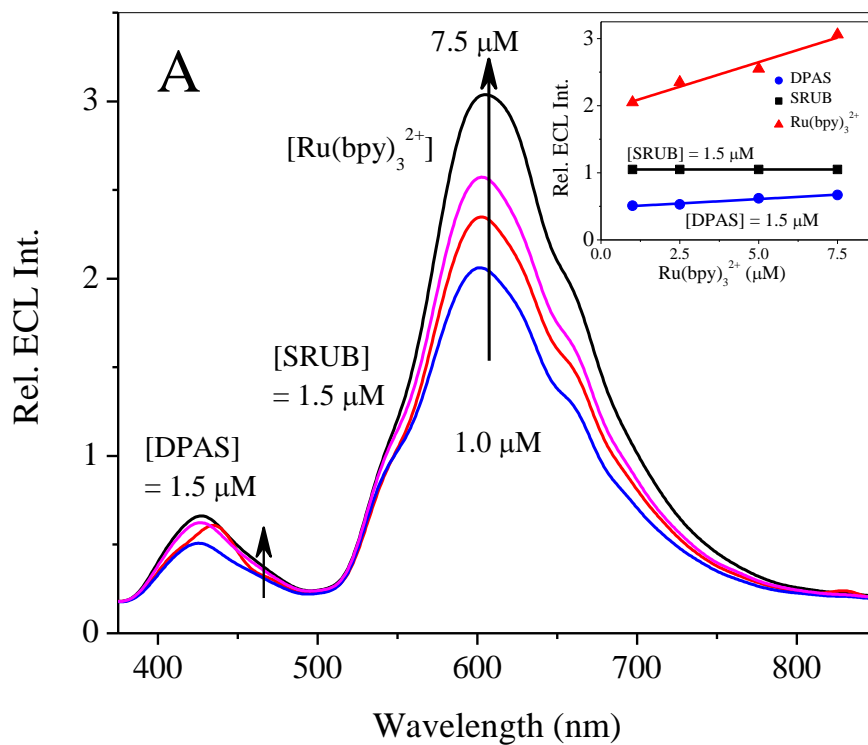


Figure 3.18 ECL spectra of (A) (DPAS-SRUB) /DBAE- $\text{NaNO}_3$  and (B) (DPAS- $\text{Ru}(\text{bpy})_3^{2+}$ )/DBAE- $\text{NaNO}_3$ .

Note: 25.0 mM DBAE as ECL coreactant and 10.0 mM  $\text{NaNO}_3$  as ECL enhancing agent were used. All ECL-intensity measurements were carried out in 0.10 M sodium phosphate buffer (pH 7.5). A 2-mm diameter Pt electrode and a scan rate of 100 mV/s were applied. LN CCD camera was used as detector.

Figure 3.19A shows the ECL spectra of mixed DPAS-SRUB- $\text{Ru}(\text{bpy})_3^{2+}$  system in the presence of 25.0 mM DBAE and 10.0 mM  $\text{NaNO}_3$ . With the increase of  $\text{Ru}(\text{bpy})_3^{2+}$  concentration, ECL intensity of DPAS increases slightly, and the ECL for SRUB remains unchanged as displayed in the inset after spectral deconvolution (see Sections 2.3.5 and 2.3.6 of Chapter II for detail). Figure 3.19B shows the effect of SRUB concentration changes on ECL signal changes of DPAS and  $\text{Ru}(\text{bpy})_3^{2+}$ . In this case, with the increase

of SRUB concentration, ECL signal changes for both DPAS and Ru(bpy)<sub>3</sub><sup>2+</sup> increase due to energy transfer interactions.



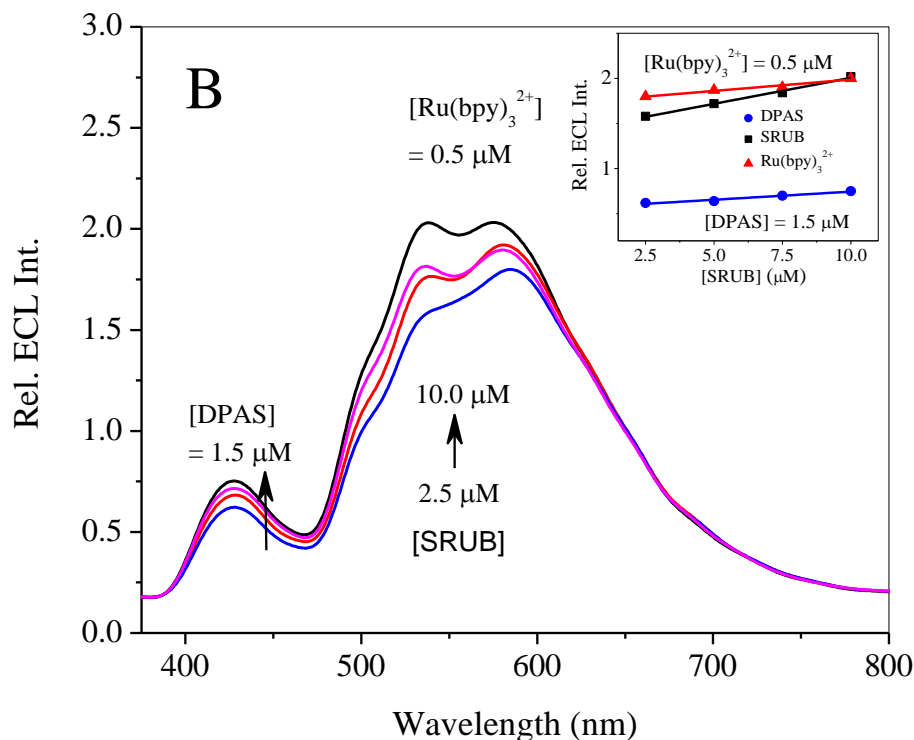


Figure 3.19 ECL spectra (DPAS-SRUB-Ru(bpy)<sub>3</sub><sup>2+</sup>)-NaNO<sub>3</sub>/DBAE with the concentration change of (A) Ru(bpy)<sub>3</sub><sup>2+</sup> and (B) SRUB.

Note: Experiments were carried out with 10.0 mM NaNO<sub>3</sub> as ECL enhancing agent in 0.10 M sodium phosphate buffer, pH 7.5. A 2-mm diameter Pt electrode and a scan rate of 100 mV/s were applied. LN CCD camera was used as detector.

### 3.5 Conclusion

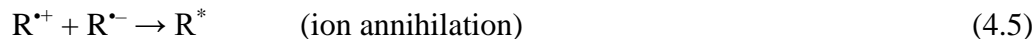
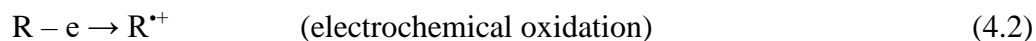
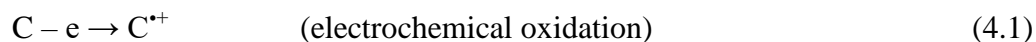
Water soluble analogues of DPA and RUB, i.e., DPAS and SRUB, were synthesized and characterized by electrochemical and ECL studies. The CV and ECL behavior of both DPAS and SRUB was very similar (in terms of redox potential, ECL emission wavelength, ECL generation potential window, etc.) to that of their precursors DPA and RUB. The weak ECL emissions of both DPAS and SRUB with DBAE as

anodic ECL coreactant were enhanced with nitrate salt. More than 10 times enhancement in ECL intensity was found for all three ECL emitters when 10.0 mM NaNO<sub>3</sub> was used. This effect was believed to be ascribed to the formation of NO<sub>3</sub><sup>•</sup> free radical, which was confirmed by EPR spectra obtained from solution phase KNO<sub>3</sub> under UV irradiation in the presence of DMPO as spin trapping agent. Finally, ECL responses from mixed ECL emitter systems were studied, where energy transfer interactions occurred, although such effects may be insignificant at a much lower concentration range.

CHAPTER IV – DIRECT ELECTRON PARAMAGNETIC RESONANCE EVIDENCE  
OF CATHODIC ECL COREACTANT INTERMEDIATES OF BENZOYL PEROXIDE  
AND AMMONIUM PERSULFATE

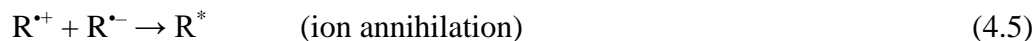
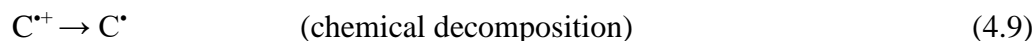
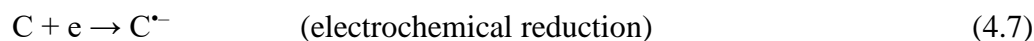
#### 4.1 Introduction

Coreactant electrogenerated chemiluminescence (ECL) is a type of ECL that is generated from an ECL emitter (R) mixed with a deliberately added chemical termed “coreactant” (C) upon anodic or cathodic potential scanning.<sup>72,81</sup> For anodic coreactant ECL (Scheme 4.1), C along with R is first electrochemically oxidized to form  $C^{*+}$  and  $R^{*+}$ , which is immediately followed by a homogeneous chemical dissociation that converts  $C^{*+}$  to a strongly reducing agent  $C^{\bullet}$  free radical.  $C^{\bullet}$  then chemically reduces R to  $R^{\bullet-}$ . Finally,  $R^{*+}$  annihilates with  $R^{\bullet-}$  to produce the excited state  $R^*$  that emits light.



Scheme 4.1 A general ECL mechanism of an anodic ECL system with R served as an ECL emitter and C as a coreactant.

On the other hand, for cathodic coreactant ECL (Scheme 4.2), C along with R is first electrochemically reduced to form  $C^{\bullet-}$  and  $R^{\bullet-}$ , which is immediately followed by a homogeneous chemical decomposition reaction that converts  $C^{\bullet-}$  to a strongly oxidizing agent  $C^{\bullet+}$  free radical.  $C^{\bullet+}$  then chemically oxidizes R to  $R^{\bullet+}$ . Finally,  $R^{\bullet+}$  annihilates with  $R^{\bullet-}$  to produce the excited state  $R^*$  that emits light.



Scheme 4.2 A general ECL mechanism of a cathodic ECL system with R served as an ECL emitter and C as a coreactant.

Examples of commonly used R include 9,10-diphenylanthracene (DPA), rubrene (RUB),  $\text{Ru}(\text{bpy})_3^{2+}$ , and their derivatives. Two commonly used anodic coreactants C are tri-*n*-propylamine (TPrA) and 2-(dibutylamino)ethanol (DBAE), and benzoyl peroxide ( $\text{C}_6\text{H}_5\text{COOCC}_6\text{H}_5$  or BPO) and persulfate ( $\text{S}_2\text{O}_8^{2-}$ ) are examples of two cathodic ECL coreactants. Coreactant ECL has been well studied and widely used in chemical and biochemical analysis. The proposed ECL mechanism is also broadly accepted; however, very limited experimental evidence in the literature that directly show the presence of

coreactant intermediates (i.e.,  $C^{*+}$ ,  $C^{*-}$ , or  $C^*$ ). This is probably because these cation, anion, or neutral free radicals are short-lived, unstable, and very reactive, which is supported by the fact that cyclic voltammetric responses of these coreactants only show irreversible behavior, even at a very fast scan rate ( $v = 5000$  mV/s).

Given the fact that all aforementioned coreactant intermediates have unpaired electrons, electron paramagnetic resonance (EPR) spectroscopy or electron spin resonance (ESR) spectroscopy could be a powerful technique to probe these species. EPR measures the absorption of electromagnetic radiation with a wavelength in microwave region (in the order of a few cm) by a sample with unpaired electron under an external magnetic field. Unlike NMR, where nuclear spins are excited, in EPR the electron spins are excited. EPR spectra is a display of the first order differentiation or derivative of absorbance. Experimentally, EPR spectrum is often measured by holding microwave frequency constant while sweeping the magnetic field, and the power absorbed is acquired as a function of the applied magnetic field.

EPR has been used to study a variety of reactive oxygen species (ROS) including peroxides, superoxide, hydroxyl radical, and singlet oxygen as well as reactive nitrogen species (RNS)<sup>298-300</sup>. EPR spectroscopy has been applied for online monitoring of species of environmental concerns,<sup>301-305</sup> thermally generated radicals,<sup>306</sup> polymers,<sup>307</sup> proteomics and genome-wise expression studies,<sup>308</sup> transition-metal proteins (metalloproteins),<sup>309-314</sup> bio-medical, clinical and pharmaceutical applications,<sup>315-318</sup> DNA-metal complex interactions, biologically relevant free radicals in cellular, ex vivo, and in vivo systems.<sup>319-322</sup>

Previously, EPR evidence of  $\text{TPrA}^{\bullet+}$ , the radical cation intermediate formed after TPrA oxidation, was reported.<sup>216</sup> Reports<sup>323,324</sup> on BPO generating  $\text{BPO}^{\bullet}$  (i.e., benzoyloxyl radical  $\text{C}_6\text{H}_5\text{COO}^{\bullet}$ ) in solid state are also available. In this chapter, EPR data of cathodic coreactant intermediates  $\text{BPO}^{\bullet}$  radical generated from BPO and  $\text{SO}_4^{\bullet-}$  anion radical generated from persulfate ( $\text{S}_2\text{O}_8^{2-}$ ) are presented. The electrochemical and chemical reaction pathways of generating  $\text{BPO}^{\bullet}$  from BPO at electrode surface have been described in Scheme 2.1 in Chapter II. Moreover, BPO yielded the strongest ECL emission in comparison to TPrA and DBAE when mixed with ECL emitter DPA, RUB, or  $\text{Ru}(\text{bpy})_3^{2+}$  (Chapter II). BPO and persulfate have similar ECL mechanisms and both contain common ECL peroxide linkage moiety (-O-O-), allowing one to generate their intermediates using similar strategy.

## 4.2 Experimental Section

### 4.2.1 Chemicals and materials

Benzoyl peroxide (BPO,  $\text{C}_{14}\text{H}_{10}\text{O}_4$ , 97%) was purchased from Aldrich. Ammonium persulfate or ammonium peroxydisulfate ( $(\text{NH}_4)_2\text{S}_2\text{O}_8$ , 98%) was obtained from Fluka. Hydrazine hydrate ( $\text{N}_2\text{H}_4$ ), acetonitrile (HPLC grade), 5,5-dimethyl-1-pyrroline-*N*-oxide (DMPO,  $\geq 98\%$ ) were obtained from Cayman Chemical (Ann arbor, MI). For measuring organic samples, a thin quartz EPR tube with outer diameter (OD) 4.0 mm, inner diameter (ID) 3.0 mm, wall thickness 0.5 mm, and 250 mm long from Wilmad Lab Glass (PA) was used. For measuring EPR spectra in water, a standard glass capillary (100 mm long, 2/0.5, OD/ID (mm), World Precision Instruments, Inc., Sarasota, FL) was utilized.

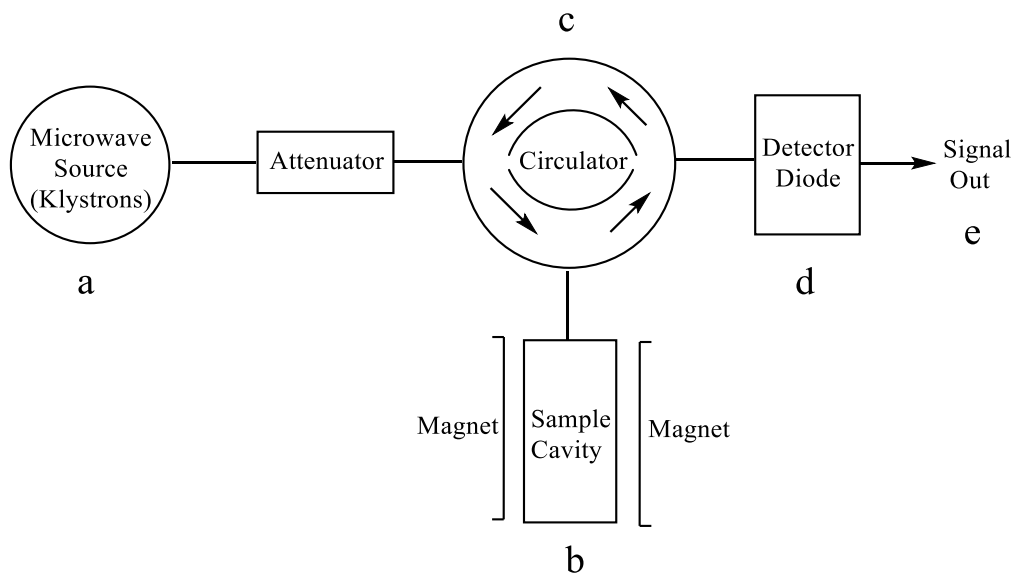


Figure 4.1 Block diagram of EPR instrumentation.

Note: (a) Microwave radiation source (klystrons or gun oscillator), (b) sample cell, (c) d.c. magnetic field and a sweeping circuit for changing the magnetic field, (d) detection system, and (e) data acquisition.

The block diagram of EPR instrumentation is shown in Figure 4.1. The experimental setup consists of (a) microwave radiation source (klystrons or gun oscillator) that provides a power output of about 300 mW holding the frequency constant, (b) a sample cell placed in the cavity where the microwave is transmitted through waveguide to convey the wave radiation to the sample, (c) a d.c. magnetic field and a sweeping circuit for changing the magnetic field., (d) a detection system (basically a rectifier crystal) for measuring the absorption, and (e) a data acquisition and a phase sensitive signal processing unit.

#### 4.2.2 EPR parameters and acquisition

EPR spectroscopy was performed with a Bruker EMX microX EPR spectrometer equipped with an ER 4119HS standard cylindrical resonator (Bruker BioSpin Corp.). Pre-

calibration was done using the manufacturer's 2,2-diphenyl-1-picrylhydrazyl (DPPH), 1,3-bisdiphenylene-2-phenylallyl (BDPA), and weak pitch standard calibration samples. Unless otherwise stated, all the EPR measurements were conducted at room temperature  $20 \pm 2$  °C.

#### 4.2.3 Spin labels (traps)

When the free radical or the molecule with unpaired electron is very unstable or has a very short life (order of nano to pico second), then a spin trap (label) is used. Spin traps are organic molecules having unpaired electrons. Most common spin traps are the class of nitrones (Figure 4.2) and have the ability to bind to the molecule (EPR inactive) and convert them to EPR active forming spin trap/ molecule adduct.

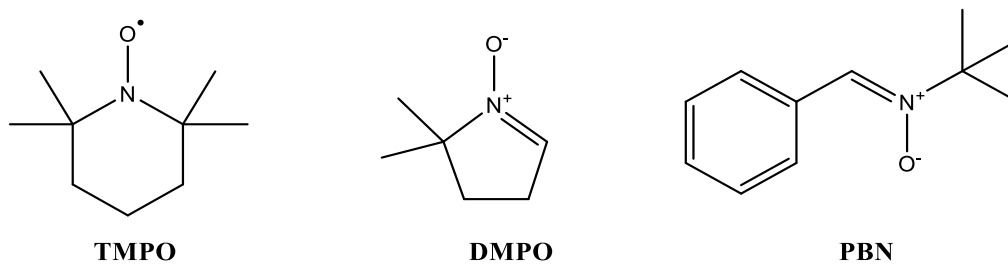
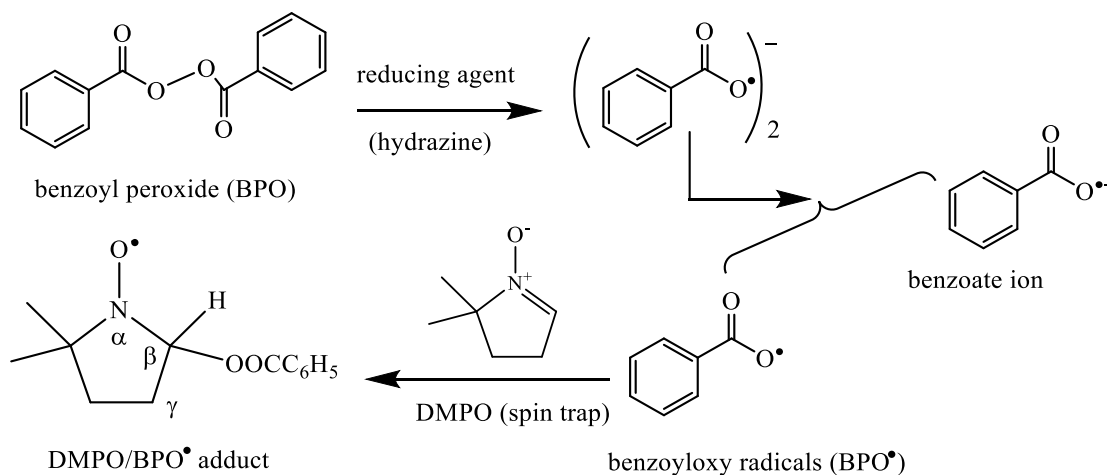


Figure 4.2 Chemical structures of common nitroxide spin labels (traps).

Note: TMPO = (3,3,5,5-tetramethyl-1-pyrroline-1-oxide), DMPO = (5,5-dimethyl-1-pyrroline *N*-oxide), and PBN = alpha-phenyl *N*-tertiary-butyl nitron.

## 4.3 Results and Disussion

### 4.3.1 Measurement of EPR spectra of benzoyloxy free radical (BPO• or PhCO<sub>2</sub>•)



Scheme 4.3 Formation of benzoyloxy radical (BPO•) by chemically reducing BPO with hydrazine, followed by spin trapping with DMPO.

As shown in Scheme 4.3, BPO is reduced by hydrazine to  $(\text{PhC(O)O})_2^{2-}$  that further decomposes to benzoyloxy radical (BPO•) and  $\text{PhC(O)O}^-$ . Finally, BPO• reacts with the spin trapping agent DMPO to form EPR active DMPO/BPO• adduct. The EPR spectra of such a system is shown in Figure 4.3, where (a) is the experimentally obtained spectra, and (b) is the simulation of (a). Considering the adduct structure (Scheme 4.3), the unpaired electrode could couple with  $\alpha$ -N,  $\beta$ -H (two possible conformation sites),<sup>293</sup> and 2  $\gamma$ -H.<sup>292</sup> The simulated EPR spectra (Figure 4.3b) essentially matches the experimental one. The simulated EPR spectra of hydroxyl radical (Figure 4.3c) does not match the experimental one, especially the first peak at  $\sim 3485$  G, suggesting that no significant hydroxyl radical is formed under current experimental conditions. This is easily understood, because in the reaction media, the initial concentration ratio of

DMPO/BPO was 20, and newly produced BPO<sup>•</sup> free radicals were immediately caught by DMPO, so that no free BPO<sup>•</sup> was left for water oxidation and OH<sup>•</sup> free radical production.

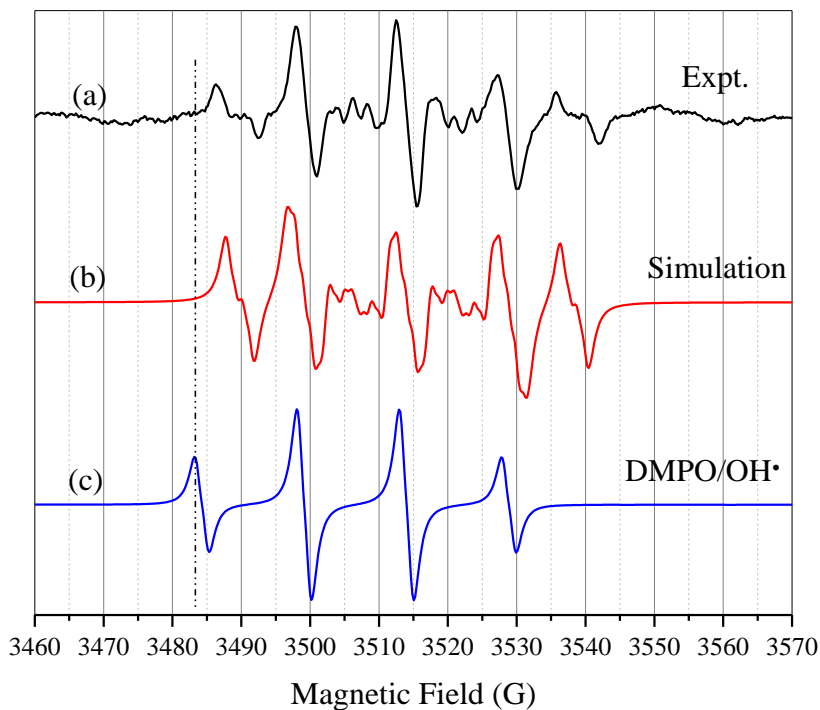


Figure 4.3 EPR spectra of DMPO/OOC<sub>6</sub>H<sub>5</sub> adduct.

Note: 10.0 mM BPO was chemically reduced by 75.0  $\mu$ M hydrazine and 200.0 mM DMPO was used as the spin trapping agent in MeCN-H<sub>2</sub>O mixture media. The experimental parameters were: microwave power = 2.69 mW, resonant frequency = 19 GHz, Q value = 8900, time constant = 20.48 ms, Modulation amplitude = 4 G. The EPR spectra was the average of 4 consecutive scans. For simulation of spectra (b),  $a^N = 14.85$  G,  $a_{\beta}^H = 10.00$  G,  $a_{\beta}^{H'} = 8.80$  G,  $a_{\gamma}^{H1} = 2.15$  G, and  $a_{\gamma}^{H2} = 1.00$  G were used. For simulation of DMPO/OH<sup>•</sup> spectra shown in (c).  $aN = a_{\beta}^H = 14.85$  G were used.

Under UV irradiation, solid and solution phase benzoyloxy peroxide radicals are produced as indicated in Equation 4.11.

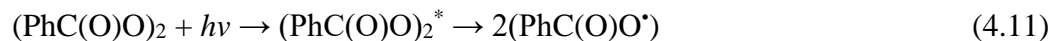
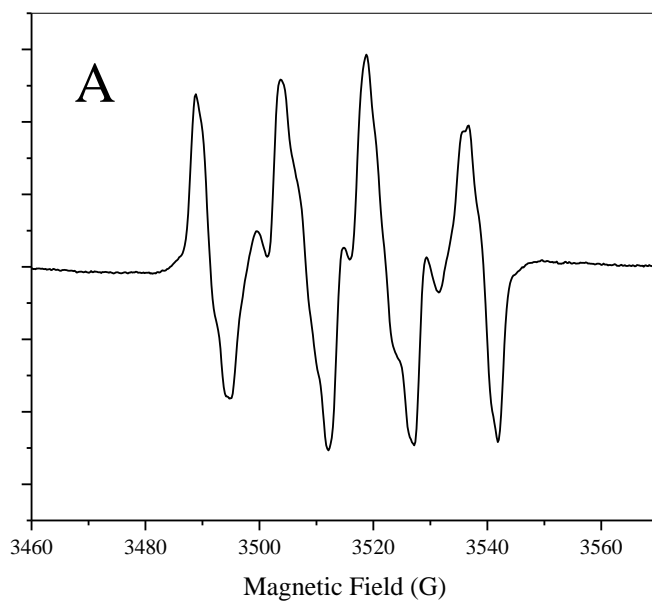


Figure 4.4A shows the EPR spectra from solid BPO without DMPO using UV irradiation. Simulations of these spectra were found to be challenging and further investigations are needed.

When solid BPO was mixed with a drop of 200 mM DMPO, and undertaken irradiation of UV, the obtained EPR spectra (Figure 4.4B) were found to be very similar to those resulted from the chemical reactions of BPO and hydrazine (Figure 4.3a), confirming that the same radical (i.e.,  $\text{BPO}\cdot$ ) was produced from the two-different means. Again, in Figure 4.4B, DMPO/ $\text{OH}\cdot$  adduct seems to be not present.



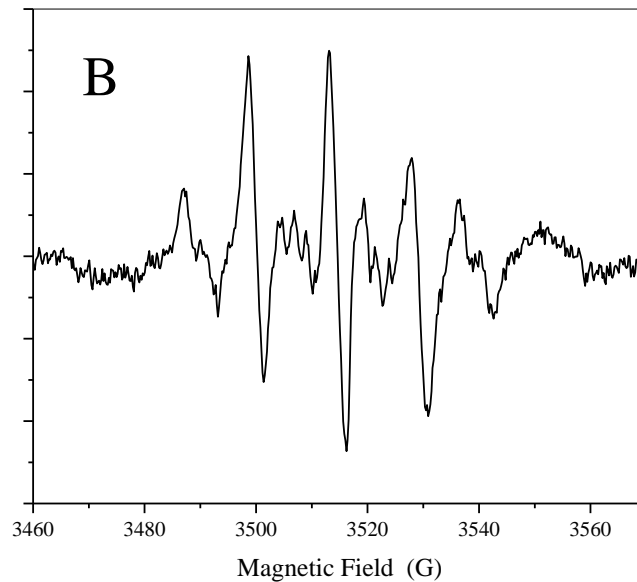


Figure 4.4 EPR spectra obtained from (A) solid BPO without DMPO under UV irradiation, and (B) solid BPO mixed with a drop of 200 mM DMPO solution under UV irradiation.

Note: EPR experimental parameters were the same as in Figure 4.4.

#### 4.3.2 Measurement of EPR spectra of sulfate anion radical ( $\text{SO}_4^{\cdot-}$ )

Under UV irradiation, solid or solution phase persulfate forms sulfate anion radical ( $\text{SO}_4^{\cdot-}$ ), which further reacts with the added DMPO to produce EPR active adduct (Equations 4.12-13).



Persulfate anion radical can also be produced through chemical reactions between persulfate and hydrazine (Equation 4.14).

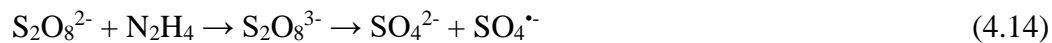
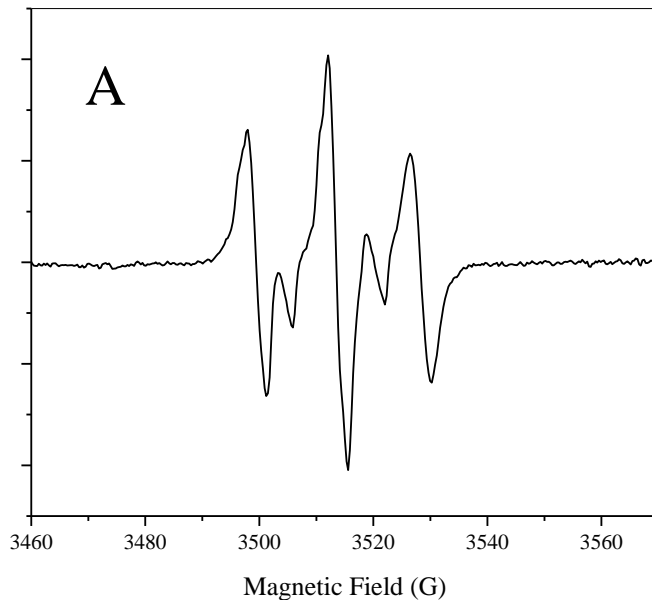


Figure 4.5A shows the EPR spectra of solid persulfate with DMPO under UV irradiation and Figure 4.5B shows solution phase EPR spectra of persulfate in water with hydrazine and DMPO in the absence of UV irradiation. Clearly, many more EPR signals are present in the second case, which probably due to the existence of DMPO/OH<sup>•</sup> adduct formed from the following reaction (Equation 4.15).<sup>325</sup>



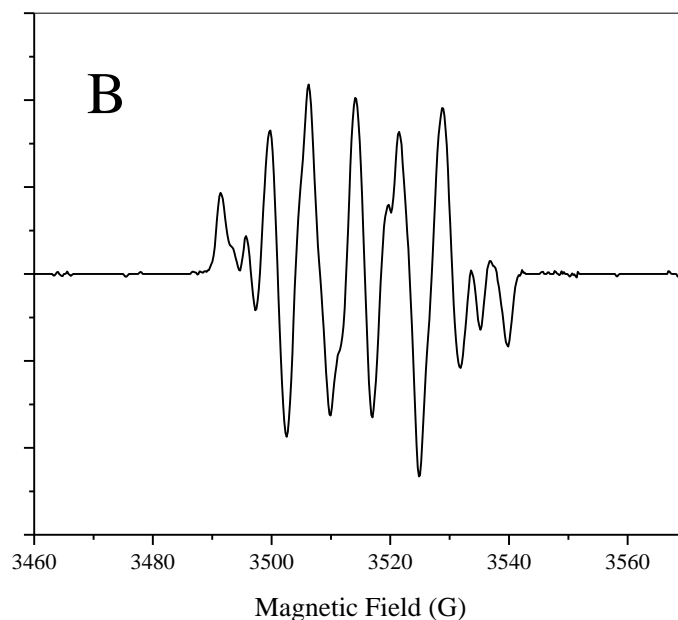


Figure 4.5 EPR spectra of (A) solid persulfate with DMPO under UV irradiation, and (B) persulfate in water with hydrazine and DMPO without UV irradiation.

Note: (A) EPR spectra were obtained with a resonant frequency of 9.87 GHz, a modulation frequency of 100 kHz, microwave power of 9.93 mW, and time constant of 327.68 ms. The concentrations of ammonium persulfate and DMPO were 10 mM and 200 mM, respectively. (B) EPR spectra were obtained with a resonant frequency of 9.87 GHz, attenuation 10 dB, a modulation frequency of 100 kHz, microwave power of 18.97 mW, and time constant of 20.48 ms. The concentrations of ammonium persulfate, hydrazine, and DMPO were 10 mM, 75  $\mu$ M, and 200 mM, respectively. The EPR spectra is the collection of 4 consecutive scans. The EPR spectra is the collection of 4 consecutive scans.

#### 4.4 Conclusion

The free radical intermediates of cathodic coreactants such as ammonium persulfate and BPO generates sulfate anion radical ( $\text{SO}_4^{\cdot-}$ ) and benzoyloxy free radicals ( $\text{C}_6\text{H}_5\text{CO}_2^{\cdot}$  or  $\text{BPO}^{\cdot}$ ) after electrochemical reduction of the coreactants in aqueous and acetonitrile respectively. The direct EPR evidence of such free radical intermediates

generated was mimicked by reducing these ECL coreactants chemically by hydrazine as the reducing agent and DMPO as the spin trapping agent. Both DMPO (as spin trap) and hydrazine (as reducing agent) respectively are needed to obtain the EPR spectrum  $C_6H_5CO_2^{\bullet}$  or  $BPO^{\bullet}$  in solution phase in MeCN solvent. Whereas neither the spin trap nor the reducing agent are needed to obtain EPR spectrum of solid BPO which just needed UV irradiation. The EPR spectra obtained from solid phase (with and without UV irradiation) are very similar. For solution phase BPO in MeCN-H<sub>2</sub>O mixed solvent, it is easy to tune the system in capillary tube rather than using the regular quartz EPR tube. The EPR spectra of persulfate radical anion in aqueous medium using hydrazine as the reducing agent and DMPO as the spin trapping agent as well as solid phase with UV irradiation with DMPO spin trapping were collected and interpreted. For solution phase persulfate in aqueous medium, it was easy to tune the system in capillary tube and could not be tuned with a regular quartz EPR tube because aqueous solution can be heated by the microwave resulting drift of the signals.

Some EPR spectra presented in this chapter need to be simulated so that identity of the radicals can be confirmed.

CHAPTER V – ULTRASENSITIVE ELECTROGENERATED  
CHEMILUMINESCENCE BASED IMMUNOASSAYS FOR THE DETECTION OF  
ZIKA AND DENGUE VIRUSES<sup>1</sup>

### 5.1 Introduction

Zika virus (ZIKV) is a member of the Flavivirus genus of the Flaviviridae family, which includes other globally important pathogens, such as West Nile (WNV), dengue (DENV), and yellow fever viruses.<sup>326,327</sup> Recent outbreaks of ZIKV have linked this previously neglected virus to the development of severe fetal abnormalities including spontaneous abortion, stillbirth, microcephaly, and Guillain-Barré syndrome (GBS), a neurological disorder.<sup>328</sup> Autochthonous transmission of ZIKV infection has been reported in Asia, Africa, Micronesia, and Latin America with increasing descriptions of travel related cases worldwide.<sup>329-333</sup> Since the *Aedes* species of mosquitoes that transmit ZIKV circulate globally, there is a significant risk of ZIKV spread worldwide.<sup>334,335</sup> Thus, ZIKV is Organization estimated that as many as four million people could have been infected in American countries in 2016.<sup>336</sup> Currently, there is no approved therapy or vaccine against ZIKV.

Dengue virus (DENV), on the other hand, is believed to be a leading cause of illness and death in the tropics and subtropics, where about one-third of the world's population could be at risk for infection, as reported by the Centers for Disease Control and Prevention. There are four serotypes of DENV (i.e., DENV1, DENV2, DENV3, and

---

<sup>1</sup>Part of this work has been published: Acharya, D.; Bastola, P.; Le, L.; Paul, A. M.; Fernandez, E.; Diamond, M. S.; Miao, W.; Bai, F., An ultrasensitive electrogenerated chemiluminescence-based immunoassay for specific detection of Zika virus. *Sci. Rep.* **2016**, *6*, 32227.

DENV4), all of which are transmitted by mosquitoes and could cause up to 400 million people infected each year. Unfortunately, no any vaccines to prevent infection with DENV is currently available.

Similar to DENV, WNV and chikungunya virus (CHIKV), ZIKV infection in humans can result in a range of clinical signs and symptoms including fever, rash, joint pain, and conjunctivitis, which poses a challenge for differential diagnosis of these viral infections as they often are co-transmitted in the same areas.<sup>337,338</sup>

In addition, ZIKV has been detected in semen, urine, and saliva,<sup>339-341</sup> suggesting a potential for transmission through routes other than mosquito bite, such as sexual contact.<sup>342-344</sup> Therefore, a highly sensitive and specific method for detection of ZIKV is urgently needed to facilitate efficient case management, surveillance, and implementation of control programs. Current methods for detection and diagnosis of ZIKV DENV infections include nuclear acid-based assays, such as quantitative polymerase chain reaction (qPCR), and antibody-based assays, such as enzyme-linked immunosorbent assay (ELISA) or neutralization tests.<sup>345-347</sup> Since the conventional nuclear acid-based assays require expensive reagents and instruments, and ELISAs are time consuming and have specificity concerns,<sup>348,349</sup> a rapid and simple-to-use methodology with high sensitivity, reliability, and cost effectiveness is needed.<sup>350,351</sup>

Electrogenerated chemiluminescence (ECL) is a phenomenon of light emission by an excited state of species generated at electrodes that undergoes high-energetic electron-transfer reactions.<sup>113</sup> The emitted light can be measured easily by simple instrumentation,<sup>113,155</sup> thus providing an efficient sensor for rapid and simple-to-use

devices for separation, detection, and quantification of a diverse range of analytes in a small quantity (up to femtomolar scale) of starting sample. Applications of ECL-based detection have been demonstrated successfully in a wide range of immunological and molecular assay systems including clinical diagnosis,<sup>155,163,352</sup> biosensing,<sup>353-355</sup> drug assays,<sup>356</sup> food quality analysis,<sup>357,358</sup> environmental monitoring,<sup>161,359</sup> and forensic chemistry.<sup>360-362</sup> Several strategies have been developed to optimize and amplify ECL detection signals. For example, it has been previously reported that the polystyrene beads (PSBs) could be loaded with several billions of water-insoluble homemade  $\text{Ru}(\text{bpy})_3[\text{B}(\text{C}_6\text{F}_5)_4]_2$  ( $\text{bpy} = 2,2'$ -bipyridine) ECL labels. This step increased the ratio of ECL label to bioanalyte and amplified ECL signals by several order of magnitudes.<sup>155,156</sup> By conjugating ECL label-loaded PSBs with specific antibody or antigen, a highly sensitive detection platform of diverse repertoire of analytes can be achieved.

In this chapter, highly sensitive and specific ECL-based immunoassays for detection and quantification of ZIKV and DENV4 in biological fluids with a limit of detection of 1 plaque-forming unit (PFU) in 100  $\mu\text{L}$  of samples are reported. The rubrene (RUB)/benzoyl peroxide (BPO) system will be our choice of sensing, because it showed the most efficient ECL emissions in MeCN as described in Chapter II. This study provides an essential proof-of-concept that ECL-based immunoassays can be developed for the detection and quantification of viruses.

## **5.2 Experimental**

### **5.2.1 Chemicals and reagents**

Monoclonal antibody (mAb) against ZIKV (ZV2, IgG2c) specifically recognizes the E protein on ZIKV and was generated after immunization of mice with infectious ZIKV.<sup>363</sup> Mouse mAb specific to flaviviruses (4G2) was produced and purified by culturing hybridoma (HB-112, ATCC) as previously described.<sup>364</sup> Carboxylate polystyrene beads (referred as PSB, 10  $\mu\text{m}$  diameter, 2.6% (w/w) aqueous suspension with approximately  $6.5 \times 10^4$  beads  $\mu\text{L}^{-1}$ ) and streptavidin-coated super-paramagnetic polystyrene beads (referred as MB, 1.0  $\mu\text{m}$  diameter, 10 mg  $\text{mL}^{-1}$  aqueous suspension with approximately  $9.5 \times 10^6$  beads  $\mu\text{L}^{-1}$ ) were purchased from PolySciences Inc. and Dynal Biotech Inc., respectively. Other reagents were purchased from either Sigma or other commercial vendors.

### **5.2.2 Preparation and titration of virus stocks**

A recent strain of ZIKV (PRVABC59) was obtained from B. Johnson (CDC Arbovirus Branch, Fort Collins CO). CHIKV (LR-OPY1-2006 strain) was provided by R. Tesh (University of Texas Medical Branch). WNV isolate (CT2741) and the four serotypes of dengue viruses (DENV1, DENV2, DENV3, and DENV4) were provided by J. Anderson (Connecticut Agricultural Experiment Station). WNV, ZIKV, and CHIKV were propagated in African green monkey kidney cells (Vero cells, ATCC CCL-81) and DENV (DENV1, DENV2, DENV3 and DENV4) were propagated in C6/36 *Aedes albopictus* cells. All virus stocks were titered in Vero cells (ATCC CCL-81) by plaque assay as previously described.<sup>365</sup>

### **5.2.3 ECL label loading and avidin conjugation of PSBs.**

Loading of ECL-labels to PSBs was performed as previously described<sup>113,156</sup> with some modifications. Briefly, carboxylated PSBs were loaded with RUB by immersing the beads into a saturated solution of RUB (~0.7 mM) in 5% benzene–95% MeOH (v/v) for 2 h, followed by a series of centrifugation, washing, and drying. Prepared PSBs were designated as PSB(RUB). For avidin conjugation, the PSB(RUB) beads were reacted with a freshly prepared avidin solution (25  $\mu$ M), activated in a 1-methylimidazole-HCl buffer (0.10 M, pH 7.2) containing 0.10 M EDAC and 0.10 M NHS for 1h, followed by centrifugation, washing and re-suspension in PBS buffer (pH 7.2). The final solution containing approximately  $6.5 \times 10^4 \mu\text{L}^{-1}$  of avidin conjugated PSB(RUB) beads was stored at 4 °C until use.

### **5.2.4 Attachment of biotinylated antibodies to the surface of ECL-label loaded PSBs and MBs.**

Biotinylation of antibody was performed as described.<sup>155</sup> Biotinylated antibody was immobilized on the surface of ECL-label loaded PSBs by mixing 400  $\mu$ L of avidin-coated beads with 1.5 mL of biotinylated antibody (0.05 mg/ml) and rotating the mixture in a Dynal sample mixer at 20 rpm for 1 h. Free antibodies then were removed from the newly formed mAb-PSB(RUB) conjugates by washing four times with PBS and conjugates were re-suspended in 400  $\mu$ L of PBS (pH 7.2). Likewise, freshly washed MBs corresponding to 100  $\mu$ L of the original MBs suspension was immersed in 1.5 mL of 0.05 mg/mL of biotinylated antibody, and the mixture was then rotated with a Dynal sample mixer at 20 rpm for 1 h. Newly formed mAb-MB conjugates were separated from the solution mixture with a magnet (Dynal MPC-S), followed by washing and re-

suspension in 100  $\mu\text{L}$  of PBS buffer (pH 7.2). The resulting mAb-MB and mAb-PSB(RUB) conjugates were stored at  $4^\circ\text{C}$  until use.

### 5.2.5 ECL and electrochemical measurements

To measure ECL-intensity, aggregates were dissolved in a 2.0 mL solution of 10.0 mM BPO-0.10 M TBAP in MeCN for optimized ECL measurements (see results for details). A three-electrode system with a 2.0-mm diameter Pt disk as the working electrode, a Pt wire as the counter electrode, and a Ag/Ag<sup>+</sup> (10 mM AgNO<sub>3</sub> and 0.10 M TBAP in MeCN) as the reference electrode were used. All three electrodes were incorporated in a 5-mL disposable glass vial cell containing assay samples. Before each measurement, the Pt electrode was polished with a 0.3  $\mu\text{m}$  alumina slurry, and all electrodes were cleaned carefully by washing with excess water followed by rinsing with MeCN. The ECL intensities along with the cyclic voltammetry signals (CV) were recorded simultaneously in a home-built ECL instrument as described previously.<sup>161</sup> This instrument consists of a 660A electrochemical workstation (CH Instruments, Austin, TX, USA) combined with a photomultiplier tube (PMT, Hamamatsu R928, Japan) installed under the electrochemical cell. A voltage of  $-700\text{ V}$  was supplied to the PMT with a high voltage power supply (Model 472A Brandenburg PMT power supply, England). The light signal (as photocurrent) was detected with a high sensitive Keithley 6514 electrometer (Keithley, Cleveland, OH, USA) and converted to voltage (in  $\pm 2\text{ V}$ ) that was collected to the electrochemical workstation computer. Unlike the commercially available BioVeris ECL system, where flow-cell based ECL detection is used; our ECL instrument uses conventional electrochemical cells. For cathodic ECL measurements, the testing solutions were pre-degassed with ultra-high purity of nitrogen (Airgas South,

Hattiesburg, MS) for 7-10 min. All measurements were conducted at a temperature of  $23 \pm 2^{\circ}\text{C}$ .

### **5.2.6 Confocal Microscopy**

ECL label loaded PSBs and PSB-virus-MB aggregates were imaged in a Zeiss LSM510 META confocal microscope (Carl Zeiss, NY).

### **5.2.7 Transmission Electron Microscopy**

Transmission electron microscopy (TEM) images were obtained using a JEOL 2100 transmission microscope operating at 200 kV. TEM images of ZIKV, PSB, and PSB<ZIKV>MB were obtained using copper mesh grids with Formvar support film.

### **5.2.8 Real time-quantitative PCR (RT-qPCR)**

ZIKV particles attached on the surface of beads (i.e., PSB<ZIKV>MB) were quantified by RT-qPCR, as described previously.<sup>365</sup> Briefly, PSB<ZIKV>MB complexes prepared with different concentrations of ZIKV were treated with TRI-reagent (Molecular Research Center) to lyse viral particles, and viral RNA was isolated after adding 1  $\mu\text{g}$  of tRNA (ThermoFisher Scientific) as carrier. The complementary DNA (cDNA) was synthesized using the iSCRIPT cDNA synthesis kit (Bio-Rad) and RT-qPCR assays were performed in a CFX96 Real-Time system (Bio-Rad) using iTaq universal probe supermix (Bio-Rad). Primers (Forward, GGAGTCAGCAATAGGGACTTTG; Reverse, CGGTTTGTCTGTGCCATTA) and probe (FAM/AGGTGGGAC/ZEN/TTGGGTTGATGTTGT/3IABkFQ) specific to the Envelope gene of ZIKV were designed and synthesized by Integrated DNA Technologies.

### **5.2.9 Western blotting**

Antibody conjugation to beads was analyzed by immunoblotting as previously described.<sup>365</sup> Briefly, the beads were treated with Laemmli sample buffer (Bio-Rad) and proteins were separated by 10% SDS-polyacrylamide gel electrophoresis, followed by transfer to a nitrocellulose membrane (Bio-Rad). Heavy chain and light chain of antibody were detected by probing the membrane with horseradish peroxidase conjugated goat anti-mouse IgG antibody (Jackson ImmunoResearch). Images were acquired in a ChemiDoc MP system (Bio-Rad) by using SuperSignal West Pico Chemiluminescence Substrate (Thermo Scientific).

## **5.3 Results**

### **5.3.1 Assay design, ECL-label loading and antibody conjugation of polystyrene and magnetic beads**

A scheme of the ECL-based strategy for detection of viruses is shown in Figure 5.1A, which is developed based on previous studies<sup>155,156,161</sup> with a more sensitive RUB/BPO sensing system. Briefly, the loading of ECL-labels (e.g., RUB) to PSBs amplifies the signal intensity several orders of magnitudes, generating a highly sensitive detection system. Subsequent conjugation of ECL label loaded PSBs with virus-specific antibody allow specific binding of virus particles to the PSBs surface. By using magnetic beads (MBs) conjugated with virus-specific antibody as a capture element, virus bound to ECL-label loaded PSBs can be separated magnetically and subjected to measurement of ECL-intensity after the dissolution of the PSB<virus>MB aggregates in MeCN, the latter signal is proportional to the amount of virus present in the samples. To develop a specific and highly sensitive ECL-based immunoassay for detection of ZIKV, PSBs were loaded

with RUB by immersing the beads into a saturated solution of RUB. These PSBs, designated as PSB(RUB), had a typical loading capacity of  $\sim 3.3 \times 10^9$  RUB molecules per bead, which was estimated on the basis of the ECL data obtained from the PSB(RUB) dissolved in MeCN and a set of standard RUB solutions using BPO as a coreactant. ECL label loading of PSBs with RUB was confirmed with a fluorescence microscope, which shows that PSB(RUB) beads glow as intense yellow color when exposed to UV light (Figure 5.1B). No such signal was detected from unloaded (bare) PSBs (data not shown). Subsequently, avidin was covalently attached to the surface of the PSB(RUB) beads via amide bonding. Avidin conjugated PSB(RUB) beads then were mixed with a biotinylated monoclonal antibody (mAb ZV-2) that is specific to ZIKV and does not recognized closely related flaviviruses, including DENV (data not shown). This step generated an antibody-conjugated PSB(RUB) (abbreviated as anti-ZIKV-PSB in following text) for specific detection of ZIKV. In addition, magnetic beads (MBs) were conjugated with ZV-2 mAb through biotin-streptavidin conjugation (anti-ZIKV-MB), which can serve as a capture element for magnetically separating ZIKV bound to PSB(RUB) in subsequent ECL-intensity measurements. Conjugation of ZV-2 to PSB (Figure 5.1C, left) and MB (Figure 5.1C, right) was confirmed by Western blotting. The ECL behavior of anti-ZIKV-PSB complexes were studied. These complexes exhibited a stable and consistent ECL response similar to those shown in Figure 5.1C for RUB/BPO solutions, suggesting no alteration in ECL behavior of RUB after loading to PSB and antibody conjugation. Taken together, these data suggest that the anti-ZIKV-PSB complexes serve as both target binding reagent and ECL signal generator, and are suitable to capture ZIKV from solution.

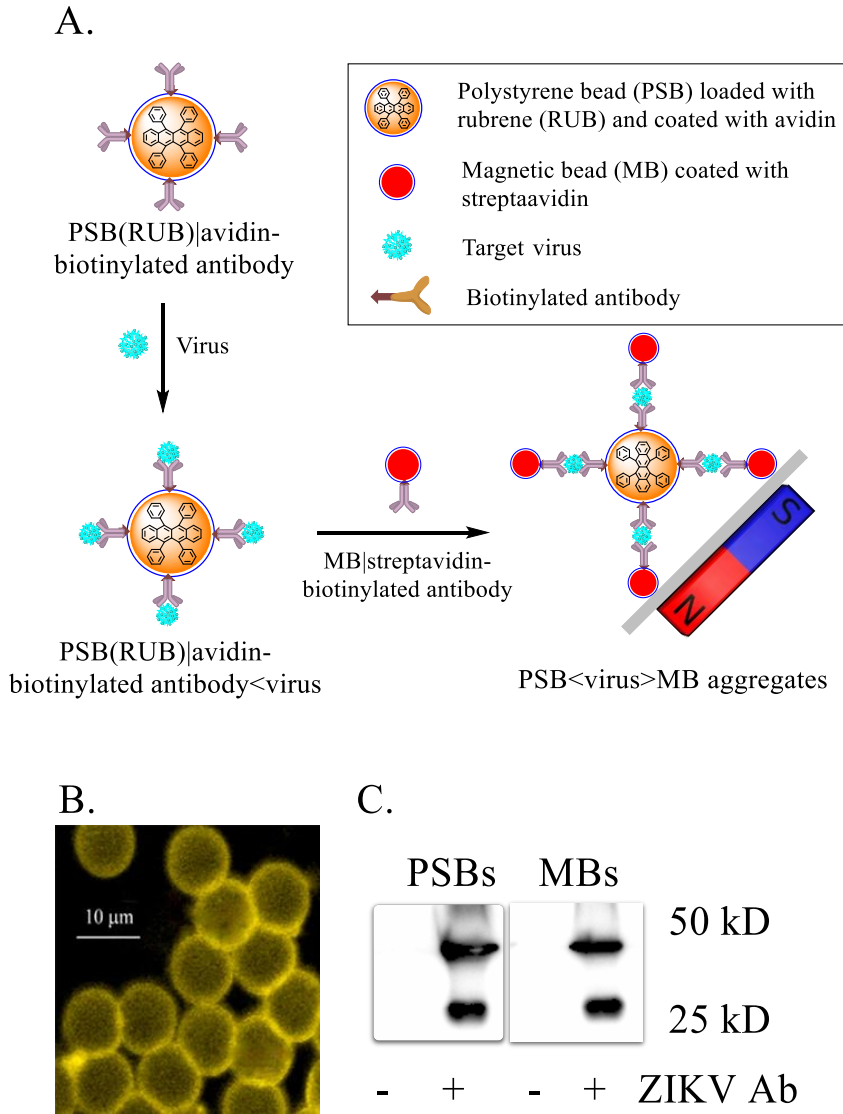


Figure 5.1 Assay design and preparation of immuno-conjugated and ECL-loaded beads.

Note: (A) Cartoon representation of fabrication of immunosensor for ZIKV and DENV4 (B) Image of rubrene loaded PSBs (golden yellow, right) taken under UV-light (385 nm excitation) in a confocal microscope. (C) Antibody conjugation to PSBs and MBs was analyzed by immunoblotting assay. Note: All experiments were performed in duplicates and repeated at least one time.

### 5.3.2 Anti-ZIKV-PSB capture of ZIKV

To test whether anti-ZIKV-PSB can capture ZIKV,  $10^4$  PFU of ZIKV (strain PRVABC59) in 0.1 M PBS (pH 7.4, 100  $\mu$ L) containing 2% BSA were incubated with

anti-ZIKV-PSB (40  $\mu$ L) for 45 min in a Dynal mixer to form ZIKV-anti-ZIKV-PSB complexes. These complexes were washed twice (8,000 g, 3 min) with PBS, re-suspended in 100  $\mu$ L PBS containing 2% BSA, then reacted with 10  $\mu$ L of capture element (anti-ZIKV-MBs) for 45 min in a Dynal mixer form PSB<ZIKV>MB aggregates, which were separated by using Dynal magnetic separator. After centrifugation, some of the PSBs in the control samples (without virus) attach on the wall of the microfuge tube. In comparison, after addition of viruses followed by centrifugation, the virus-PSB complexes settled down at the bottom of microfuge tube (Figure 5.2A), indicating that the ZIKV causes aggregation of anti-ZIKV-PSBs. In addition, after magnetic separation, the beads that bound the PSBs can be observed in the wall of tube (Figure 5.2B), suggesting the formation of PSB<ZIKV>MB aggregates in the presence of ZIKV. As shown in a micrograph (Figure 5.2C), anti-ZIKV-PSB complexes undergo aggregation in the presence of ZIKV and anti-ZIKV-MBs. To detect and quantify the ZIKV bound to PSB<ZIKV>MB aggregates, different amounts of ZIKV (0 to  $10^4$  PFU) were used to form aggregates, which were separated magnetically and subjected to extraction and RT-qPCR analysis of ZIKV RNA. The PCR results confirmed that ZIKV bound to PSB<ZIKV>MB aggregates validating the efficiency of ECL-based assay to capture ZIKV (Figure 5.2D). Collectively, these results suggest that conjugation to ECL label loaded PSBs does not alter the specificity of anti-ZIKV antibody, suggesting that this system can be used to selectively capture the target ZIKV particles.

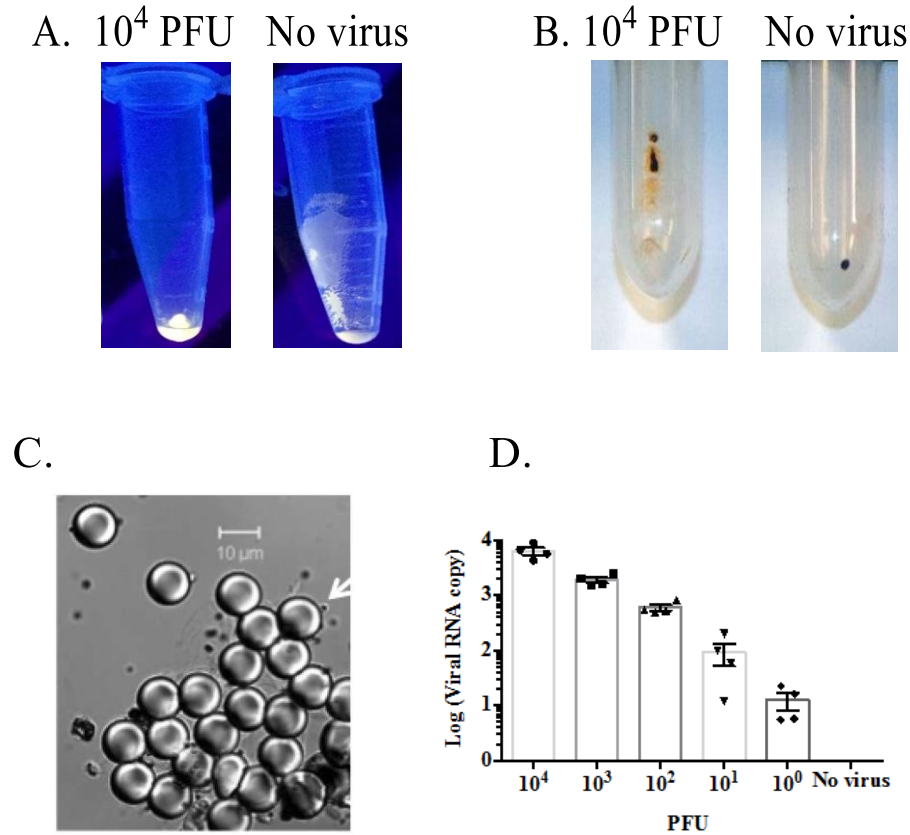


**Figure 5.2 Immuno-conjugated and ECL label loaded polystyrene beads capture ZIKV.**

Note: **(A)** Photograph of a microcentrifuge tubes after addition of ZIKV containing samples to ZV2-PSB(RUB), showing the aggregation of PSBs at the bottom of tube in the presence of ZIKV. **(B)** Photograph of a microcentrifuge tubes after magnetic separation showing (arrow) the free MBs (right), and binding of PSBs to MBs (left) in the presence of ZIKV. **(C)** A phase-contrast image of PSB<ZIKV>MB aggregates showing the binding of anti-ZV2-MB (1  $\mu$ m diameter, arrow) to the surface of anti-ZV2-PSB (10  $\mu$ m diameter) in the presence of ZIKV. **(D)** PSB<ZIKV>MB aggregates that were obtained from samples containing different PFUs of ZIKV were analyzed by RT-qPCR assay to quantify copy number of ZIKV envelope gene. All experiments were performed in duplicates and repeated at least one time.

Figure 5.3 shows TEM images during detection of ZIKV. More specifically, Figure 5.3 (A) shows white illumination of ZIKV under negative stain of phosphotungstic acid, indicating the ZIKV viral particle size was 40 nm. Figure 5.3 (B) shows only PSBs that are loaded with rubrene and coated with neutravidin, designated as

PSB(RUB)|avidin. Figure 5.3 (C) shows PSB<ZIKV>MB final aggregates showing many MBs attached to a PSB, and Figure 5.3 (D) is the zoomed image of PSB<ZIKV>MB final aggregate showing only one MB.

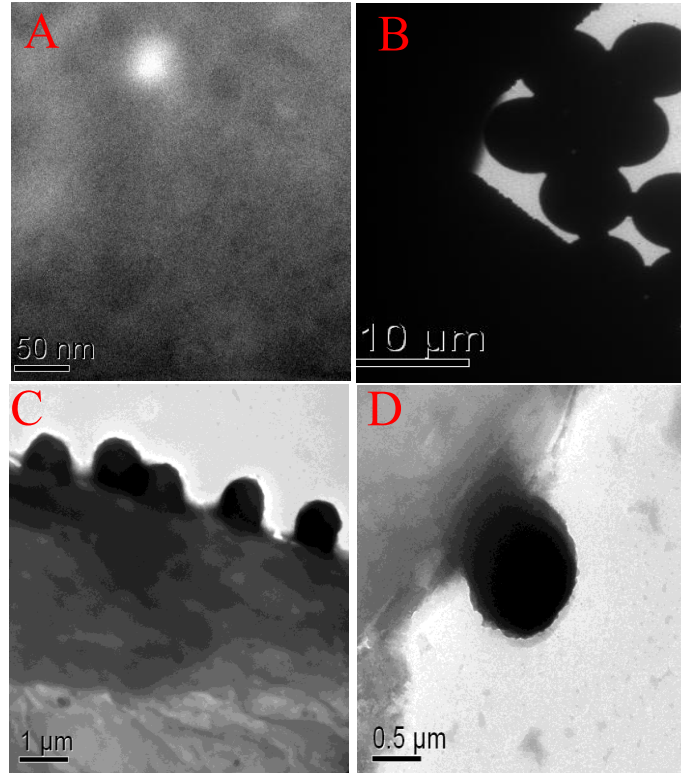


Figure 5.3 TEM images during detection of ZIKV.

Note: (A) white illumination of ZIKV under negative stain of phosphotungstic acid, (B) PSB(RUB)|avidin, (C) PSB<ZIKV>MB final aggregates showing many MBs attached to a PSB, and (D) zoomed image of PSB<ZIKV>MB final aggregate showing only one MB.

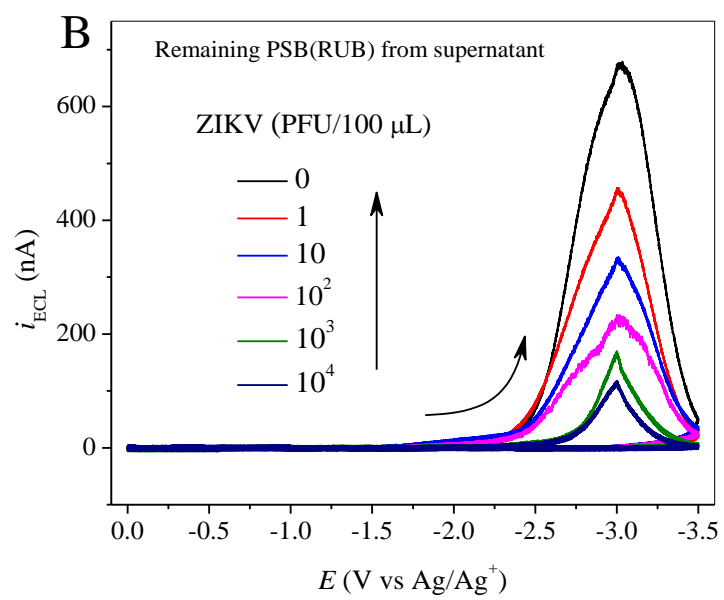
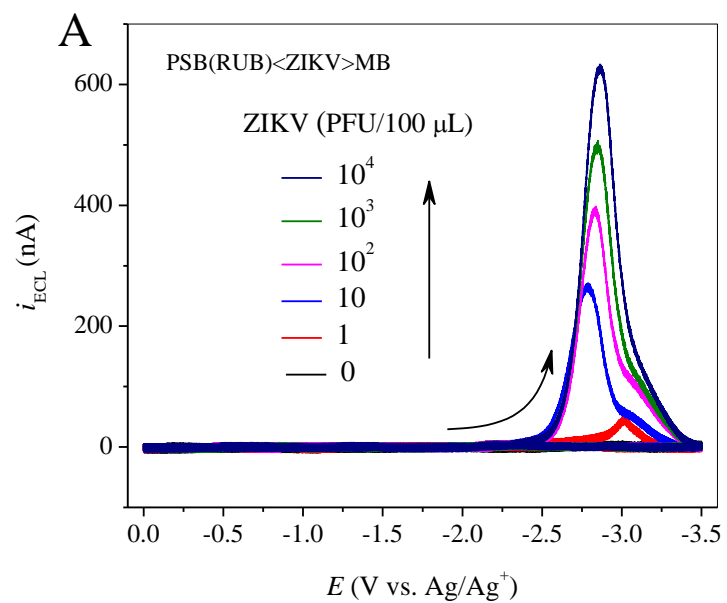
### 5.3.3 Anti-ZIKV-PSB specifically detects ZIKV in a highly sensitive manner

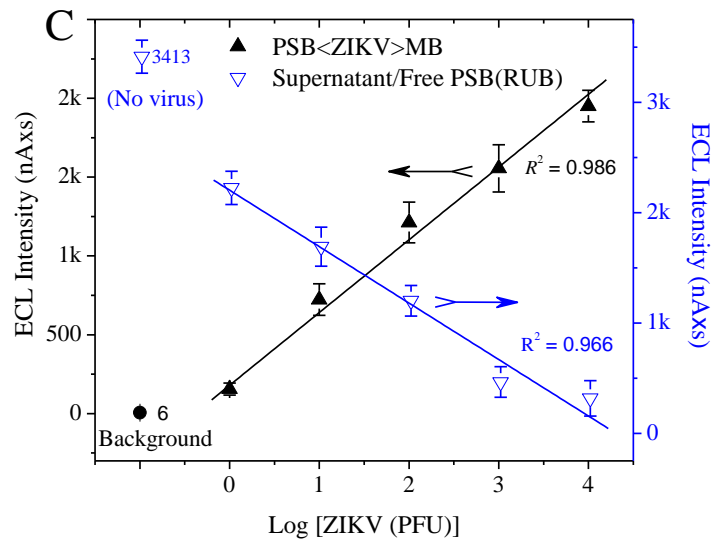
To detect ZIKV, anti-ZIKV-PSBs were mixed with different amounts of ZIKV (0 to  $10^4$  PFU) diluted in PBS with 2% BSA. The resulting virus-PSB conjugates were washed to remove unbound viruses and re-suspended. Virus-PSB conjugates then were allowed to react with the capture element (i.e., anti-ZIKV-MB) to form sandwich-type

PSB<ZIKV>MB aggregates, which were magnetically separated from the reaction medium. PSBs that did not have bound viruses do not form aggregates and remain in solution during magnetic separation. Thus the ECL-intensity obtained from the PSB<ZIKV>MB aggregate is proportional to the concentration of virus in a sample. Figure 5.4A shows that the ECL intensity of the purified MB-ZIKV-PSB aggregates increase with the amount of virus in the samples. Notably, the ECL response obtained from sample containing 1 PFU of ZIKV is distinguishable from the background (i.e., no virus in the system), indicating that the present detection platform has a detection limit of as low as 1 PFU, which is comparable to RT-PCR (see Figure 5.2D). If the concentration of virus in a sample is low, the amount of PSB-virus-MB species formed should be also low. In this case, most of the ECL-signal remains in free (virus-unbound) PSBs that are left in solution during magnetic separation. To confirm these results, the ECL intensity of virus-free PSBs was measured, which was expected to be complementary with the ECL signals obtained from PSB-virus-MB aggregates. Indeed, the ECL signals from the virus-unbound PSBs displayed an inversed relationship with the original amount of ZIKV added to samples (Figure 5.4B). This was expected, because each sample used the same amount of PSBs; the more PSB<ZIKV>MB aggregates are formed, the less PSBs remain in the solution. These results also show that there is no loss of ECL-intensity during the assay, confirming that the ECL-intensity of PSB-virus-MB is proportional to the amount of complex formed, hence the amount of virus present in the samples. To analyze further the relationship between ECL-intensity and the amount of virus in the samples, area under the ECL-curves were calculated and plotted the average values against the amount of virus added to the samples. The results showed a linear relationship between the virus

amount and the ECL-intensity of PSB<ZIKV>MB aggregates as well as free PSBs in the supernatant (Figure 5.4C). These results suggest that the ECL-intensity proportionally reflects the amount of viral particles present in samples in a sensitive manner.

To determine whether anti-ZIKV-PSB specifically binds to ZIKV, unrelated (chikungunya virus (CHIKV)) or related (West Nile virus (WNV) and dengue (DENV, serotype 1-4)) mosquito-transmitted viruses were tested with the developed ECL-based immunoassay. As shown in Figure 5.4D, the ECL-intensity of samples containing  $10^3$  PFU of CHIKV, WNV, or DENV has a substantially lower ECL signal as compared to ZIKV. The inset of Figure 5.4D illustrates the normalized ECL intensity of six viruses compared to ZIKV, and suggests that the detection of ZIKV by an anti-ZIKV-PSB based immunoassay has an acceptable selectivity of ~90%. In addition, ECL label loaded PSBs and MBs were conjugated with a mAb (4G2) that binds to the conserved fusion loop epitope of the E protein of most flaviviruses.<sup>366</sup> The stability of the ECL-based immunoassay based on PSB<ZIKV>MB system is actually determined by the stability of the RUB/BPO ECL system, because trace amounts of PSB and MB debris as well as bio-substances present in MeCN solution do not interfere the ECL generation. Stable and reproducible ECL signals were observed from the same test solution over different potential cycles and on different testing days.





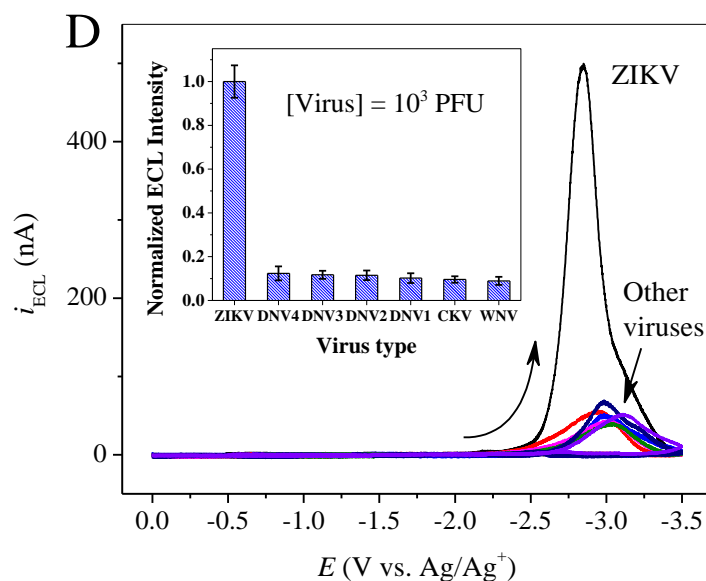


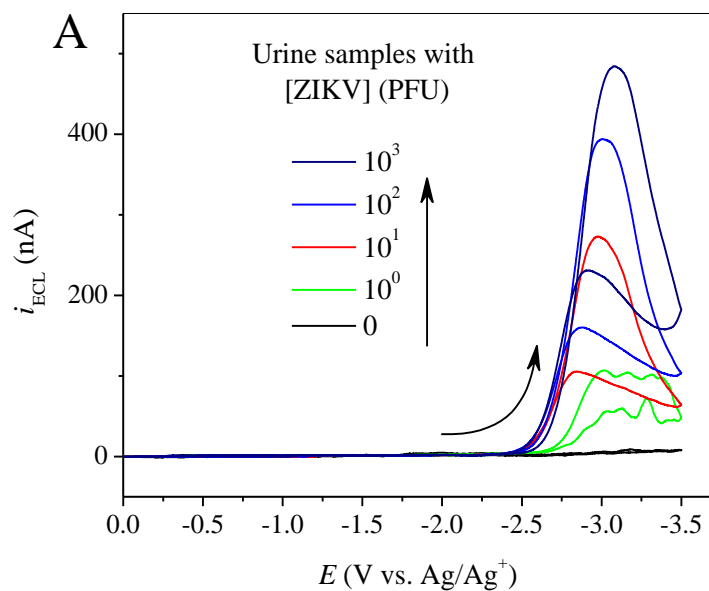
Figure 5.4 Anti-ZIKV-PSB specifically detects ZIKV in a highly sensitive manner.

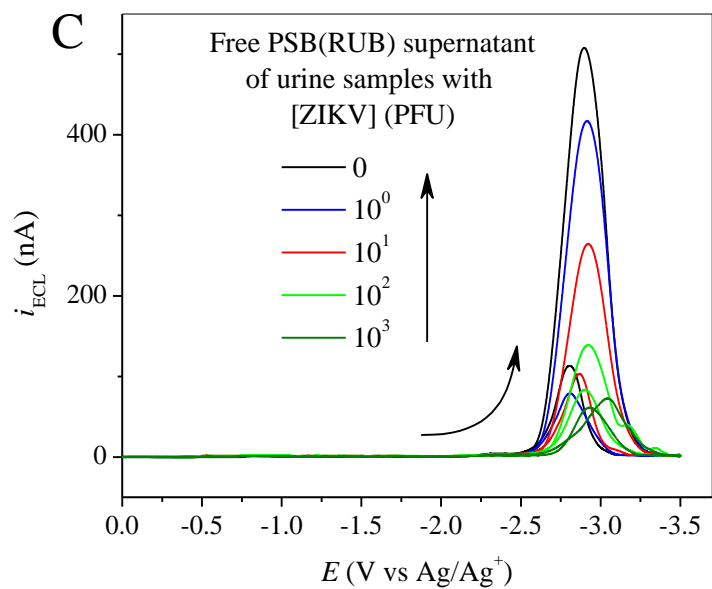
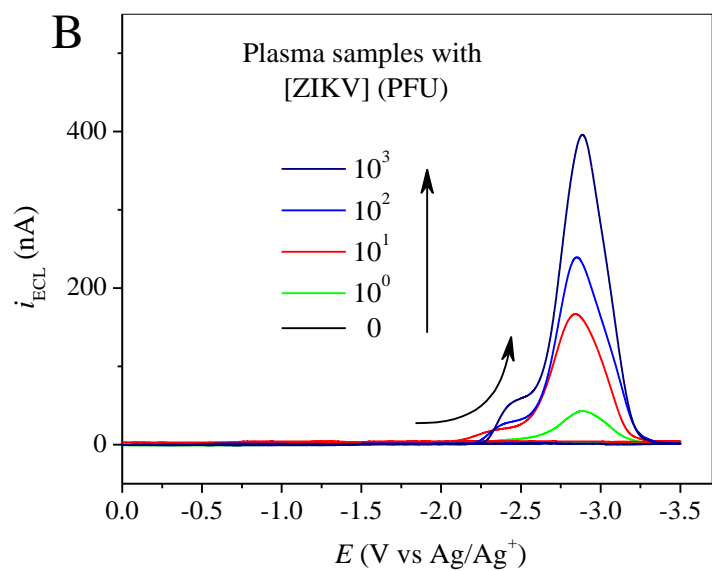
Note: Samples containing different amounts of ZIKV ( $0-10^4$  PFU) were prepared in PBS containing 2% BSA and allowed to form PSB<ZIKV>MB complexes by reacting with ZV2-PSB(RUB) and ZV2-MB. PSB<ZIKV>MB complexes were separated magnetically and subjected to ECL-intensity measurement. (A) ECL-response curves of PSB<ZIKV>MB aggregates obtained from samples containing different PFUs of ZIKV in PBS. (B) ECL-response of free (unliganded) PSB(RUB) that remained in solution after magnetic separation. (C) A calibration curve of mean ECL intensity of magnetically separated PSB<ZIKV>MB aggregates (upward line, black) and free PSB(RUB) (downward line, blue) that remained in solution after magnetic separation. (D) ECL response of PSB<ZIKV>MB aggregates obtained from samples containing related (DENV and WNV) or unrelated (CHIKV) viruses ( $10^3$  PFU) prepared in PBS containing 2% BSA. Sample containing no virus was used as a control to determine background signal ( $\sim 0$ , see Figure 5.4C). All experiments were performed in duplicates and repeated at least one time.

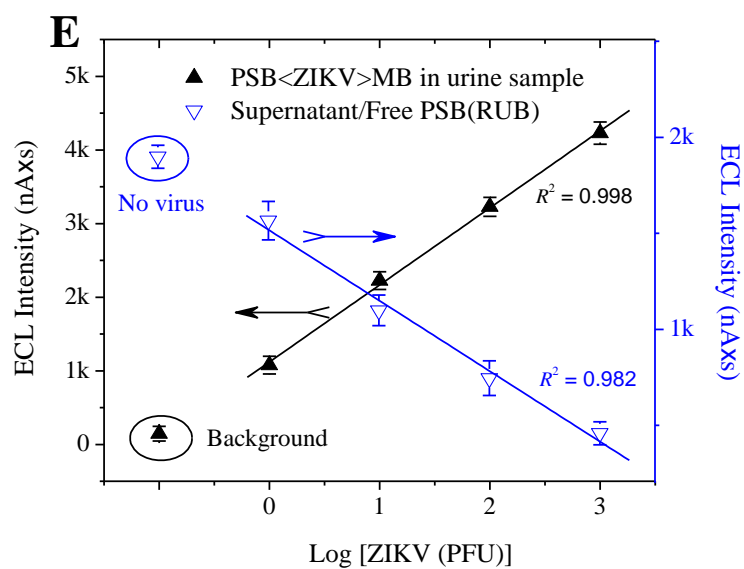
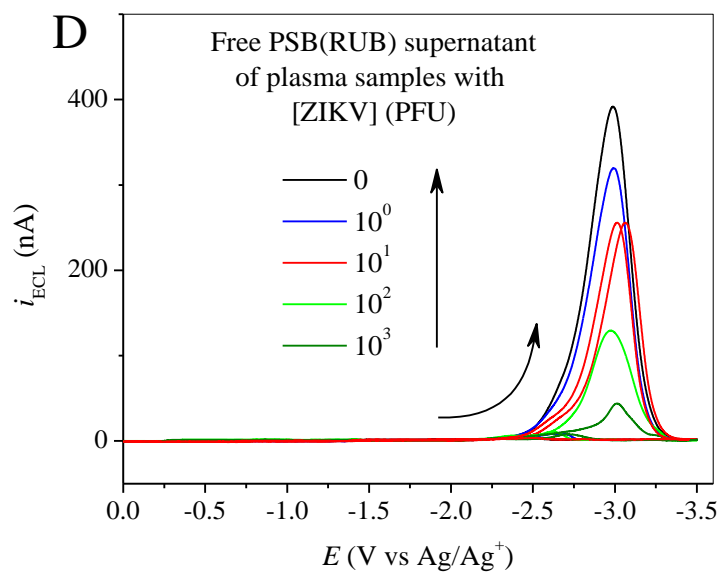
### 5.3.4 ECL-based immunoassay can detect ZIKV in human biological fluids

ZIKV is present in human blood, urine and other body fluids.<sup>339,340,367</sup> To test whether our ECL-based immunoassay can detect ZIKV in human body fluids, we collected plasma and urine specimens from healthy human volunteers and spiked in different amount of ZIKV. In these samples, we performed ECL-based immunoassay and measured the ECL-intensity of PSB<ZIKV>MB aggregates. Consistent with the results

obtained in PBS, our ECL-based assay detected as few as 1 PFU of ZIKV in 100  $\mu$ L of human urine (Figure 5.5A) and plasma (Figure 5.5B). These results were complemented by measuring the ECL intensity of virus-free PSBs that remain in solution after magnetic separations (Figures 5.5C and 5.5D), which show a progressive decrease of ECL-intensity with increasing amount of ZIKV present in samples. The area under the ECL curves were plotted against amount of PFUs added to the samples (Figures 5.5E and 5.5F) and produced a linear curve, suggesting that the ECL-intensity of the PSB-virus-MB aggregates formed is proportional to the amount of ZIKV in the sample. These results establish that the ECL-based immunoassay can detect ZIKV in clinical samples in an ultrasensitive and specific manner.







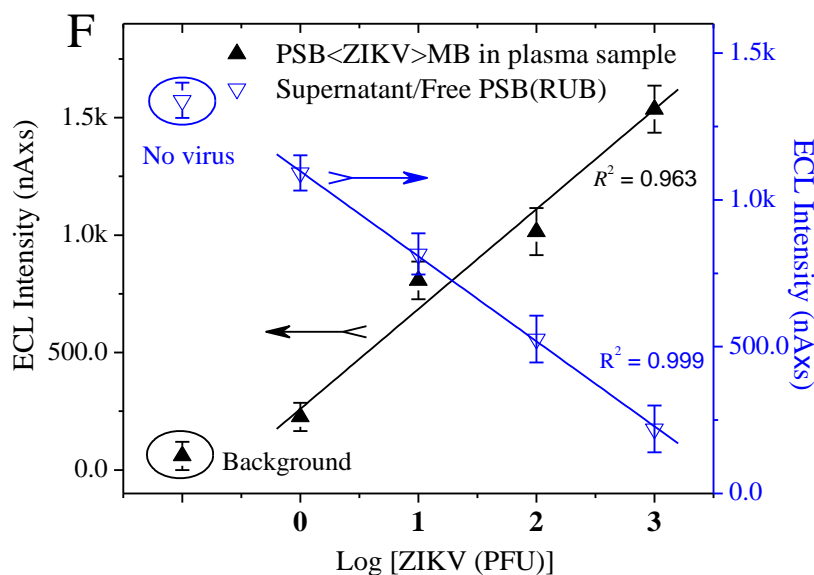


Figure 5.5 ECL-based immunoassay detects ZIKV in human biofluids.

Note: Samples containing different amounts of ZIKV ( $0-10^3$  PFU) were prepared in human urine or plasma specimens collected from healthy human volunteers. ECL-response from PSB<ZIKV>MB aggregates obtained from (A) plasma, and (B) urine samples containing different PFUs of ZIKV. ECL-response of virus-free PSB(RUB) that remained in solution after magnetic separation from (C) urine and (D) plasma samples. A calibration curve of mean ECL intensity of magnetically separated PSB<ZIKV>MB aggregates (upward line, black) and free PSB(RUB) (downward line, blue) that remained in solution after magnetic separation were generated from (E) urine and (F) plasma samples. No virus control was used to determine background signal. All the experiments were performed in duplicates and repeated at least one time.

### 5.3.5 ECL Detection of DENV4

For the detection of DENV4, similar strategy to the ZIKV detection as described above was used, where the experimental conditions and the procedures remained the same but the antibody was changed to anti-4G2 that detects most of the flaviviruses. Experimentally, the samples containing different amounts ( $0-10^4$  PFU) of DENV4 in PBS containing 2% BSA were allowed to form PSB<DENV4>MB aggregates by reacting with anti-4G2-PSB(RUB) and anti-4G2-MB. The final PSB<DENV4>MB aggregates

were dissolved with 2.0 mL of 10.0 mM BPO followed by ECL measurements after degassing with N<sub>2</sub>.

Figure 5.6 shows the photographs of centrifuge tubes at different stages of DENV4 detection. More specifically, Figure 5.6A shows the PSB-DENV4 conjugates before MB separation, where large numbers of DENV4 correspond to more precipitates of PSB-DENV4 conjugates at the bottom of the tube. Figure 5.6B shows that the spot size of PSB<DENV4>MB aggregates on the wall of the tube progressively decreases with the decrease of DENV4 concentration. This is expected, because the less numbers of DENV4 are, the less conjugates of PSB-DENV4 are formed, and the less numbers of PSB<DENV4>MB aggregates can be collected. Consistent with the above observations, the number of free unbound PSB(RUB) beads collected from the supernatant increase with the decrease of DENV4 concentration as illustrated in Figure 5.6C.

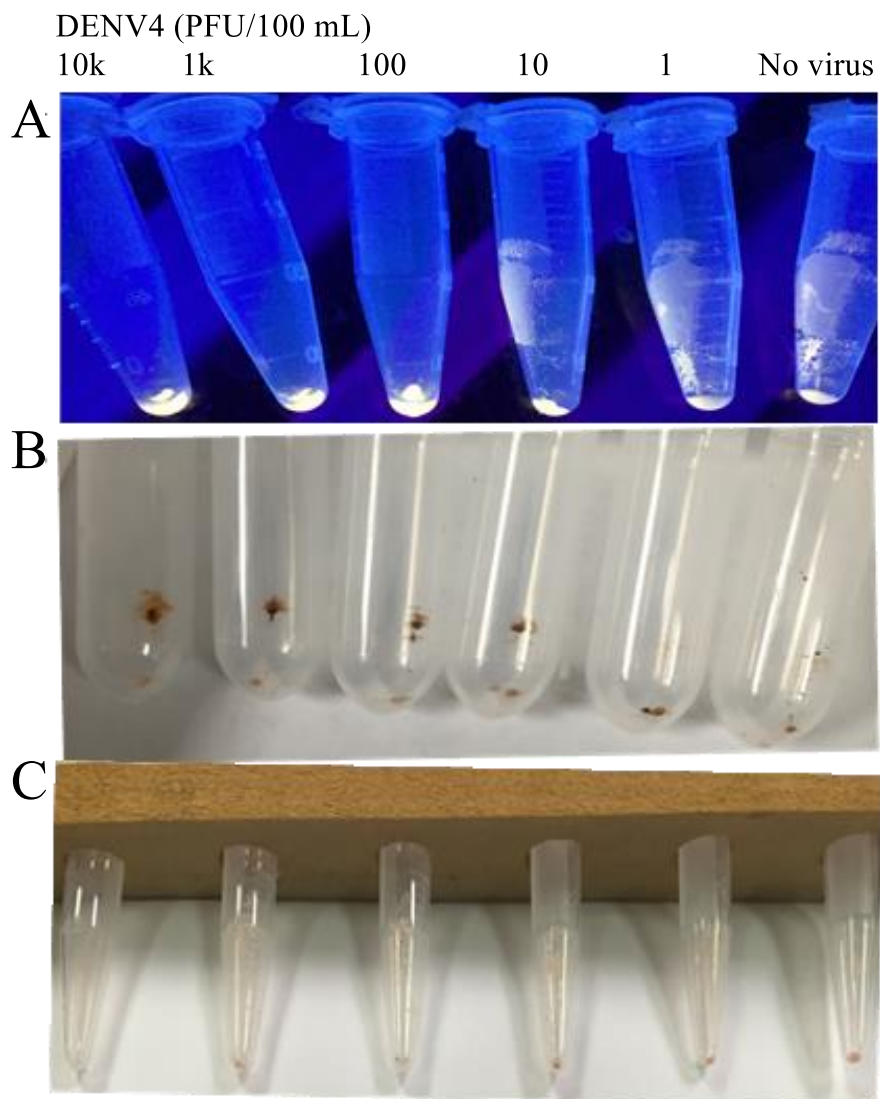
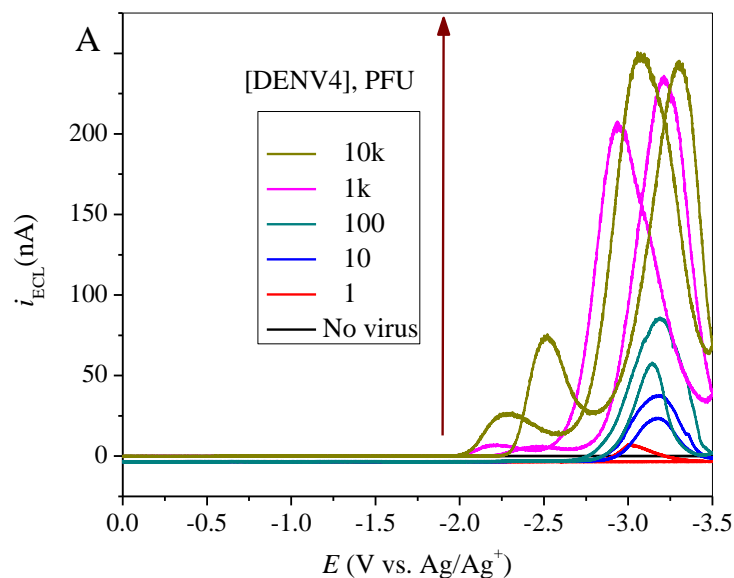


Figure 5.6 (A) PSB(RUB)-anti-4G2 conjugates, (B) PSB(RUB)<DENV4>MB final aggregates and (C) Free (unbound) PSB(RUB) from the supernatant.

The final aggregates of PSB<DENV4>MB shown in Figure 5.6B were dissolved in 2.0 mL of 10.0 mM BPO and subjected to ECL measurements. Figure 5.7A shows the ECL-potential profiles of solutions associated with different concentrations of DENV4, where progressive increase of ECL signal along with the increase of DENV4

concentration is generally seen. Figure 5.7B displays the linear relationship between the integrated ECL intensity and the logarithmic concentration of DENV4, where the upward line is obtained from the solution containing dissolved PSB<DENV4>MB aggregates, and the downward line corresponds to the solution containing dissolved free PSB(RUB) that remained in solution after magnetic separation. Because a constant number of PSB(RUB) was used for each DENV4 test, an opposite ECL intensity change is expected from the test solution associated with PSB<DENV4>MB aggregates and free PSB(RUB) beads. Notably, the ECL signal of 1 PFU DENV4 can be clearly distinguished from the background, indicating a limit of detection of 1 PFU/100 mL DENV4 with the present ECL method.



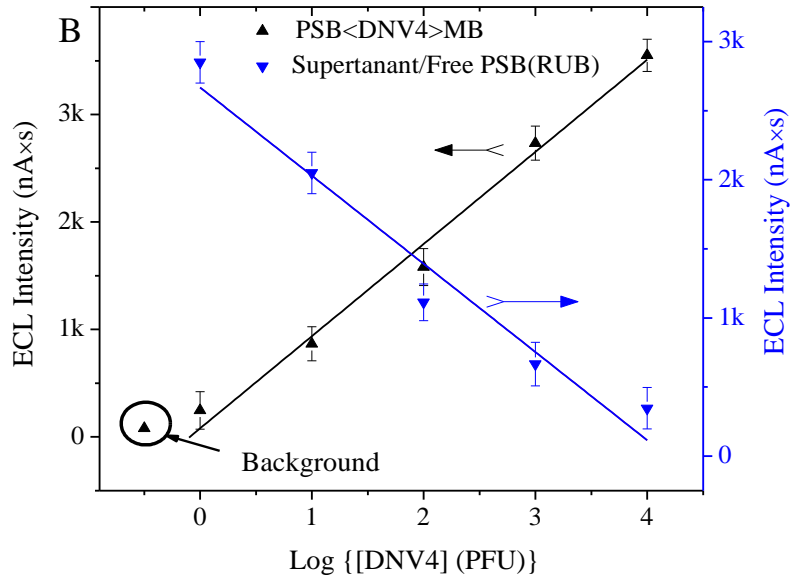


Figure 5.7 ECL-responses from PSB-DENV4-MB aggregates obtained from samples containing different concentrations of DENV4 viruses.

Note: (A) Samples containing different amounts ( $0-10^4$  PFU) of DENV4 in PBS containing 2% BSA were allowed to form PSB-DENV4-MB aggregates by reacting with anti-4G2-PSB(RUB) and anti-4G2-MB. All the experiments were performed in duplicates and repeated at least one time. (B) Plot of a calibration curve of mean ECL intensity of magnetically separated PSB<DENV4>MB aggregates (upward line, black) and free PSB(RUB) (downward line, blue) that remained in solution after magnetic separation were generated in PBS buffer.

## 5.4 Discussion

Mosquito transmitted viruses, such as DENV, Japanese encephalitis virus, and WNV are worldwide public health challenges.<sup>368</sup> Recent emergence of CHIKV<sup>369</sup> and ZIKV<sup>370,371</sup> has prompted a global public health emergency. Besides mosquito transmission, these viruses also can be transmitted through other routes, such as blood transfusion, organ transplantation, and in utero.<sup>372,373</sup> For instance, ZIKV virions or RNA can be detected in semen, urine, and saliva, and is categorized as a high-priority

infectious agent with the risk of sexual-transmission.<sup>342-344</sup> Importantly, there is no approved vaccine or specific therapy against the most of these mosquito-transmitted viruses. Early and accurate diagnosis of viral infection can reduce the risk of severe consequences, such as DENV hemorrhagic fever, shock syndrome and ZIKV-related developmental defects. Most of the currently available diagnostic methods for viral infection are based on detection of viral antigens, antiviral antibodies, or viral nucleic acid. Although the nucleic acid-based methods are sensitive, they require expensive reagents and instruments. For immunoassays, the performance is often poor due to cross-reactivity with other flaviviruses (e.g. Dengue) and difficulty in clinical correlation. Direct detection of viruses is challenged by requirement of facilities, such as cell culture or electron microscopy, which are not available in most diagnostic laboratories. Thus, a rapid, simple-to-use, sensitive, and cost-effective assay for virus detection in clinical specimen is highly desirable.

An ECL-based detection assay may be ideal for virus detection as it offers several advantages including ultrasensitivity, reproducibility, cost-effectiveness, and rapidness over conventional immunoassays and PCR-based assay,<sup>85,374,375</sup> as demonstrated in this chapter for detection of ZIKV and DENV4 in human biological fluids. Moreover, as ZIKV has been suggested to be transmitted by blood transfusion, the ECL-based assay could be developed for blood screening of ZIKV. By utilizing various ECL-emitters (such as RUB, Ru(bpy)<sub>3</sub><sup>2+</sup> and DPA) that have easily distinguishable excitation and emission properties,<sup>376</sup> ECL-based immunoassays have multiplexing capacity for simultaneous detection of several types of viruses in a single sample.

## **5.5 Conclusion**

Ultrasensitive ECL based immunoassays were fabricated for sensitive and specific detection of zika virus (ZIKV) and dengue virus (DENV4) in human body fluids. As low as 1 PFU/100  $\mu$ L or 10 PFU/mL of ZIKV and DENV4 were detected using sensitive RUB/BPO ECL system in MeCN. This was achieved by amplifying the ECL signal using two particles (beads) assay using polystyrene bead as ECL label carrier whereas magnetic bead as conjugates or aggregates separation moderator. This proof-of-concept study can be extended to the detection of other viruses or pathogens.

## CHAPTER VI – CONCLUDING REMARKS

Electrogenerated chemiluminescence (ECL) is a process of light emission at the surface of the working electrode resulting from electrochemical and chemical reactions of the ECL emitters (labels) with or without the use of deliberately added ECL coreactants. ECL is electrode potential controlled. ECL is “on” when potential is applied and ECL is “off” once the potential is disconnected. For the process of ECL to be relatively efficient or ECL to be strong (ECL intensity in the scale of microampere range scale when micromolar concentrations of ECL emitters are used), the electrogenerated emitter radicals must be sufficiently stable in the reaction media. The highly efficient ECL could be produced by adding coreactants that allow the ECL process to occur upon either anodic potential scanning or cathodic scanning. ECL can be detected by using various light detectors coupled with or without wavelength selectors including photomultiplier tube (PMT), charge coupled devices (CCDs), and complementary metal–oxide–semiconductor (CMOS). Thus, ECL can also be understood as a marriage between electrochemistry and spectroscopy. Most diagnostic methods are often challenged by three factors—sensitivity, selectivity and stability of the biosensor. ECL based biosensors are promising when addressing these issues.

After an introduction chapter of the dissertation (Chapter I), systematic ECL studies of unmixed and mixed systems of three most efficient ECL emitters, namely, 9,10-diphenylanthracene (DPA), rubrene (RUB), and tris(2,2'-bipyridine)ruthenium(II) complex ( $\text{Ru}(\text{bpy})_3^{2+}$ ), using benzoyl peroxide (BPO) as a common cathodic coreactant and 2-(dibutylamino)ethanol (DBAE) or tri-*n*-propylamine (TPrA) as an anodic

coreactant in acetonitrile, were studied for their potential applications in multiplexing ECL detection of multiple target analytes (Chapter II). The experiments were performed with a homemade, portable, and inexpensive spectral ECL instrument. The search for most favorable coreactant turned out to be the cathodic coreactant BPO among tested coreactants of DBAE, TPrA, and BPO. Certain interactions associated with energy transfer were observed when different ECL emitters were mixed in the same system, which was confirmed by fluorescence titrations and consistent with their emission and absorption spectra. The experiments and spectral ECL instrument can be well-adapted by college level chemistry laboratories especially senior undergraduate analytical chemistry and instrumental analysis courses.

In Chapter III, an extension of the study done from Chapter II was explored. Synthesis, electrochemistry, and ECL studies of water soluble analogues of DPA and RUB were carried out. Different ECL coreactants and electrode materials on the ECL behavior of sulfonated DPA (DPAS), sulfonated RUB (SRUB), and  $\text{Ru}(\text{bpy})_3^{2+}$  were systematically examined. DBAE and Pt electrode were found to be most favorable coreactant and electrode, respectively. The relatively weak ECL responses can be remarkably enhanced by adding 10.0 mM nitrate salt to the ECL system. The proposed mechanism involving the production of  $\text{NO}_3^\cdot$  free radicals, which chemically reacted with ECL emitter and coreactant to form species crucial for ECL production. Electron spin resonance spectroscopy (EPR) experiments with solution phase  $\text{KNO}_3$  mixed with spin trapping agent DMPO under UV irradiation provided direct evidence of the existence of such a free radical. ECL titration studies of mixed systems of the emitters using DBAE and nitrate salt were also carried out.

In Chapter IV, EPR studies of radical intermediates ( $C_6H_5COO^{\bullet}$  and  $SO_4^{\bullet-}$ ) of cathodic ECL coreactants benzoyl peroxide (BPO) and persulphate salt were presented. Several strategies were used for the generation of radicals, which included solid and solution phase coreactant with and without DMPO under UV irradiation and chemical reductions of coreactants with hydrazine. These data provided direct evidence that supports various ECL mechanisms proposed previously, although detailed explanation or interpretation of such EPR spectra are yet to be done.

In Chapter V, sensitive and selective detection of viruses, namely zika virus (ZIKV) and dengue virus (DENV4) was reported using two particles (beads) based ECL immunoassay, where polystyrene bead was used as ECL label carrier and magnetic bead as conjugate or aggregate separation moderator. The loading of ECL label rubrene inside the polystyrene allowed huge amplifications resulting in sensitive detection of viruses (DENV4 and ZIKV) with a LOD of 10 plaque forming unit (PFU)/mL or 1 PFU/100  $\mu$ L sample.

One of the important future direction of the studies can lead to the application of the studied multiple efficient emitters and coreactants for multiplexed assays for detecting multiple analytes simultaneously. For example, using two efficient ECL emitters DPA and RUB with effective combination of cathodic ECL coreactant BPO could generate ECL at two distinct emission wavelengths of  $\sim 420$  nm and  $\sim 550$  nm, respectively, for the detection of two analytes of interest simultaneously without pre-separation.

## REFERENCES

- (1) Scholz, F.; Editor *Electroanalytical Methods: Guide to Experiments and Applications*, 2nd printing; Springer, 2005.
- (2) Bard, A. J.; Faulkner, L. R. *Electrochemical Methods: Fundamentals and Applications*; 2nd ed. ed.; John Wiley & Sons, Inc.: New York, 2001.
- (3) Skoog, D. A. *Principles of Instrumental Analysis. 3rd Ed*; CBS College Publishing, 1985.
- (4) Arribas, A. S.; Martinez-Fernandez, M.; Chicharro, M. *TrAC, Trends Anal. Chem.* **2012**, *34*, 78.
- (5) Bozal, B.; Uslu, B.; Ozkan, S. A. *Int. J. Electrochem.* **2011**, 343947.
- (6) Cepria, G.; Perez-Arantegui, J.; Barcelona, R. *Curr. Top. Anal. Chem.* **2006**, *6*, 19.
- (7) Apak, R.; Capanoglu, E.; Arda, A. U. *ACS Symp. Ser.* **2015**, *1191*, 209.
- (8) Baldo, M. A.; Oliveri, P.; Simonetti, R.; Daniele, S. *Talanta* **2016**, *161*, 881.
- (9) Baval, D.; Dejmikova, H.; Scampicchio, M.; Zima, J.; Berek, J. *Electroanalysis* **2017**, *29*, 182.
- (10) Costa, D. J. E.; Martinez, A. M.; Ribeiro, W. F.; Bichinho, K. M.; Di Nezio, M. S.; Pistonesi, M. F.; Araujo, M. C. U. *Talanta* **2016**, *154*, 134.

- (11) de Macedo, I. Y. L.; Garcia, L. F.; Oliveira Neto, J. R.; de Siqueira Leite, K. C.; Ferreira, V. S.; Ghedini, P. C.; de Souza Gil, E. *Food Chem.* **2017**, *217*, 326.
- (12) El Kasmi, S.; Lahrich, S.; Farahi, A.; Zriouil, M.; Ahmamou, M.; Bakasse, M.; El Mhammedi, M. A. *J. Taiwan Inst. Chem. Eng.* **2016**, *58*, 165.
- (13) Kilmartin, P. A. *Electrochem. Commun.* **2016**, *67*, 39.
- (14) Mohammed, G. I.; Bashammakh, A. S.; Alsibaai, A. A.; Alwael, H.; El-Shahawi, M. S. *TrAC, Trends Anal. Chem.* **2016**, *78*, 84.
- (15) Andrade, A. F. B.; Mamo, S. K.; Gonzalez-Rodriguez, J. *Anal. Chem.* **2016**, Ahead of Print.
- (16) Attia, A. K.; Frag, E. Y. Z.; Ahmed, H. E. *Arabian J. Chem.* **2016**, Ahead of Print.
- (17) Colkesen, B.; Ozturk, F.; Erden, P. E. *J. Braz. Chem. Soc.* **2016**, *27*, 849.
- (18) Karimi Shervedani, R.; Bahrani, S.; Samiei Foroushani, M.; Momenbeik, F. *Electroanalysis* **2017**, *29*, 272.
- (19) Lete, C.; Lakard, B.; Hihn, J.-Y.; del Campo, F. J.; Lupu, S. *Sens. Actuators, B* **2017**, *240*, 801.
- (20) Li, J.; Liu, M.; Zhang, F.; Xu, Z.; Deng, P.; Tang, S.; Liu, X.; Hengyang Normal University, Peop. Rep. China . 2016, p 11pp.

- (21) Mahmoud, B. G.; Khairy, M.; Rashwan, F. A.; Banks, C. E. *Anal. Chem.* **2017**, Ahead of Print.
- (22) Mbokou, S. F.; Pontie, M.; Bouchara, J.-P.; Tchieno, F. M. M.; Njanja, E.; Mogni, A.; Pontalier, P. Y.; Tonle, I. K. *Int. J. Electrochem.* **2016**, 1953278/1.
- (23) Narang, J.; Malhotra, N.; Singhal, C.; Mathur, A.; Chakraborty, D.; Anil, A.; Ingle, A.; Pundir, C. S. *Biosens. Bioelectron.* **2017**, 88, 249.
- (24) Ngai, K. S.; Tan, W. T.; Zainal, Z.; Zawawi, R. M.; Juan, J. C. *Sci. Adv. Mater.* **2016**, 8, 788.
- (25) Nigovic, B.; Juric, S.; Mitrovic, I. *Talanta* **2017**, 164, 201.
- (26) Norouzi, P.; Haji-Hashemi, H.; Larijani, B.; Aghazadeh, M.; Pourbasheer, E.; Ganjali, M. R. *Curr. Anal. Chem.* **2017**, 13, 70.
- (27) Ochiai, L. M.; Agustini, D.; Figueiredo-Filho, L. C. S.; Banks, C. E.; Marcolino-Junior, L. H.; Bergamini, M. F. *Sens. Actuators, B* **2017**, 241, 978.
- (28) Ribeiro, J. A.; Fernandes, P. M. V.; Pereira, C. M.; Silva, F. *Talanta* **2016**, 160, 653.
- (29) Suresh, E.; Sundaram, K.; Kavitha, B.; Kumar, N. S. *Int. J. PharmTech Res.* **2016**, 9, 182.
- (30) Adams, R. N. *Anal. Chem.* **1976**, 48, 1126A.
- (31) Bogdanov, M. B. *Farmakol. Toksikol.* **1991**, 54, 11.

- (32) Chandra, S.; Wong, D. K. Y.; Nova Science Publishers, Inc.: 2009, p 317.
- (33) Ewing, A. G.; American Chemical Society: Conf. Proc. ANYL-200, 2013
- (34) Fagan-Murphy, A.; Patel, B. A. *Electrochim. Acta* **2014**, *138*, 392.
- (35) Kimble, C. J.; Johnson, D. M.; Winter, B. A.; Whitlock, S. V.; Kressin, K. R.; Horne, A. E.; Robinson, J. C.; Bledsoe, J. M.; Tye, S. J.; Chang, S.-Y.; Agnesi, F.; Griessenauer, C. J.; Covey, D.; Shon, Y.-M.; Bennet, K. E.; Garris, P. A.; Lee, K. H. *Conf Proc IEEE Eng Med Biol Soc* **2009**, *2009*, 4856.
- (36) Kita, J. M., Electroanalytical Techniques for Probing Neurochemical Mechanisms, PhD Dissertation; University of North Carolina at Chapel Hill, 2008.
- (37) Lebedev, V. P.; Savchenko, A. B.; Otellin, V. A.; Kucherenko, R. P. *Fiziol Zh Im I M Sechenova* **1995**, *81*, 36.
- (38) Lin, Y.; Zhang, Z.; Mao, L. *Neuromethods* **2013**, *75*, 121.
- (39) Strope, E. R., Electroanalytical Techniques: Applications to Neurochemistry; Univ. Kansas, Lawrence, 1978.
- (40) Troyer, K. P.; Heien, M. L. A. V.; Venton, B. J.; Wightman, R. M. *Curr. Opin. Chem. Biol.* **2002**, *6*, 696.
- (41) Rotureau, E.; Waldvogel, Y.; Present, R. M.; Pinheiro, J. P. *J. Electroanal. Chem.* **2015**, *752*, 68.

- (42) Abdalsamed, I.; Zidan, M. *Int. J. Chem. Sci.* **2015**, *13*, 1.
- (43) Esteban, M.; Casassas, E. *Trends Anal. Chem.* **1994**, *13*, 110.
- (44) Hoeflich, L. K., Application of Electroanalytical Techniques to Environmental Thallium Compounds, PhD Dissertation; Louisiana State Univ., Baton Rouge, 1982.
- (45) Magee, R. J. *Trans. SAEST* **1985**, *20*, 135.
- (46) Senturk, Z. *Curr. Drug Delivery* **2013**, *10*, 76.
- (47) Erturan, S.; Yalcin, M.; Marmara Univ. Fac. Sci. Lett.: 1992; Vol. 3, p 129.
- (48) Fortin, D.; Clement, S.; Gagnon, K.; Berube, J.-F.; Stewart, M. P.; Geiger, W. E.; Harvey, P. D. *Inorg. Chem.* **2009**, *48*, 446.
- (49) Montenegro, M. I.; Queiros, M. A. M. *Port. Electrochim. Acta* **1987**, *5*, 207.
- (50) Qin, J.; Green, M. L. H.; Green, J. C.; Bandy, J. A. *Youji Huaxue* **1989**, *9*, 422.
- (51) Bolhuis, P. A. *J. Electroanal. Chem. Interfacial Electrochem.* **1980**, *110*, 285.
- (52) Gucle, H.; Ozyoruk, H.; Yildiz, A. *Ber. Bunsen-Ges. Phys. Chem.* **1994**, *98*, 828.

- (53) Ribeiro, M. S.; Ticianelli, E. A.; Avaca, L. A.; Gonzalez, E. R.; Dep. Quim. Univ. Fed. Sao Carlos: 1984, p 13.
- (54) Santhanam, K. S. V.; Bard, A. J. *J. Am. Chem. Soc.* **1966**, *88*, 2669.
- (55) Ticianelli, E. A.; Avaca, L. A.; Gonzalez, E. R. *J. Electroanal. Chem. Interfacial Electrochem.* **1989**, *258*, 379.
- (56) Kim, D.-H.; Abidian, M.; Martin, D. C. *J. Biomed. Mater. Res., Part A* **2004**, *71A*, 577.
- (57) Petrov, A. V.; Bazanov, M. I.; Siling, S. A.; Scholl, H.; Girnchev, E. G.; Izdatel'stvo Saratovskogo Universiteta: 2002, p 132.
- (58) Zagorska, M.; Kulszewicz-Bajer, I.; Lapkowski, M.; Laska, J.; Hasik, M.; Pron, A. *Synth. Met.* **1991**, *43*, 3009.
- (59) Yan, J.; Yang, X.; Wang, E. *Anal. Bioanal. Chem.* **2005**, *381*, 48.
- (60) Forry, S. P.; Wightman, R. M.; Marcel Dekker, Inc.: 2004, p 273.
- (61) Kissinger, P. T.; Heineman, W. R.; Editors *Monographs in Electroanalytical Chemistry and Electrochemistry, Vol. 5: Laboratory Techniques in Electroanalytical Chemistry*; Dekker, 1984.
- (62) DuVall, S. H.; McCreery, R. L. *Anal. Chem.* **1999**, *71*, 4594.
- (63) Bond, A. M.; Feldberg, S. W. *J. Phys. Chem. B* **1998**, *102*, 9966.

- (64) Jorgensen, L. V.; Andersen, H. J.; Skibsted, L. H. *Free Radical Res.* **1997**, 27, 73.
- (65) Sawyer, D. T.; Komai, R. Y. *Anal. Chem.* **1972**, 44, 715.
- (66) Carriedo, G. A. *J. Chem. Educ.* **1988**, 65, 1020.
- (67) Collinson, M. M.; Wightman, R. M. *Science* **1995**, 268, 1883.
- (68)
- <http://community.asdlib.org/imageandvideoexchangeforum/2013/07/31/pulse-polarography/>.
- (69) Bard, A. J.; Debad, J. D.; Leland, J. K.; Sigal, G. B.; Wilbur, J. L.; Wohlsatdter, J. N. In *Encyclopedia of Analytical Chemistry: Applications, Theory and Instrumentation*; Meyers, R. A., Ed.; John Wiley & Sons: New York, 2000; Vol. 11, p 9842.
- (70) Massey, R. J.; Powell, M. J.; Mied, P. A.; Feng, P.; Della Ciana, L.; Dressick, W. J.; Poonian, M. S. In *United States Patent US*, 1995.
- (71) *Electrogenerated Chemiluminescence*; Bard, A. J., Ed.; Marcel Dekker, Inc.: New York, 2004.
- (72) Miao, W. *Chem. Rev.* **2008**, 108, 2506.
- (73) Miao, W. In *Handbook of Electrochemistry*; Elsevier: Amsterdam, 2007, p 541.

- (74) Bezman, R.; Faulkner, L. R. *J. Amer. Chem. Soc.* **1972**, *94*, 6324.
- (75) Faulkner, L. R.; Tachikawa, H.; Bard, A. J. *J. Amer. Chem. Soc.* **1972**, *94*, 691.
- (76) Faulkner, L. R.; Bard, A. J. *J. Amer. Chem. Soc.* **1969**, *91*, 209.
- (77) Periasamy, N.; Santhanam, K. S. V. *Proc. Indian Acad. Sci., Sect. A* **1974**, *80*, 194.
- (78) Pighin, A. *Can. J. Chem.* **1973**, *51*, 3467.
- (79) Pighin, A.; Conway, B. E. *J. Electrochem. Soc.* **1975**, *122*, 1643.
- (80) Tachikawa, H.; Bard, A. J. *Chem. Phys. Lett.* **1974**, *26*, 568.
- (81) Miao, W.; Choi, J.-P. In *Electrogenerated Chemiluminescence*; Bard, A. J., Ed.; Marcel Dekker, Inc.: New York, 2004, p 213.
- (82) Miao, W.; Wang, S. In *Handbook of Chemiluminescent Methods in Oxidative Stress Assessment*; Popov, I., Lewin, G., Eds.; Transworld Research Network: Kerala, 2008, p 41.
- (83) Hesari, M.; Ding, Z. *J. Electrochem. Soc.* **2016**, *163*, H3116.
- (84) Fichorova, R. N.; Richardson-Harman, N.; Alfano, M.; Belec, L.; Carbonneil, C.; Chen, S.; Cosentino, L.; Curtis, K.; Dezzutti, C. S.; Donoval, B.; Doncel, G. F.; Donaghay, M.; Grivel, J.-C.; Guzman, E.; Hayes, M.; Herold, B.; Hillier, S.; Lackman-Smith, C.; Landay, A.; Margolis, L.; Mayer, K. H.; Pasicznyk, J.-M.;

Pallansch-Cokonis, M.; Poli, G.; Reichelderfer, P.; Roberts, P.; Rodriguez, I.; Saidi, H.; Sassi, R. R.; Shattock, R.; Cummins, J. J. E. *Anal. Chem.* **2008**, *80*, 4741.

(85) Toedter, G.; Hayden, K.; Wagner, C.; Brodmerkel, C. *Clin. Vaccine Immunol.* **2008**, *15*, 42.

(86) Chowdhury, F.; Williams, A.; Johnson, P. *J. Immunol. Methods* **2009**, *340*, 55.

(87) Christodoulides, N.; Tran, M.; Floriano, P. N.; Rodriguez, M.; Goodey, A.; Ali, M.; Neikirk, D.; McDevitt, J. T. *Anal. Chem.* **2002**, *74*, 3030.

(88) Kenten, J. H.; Gudibande, S.; Link, J.; Willey, J. J.; Curfman, B.; Major, E. O.; Massey, R. J. *Clin. Chem.* **1992**, *38*, 873.

(89) Z. Liron, A. B. a. M. F., *Novel Approaches in Biosensors and Rapid Diagnostic Assays*, Springer, US, 2001

(90) Heller, M. J. *Annu. Rev. Biomed. Eng.* **2002**, *4*, 129.

(91) Nelson, M. S.; Benzinger, E. A.; Budzynski, M. J.; Boodee, M. T.; Matthews, A.; Buel, E.; Schwartz, M. B.; von Beroldingen, C.; Wampler, R. L.; et, a. *J. Forensic Sci.* **1996**, *41*, 557.

(92) Lucarelli, F.; Palchetti, I.; Marrazza, G.; Mascini, M. *Talanta* **2002**, *56*, 949.

(93) Pollice, M.; Yang, H. L. *Clin Lab Med* **1985**, *5*, 463.

- (94) Gao, Y.; Xiang, Q.; Xu, Y.; Tian, Y.; Wang, E. *Electrophoresis* **2006**, *27*, 4842.
- (95) Gubitz, G.; Schmid, M. G.; Silviaeh, H.; Aboul-Enein, H. Y. *Crit. Rev. Anal. Chem.* **2001**, *31*, 167.
- (96) Iqbal, S. S.; Mayo, M. W.; Bruno, J. G.; Bronk, B. V.; Batt, C. A.; Chambers, J. P. *Biosens. Bioelectron.* **2000**, *15*, 549.
- (97) McBride, M. T.; Gammon, S.; Pitesky, M.; O'Brien, T. W.; Smith, T.; Aldrich, J.; Langlois, R. G.; Colston, B.; Venkateswaran, K. S. *Anal. Chem.* **2003**, *75*, 1924.
- (98) Merrill, G. A.; Rivera, V. R.; Neal, D. D.; Young, C.; Poli, M. A. *Anal. Biochem.* **2006**, *357*, 181.
- (99) Miao, W.; Bard, A. J. *Anal. Chem.* **2003**, *75*, 5825.
- (100) Sadik, O. A.; Land, W. H., Jr.; Wang, J. *Electroanalysis* **2003**, *15*, 1149.
- (101) Shah, J.; Wilkins, E. *Electroanalysis* **2003**, *15*, 157.
- (102) Song, L.; Ahn, S.; Walt, D. R. *Anal. Chem.* **2006**, *78*, 1023.
- (103) Uithoven, K. A.; Schmidt, J. C.; Ballman, M. E. *Biosens. Bioelectron.* **2000**, *14*, 761.
- (104) Bertoncetto, P.; Stewart, A. J.; Dennany, L. *Anal. Bioanal. Chem.* **2014**, *406*, 5573.

- (105) Deng, S.; Ju, H. *Analyst* **2013**, *138*, 43.
- (106) Doeven, E. H.; Barbante, G. J.; Hogan, C. F.; Francis, P. S. *ChemPlusChem* **2015**, *80*, 456.
- (107) Gross, E. M.; Maddipati, S. S.; Snyder, S. M. *Bioanalysis* **2016**, *8*, 2071.
- (108) Kargbo, O.; Ding, S.-N.; Li, Q.-L. *Curr. Anal. Chem.* **2014**, *10*, 622.
- (109) Kerr, E.; Doeven, E. H.; Wilson, D. J. D.; Hogan, C. F.; Francis, P. S. *Analyst* **2016**, *141*, 62.
- (110) Li, H.-J.; Han, S.; Hu, L.-Z.; Xu, G.-B. *Fenxi Huaxue* **2009**, *37*, 1557.
- (111) Miao, W.; Choi, J.-P.; Marcel Dekker, Inc.: 2004, p 213.
- (112) Miao, W.; Wang, S.; Transworld Research Network: 2008, p 41.
- (113) Miao, W. *Chem. Rev.* **2008**, *108*, 2506.
- (114) Ogi, O. *Bunko Kenkyu* **2013**, *62*, 135.
- (115) Wang, J.; Han, H. *Rev. Anal. Chem.* **2013**, *32*, 91.
- (116) Asamoto, H.; Nobushi, Y.; Oi, T.; Uchikura, K. *Chem. Pharm. Bull.* **2015**, *63*, 476.
- (117) Jiang, G.-m.; Zhan, W.-y.; Yan, R.; Lu, M.-f.; Jiang, G.-q. *Nantong Daxue Xuebao, Ziran Kexueban* **2013**, *12*, 48.

- (118) Kodamatani, H.; Kanzaki, R.; Tomiyasu, T.; Saito, K.; Kono, Y. *Anal. Lett.* **2011**, *44*, 2769.
- (119) Liao, H. *Dangdai Huagong* **2012**, *41*, 767.
- (120) Sun, Y.; Zhang, Z.; Zhang, X. *Spectrochim. Acta, Part A* **2013**, *116*, 361.
- (121) Sun, Y.; Zhang, Z.; Zhang, X. *Spectrochim. Acta, Part A* **2013**, *105*, 171.
- (122) Yamanaka, Y.; Miyamoto, M.; Tanaka, Y.; Nagumo, A.; Katsuki, Y.; Fukuda, Y.; Yoshimatsu, M.; Takeshige, A.; Kondo, T.; Fujishima, A.; Honda, K. *Electrochim. Acta* **2008**, *53*, 5397.
- (123) Yi, C.; Li, P.; Tao, Y.; Chen, X. *Microchim. Acta* **2004**, *147*, 237.
- (124) Danielson, N. D.; Marcel Dekker, Inc.: 2004, p 397.
- (125) Lin, M. S.; Wang, J. S.; Lai, C. H. *Electrochim. Acta* **2008**, *53*, 7775.
- (126) Li, X.-r.; Wang, Q.-f.; Shen, J.-s.; Tong, R.-t. *Hebei Shifan Daxue Xuebao, Ziran Kexueban* **2005**, *29*, 491.
- (127) Yang, L. *Yejin Fenxi* **2008**, *28*, 15.
- (128) Alarfaj, N. A.; Aly, F. A.; Al-Qahtany, A. A. *Luminescence* **2013**, *28*, 84.
- (129) Nobushi, Y.; Uchikura, K. *Chem. Pharm. Bull.* **2010**, *58*, 117.
- (130) Deng, B.; Shi, A.; Kang, Y.; Li, L. *Luminescence* **2011**, *26*, 592.

- (131) Deng, B.; Shi, A.; Li, L.; Kang, Y. *J. Pharm. Biomed. Anal.* **2008**, *48*, 1249.
- (132) Deng, B.; Shi, A.; Li, L.; Xie, F.; Lu, H.; Xu, Q. *Microchim. Acta* **2009**, *165*, 279.
- (133) Ji, Y.; Ma, Y.; Sun, X. *Anal. Methods* **2013**, *5*, 1542.
- (134) Muzyka, E. N.; Rozhitskii, N. N. *J. Anal. Chem.* **2010**, *65*, 550.
- (135) Wei, W.; Wei, M.; Cai, Z.; Liu, S. *Chromatographia* **2011**, *74*, 349.
- (136) Yu, H.; Raymonda, J. W.; McMahon, T. M.; Campagnari, A. A. *Biosens. Bioelectron.* **2000**, *14*, 829.
- (137) Li, S.; Wu, X.; Liu, C.; Yin, G.; Luo, J.; Xu, Z. *Anal. Chim. Acta* **2016**, *941*, 94.
- (138) Li, Z.; Sun, L.; Zhao, Y.; Yang, L.; Qi, H.; Gao, Q.; Zhang, C. *Talanta* **2014**, *130*, 370.
- (139) Dong, Y.-P.; Zhou, Y.; Wang, J.; Zhu, J.-J. *Anal. Chem.* **2016**, *88*, 5469.
- (140) Xu, H.; Liang, S.; Zhu, X.; Wu, X.; Dong, Y.; Wu, H.; Zhang, W.; Chi, Y. *Biosens. Bioelectron.* **2016**, Ahead of Print.
- (141) Hong, L.-R.; Chai, Y.-Q.; Zhao, M.; Liao, N.; Yuan, R.; Zhuo, Y. *Biosens. Bioelectron.* **2015**, *63*, 392.

- (142) Sun, L.-j.; Yang, J.; Zhang, Y.; Qi, H.-l.; Gao, Q.; Zhang, C.-x. *Fenxi Kexue Xuebao* **2014**, *30*, 651.
- (143) Gui, G.-F.; Zhuo, Y.; Chai, Y.-Q.; Xiang, Y.; Yuan, R. *Anal. Chem.* **2014**, *86*, 5873.
- (144) Li, Y.; Qi, H.; Gao, Q.; Zhang, C. *Biosens. Bioelectron.* **2011**, *26*, 2733.
- (145) Dang, J.; Guo, Z.; Zheng, X. *Anal. Chem.* **2014**, *86*, 8943.
- (146) Guo, X.; Wu, S.; Duan, N.; Wang, Z. *Anal. Bioanal. Chem.* **2016**, *408*, 3823.
- (147) He, Y.; Li, J.; Liu, Y. *Anal. Chem.* **2015**, *87*, 9777.
- (148) Gui, G.-F.; Zhuo, Y.; Chai, Y.-Q.; Xiang, Y.; Yuan, R. *Biosens. Bioelectron.* **2016**, *77*, 7.
- (149) Yang, H.; Yang, Q.; Li, Z.; Du, Y.; Zhang, C. *Sens. Actuators, B* **2016**, *236*, 712.
- (150) Xie, L.; You, L.; Cao, X. *Spectrochim. Acta, Part A* **2013**, *109*, 110.
- (151) Zhang, J.; Chen, P.; Wu, X. Y.; Chen, J. H.; Xu, L. J.; Chen, G. N.; Fu, F. *Biosens. Bioelectron.* **2011**, *26*, 2645.
- (152) Ji, X.; Yao, C.; Wan, Y.; Song, H.; Xin, P.; Cui, H.; Zheng, C.; Deng, S. *Chin. J. Chem.* **2016**, *34*, 331.

- (153) Chen, X.; He, Y.; Zhang, Y.; Liu, M.; Liu, Y.; Li, J. *Nanoscale* **2014**, *6*, 11196.
- (154) Wang, Z. G., X.; Wu, S.; Duan, N; Ma, X.; Xia, Y. China Patent CN105241869A, 2016.
- (155) Miao, W.; Bard, A. J. *Anal. Chem.* **2004**, *76*, 7109.
- (156) Miao, W.; Bard, A. J. *Anal. Chem.* **2004**, *76*, 5379.
- (157) Zhan, W.; Bard, A. J. *Anal. Chem.* **2007**, *79*, 459.
- (158) Maeda, M. *Bunseki* **1996**, 452.
- (159) Habtamu, H. B.; Sentic, M.; Silvestrini, M.; De Leo, L.; Not, T.; Arbault, S.; Manojlovic, D.; Sojic, N.; Ugo, P. *Anal. Chem.* **2015**, *87*, 12080.
- (160) Lee, W. Y. *Mikrochim. Acta* **1997**, *127*, 19.
- (161) Pittman, T. L.; Thomson, B.; Miao, W. *Anal. Chim. Acta* **2009**, *632*, 197.
- (162) Liu, Q.; Han, M.; Bao, J.; Jiang, X.; Dai, Z. *Analyst* **2011**, *136*, 5197.
- (163) Wang, S.; Harris, E.; Shi, J.; Chen, A.; Parajuli, S.; Jing, X.; Miao, W. *Phys. Chem. Chem. Phys.* **2010**, *12*, 10073.
- (164) Li, L.-L.; Liu, K.-P.; Yang, G.-H.; Wang, C.-M.; Zhang, J.-R.; Zhu, J.-J. *Adv. Funct. Mater.* **2011**, *21*, 869.
- (165) Lei, J.; Ju, H. *TrAC, Trends Anal. Chem.* **2011**, *30*, 1351.

- (166) Li, J.; Xu, Q.; Wei, X.; Hao, Z. *J. Agric. Food Chem.* **2013**, *61*, 1435.
- (167) Huang, R.; Wei, M.-Y.; Guo, L.-H. *J. Electroanal. Chem.* **2011**, *656*, 136.
- (168) Xu, Q.; Li, J.; Li, S.; Pan, H. *J. Solid State Electrochem.* **2012**, *16*, 2891.
- (169) Xiong, C.-Y.; Wang, H.-J.; Liang, W.-B.; Yuan, Y.-L.; Yuan, R.; Chai, Y.-Q. *Chem. - Eur. J.* **2015**, *21*, 9825.
- (170) Giokas, D. L.; Vlessidis, A. G.; Tsogas, G. Z.; Evmiridis, N. P. *TrAC, Trends Anal. Chem.* **2010**, *29*, 1113.
- (171) Ma, H.; Li, X.; Yan, T.; Li, Y.; Liu, H.; Zhang, Y.; Wu, D.; Du, B.; Wei, Q. *ACS Appl. Mater. Interfaces* **2016**, *8*, 10121.
- (172) Choi, H. N.; Yoon, S. H.; Lyu, Y.-K.; Lee, W.-Y. *Electroanalysis* **2007**, *19*, 459.
- (173) Guo, Z.; Dong, S. *Anal. Chem.* **2004**, *76*, 2683.
- (174) Dong, Y.-P. *J. Lumin.* **2010**, *130*, 1539.
- (175) Huang, R.; Zheng, X.; Qu, Y. *Anal. Chim. Acta* **2007**, *582*, 267.
- (176) Zhang, L.; Guo, Z.; Xu, Z.; Dong, S. *J. Electroanal. Chem.* **2006**, *592*, 63.
- (177) Choi, H. N.; Lee, J.-Y.; Lyu, Y.-K.; Lee, W.-Y. *Anal. Chim. Acta* **2006**, *565*, 48.

- (178) Chen, H.; Li, W.; Zhao, P.; Nie, Z.; Yao, S. *Electrochim. Acta* **2015**, *178*, 407.
- (179) Zou, X.; Shang, F.; Wang, S. *Spectrochim. Acta, Part A* **2017**, *173*, 843.
- (180) Yang, H.; Li, Z.; Shan, M.; Li, C.; Qi, H.; Gao, Q.; Wang, J.; Zhang, C. *Anal. Chim. Acta* **2015**, *863*, 1.
- (181) Dong, Y.-P.; Wang, J.; Peng, Y.; Zhu, J.-J. *J. Electroanal. Chem.* **2016**, *781*, 109.
- (182) Wu, D.; Fan, D.; Ma, H.; Ren, X.; Wang, Y.; Wang, H.; Hu, L.; Wei, Q.; China Patent CN105136879A, 2015.
- (183) Dong, Y.; Gao, T.; Zhou, Y.; Chu, X.; Wang, C. *Spectrochim. Acta, Part A* **2015**, *134*, 225.
- (184) Ma, H.; Wei, Q.; Lv, X.; Pang, X.; Wang, X.; Wu, D.; Fan, D.; Cao, W.; China Patent CN104931698A, 2015, p 10pp.
- (185) Hosseini, M.; Mirzanasiri, N.; Rezapour, M.; Sheikha, M. H.; Faridbod, F.; Norouzi, P.; Ganjali, M. R. *Luminescence* **2015**, *30*, 376.
- (186) Cristarella, T. C.; Chinderle, A. J.; Hui, J.; Rodriguez-Lopez, J. *Langmuir* **2015**, *31*, 3999.
- (187) Siddiqi, A. M.; Jennings, V. M.; Kidd, M. R.; Actor, J. K.; Hunter, R. L. *J. Clin. Lab. Anal.* **1996**, *10*, 423.

- (188) de Jong, M. D.; Weel, J. F. L.; Schuurman, T.; Wertheim-van Dillen, P. M. E.; Boom, R. *J. Clin. Microbiol.* **2000**, *38*, 2568.
- (189) Stevens, S. J. C.; Vervoort, M. B. H. J.; Van den Brule, A. J. C.; Meenhorst, P. L.; Meijer, C. J. L. M.; Middeldorp, J. M. *J. Clin. Microbiol.* **1999**, *37*, 2852.
- (190) Motmans, K.; Raus, J.; Vandevyver, C. *J. Immunol. Methods* **1996**, *190*, 107.
- (191) O'Connell, C. D.; Juhasz, A.; Kuo, C.; Reeder, D. J.; Hoon, D. S. B. *Clinical Chemistry* **1998**, *44*, 1161.
- (192) Delaney, J. L.; Hogan, C. F.; Tian, J.; Shen, W. *Anal. Chem.* **2011**, *83*, 1300.
- (193) Ge, L.; Wang, S.; Ge, S.; Yu, J.; Yan, M.; Li, N.; Huang, J. *Chem. Commun.* **2014**, *50*, 5699.
- (194) Ge, L.; Yu, J.; Ge, S.; Yan, M. *Anal. Bioanal. Chem.* **2014**, *406*, 5613.
- (195) Zhang, C. L., R. China Patent CN104198469A, 2014.
- (196) Miao, W.; Bard, A. J. *Anal. Chem.* **2003**, *75*, 5825.
- (197) Miao, W.; Bard, A. J. *Anal. Chem.* **2004**, *76*, 5379.
- (198) Miao, W.; Bard, A. J. *Anal. Chem.* **2004**, *76*, 7109.

- (199) Ma, F.; Zhang, Y.; Qi, H.; Gao, Q.; Zhang, C.; Miao, W. *Biosens. Bioelectron.* **2012**, *32*, 37.
- (200) Miao, W.; Pittman, T. L.; Thompson, B. In *PITTCON* Chicago, IL, 2007, p 790.
- (201) Shankaran, D. R.; Gobi, K. V.; Sakai, T.; Matsumoto, K.; Imato, T.; Toko, K.; Miura, N. *IEEE Sensors J.* **2005**, *5*, 616.
- (202) Zhan, W.; Bard, A. J. *Anal. Chem.* **2007**, *79*, 459.
- (203) Delaney, J. L.; Hogan, C. F.; Tian, J.; Shen, W. *Anal. Chem.* **2011**, *83*, 1300.
- (204) Mole, F.; Wang, J.; Clayton, D. A.; Xu, C.; Pan, S. *Langmuir* **2012**, *28*, 10610.
- (205) Li, Y.; Qi, H.; Fang, F.; Zhang, C. *Talanta* **2007**, *72*, 1704.
- (206) Acharya, D.; Bastola, P.; Le, L.; Paul, A. M.; Fernandez, E.; Diamond, M. S.; Miao, W.; Bai, F. *Sci. Rep.* **2016**, *6*, 32227.
- (207) Guo, Z.; Kong, H.; Yang, F.; Chen, T. *Sens. Actuators, B* **2015**, *220*, 270.
- (208) Guo, Z.; Yang, F.; Zhang, L.; Zheng, X. *Sens. Actuators, B* **2013**, *177*, 316.
- (209) Ishimatsu, R.; Matsunami, S.; Kasahara, T.; Mizuno, J.; Edura, T.; Adachi, C.; Nakano, K.; Imato, T. *Angew. Chem., Int. Ed.* **2014**, *53*, 6993.

- (210) Shen, M.; Zhu, X.-H.; Bard, A. J. *J. Am. Chem. Soc.* **2013**, *135*, 8868.
- (211) Dong, Y.-P.; Zhou, Y.; Wang, J.; Zhu, J.-J. *Sens. Actuators, B* **2016**, *226*, 444.
- (212) Odom, B.; Hanneke, D.; D'Urso, B.; Gabrielse, G. *Phys. Rev. Lett.* **2006**, *97*, 030801/1.
- (213) *Anon Anal. Chem.* **2008**, *80*, 1380.
- (214) Nugent, J. H. A. *Trends Biochem. Sci.* **1994**, *19*, 434.
- (215) Weil, J. A.; Bolton, J. R. *J. Chem. Educ.* **2009**, *86*, 33.
- (216) Miao, W.; Choi, J.-P.; Bard, A. J. *J. Am. Chem. Soc.* **2002**, *124*, 14478.
- (217) Parajuli, S.; Miao, W. *Anal. Chem.* **2013**, *85*, 8008.
- (218) Bard, A. J.; Editor *Electrogenerated Chemiluminescence*; Marcel Dekker, Inc., 2004.
- (219) Alexander, C.; McCall, J.; Richter, M. M. *Chem. Educ.* **1998**, *3*, No pp. Given.
- (220) Bolton, E.; Breyfogle, B.; Gordon, A.; Richter, M. M. *Chem. Educ.* **2007**, *12*, 15.
- (221) Hamamatsu.
- (222) Maness, K. M.; Wightman, R. M. *J. Electroanal. Chem.* **1995**, *396*, 85.

- (223) Lai, R. Y.; Bard, A. J. *J. Phys. Chem. A* **2003**, *107*, 3335.
- (224) Richter, M. M. *Chem. Rev.* **2004**, *104*, 3003.
- (225) Forry, S. P.; Wightman, R. M. In *Electrogener. Chemilumin.*; Bard Allen, J., Ed.; Marcel Dekker, Inc: New York, 2004, p 273.
- (226) Wallace, W. L.; Bard, A. J. *J. Phys. Chem.* **1979**, *83*, 1350.
- (227) Gao, X.; Lv, B.; Zhou, Z.; Xiao, D. *Microchim. Acta* **2008**, *161*, 163.
- (228) McCall, J.; Richter, M. M.; American Chemical Society: 1999, p ANYL.
- (229) Zheng, H.; Zu, Y. *J. Phys. Chem. B* **2005**, *109*, 16047.
- (230) Tokel-Takvoryan, N. E.; Hemingway, R. E.; Bard, A. J. *J. Am. Chem. Soc.* **1973**, *95*, 6582.
- (231) Matsuo, Y.; Seiko Epson Corp., Japan . 2015, p 18pp.
- (232) Dong, G. R.; Kariminia, H.-R.; Chen, Z. W.; Parker, W.; Pritzker, M. D.; Legge, R. L. *Energy Fuels* **2017**, *31*, 959.
- (233) He, X.; Yin, F.; Li, G.; Changzhou Institute of Advanced Materials, Beijing University of Chemical Technology, Peop. Rep. China . 2016, p 4pp.
- (234) Kitagawa, R.; Sugano, Y.; Yamagiwa, M.; Tsutsumi, E.; Tamura, J.; Ono, A.; Kudo, Y.; Mikoshiba, S.; Kabushiki Kaisha Toshiba, Japan . 2017, p 17pp.

- (235) Xia, Y.; Xie, S.; Choi, S.-I.; Wang, X.; Park, J.; Zhang, L.; Georgia Tech Research Corporation, USA . 2016, p 39pp.
- (236) Yamaguchi, T.; Tamaki, T.; Yamada, Y.; Tokyo Institute of Technology, Japan; Kanagawa Academy of Science and Technology; Noritake Co., Ltd. . 2016, p 11pp.
- (237) Bogdanovskaya, V. A.; Kol'tsova, E. M.; Tarasevich, M. R.; Radina, M. V.; Zhutaeva, G. V.; Kuzov, A. V.; Gavrilova, N. N. *Russ. J. Electrochem.* **2016**, 52, 723.
- (238) Chandross, E. A.; Sonntag, F. I. *J. Am. Chem. Soc.* **1966**, 88, 1089.
- (239) Rosado, D. J., Jr.; Miao, W.; Sun, Q.; Deng, Y. *J. Phys. Chem. B* **2006**, 110, 15719.
- (240) *Surface Analysis by Auger and X-ray Photoelectron Spectroscopy*; Briggs, D.; Grant, J. T., Eds.; IM Publications, 2003.
- (241) Kong, D.-x.; Li, Q.-l.; Chi, Y.-w.; Chen, G.-n. *Fenxi Ceshi Xuebao* **2013**, 32, 1283.
- (242) Gao, Y.; Wang, T.; Liu, F. *Electroanalysis* **2016**, Ahead of Print.
- (243) Dong, L.; Weng, L.; Qian, Y.; An, D.; Ping, T.; Wang, L. *Zhongguo Shipin Xuebao* **2014**, 14, 248.
- (244) Wang, F.; Bai, L. *Fenxi Kexue Xuebao* **2014**, 30, 291.

- (245) Kong, D.; Huang, X.; Lin, B.; Jiang, J.; Li, Q.; Wei, Q.; Chi, Y.; Chen, G. *Talanta* **2015**, *134*, 524.
- (246) Yu, X.; Zhang, W.; Ye, Z.; Song, B.; Yuan, J. *J. Fluoresc.* **2015**, *25*, 997.
- (247) Spehar-Deleze, A.-M.; Gransee, R.; Martinez-Montequin, S.; Bejarano-Nosas, D.; Dulay, S.; Julich, S.; Tomaso, H.; O'Sullivan, C. K. *Anal. Bioanal. Chem.* **2015**, *407*, 6657.
- (248) Parajuli, S.; Jing, X.; Miao, W. *Electrochim. Acta* **2015**, *180*, 196.
- (249) Liu, J.-L.; Zhao, M.; Zhuo, Y.; Chai, Y.-Q.; Yuan, R. *Chem. - Eur. J.* **2017**, Ahead of Print.
- (250) Lin, Y.; Yang, L.; Yue, G.; Chen, L.; Qiu, B.; Guo, L.; Lin, Z.; Chen, G. *Anal. Bioanal. Chem.* **2016**, *408*, 7105.
- (251) Li, X.; Lv, S.; Chen, M.; Tang, X.; Zou, Z.; Lu, L.; Inspection and Quarantine Technique Center of Fujian Entry-Exit Inspection and Quarantine Bureau, Peop. Rep. China . 2014, p 9pp.
- (252) Guo, H.; Wu, X.; Wang, A.; Luo, X.; Ma, Y.; Zhou, M. *New J. Chem.* **2015**, *39*, 8922.
- (253) Wang, S.-w.; Deng, G.-h.; Qu, Z.-k.; Wang, H. *Fenxi Shiyanshi* **2014**, *33*, 1198.
- (254) Jie, G.; Zhao, Y.; Niu, S. *Biosens. Bioelectron.* **2013**, *50*, 368.

- (255) Huan, J.; Liu, Q.; Fei, A.; Qian, J.; Dong, X.; Qiu, B.; Mao, H.; Wang, K. *Biosens. Bioelectron.* **2015**, *73*, 221.
- (256) Jie, G.; Qin, Y.; Meng, Q.; Wang, J. *Analyst* **2015**, *140*, 79.
- (257) Shan, D.; Zhu, R.; Niu, W.; Wei, X.; Lv, Y.; Jing, H.; Nanjing University of Science and Technology, Peop. Rep. China . 2016, p 13pp.
- (258) Zhang, J.; Cai, F.; Deng, A.; Li, J. *Electroanalysis* **2014**, *26*, 873.
- (259) Cai, F.; Wang, N.; Dong, T.; Deng, A.; Li, J. *Analyst* **2015**, *140*, 5885.
- (260) Zhou, H.; Han, T.; Wei, Q.; Zhang, S. *Anal. Chem. (Washington, DC, U. S.)* **2016**, *88*, 2976.
- (261) Liu, Y.-M.; Yang, J.-J.; Cao, J.-T.; Zhang, J.-J.; Chen, Y.-H.; Ren, S.-W. *Sens. Actuators, B* **2016**, *232*, 538.
- (262) Bin, N.; Li, W.; Yin, X.; Huang, X.; Cai, Q. *Talanta* **2016**, *160*, 570.
- (263) Yu, Y.; Shi, J.; Zhao, X.; Yuan, Z.; Lu, C.; Lu, J. *Analyst (Cambridge, U. K.)* **2016**, *141*, 3305.
- (264) Chen, Y.; Dong, Y.; Wu, H.; Chen, C.; Chi, Y.; Chen, G. *Electrochim. Acta* **2015**, *151*, 552.
- (265) Wu, D.; Fan, D.; Ma, H.; Ren, X.; Wang, Y.; Wang, H.; Hu, L.; Wei, Q.; University of Jinan, Peop. Rep. China . 2015, p 8pp.

- (266) Zhang, Q.; Xu, G.; Gong, L.; Dai, H.; Zhang, S.; Li, Y.; Lin, Y.  
*Electrochim. Acta* **2015**, *186*, 624.
- (267) Chen, Y.; Xiang, Y.; Yuan, R.; Chai, Y. *Anal. Chim. Acta* **2015**, *891*, 130.
- (268) Bard, A. J.; Richards, T. C.; Leland, J. K.; Igen, Inc., USA . 1996, p 67 pp.
- (269) Richards, T. C.; Bard, A. J. *Anal. Chem.* **1995**, *67*, 3140.
- (270) Rosado, D. J., Jr.; Miao, W.; Sun, Q.; Deng, Y. *J. Phys. Chem. B* **2006**, *110*, 15719.
- (271) Catalani, L. H.; Wilson, T.; Bechara, E. J. H. *Photochem. Photobiol.* **1987**, *45*, 273.
- (272) Duran, N.; Faljoni, A. *Biochem. Biophys. Res. Commun.* **1978**, *83*, 287.
- (273) American Cyanamid Co., USA . 1985, p 6 pp.
- (274) Bard, A. J.; Richards, T.; Leland, J. K.; Google Patents: 1998.
- (275) Catalani, L. H.; Wilson, T.; Bechara, E. J. H. *Photochemistry and Photobiology* **1987**, *45*, 273.
- (276) Rauhut, M. M.; Mohan, A. G.; American Cyanamid Co., USA . 1982, p 19 pp.
- (277) Becker, C. M.; Biagini, A. B.; Forte, M. M. C.; Amico, S. C.; Vargas, J. V. C.; Azambuja, D. S. *Polímeros* **2012**, *22*, 395.

- (278) Becker, C. M.; Biagini, A. B.; Forte, M. M. C.; Amico, S. C.; Vargas, J. V. C.; Azambuja, D. S. *Polim.: Cienc. Tecnol.* **2012**, *22*, 395.
- (279) Rudge, A.; Davey, J.; Raistrick, I.; Gottesfeld, S.; Ferraris, J. P. *Journal of Power Sources* **1994**, *47*, 89.
- (280) Suganuma, S.; Nakajima, K.; Kitano, M.; Yamaguchi, D.; Kato, H.; Hayashi, S.; Hara, M. *J. Am. Chem. Soc.* **2008**, *130*, 12787.
- (281) Parajuli, S.; Miao, W. *Anal. Chem.* **2009**, *81*, 5267.
- (282) da Cunha, M. C. P. M.; Weber, M.; Nart, F. C. *J. Electroanal. Chem.* **1996**, *414*, 163.
- (283) Horányi, G.; Rizmayer, E. M. *J. Electroanal. Chem. Interfacial Electrochem.* **1985**, *188*, 273.
- (284) Mayell, J. S.; Longer, S. H. *J. Electrochem. Soc.* **1964**, *111*, 438.
- (285) Mishima, H.; Iwasita, T.; Macagno, V. A.; Giordano, M. C. *Electrochim. Acta* **1973**, *18*, 287.
- (286) Tracy, M. L.; Nash, C. P. *J. Phys. Chem.* **1985**, *89*, 1239.
- (287) Rao, R. R.; Milliken, S. B.; Robinson, S. L.; Mann, C. K. *Anal. Chem.* **1970**, *42*, 1076.
- (288) Attri, P.; Kim, Y. H.; Park, D. H.; Park, J. H.; Hong, Y. J.; Uhm, H. S.; Kim, K.-N.; Fridman, A.; Choi, E. H. *Scientific Reports* **2015**, *5*, 9332.

- (289) Hering, T.; Slanina, T.; Hancock, A.; Wille, U.; Konig, B. *Chem. Commun.* **2015**, *51*, 6568.
- (290) Mack, J.; Bolton, J. R. *Journal of Photochemistry and Photobiology A: Chemistry* **1999**, *128*, 1.
- (291) Uchiyama, H.; Zhao, Q.-L.; Hassan, M. A.; Andocs, G.; Nojima, N.; Takeda, K.; Ishikawa, K.; Hori, M.; Kondo, T. *PLOS ONE* **2015**, *10*, e0136956.
- (292) Rosen, G. M.; Beselman, A.; Tsai, P.; Pou, S.; Mailer, C.; Ichikawa, K.; Robinson, B. H.; Nielsen, R.; Halpern, H. J.; MacKerell, A. D. *The Journal of Organic Chemistry* **2004**, *69*, 1321.
- (293) Houriez, C.; Ferré, N.; Siri, D.; Tordo, P.; Masella, M. *J. Phys. Chem. B* **2010**, *114*, 11793.
- (294) Frejaville, C.; Karoui, H.; Tuccio, B.; Moigne, F. L.; Culcasi, M.; Pietri, S.; Lauricella, R.; Tordo, P. *J. Med. Chem.* **1995**, *38*, 258.
- (295) Mottley, C.; Mason, R. P. *Arch. Biochem. Biophys.* **1988**, *267*, 681.
- (296) Rangelova, K.; Mason, R. P. *Magn. Reson. Chem.* **2011**, *49*, 152.
- (297) Reuveni, A.; Luz, Z. *Journal of Magnetic Resonance (1969)* **1976**, *23*, 271.
- (298) Jackson, S. K.; James, P. E. *Electron Paramagn. Reson.* **2008**, *21*, 15.
- (299) Fang, F. C. *Nat Rev Micro* **2004**, *2*, 820.

- (300) Kohno, M. *Journal of Clinical Biochemistry and Nutrition* **2010**, *47*, 1.
- (301) Shakerkhatibi, M.; Mohammadi, N.; Benis, K. Z.; Sarand, A. B.; Fatehifar, E.; Hashemi, A. A. *Environ. Health Eng. Manage. J.* **2015**, *2*, 117.
- (302) Song, Y.; She, X.; Yi, J.; Mo, Z.; Liu, L.; Xu, H.; Li, H. *Phys. Status Solidi A* **2016**, Ahead of Print.
- (303) Arangio, A. M.; Tong, H.; Socorro, J.; Poeschl, U.; Shiraiwa, M. *Atmos. Chem. Phys.* **2016**, *16*, 13105.
- (304) Yang, J.; Peop. Rep. China . 2016, p 8pp.
- (305) Jiang, B.; Dai, D.; Yao, Y.; Xu, T.; Li, R.; Xie, R.; Chen, L.; Chen, W. *Chem. Commun. (Cambridge, U. K.)* **2016**, *52*, 9566.
- (306) Bidzinska, E. *Carbohydr. Polym.* **2015**, *124*, 139.
- (307) Hinderberger, D. In *EPR Spectroscopy: Applications in Chemistry and Biology*; Drescher, M., Jeschke, G., Eds.; Springer Berlin Heidelberg: Berlin, Heidelberg, 2012, p 67.
- (308) Cammack, R.; CRC Press LLC: 2007, p 391.
- (309) Fee, J. A. *Methods Enzymol.* **1978**, *49*, 512.
- (310) Quintanar, L.; Rivillas-Acevedo, L. *Methods Mol. Biol. (N. Y., NY, U. S.)* **2013**, *1008*, 267.

- (311) Calle, C.; Sreekanth, A.; Fedin, M. V.; Forrer, J.; Garcia-Rubio, I.; Gromov, I. A.; Hinderberger, D.; Kasumaj, B.; Leger, P.; Mancosu, B.; Mitrikas, G.; Santangelo, M. G.; Stoll, S.; Schweiger, A.; Tschaggelar, R.; Harmer, J. *Helv. Chim. Acta* **2006**, *89*, 2495.
- (312) Pritchard, D.; Dehal, P.; Geekie, C.; ITI Scotland Limited, UK . 2009, p 63pp.
- (313) Sakurai, H. *Kassei Sanso, Furi Rajikaru* **1992**, *3*, 466.
- (314) Cammack, R. *Appl. Magn. Reson.* **2009**, *37*, 257.
- (315) Kuzuya, M. *Gifu Yakka Daigaku Kiyo* **2006**, *55*, 19.
- (316) Carini, M.; Aldini, G.; Orioli, M.; Facino, R. M. *Curr. Pharm. Anal.* **2006**, *2*, 141.
- (317) Swartz, H. M.; Khan, N.; Buckey, J.; Comi, R.; Gould, L.; Grinberg, O.; Hartford, A.; Hopf, H.; Hou, H.; Hug, E.; Iwasaki, A.; Lesniewski, P.; Salikhov, I.; Walczak, T. *NMR Biomed* **2004**, *17*, 335.
- (318) Lee, M. C.; Monduzzi Editore: 2005, p 159.
- (319) Mendu, P.; Kumari, C. G.; Ragi, R. *J. Fluoresc.* **2015**, *25*, 369.
- (320) El-Metwally, N. M.; Al-Hazmi, G. A. A. *Spectrochim. Acta, Part A* **2013**, *107*, 289.

- (321) Chen, X. J.; Schramm, J.; Tuohy, C.; Skiff, H.; Hummel, K.; Szklarski, A. R.; Vacirca, N.; Wolf, B. A.; Hirsh, D. J. *Biophys. Chem.* **2007**, *129*, 148.
- (322) Anupama, B.; Venkata Ramana Reddy, C.; Gyana Kumari, C. *Chem. Sci. Trans.* **2013**, *2*, 461.
- (323) Barchuk, V. I.; Dubinsky, A. A.; Grinberg, O. Y.; Lebedev, Y. S. *Chemical Physics Letters* **1975**, *34*, 476.
- (324) Hazlewood, C.; Davies, M. J. *Arch Biochem Biophys* **1996**, *332*, 79.
- (325) Wei, Z.; Villamena, F. A.; Weavers, L. K. *Environ. Sci. Technol.* **2017**, *51*, 3410.
- (326) Shuaib, W.; Stanazai, H.; Abazid, A. G.; Mattar, A. A. *Am. J. Med.* , *129*, 879.e7.
- (327) Petersen, L. R.; Jamieson, D. J.; Powers, A. M.; Honein, M. A. *N. Engl. J. Med.* **2016**, *374*, 1552.
- (328) Lazear, H. M.; Diamond, M. S. *J. Virol.* **2016**, *90*, 4864.
- (329) Perkasa, A.; Yudhaputri, F.; Haryanto, S.; Hayati, R. F.; Ma'roef, C. N.; Antonjaya, U.; Yohan, B.; Myint, K. S. A.; Ledermann, J. P.; Rosenberg, R.; Powers, A. M.; Sasmono, R. T. *Emerg. Infect. Dis.* **2016**, *22*, 924.

(330) Li, J.; Xiong, Y.; Wu, W.; Liu, X.; Qu, J.; Zhao, X.; Zhang, S.; Li, J.; Li, W.; Liao, Y.; Gong, T.; Wang, L.; Shi, Y.; Xiong, Y.; Ni, D.; Li, Q.; Liang, M.; Hu, G.; Li, D. *Emerg. Infect. Dis.* **2016**, *22*, 1133.

(331) Armstrong, P.; Hennessey, M.; Adams, M.; Cherry, C.; Chiu, S.; Harrist, A.; Kwit, N.; Lewis, L.; McGuire, D. O.; Oduyebo, T.; Russell, K.; Talley, P.; Tanner, M.; Williams, C. *Morb. Mortal. Wkly. Rep.* **2016**, *65*, 286.

(332) Thomas, D. L.; Sharp, T. M.; Torres, J.; Armstrong, P. A.; Munoz-Jordan, J.; Ryff, K. R.; Martinez-Quinones, A.; Arias-Berrios, J.; Mayshack, M.; Garayalde, G. J.; Saavedra, S.; Luciano, C. A.; Valencia-Prado, M.; Waterman, S.; Rivera-Garcia, B. *Morb. Mortal. Wkly. Rep.* **2016**, *65*, 154.

(333) Bachiller-Luque, P.; Domínguez-Gil González, M.; Álvarez-Manzanares, J.; Vázquez, A.; De Ory, F.; Sánchez-Seco Fariñas, M. P. *Enferm. Infecc. Microbiol. Clin.* **2016**, *34*, 243.

(334) Gardner, L. M.; Chen, N.; Sarkar, S. *Lancet Infect. Dis.* **2016**, *16*, 522.

(335) McCarthy, M. *BMJ* **2016**, 353.

(336) <http://www.who.int/mediacentre/factsheets/zika/en/>.

(337) Cerbino-Neto, J.; Mesquita, E. C.; Souza, T. M. L.; Parreira, V.; Wittlin, B. B.; Durovni, B.; Lemos, M. C. F.; Vizzoni, A.; Bispo, d. F. A. M.; Sampaio, S. A.; Goncalves, B. d. S.; Bozza, F. A. *Emerg Infect Dis* **2016**, *22*, 1318.

- (338) Ioos, S.; Mallet, H. P.; Leparc Goffart, I.; Gauthier, V.; Cardoso, T.; Herida, M. *Med. Maladies. Infect.* **2014**, *44*, 302.
- (339) Barry, A.; Pasco, H.; Babak, A.; Sarah, L.; Daniel, C.; Emma, J. A.; Andrew, J. S.; Timothy, J. B.; Roger, H. *Emerg. Infect. Dis.* **2016**, *22*, 940.
- (340) de M. Campos, R.; Cirne-Santos, C.; Meira, G. L. S.; Santos, L. L. R.; de Meneses, M. D.; Friedrich, J.; Jansen, S.; Ribeiro, M. S.; da Cruz, I. C.; Schmidt-Chanasit, J.; Ferreira, D. F. *J. Clin. Virol.* **2016**, *77*, 69.
- (341) Musso, D.; Roche, C.; Nhan, T.-X.; Robin, E.; Teissier, A.; Cao-Lormeau, V.-M. *J. Clin. Virol.* **2015**, *68*, 53.
- (342) Deckard, D. T.; Chung, W. M.; Brooks, J. T.; Smith, J. C.; Woldai, S.; Hennessey, M.; Kwit, N.; Mead, P. *MMWR Morb Mortal Wkly Rep* **2016**, *65*, 372.
- (343) D'Ortenzio, E.; Yazdanpanah, Y.; Piorowski, G.; Descamps, D.; Damond, F.; Matheron, S.; de, L. X.; Hubert, B.; Maquart, M.; Leparc-Goffart, I. *N Engl J Med* **2016**, *374*, 2195.
- (344) Moreira, J.; Lamas, C. C.; Siqueira, A. *Clin Infect Dis* **2016**, *63*, 141.
- (345) Rabenau, H. F.; Kessler, H. H.; Kortenbusch, M.; Steinhorst, A.; Raggam, R. B.; Berger, A. *J. Clin. Virol.* **2007**, *40*, 93.
- (346) Balm, M. N. D.; Lee, C. K.; Lee, H. K.; Chiu, L.; Koay, E. S. C.; Tang, J. W. *J. Med. Virol.* **2012**, *84*, 1501.

- (347) Faye, O.; Faye, O.; Dupressoir, A.; Weidmann, M.; Ndiaye, M.; Alpha Sall, A. *J.Clin. Virol.* **2008**, *43*, 96.
- (348) Koraka, P.; Zeller, H.; Niedrig, M.; Osterhaus, A. D. M. E.; Groen, J. *Microbes Infect.* **2002**, *4*, 1209.
- (349) Robert, S. L.; Olga, L. K.; Janeen, J. L.; Jason, O. V.; Amy, J. L.; Alison, J. J.; Stephanie, M. S.; Mark, R. D. *Emerg. Infect.Dis.* **2008**, *14*, 1232.
- (350) Pardee, K.; Green, A. A.; Takahashi, M. K.; Braff, D.; Lambert, G.; Lee, J. W.; Ferrante, T.; Ma, D.; Donghia, N.; Fan, M.; Daringer, N. M.; Bosch, I.; Dudley, D. M.; O'Connor, D. H.; Gehrke, L.; Collins, J. J. *Cell* **2016**, *165*, 1255.
- (351) Kilianski, A.; Roth, P. A.; Liem, A. T.; Hill, J. M.; Willis, K. L.; Rossmair, R. D.; Marinich, A. V.; Maughan, M. N.; Karavis, M. A.; Kuhn, J. H.; Honko, A. N.; Rosenzweig, C. N. *Emerg. Infect. Dis.* **2016**, *22*, 1448.
- (352) Liu, Y.-M.; Cao, J.-T.; Zheng, Y.-L.; Chen, Y.-H. *J. Sep. Sci.* **2008**, *31*, 2463.
- (353) Xu, S.-J.; Liu, Y.; Wang, T.-H.; Li, J.-H. *Anal. Chem.* **2010**, *82*, 9566.
- (354) Liu, X.; Ju, H. *Anal. Chem.* **2008**, *80*, 5377.
- (355) Li, Y.; Qi, H.; Peng, Y.; Gao, Q.; Zhang, C. *Electrochem. Commun.* **2008**, *10*, 1322.

- (356) Liu, Y.-M.; Cao, J.-T.; Tian, W.; Zheng, Y.-L. *Electrophoresis* **2008**, *29*, 3207.
- (357) Hao, N.; Wang, K. *Anal. Bioanal. Chem.* **2016**, *408*, 7035.
- (358) Rivera, V. R.; Gamez, F. J.; Keener, W. K.; White, J. A.; Poli, M. A. *Anal. Biochem.* **2006**, *353*, 248.
- (359) Ma, F.; Zhang, Y.; Qi, H.; Gao, Q.; Zhang, C.; Miao, W. *Biosens. Bioelectron.* **2012**, *32*, 37.
- (360) Parajuli, S.; Miao, W. *Anal. Chem.* **2009**, *81*, 5267.
- (361) Parajuli, S.; Miao, W. *Anal. Chem.* **2013**, *85*, 8008.
- (362) Sun, B.; Qi, H.; Ma, F.; Gao, Q.; Zhang, C.; Miao, W. *Anal. Chem.* **2010**, *82*, 5046.
- (363) Miner, Jonathan J.; Cao, B.; Govero, J.; Smith, Amber M.; Fernandez, E.; Cabrera, Omar H.; Garber, C.; Noll, M.; Klein, Robyn S.; Noguchi, Kevin K.; Mysorekar, Indira U.; Diamond, Michael S. *Cell* **2016**, *165*, 1081.
- (364) Paul, A. M.; Shi, Y.; Acharya, D.; Douglas, J. R.; Cooley, A.; Anderson, J. F.; Huang, F.; Bai, F. *J. Gen. Virol.* **2014**, *95*, 1712.
- (365) Acharya, D.; Paul, A. M.; Anderson, J. F.; Huang, F.; Bai, F. *PLoS Negl. Trop. Dis.* **2015**, *9*, e0004139.

- (366) Henschel, E. A.; McCown, J. M.; Burke, D. S.; Seguin, M. C.; Brandt, W. *E. Am. J. Trop. Med. Hyg.* **1985**, *34*, 162.
- (367) Roze, B.; Najioullah, F.; Ferge, J.-L.; Apetse, K.; Brouste, Y.; Cesaire, R.; Fagour, C.; Fagour, L.; Hochedez, P.; Jeannin, S.; Joux, J.; Mehdaoui, H.; Valentino, R.; Signate, A.; Cabie, A. *Euro. Surveill.* **2016**, *21*.
- (368) Weaver, S. C.; Reisen, W. K. *Antiviral Res.* **2010**, *85*, 328.
- (369) Rougeron, V.; Sam, I. C.; Caron, M.; Nkoghe, D.; Leroy, E.; Roques, P. J. *Clin. Virol.* **2015**, *64*, 144.
- (370) Hajra, A.; Bandyopadhyay, D.; Hajra, S. *N. Am. J. Med. Sci.* **2016**, *8*, 123.
- (371) Fauci, A. S.; Morens, D. M. *New Eng. J. Med.* **2016**, *374*, 601.
- (372) Paty, M. C. *Transfus. Clin. Biol.* **2013**, *20*, 165.
- (373) Tambyah, P. A.; Koay, E. S. C.; Poon, M. L. M.; Lin, R. V. T. P.; Ong, B. K. C. *New Eng. J. Med.* **2008**, *359*, 1526.
- (374) Fichorova, R. N.; Richardson-Harman, N.; Alfano, M.; Belec, L.; Carbonneil, C.; Chen, S.; Cosentino, L.; Curtis, K.; Dezzutti, C. S.; Donoval, B.; Doncel, G. F.; Donaghay, M.; Grivel, J.-C.; Guzman, E.; Hayes, M.; Herold, B.; Hillier, S.; Lackman-Smith, C.; Landay, A.; Margolis, L.; Mayer, K. H.; Pasicznyk, J.-M.; Pallansch-Cokonis, M.; Poli, G.; Reichelderfer, P.; Roberts, P.; Rodriguez, I.; Saidi, H.; Sassi, R. R.; Shattock, R.; Cummins, J. E., Jr. *Anal. Chem.* **2008**, *80*, 4741.

(375) Chowdhury, F.; Williams, A.; Johnson, P. *J. Immunol. Methods* **2009**, *340*, 55.

(376) Doeven, E. H.; Barbante, G. J.; Kerr, E.; Hogan, C. F.; Endler, J. A.; Francis, P. S. *Anal. Chem.* **2014**, *86*, 2727.